
Department of Neurology
Faculty2: Medicine Clinical Medicine
Saarland University Medical Center, Homburg/Saar

Pathogenic roles of GPR109a in Alzheimer's Disease

Dissertation for the degree of

Doctor of Medicine and Natural Sciences (MD/PhD)

Faculty of Medicine

SAARLAND UNIVERSITY

2022

Submitted by Qinghua Luo

Born on February, 1993 in Jiangxi, P. R. China

Aus der Klinik für Neurologie
Klinische Medizin der Medizinischen Fakultät
Universitätsklinikum des Saarlandes (UKS), Homburg/Saar

Pathogene Rolle von GPR109a bei der Alzheimer- Krankheit

Dissertation zur Erlangung des Grades eines

Doktors der Medizin und der Naturwissenschaften (MD/PhD)

der Medizinischen Fakultät

der UNIVERSITÄT DES SAARLANDES

2022

vorgelegt von Qinghua Luo

Geb. im February 1993 in Jiangxi, V. R. China

To
My Dear Parents
&
Dear Myself

Declaration

I hereby declare that this thesis is my own original work and effort. All experiments, except for those specified, were exclusively performed by me. Except for the publications written by myself listed in the publication list, the data presented here have not been submitted anywhere else for any award. Where other sources of information and help have been used, they have been indicated and acknowledged.

Homburg/Saar,

Qinghua Luo

Qinghua Luo

Tag der Promotion: 20.12.2022

Dekan: Prof. Dr. M.D. Menger

Berichterstatter:

Prof. Dr. Frank Kirchhoff,

Prof. Dr. Klaus Faßbender,

Prof. Dr. Martin Jung,

Prof. Dr. Tobias Hartmann (Prüfer)

ABBREVIATIONS

% (v/v)	Volume/volume percentage solution
% (w/v)	Weight/volume percentage solution
ABC	ATP-binding cassette
ABCB	ATP Binding Cassette Subfamily B Member
AD	Alzheimer's disease
ADAM10	A disintegrin and metalloproteinase domain-containing protein 10
AICD	Amyloid precursor protein intracellular domain
APOE	Apolipoprotein E
APP	Amyloid precursor protein
APP-KI	APP-knock-in
APS	Ammonium persulfate
AQP4	Aquaporin 4
ASC	Apoptosis-associated speck-like protein containing a CARD
ASF	Altered Schaedler flora
Axl	AXL tyrosine kinase receptor
A β	Amyloid β -peptide
BACE-1	B-site APP-cleaving enzyme
BBB	Blood-brain barrier
BDNF	Brain-derived neurotrophic factor
BIN1	Bridging Integrator 1
BMDM	Bone marrow derived macrophage
BSA	Bovine serum albumin
CD	Cluster of differentiation
CD2AP	CD2-associated protein
CE	Coefficient of error
CLU	Clusterin
CMA	Chaperone-mediated autophagy
CNS	Central nervous system
CR1	Complement receptor type 1
CSF	Cerebrospinal fluid
Ct	Threshold cycle
CTF	C-terminal fragment
CX3CL1	C-X3-C Motif Chemokine Ligand 1
CX3CR1	C-X3-C Motif Chemokine Receptor 1
DAM	Disease-associated microglia
DAPI	4',6-diamidino-2-phenylindole
Ddit4	DNA-damage-inducible transcript 4
DMEM	Dulbecco's Modified Eagle Medium
DMSO	Dimethyl sulfoxide
DNA	Deoxyribonucleic acid
dsDNA	Double-strand deoxyribonucleic acid
dsRNA	Double-strand ribonucleic acid
DT	Diphtheria toxin
DTT	Dithiothreitol
<i>e.g.</i>	<i>Exempli gratia</i> , for example
eA β	Extracellular A β
EDTA	Ethylenediaminetetraacetic acid
ELISA	Enzyme-linked immunosorbent assay
ELN	Endosomal-lysosomal Network
EOAD	Early-onset Alzheimer's disease

FAD	Familial AD
FBS	Fetal bovine serum
FSC	Forward-scatter
g	Gram
<i>g</i>	<i>Gravity</i>
Gau-HCl	Guanidine chloride buffer
GF	Germ-free
GFAP	Glial fibrillary acidic protein
GFP	Green fluorescence protein
GPCRs	G protein-coupled receptors
GPER	G protein-coupled estrogen receptor
GWASs	Genome-wide association studies
H ₂ O ₂	Hydrogen peroxide
HBSS	Hanks Balanced Salt Solution
HEPES	N-2-Hydroxyethylpiperazine-N-2-Ethane Sulfonic Acid
HRP	Horseradish Peroxidase
Iba1	Ionized calcium-binding adaptor molecule 1
IDE	Insulin-degrading enzyme
IF	Immunofluorescence
IFN	Interferon
IGF	Insulin-like growth factor
IgG	Immunoglobulin G
IL-10	Interleukin-10
IL-34	Interleukin-34
iNOS	Inducible nitric oxide synthase
IRF	Interferon regulatory factor
ISF	Interstitial fluid
kb	Kilo base pairs
KBs	Ketone bodies
kDa	Kilodalton
KO/ko	Knockout
LDLR	Low Density Lipoprotein Receptor
LOAD	Late-onset Alzheimer's disease
LPS	Lipopolysaccharide
LRP1	Low-density lipoprotein-related protein 1
M	Molar/L
MCI	Mild cognitive impairment
MeX04	Methoxy-X04
mFI	Mean fluorescence intensity
min	minute
mRFP	Monomeric red fluorescent protein
mTOR	Mammalian target of the rapamycin
Munc18-1	Mammalian uncoordinated-18
NAD	Nicotinamide adenine dinucleotide
NEP	Neprilysin
NFT	Neurofibrillary tangles
NLRP3	NOD-, LRR- and pyrin domain-containing protein 3
NOD1/2	Nucleotide-binding domain-containing protein 1/2
O.D.	Optical density
OFP	Open-field test
PAGE	Polyacrylamide gel electrophoresis
PBS	Phosphate-Buffered Saline

PCR	Polymerase chain reaction
PE	Porter-Elvehjem
PET	Positron emission tomography
PFA	Paraformaldehyde
PGLYRP1	Peptidoglycan recognition protein 1
P-gp	P-Glykoprotein
PICALM	Phosphatidylinositol Binding Clathrin Assembly Protein
PPs	Peyer's patches
PSD95	Postsynaptic density protein 95
PSEN1	Presenilin 1
PSEN2	Presenilin 2
p-Tau	Hyperphosphorylated Tau protein
PVC	Polyvinyl chloride
PVDF	Polyvinylidene difluoride
RNA	Ribonucleic acid
RNA-seq	Single-cell RNA sequencing
RNS	Nitrogen species
ROS	Reactive oxygen
rpm	Revolutions per minute
RPMI	Roswell Park Memorial Institute
RT-RCR	Real-time reverse transcription polymerase chain reaction
s	Second
sAPP α	Soluble ectodomain of APP
sAPP β	Soluble APP β fragment
SCARA1	Scavenger receptor 1
SCFA	Short chain fatty acid
SDS	Sodium dodecyl sulfate
SEM	Standard Error of Mean
sLRP1	Soluble low-density lipoprotein-related protein 1
SNAP25	Synaptosome-associated protein 25
SORL1	Sortilin Related Receptor 1
SPF	Specific pathogen-free
SRs	Scavenger receptors
SSC	Side-scatter
sTREM2	Soluble TREM2
TBS	Tris buffer with salt
TCR	T-cell receptor
TEMED	N, N, N', N'-Tetramethyl ethylenediamine
TGF β	Transforming growth factor β
TLR	Toll-like receptor
TNF	Tumor necrosis factor
TREM2	Triggering receptors expressed on myeloid cells 2
Tris	Tris(hydroxymethyl)aminomethane
TYROBP	Transmembrane immune signaling adaptor TYROBP
U	Unit
UPS	Ubiquitin-proteasome system
V	Volt
WB	Western blot
WT/wt	Wildtype
α 2M	α 2-Macroglobulin

CONTENT

1. ABSTRACT.....	1
2. ZUSAMMENFASSUNG.....	2
3. INTRODUCTION.....	3
3.1 Epidemiology of Alzheimer’s disease	3
3.2 Risk factor in AD	3
3.3 Pathological hallmarks of Alzheimer’s Disease	4
3.3.1 Amyloid β	4
3.3.1.1 Accumulation of A β in AD.....	5
3.3.1.2 A β clearance systems.....	5
3.3.2 Microglia.....	11
3.3.2.1 The origin of microglia	11
3.3.2.2 Microglia physiology	12
3.3.2.3 Microglia in the AD brain: blessing or curse?.....	12
3.3.2.4 A β clearance by microglia	15
3.3.2.5 Regulation of microglial activation	15
3.4 Gut microbiota in Alzheimer’s disease.....	16
3.5 Microbiome-microglia connections in AD	17
4. AIM OF THIS WORK.....	21
5. MATERIALS AND METHODS	22
5.1 Materials	22
5.1.1 Instruments.....	22
5.1.2 General experimental materials and consumables.....	23
5.1.3 Chemicals, reagents, Kits, Antibodies	24
5.1.4 Buffer	28
5.2 Mice	30
5.3 Methods.....	31
5.3.1 Y maze test.....	31
5.3.2 Open field test.....	32
5.3.3 Tissue preparation.....	32
5.3.4 Separation of cerebral vessels in mice	33

5.3.5	Positive selection of CD11b ⁺ cells in adult mouse brain.....	35
5.3.6	Isolation of T cells from mouse small intestinal lamina propria and Peyer's patches.....	36
5.3.7	Bone marrow-derived macrophages (BMDMs) culture and treatment	38
5.3.8	Flow cytometric analysis of HiLyte Flour TM 488-A β 42 internalization in primary macrophages.....	39
5.3.9	Bio-Rad Protein Assay.....	39
5.3.10	ELISA	40
5.3.11	Extraction of A β from mouse brain into TBS-soluble, TBS-T-soluble, guanidine HCl-soluble fractions	41
5.3.12	A β ELISA	42
5.3.13	Western blot analysis	43
5.3.14	Methoxy-X04 staining for A β deposition.....	46
5.3.15	Immunofluorescent staining.....	47
5.3.16	Analysis of microglial morphology	50
5.3.17	Phagocytosis assays <i>in vivo</i>	51
5.3.18	Reverse transcription and quantitative PCR for analysis of gene transcripts ..	52
5.3.19	Statistical analysis.....	55
6.	RESULTS	57
6.1	GPR109a specifically expresses in A β -associated microglia	57
6.2	Deficiency of GPR109a ameliorates cognitive deficits in APP-knock-in mice	58
6.3	Deficiency of GPR109a reduces synaptic impairment of APP-knock-in AD mice	59
6.4	Deficiency of GPR109a reduces A β load in the brain of APP-knock-in mice.....	62
6.5	Deficiency of GPR109a does not change neuroinflammatory activation in APP-knock-in mice.....	66
6.6	Deficiency of GPR109a regulates morphological changes of A β plaque-associated microglia in APP-knock-in mice	67
6.7	Deficiency of GPR109a shifts microglial activation to homeostatic profile	69
6.8	Deficiency of GPR109a increases microglial recruitment around the plaques and promotes microglial A β phagocytosis	70
6.9	Deficiency of GPR109a enhances anti-inflammatory activation and A β phagocytosis in macrophages upon niacin treatment	72

6.10	LRP1 upregulation in neurons and astrocytes from GPR109a-deficient APP ^{ki/ki} mice	76
6.11	Deficiency of GPR109a decreases IL-17a expression in intestinal CD4 ⁺ T lymphocytes of APP ^{ki/ki} mice.....	79
6.12	IL17a-expressing lymphocytes might be involved in the improvements of A β pathologies in GPR109a-deficient APP ^{ki/ki} mice	81
7.	DISCUSSION.....	86
7.1	Deficiency of GPR109a ameliorates Alzheimer’s pathologies	86
7.2	Deficiency of GPR109a modifies microglial activation and response in AD brain	86
7.3	Deficiency of GPR109a promotes construction of microglia physical barrier around A β deposits	89
7.4	Deficiency of GPR109a facilitates A β clearance in the brain	90
7.4.1	Deficiency of GPR109a increases microglia-mediated A β clearance	91
7.4.2	Deficiency of GPR109a elevates LRP1-mediated A β clearance.....	92
7.5	IL-17a-producing CD4-positive lymphocytes may regulate the pathogenic role of GPR109a in APP knock-in mice.....	93
8.	APPENDIX.....	95
9.	REFERENCES.....	114
10.	LIST OF FIGURES AND COOPERATIONS.....	131
11.	PUBLICATIONS AND PRESENTATIONS.....	133
11.1	Publications.....	133
11.2	Poster presentations	133
12.	ACKNOWLEDGEMENTS	134
13.	CURRICULUM VITAE.....	136

1. ABSTRACT

As a significant environmental factor for Alzheimer's disease (AD), gut microbiota have been observed to regulate microglial activation and amyloid pathology. However, the mechanisms through which gut microbiota modify AD progression remain unclear. We hypothesized that GPR109a, a receptor for bacterial metabolites, might link the intestinal microbiota to AD pathology. By cross-breeding *App*^{NL-G-F/NL-G-F} knock-in (APP-KI) AD mouse model with GPR109a knockout mice, we showed that deficiency of GPR109a increases microglial internalization of amyloid- β (A β) and substantially reduces A β load in the brain. As a result, deficiency of GPR109a prevents neuronal impairment and improves cognitive function of AD mice. Deficiency of GPR109a does not affect neuroinflammation, as neither the number of microglia nor the transcription of inflammatory genes (*e.g.*, *tnf- α* and *il-1 β*) in the brain tissue is changed compared with GPR109a-wildtype AD mouse.

In further experiments, we observed 3 potential molecular mechanisms: 1) GPR109a deficiency up-regulates the transcription of the *trem2* gene in microglia, which promotes microglial response to extracellular environmental changes. In GPR109a-deficient AD mice, there are more microglia clustered around A β deposits than in GPR109a-wildtype APP-KI mice, which may facilitate A β clearance; 2) Deficiency of GPR109a increases transcription of *cx3cr1* gene. In cultured bone marrow-derived macrophages, GPR109a deficiency enhances CX3CR1 expression induced by niacin treatment compared with GPR109a wild-type cells. CX3CR1 expression is correlated with phagocytosis of A β oligomers. Concurrent treatment with CX3CR1 antagonist, AZD 8797, prevents niacin from promoting A β -phagocytosis by GPR109a-deficient macrophages; and 3) deficiency of GPR109a increases the expression of LRP1 on neurons and astrocytes, which might also facilitate uptake of A β by these cells.

In conclusion, deficiency of GPR109a increases A β clearance by microglia and possibly also by neurons and astrocytes, which subsequently attenuates amyloid pathology and protects neurons in AD mice.

2. ZUSAMMENFASSUNG

Es wurde beobachtet, dass die Darmmikrobiota als wichtiger Umweltfaktor für die Alzheimer-Krankheit (AD) die Mikroglia-Aktivierung und die Amyloid-Pathologie reguliert. Die Mechanismen, durch die die Darmmikrobiota das Fortschreiten der Alzheimer-Krankheit beeinflusst, sind jedoch noch unklar. Wir stellten die Hypothese auf, dass GPR109a, ein Rezeptor für bakterielle Stoffwechselprodukte, eine Verbindung zwischen der Darmmikrobiota und der AD-Pathologie herstellen könnte. Durch die Kreuzung von *App^{NL-G-F/NL-G-F}* (APP-KI) AD-Mausmodell mit GPR109a-Knockout-Mäusen konnten wir zeigen, dass ein Mangel an GPR109a die mikrogliale Internalisierung von Amyloid- β ($A\beta$) erhöht und die $A\beta$ -Belastung im Gehirn erheblich reduziert. Ein Mangel an GPR109a verhindert also neuronale Beeinträchtigungen und verbessert die kognitiven Funktionen von AD-Mäusen. Der Mangel an GPR109a hat keinen Einfluss auf die Neuroinflammation, da weder die Anzahl der Mikroglia noch die Transkription von Entzündungsgenen (z.B. $\text{tnf-}\alpha$ und $\text{il-1}\beta$) im Hirngewebe im Vergleich zur GPR109a-Wildtyp-AD-Maus verändert ist.

In weiteren Experimenten haben wir 3 mögliche molekulare Mechanismen beobachtet: 1) Der Mangel an GPR109a regt die Transkription des *trem2*-Gens in Mikroglia an, was die Reaktion der Mikroglia auf extrazelluläre Umweltveränderungen fördert. In GPR109a-defizienten AD-Mäusen gibt es mehr Mikroglia, die sich um $A\beta$ -Ablagerungen gruppieren, als in GPR109a-Wildtyp-APP-KI-Mäusen, was die $A\beta$ -Clearance erleichtern könnte; 2) Ein Mangel an GPR109a erhöht die Transkription des *cx3cr1*-Gens. In kultivierten Makrophagen aus dem Knochenmark verstärkt ein GPR109a-Mangel die durch Niacin-Behandlung induzierte CX3CR1-Expression im Vergleich zu GPR109a-Wildtyp-Zellen. Die CX3CR1-Expression korreliert mit der Phagozytose von $A\beta$ -Oligomeren. Die gleichzeitige Behandlung mit dem CX3CR1-Antagonisten AZD 8797 verhindert, dass Niacin die $A\beta$ -Phagozytose durch GPR109a-defiziente Makrophagen fördert; und 3) Der Mangel an GPR109a erhöht die Expression von LRP1 auf Neuronen und Astrozyten, was auch die Aufnahme von $A\beta$ durch diese Zellen erleichtern könnte.

Zusammenfassend lässt sich sagen, dass ein Mangel an GPR109a die $A\beta$ -Clearance durch Mikroglia und möglicherweise auch durch Neuronen und Astrozyten erhöht, was in der Folge die Amyloid-Pathologie abschwächt und die Neuronen in AD-Mäusen schützt.

3. INTRODUCTION

3.1 Epidemiology of Alzheimer's disease

Alzheimer's disease (AD) is an irreversible neurodegenerative disease responsible for about two-thirds of dementia in the elderly. There are over 50 million people worldwide living with dementia in 2020 (<https://www.alzint.org/resource/numbers-of-people-with-dementia-worldwide/>). There are more than 9.9 million new AD cases each year worldwide, equivalent to one new case every 3.2 seconds, and the number of people with dementia is expected to increase to 152 million in 2050 (MARTIN PRINCE, 2015; PRINCE et al., 2016). AD also is one of the fifth-leading causes of mortality among the elderly, the number of deaths from AD jumped 145% between 2000 and 2019 (2021). With increasing life expectancy and the progressive demographic aging, the prevalence of AD will climb further (<https://www.dementiastatistics.org/>). Alzheimer's disease is becoming a serious and growing worldwide health challenge.

3.2 Risk factor in AD

AD is a complex and multifactorial disease caused by genetic susceptibility and environmental factors throughout the life course. Most people with AD are 65 years or older, called late-onset Alzheimer's disease (LOAD). Aging is the most potent risk factor contributing to LOAD. AD affects more than one in every nine persons aged 65 and over, and the proportion of people with AD rises sharply with age (RAJAN et al., 2021). Genetic factors are additional significant contributor to AD, with nearly 60-80% heritability rate (GATZ et al., 2006). Genome-wide association studies (GWASs) have identified more than forty AD-associated genetic loci, of which APOE4 is the most vital risk gene, presenting in 40-65% of AD patients. These GWASs-identified variants are predominantly associated with amyloid β metabolism (ADAM10, APOE4, ABCA7), lipid metabolism (APOE4, ABCA7, CLU), inflammatory response (TREM2, CD33, CR1), and endocytosis (PICALM, CD2AP, SORL1, BIN1) (SCHELTENS et al., 2021). In addition, mutations in β -amyloid precursor protein (APP), presenilin 1 (PSEN1), and presenilin 2 (PSEN2) cause dominantly inherited familial AD (FAD),

which represent fewer than 1% of all AD patients, and their symptoms typically appear between the ages of 40s and 50s (2021). Although age, genetics, and family history are all risk factors that cannot be changed, AD is also affected by many modifiable risk factors, such as cardiovascular disease, physical activity, diet, gut microbiota, and education. According to the 2020 recommendations of The Lancet Commission on dementia prevention, intervention, and care (LIVINGSTON et al., 2020) suggest that addressing modifiable risk factors might prevent or postpone up to 40% of dementia cases.

3.3 Pathological hallmarks of Alzheimer’s Disease

The pathological changes in Alzheimer’s disease occur decades before the onset of clinical symptoms and subtly affect various brain parenchyma cells such as neurons, microglia, and astrocytes (JACK et al., 2018). The abnormalities in these brain parenchyma cells drive a relentless progression of the underlying pathology of AD, with cognitive decline, disrupted language, and cumulative behavioral changes that diminish a person’s independence. Extensive neuronal loss, extracellular deposits of amyloid β peptide ($A\beta$), intracellular neurofibrillary tangles (NFT) containing the hyperphosphorylated Tau protein (p-Tau), and microglia-associated inflammatory activation are hallmarks of the Alzheimer’s pathology. The progression of AD is a continuum from preclinical to mild cognitive impairment (MCI) and eventually to severe Alzheimer’s disease dementia, a process that typically lasts 15-25 years (2021; ALBERT et al., 2011; SPERLING et al., 2011).

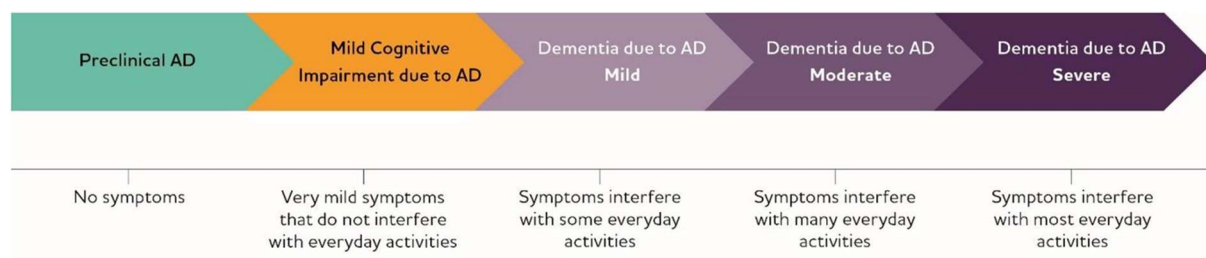


Fig. 3.3, Alzheimer’s disease (AD) continuum lasts 15-25 years. Although these arrows are of equal size, the components of the AD continuum are not equal in duration (2021).

3.3.1 Amyloid β

Amyloid β plaques are one of the crowning features of AD pathology. For the last 20 years, the amyloid cascade hypothesis has dominated AD pathology research, claiming that

amyloid deposition in the brain is a significant event that leads to tau aggregation, synaptic loss, and cell death (KARRAN et al., 2011).

3.3.1.1 Accumulation of A β in AD

A β is a 40-42 amino acid peptide (~4 kDa) derived from the sequential proteolytic cleavage of the amyloid precursor protein (APP). APP, encoded by a gene at locus 21q21.3, is a conserved type I integral membrane protein expressed in many tissues (NHAN et al., 2015). APP is available in a variety of sizes ranging from 695 to 770 amino acids, with APP695 being the most abundant in the brain and mainly generated by neurons. Under physiological conditions, APP is essential for neuronal growth and survival. There are two major processing pathways of APP degradation: nonamyloidogenic and amyloidogenic pathways. In the nonamyloidogenic pathway, α -secretase cleaves APP at the cell surface, releasing soluble ectodomain of APP (sAPP α) and a membrane-tethered intracellular 83-amino-acid C-terminal fragment (CTF α /C83). CTF α can be internalized and further processed by γ -secretase in endosomes to form p3 (3 kDa) and AICD. These fragments can be removed easily instead of depositing as plaques. In contrast, amyloidogenic processing of APP is mainly by β -secretase at endosomes. β -secretase located on the endosomal membrane cleavage APP between residues 671 and 672, yielding an N-terminal soluble APP β fragment (sAPP β) and an intracellular C-terminal β (CTF β or C99). Further hydrolysis of CTF β by γ -secretase liberates A β monomers and cytoplasmic peptides called APP intracellular domain (AICD). The A β monomers are further cleaved to form primary A β forms, A β 40 and A β 42. Soluble A β 42 is considered more toxic than A β 40, for it tends to aggregate to form fibrils. The secreted A β peptides form soluble A β , A β oligomers (from monomer to dodecamers), and larger, insoluble amyloid fibrils. A substantial body of the literature indicates that soluble oligomeric A β is the main noxious form in AD pathology, as their concentrations are linked to the onset, progression, and severity of clinical symptoms (ESPARZA et al., 2013; TOLAR et al., 2020).

3.3.1.2 A β clearance systems

In biological systems, the balance between protein anabolism and catabolism/clearance determines the amount of protein, which implies that all variables controlling A β production

and catabolism/clearance dictate A β concentration in the brain. The relative rather than the absolute rates of A β production and removal determine net A β levels (SAIDO, LEISSRING, 2012). Unlike EOAD, in which gene mutations lead to a significant increase in A β production, there is little evidence that increased total A β production leads to sporadic AD. Numerous studies strongly suggest that the failure of A β clearance, rather than an increase in its production, is the key to driving late-onset sporadic AD pathogenesis (CHEN et al., 2017; TOLAR et al., 2020). Multiple mechanisms can remove soluble A β from the brain, such as transport into the peripheral circulation and lymphatic system and catabolism in the central nervous system (CNS).

3.3.1.2.1 A β efflux from the CNS into the circulation

Extracellular A β (eA β) efflux into the peripheral circulation is an essential pathway for A β clearance. Substantial studies revealed that neurovascular, BBB, and glymphatic (glial + lymphatic) system dysfunction contributes to the development and pathogenesis of AD (LOUVEAU et al., 2015).

Blood-brain barrier (BBB) clearance

The BBB is a physical and selective barrier that restricts blood-derived components, cells, and pathogens into and out of the brain. BBB-mediated A β clearance is a key pathway for A β removal, and a dysfunctional BBB is directly associated with AD development. Endothelial cells of the BBB contain numerous transport systems, including the endocytic receptor low-density lipoprotein-related protein 1 (LRP1) and membrane transporter ATP-binding cassette (ABC) transporter, which mediate the clearance of A β .

LRP1 is a low-density lipoprotein receptor (LDLR) family member, a multifunctional scavenger and signaling receptor involved in various pathophysiological processes, such as A β clearance. It is highly expressed in all cells that make up the neurovascular unit and is involved in the endocytosis of more than 40 different ligands, including apolipoprotein (APOE), APP, and A β (KANEKIYO, BU, 2014). LRP1 is physiologically present in a cell surface-bound form and a truncated soluble form (sLRP1). The cell surface level of LRP1 is controlled by the proteolytic cleavage of its extracellular domain, such as β -secretase 1 (BACE-1), and then

released as sLRP1 in the interstitial fluid (ISF) and bloodstream. LRP1, in concert with ABCB1, mediates the excretion of free A β and A β bound to ApoE2, ApoE3, or α 2M through the BBB into the bloodstream. It has been identified that LRP1 and its ligands increased in senile plaques, and its expression decreases in aging and AD patients, both in brain tissue and capillaries (VAN GOOL et al., 2019). Brain endothelial-specific *lrp1* deletion in the 5xFAD AD mouse model lowered plasma A β levels while increasing soluble A β in the brain, resulting in worsened spatial learning and memory impairments, highlighting the significance of LRP1 in systemic A β removal through the BBB (STORCK et al., 2016).

ABCB1 (also known as p-glycoprotein, MDR1), a member of the ATP-binding cassette (ABC) transporters, is an essential cell membrane protein that pumps many foreign substances out of cells. ABCB1 is extensively distributed in the brain and highly expressed in the capillary endothelial cells composing the blood-brain barrier as well as in astrocytes, neurons, and microglia. A β is thought to be a substrate for ABCB1, and growing evidence supports that ABCB1 is a transporter protein for BBB efflux exporting A β directly from the brain to the circulation (WANG et al., 2021). In recent years, the positron emission tomography (PET) tracer [11C]-verapamil has been used to characterize the function of ABCB1, demonstrating that ABCB1 expression and function diminish with age and in individuals with AD (VAN ASSEMA et al., 2012). Research in an *in vivo* AD mouse model has shown that ABCB1 deficiency in the BBB increases brain A β levels and enhances A β deposition (CIRRITO et al., 2005). An *in vitro* study with human blood-brain barrier model further demonstrated the important role of ABCB1 in A β clearance, that ketone bodies (KBs) significantly increased the protein levels of LRP1 and P-gp, the combined use of KBs promoted A β efflux across the BBB (VERSELE et al., 2020).

Glymphatic system clearance

The glymphatic system is a highly organized cerebrospinal fluid (CSF) transport system that shares several critical functions with the lymphatics of surrounding tissues, including the export of excess interstitial fluid and proteins. The waste clearance process of the glymphatic system includes three steps: subarachnoid CSF solute flows into perivascular space driven by a bulk-flow manner; then from the perivascular space, CSF and ISF interchanged continuously

mediating by aquaporin 4 (AQP4) which enables CSF-ISF mixing; CSF-ISF fluid mixed with interstitial waste solutes is then drained along the perineural sheaths of cranial and spinal nerves, meningeal lymphatic vessels and arachnoid granulations and ultimately into the lymphatic vessels or circulation (BENVENISTE et al., 2019; RASMUSSEN et al., 2018).

Numerous preclinical investigations suggested that the glymphatic pathway, especially the AQP4-dependent CSF clearance, may play a key role in facilitating the clearance of A β (XIA et al., 2017; XU et al., 2015). Iliff et al. have demonstrated that interstitial solute clearance was reduced by approximately 70% in AQP4-deficient mice, and ^{125}I -amyloid β_{1-40} clearance was reduced by about 55% (ILIFF et al., 2012). Furthermore, deletion of AQP4 in APP/PS1 mice exacerbates brain A β accumulation without affecting the expression of proteins associated with A β formation and degradation, indicating an essential role of AQP4 in the A β clearance (XU et al., 2015). It has also been shown that glymphatic clearance is most active during sleep, paralleling with ^{125}I -amyloid β_{1-40} clearance, which was significantly increased during sleep, but that clearance is impaired with aging (XIE et al., 2013b). Genetic studies further support a role for AQP4 in A β clearance that several AQP4 genetic variants simultaneously influence sleep quality and brain A β load in humans (RAINEY-SMITH et al., 2018).

Similarly, a longitudinal cohort study of AD patients showed that AQP4 variants were also associated with the rate of cognitive decline and that loss of perivascular AQP4 localization was significantly related to increased amyloid β load (ZEPPENFELD et al., 2017). In addition, it has been shown that the dysfunction of the glymphatic system causes a decrease in A β clearance, but, on the contrary, the accumulation of A β itself also distorts the glymphatic flow. Pretreatment with A β_{40} in the CSF of normal mice reduced glymphatic transport into the brain (PENG et al., 2016). Dynamic PET studies in AD patients revealed A β could lead to reduced CSF clearance in humans, that CSF tau tracer 18F-THK5117 uptake reduced 23% and a 33% reduction in CSF clearance of the tracer 11C-Pittsburgh compound B (11C-PiB) (DE LEON et al., 2017).

3.3.1.2.2 Extracellular enzyme-mediated degradation of A β

The degradation of extracellular A β by a range of proteases (neprilysin, insulin-degrading enzyme, matrix metalloproteinases 2, 3, and 9, endothelin-converting enzyme, angiotensin-converting enzyme, etc.) secreted by neurons and astrocytes is one of the prime pathways of A β clearance. Among these A β -degrading proteases, NEP and IDE are the most investigated enzymes, and they are the only two that act both extracellular and intracellular.

Neprilysin, a type II membrane protein on the cell surface, is a prototypic A β -degrading metalloendopeptidase that is the most efficient in degrading A β (MINERS et al., 2011; SHIROTANI et al., 2001). Genetic ablation of the NEP gene has shown the importance of NEP in impeding A β accumulation in hAPP mice, and neprilysin deficiency leads to a decrease in exogenous A β degradation and an increase in intracellular A β levels in a gene-dose-dependent manner (IWATA et al., 2001). In addition, NEP expression is reduced in AD, especially in high A β load regions such as the hippocampus and temporal gyrus (YASOJIMA et al., 2001).

IDE is a ubiquitous zinc metalloprotease that can degrade soluble A β 40 and A β 42 to innocuous fragments. IDE is found mainly in the cytoplasm and various cellular compartments, extracellular vesicles, and intracellular membranes. The multiple subcellular sites of IDEs are the foundation for efficient degradation of intracellular and extracellular A β . Overexpression of IDE or NEP in neurons significantly reduces brain A β levels retards amyloid plaque accumulation in APP transgenic mice (LEISSRING et al., 2003). Partial loss-of-function mutation of the IDE gene in vivo impairs neuronal regulation of A β and increases A β levels (FARRIS et al., 2004). As well, it was discovered that IDE expression was increased around plaques, and the upregulation of IDE may be a feedback mechanism to lower toxic peptide levels, with higher A β in the brain promoting IDE expression (KUROCHKIN et al., 2018).

3.3.1.2.3 Intracellular degradation of A β

The intracellular degradation of abnormal or misfolded proteins, such as A β and tau, is dependent on the cellular quality control systems, namely ubiquitin-proteasome system (UPS), autophagy, and endosomal/lysosomal degradation (FRIEDMAN et al., 2015; ZHANG et al., 2017). Dysregulation of these systems will result in excessive protein misfolding and its

accumulation in neurons, accelerating the progression of AD.

The ubiquitin-proteasome system (UPS) is a highly selective ATP-dependent degradation pathway by labeling cytoplasmic abnormal and neurotoxic proteins with polyubiquitin chains. Briefly, the target proteins are polyubiquitinated by a series of the enzymatic cascade (including E1 ligase for activation, E2 for conjugation, and E3 for recognition) and ultimately degraded by the 26S proteasome complex. Recently, the GWAS studies have identified protein ubiquitination as one of the central modulators of AD and that dysfunction of the UPS may be a causative factor in AD (GENTIER, VAN LEEUWEN, 2015). Extensive studies have shown that UPS can downregulate APP and A β production, but both ubiquitin-binding and proteasome activity decrease with aging and in the AD brain (GENTIER, VAN LEEUWEN, 2015; ZUROFF et al., 2017). In the AD brain, proteasome activity was most significantly reduced in the parahippocampal gyrus, superior and middle temporal gyri, and inferior parietal lobe (ZHANG et al., 2017). Nonetheless, several studies have also shown that A β accumulation impedes the function of the UPS pathway and that A β binds directly to the 20S catalytic subunit attenuates the proteasome activity (TSENG et al., 2008).

Autophagy is essential for the removal of larger protein aggregates and damaged organelles in the cytoplasm, including macro-, micro-, and chaperone-mediated autophagy (CMA). Autophagy is essential for removing larger protein aggregates and damaged organelles in the cytoplasm, including macro-, micro-, and chaperone-mediated autophagy (CMA). Autophagy is severely impaired both in AD patients and ADtg models, as evidenced by the massive accumulation of unprocessed, A β -rich autophagic vacuoles (double-membrane vesicles containing cytoplasmic contents and subsequently fused with lysosomes for degradation) in dystrophic neurites (BOLAND et al., 2008; NIXON, 2007). Down-regulation of crucial autophagy proteins (beclin-1 and autophagy proteins 5 and 7) may impair autophagy, causing A β accumulation and neuronal cell death. Under pathological circumstances such as nutrient deprivation, studies have shown that inhibiting the mammalian target of the rapamycin (mTOR) pathway promotes autophagy (JUNG et al., 2010). However, excessive activation of mTOR signaling in the toxic microenvironment of the CNS in AD patients inhibits autophagic activity and leads to A β accumulation (LI et al., 2005).

The endosomal-lysosomal Network (ELN) is a dynamic communication vesicle system capable of transporting and degrading internalized extracellular substances, including A β and tau. In addition, lysosomes can also degrade substrates transported by the UPS and autophagic pathways. Lysosomal degradation is an important pathway for A β clearance. However, endosomal abnormalities and progressive loss of lysosomal function are widespread in AD, which may explain the enormous amount of A β aggregation in lysosomal vesicles observed in AD patients and models (NIXON, 2017; TAKAHASHI et al., 2002). Furthermore, AD-related causative and risk factor genes (APP, PSEN1/2, APOE4), as well as aging, directly disrupt ELN function, and ELN failure affects APP metabolism, which promotes β -amyloid formation (NIXON, 2017; WONG, 2020).

3.3.2 Microglia

Microglia belong to myeloid-derived cells that are considered to be the resident macrophages in the brain. They are the first line of immune defense in the CNS and are essential for maintaining brain homeostasis. Microglia, like other tissue-resident macrophages, are highly phenotypically plastic and dynamically monitor nearing microenvironment, their dysregulation underpinning the onset and progression of multiple CNS diseases.

3.3.2.1 The origin of microglia

Microglia are derived from the yolk sac progenitor cells at the early embryonic phase. They are capable of self-renewal independently of hematopoietic stem cells, depending on the interleukin-34 (IL-34) (WANG et al., 2012), CSF1 signaling (PRINZ, PRILLER, 2014), and interferon regulatory factor (IRF)-8 (KIERDORF et al., 2013) for their survival and development. Microglia, as well as perivascular and meningeal macrophages in the CNS, are thought to be the rare remnants of early primitive hematopoiesis that persist throughout life (GOMEZ PERDIGUERO et al., 2015). With the development of the brain, microglia evolve through three distinct temporal stages: early, pre-mature and mature. Recent comprehensive transcriptome analysis revealed microglial gene expression differed significantly from early prenatal through maturity. Early microglia are enriched in cell cycle and differentiation (*Dab2*, *Mcm5*, and *Lyz2*), genes associated with neuronal development (*Crybb1*, *Csf1*, and *Cxcr2*)

peak in pre-microglia. In contrast, genes involved in classical microglia functions (*Mafb*, *Cd14*, and *Mef2a*) are mainly expressed only in adult microglia (DUBBELAAR et al., 2018).

3.3.2.2 Microglia physiology

Microglia reside in a highly ramified resting state in healthy brains. They rapidly shift to an activated form of macrophage-like amoeboid structures when detecting any stimulus that disrupts milieu homeostasis (HICKMAN et al., 2018). In light of comprehensive gene expression profiling and functional studies, microglia have three essential functions: sentinel, housekeeping, and defense. They constitute a network that spans the entire CNS, acting as sentinels by dynamically scanning the area around their cell bodies (HICKMAN et al., 2018). These microglial essential functions are portals for housekeeping and defense. Physiological housekeeping functions include synaptic pruning, modulation of synaptic development and plasticity, neuronal structural organization, and migration to sites of neuronal death to phagocytose dead or dying cells or debris (HICKMAN et al., 2018). In addition, microglia interaction with other brain parenchyma cells is critical for homeostasis, inflammation, and neurological disorders (LIDDELOW et al., 2017). For example, microglia regulate astrocyte activation and proliferation, and mediate the complexity of the cerebral vascular network by promoting endothelial fusion (angiogenesis) (REEMST et al., 2016). Microglia also mediate host defense against infection, pathogens, and injurious self-proteins such as A β and tau. In response to pathogenic stimuli, microglia in the developing brain release neurotrophic substances to support endangered neurons and prevent neuronal damage. In contrast, microglia in the senescent brain function abnormally. They are over-activated and release excessive oxidative stress and inflammatory factors, damaging vulnerable neurons and leading to neurodegenerative disease (TAY et al., 2017).

3.3.2.3 Microglia in the AD brain: blessing or curse?

A histological feature of AD patients and animal models is the activation and recruitment of microglial cells to amyloid plaques in cerebral parenchyma, this phenomenon called Microgliosis. GWASs have shown that most AD risk genes are expressed chiefly or exclusively in microglia, such as triggering receptors expressed on myeloid cells 2 (TREM2), myeloid cell

surface antigen CD33, and CR1 (KARCH, GOATE, 2015). TREM2 mutations increase the AD risk by 3.0- to 4.5-fold, almost as high as the risk associated with Apoe ϵ 4 (GUERREIRO et al., 2013).

Microglia are recruited around A β in the early stages of AD, facilitating amyloid β clearance either by scavenger receptor (SR)-mediated microglial phagocytosis and endocytosis or by enzyme-mediated extracellular degradation. As the disease progresses, microglial genes involved in A β clearance are downregulated by pro-inflammatory cytokines, which contribute to A β accumulation (HICKMAN et al., 2008). Many studies have shown that microglia migrate to A β plaques forming a physical barrier that prevents plaque expansion and protects neurons from exposure to toxins, but TREM2 mutations eliminate these benefits (CONDELLO et al., 2018). Microglial phagocytosis modified the properties of amyloid- β , which acts as a trash compactor to uptake amyloid and agglomerate it in lysosomes, where it is then redeposited A β peptides in an inert form (HUANG et al., 2021). Single-cell RNA sequencing (RNA-seq) analysis of AD mouse brain homogenates has identified a distinct group of microglia whose gene expression profile transitions from a basal homeostatic state via an intermediate form to a disease-associated state (KEREN-SHAUL et al., 2017). This new subset of CNS resident macrophages is known as the disease-associated microglia (DAM). Analysis of microglia from TREM2-deficient 5XFAD and APP/PS1 mice revealed that the last step of DAM differentiation, intermediate-to-DAM state, appears to depend on the TREM2 (KEREN-SHAUL et al., 2017). With the upregulation of genes involved in phagocytosis and lysosomes in DAM, including TREM2, TYROBP, and the AXL tyrosine kinase receptor (AXL), it is speculated that DAM may be a protective state that promotes microglial A β phagocytosis (DECZKOWSKA et al., 2018; KEREN-SHAUL et al., 2017).

There may be no good or lousy microglia, but the function of microglia can become abnormal. In Alzheimer's patients, microglia are chronically activated, releasing inflammatory cytokines, neurotoxic reactive oxygen species, and nitrides (ROS and RNS), which activate the NLRP3 inflammasome and cause synaptic loss. A β -induced pro-inflammatory cytokines inhibit the clearance of A β by microglia and promote tau protein hyperphosphorylation, leading to a self-perpetuating cycle that ultimately contributes to disease progression (HICKMAN et

al., 2018). Similarly, when NLRP3 is activated, a microglial apoptosis-associated speck-like protein containing a CARD (ASC) is released, which interacts with A β , triggering amyloid- β aggregation and dissemination (NAKANISHI et al., 2018). Moreover, microglia may directly drive neuronal damage or apoptosis by releasing iNOS, glutamate, or microglial proteases. A study has shown that microglia deficiency suppressed tau propagation, implying that microglia are involved in spreading tau aggregates via phagocytosis and exocytosis (ASAI et al., 2015). Microglia also kill and damage neurons indirectly by releasing TNF- or reducing the production of nutritional brain-derived neurotrophic factor (BDNF) and insulin-like growth factor (IGF) (HICKMAN et al., 2018). In addition, they also cause neuronal death by inducing specific astrocyte phenotypes that have reduced nutritional support, impaired clearance capacity, and release toxins (LIDDELOW et al., 2017).

Despite the overwhelming evidence that unbridled microglial activation in AD pathology may be detrimental to pathologic progression, human genetic data suggest that appropriate microglia activation can delay AD progression. Microglia dysfunction is a major culprit in the pathogenesis of AD rather than a concomitant manifestation.

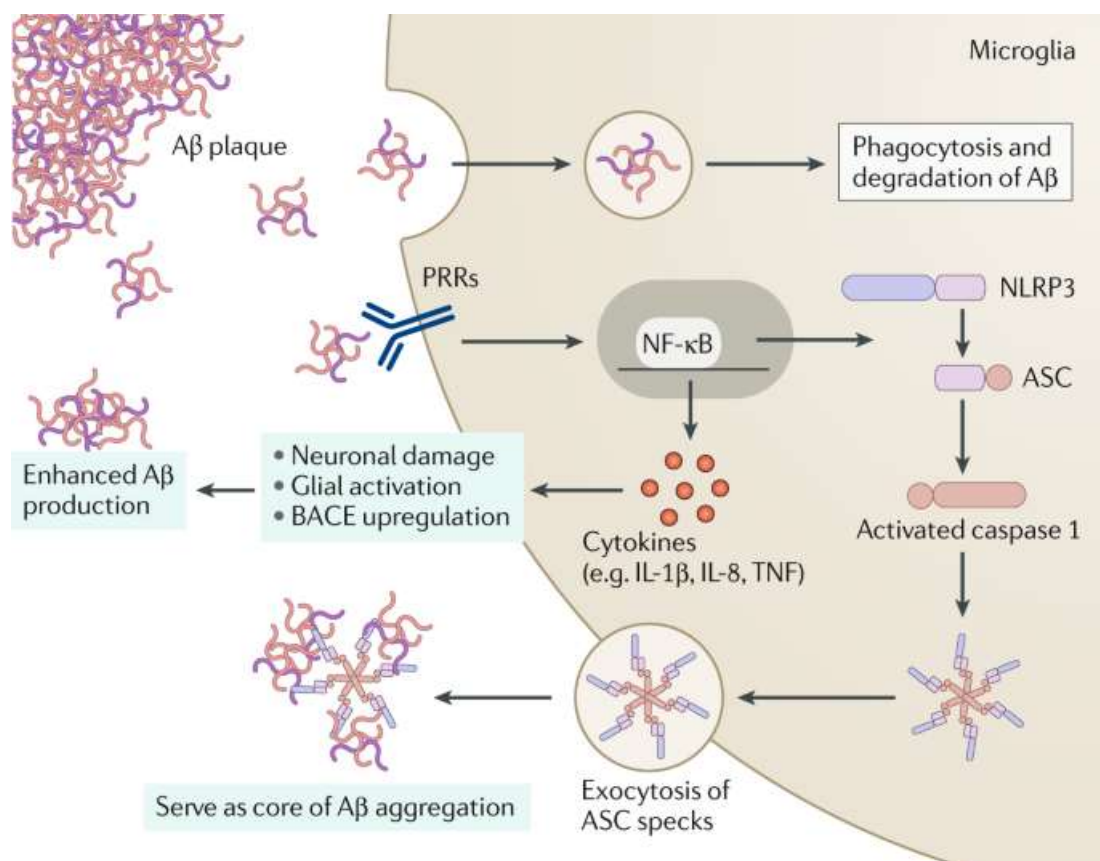


Fig. 3.3.2, Microglia response to amyloid- β . A β species can be recognized by a range of pattern recognition receptors (PRRs) on microglia, which further activate phagocytic or inflammatory pathways (LENG, EDISON, 2021).

3.3.2.4 A β clearance by microglia

Growing evidence demonstrated that activated microglia are closely associated with senile plaques in AD patients and animal models. Microglial A β phagocytosis is a critical mechanism for A β clearance but is impaired with the progression of AD (LUCIN et al., 2013).

Microglia express a variety of phagocytosis-associated receptors, such as CD14-TLRs, scavenger receptor CD36, TREM2, and macrophage scavenger receptor 1 (SCARA1), that mediate the uptake of different A β species (MALM et al., 2015). It has been shown that TLR4 and TLR2 and its co-receptor CD14 bind to protofibrillar A β , facilitating A β internalization and translocation to lysosomal degradation (LIU et al., 2005; MALM et al., 2015; REED-GEAGHAN et al., 2009). And Scara1 deficiency markedly impaired soluble amyloid- β clearance by mononuclear phagocytes, speeding up A β accumulation in APPS1 mice (FRENKEL et al., 2013). Moreover, microglia induce CD36 expression in the early stages of AD, which can mediate microglial A β phagocytosis (RICCIARELLI et al., 2004). Also, TREM2 is indispensable for microglia phagocytosis. Amounts of evidence demonstrated A β binds to lipoproteins forming complexes which are efficiently taken up by microglia in a TREM2-dependent manner (YEH et al., 2016). In addition to receptor-mediated A β phagocytosis, soluble and oligomeric A β also can be taken up through micropinocytosis in microglia. Perturbation of actin polymerization and inhibition of macropinocytosis in microglia reduced A β 40 and A β 42 uptake, highlighting the role of macropinocytosis in the accumulation of A β in AD (MANDREKAR et al., 2009; WESEN et al., 2017).

3.3.2.5 Regulation of microglial activation

It was once thought that the BBB shielded microglia from the circulatory system. However, microglia activity is now recognized to be influenced by cytokines, neurotransmitters, and other molecules that regulate signaling pathways, originating both inside and outside the CNS. The local microenvironment is crucial in regulating microglia activation. Neurons and

astrocytes release various soluble factors, such as neurotransmitters, anti-inflammatory cytokines, and neurotrophic factors, which bind to cognate receptors on microglia and exert immunomodulatory effects (BERNAUS et al., 2020). For example, transforming growth factor β (TGF β), a multifunctional cytokine that is expressed both on neurons and glial cells, is a potent regulator in down-regulating microglial responses, as demonstrated by the fact that loss of TGF β 1 leads to increased neuronal death and microgliosis in mouse brain (BRIONNE et al., 2003). Apart from soluble factors, intercellular interactions also regulate microglia activity such as CX3CL1-CX3CR1 and CD200-CD200R receptor-ligand binding inhibits microglia-neuron interactions exerting immunomodulatory effects to suppress unwanted inflammatory responses (CHAMERA et al., 2020).

Although indeed, the local environment of the CNS has the most significant impact on microglia phenotype and function, a range of peripheral stimuli also has primed microglia via neural, humoral, or metabolic pathways. Peripheral circulating inflammatory mediators and metabolites transmit signals to the CNS via receptors in vagal afferent nerve fibers, BBB-endothelial cells, and periventricular macrophages (TEELING et al., 2010). A study indicated that IFN from the periphery transduced signals across the BBB, resulting in microglia exhibiting apparent genetic and phenotypic alterations that lead to abnormal synaptic pruning (AW et al., 2020). Furthermore, studies in most recent years have demonstrated that microglia activity is also affected by the gut microbiota as well as microbiota-induced peripheral metabolites.

3.4 Gut microbiota in Alzheimer's disease

The microbiome is a complex and dynamic community of bacteria in the human body. The majority reside in the gastrointestinal system and are thought to impact physiology and disease pathology. A growing body of research has illuminated that the microbiota bidirectional communication with the CNS through the gut-brain axis, the disturbance in the gut bacterial composition might affect the neurological functions and vice versa (CARABOTTI et al., 2015). Recently, gut microbiota, as a significant environmental factor for AD, has been observed to regulate amyloid pathology. Numerous studies have shown that gut microbial composition is

altered and diversity reduced significantly in AD patient feces compared to age- and sex-matched controls (VOGT et al., 2017; ZHUANG et al., 2018). The abundance of butyrate-producing bacteria (*Butyrivibrio*, *Eubacterium*, etc.) and anti-inflammatory bacteria (*E. rectale* and *B. fragilis*) decreased in AD patients. In contrast, the abundance of taxa that are associated with neurological disorders (*Odoribacter splanchnic*) and pro-inflammatory state (*Escherichia/Shigella*) was increased (CATTANEO et al., 2017; CRYAN et al., 2020). Moreover, the abundance of specific pro-inflammatory gut bacteria taxon correlated with the blood pro-inflammatory cytokine levels in clinically diagnosed AD patients.

Meanwhile, a significant shift in gut microbiota diversity was observed in APP transgenic mouse models compared to wild-type mice: the abundance of *Firmicutes* increased while the abundance of *Bacteroides* decreased, and there is a negative correlation between the abundance of these two phyla, which is consistent with AD patients (CATTANEO et al., 2017; VOGT et al., 2017). Harach et al. (HARACH et al., 2017) found a significantly lower cerebral A β amyloid pathology in germ-free APP transgenic mice than control mice with the gut microbiome. However, cerebral A β pathology was elevated considerably after fecal transplantation from conventionally reared APP transgenic mice to germ-free APP transgenic mice. In contrast, colonization with microbiota from wild-type mice was less productive in increasing cerebral A β levels. Normally, intestinal pro-inflammatory and anti-inflammatory bacteria are in equilibrium under physiological circumstances. Nevertheless, the bacteria composition of Alzheimer's patients is changed, and substantial amounts of microbial metabolites (e.g. SCFA, pro-inflammatory cytokines) and neurotransmitters enter the bloodstream, increasing systemic inflammation, tau, and A β aggregation in the CNS (BLACHER et al., 2017). In summary, these studies revealed that gut microbiomes have powerful connections with the pathogenesis of AD and diminished microbiota diversity, which may trigger inflammation, cerebrovascular degeneration, A β aggregation, and tau pathology.

3.5 Microbiome-microglia connections in AD

Gut microbiota affects the cellular proportions, migration, and functions of various immune cells in the brain. Most gut microbiome-associated CNS diseases, including AD, are

closely intertwined with microglial dysfunction (TSE, 2017; WANG et al., 2018), suggesting that microglia might be a critical mediator between gut microbiota and CNS disorders. It was found that the gut microbiota is crucial for microglial maturation, identity, and functional regulation (ABDEL-HAQ et al., 2019). Microglia from germ-free (GF) mice exhibit a defective phenotype with upregulation of surface proteins such as colony-stimulating factor 1 receptor (CSF1-R), F4/80, and CD31 compared to microglia from specific pathogen-free (SPF) mice (ERNY et al., 2015; MOSSAD, ERNY, 2020). Genes linked to microglia activation (*Mapk8*), premature immune function (*B2m*), and pathogen recognition and regulation of transcriptional pathways in host defense (*Trim30*) were down-regulated in GF animals (ERNY et al., 2015). However, transcriptional repressors and genes involved in microglia proliferation and apoptosis inhibition were substantially elevated in microglia of GF mice (ERNY et al., 2015). The gene DNA-damage-inducible transcript 4 (*Ddit4*), which promotes cell growth, proliferation, and survival, was most amplified in microglia from GF mice. Moreover, microglia from germ-free mice exhibit inhibited inflammatory responses to viral infection and lipopolysaccharide (LPS) stimulation. Antibiotic treatments-induced perturbations of microbial diversity in the gut are ready to attenuate A β deposition and related microgliosis and astrocytosis (MINTER et al., 2017).

It is not well understood how gut microbiota regulates microglial functions. Gut microbes jointly mediated communication with the CNS through neural, immune, enteric, and metabolic signaling, including physical and chemical connections. It was reported that gut bacteria release peptidoglycan to blood and then systemically primed the innate immune system (BERSCH et al., 2021). As an essential structural component of the bacterial cell wall, peptidoglycan can be recognized by multiple pattern recognition receptors, including nucleotide-binding domain-containing protein 1/2 (NOD1/2), NLRP3, and peptidoglycan recognition protein 1 (PGLYRP1) (WOLF, UNDERHILL, 2018). And this recognition can trigger inflammatory responses in immune and non-immune cells of various systems (WOLF, UNDERHILL, 2018). The deficiency of gut microbiota dramatically reduced microglial immune activity. Furthermore, mice with a changed microbiota have a defective microglia phenotype, such as altered Schaedler flora (ASF) mice (WYMORE BRAND et al., 2015), which contain a defined set of

reduced bacterial strains. Maintaining microglia in their normal phenotype and function requires a constant input of a complex microbiota.

Interestingly, as effectively as fecal recolonization, SCFAs supplementation in drinking water reversed microglia immaturity in germ-free mice (ERNY et al., 2015). SCFAs are the bacterial fermentation of insoluble fiber products from dietary plant matter, including acetate, propionate, and butyrate. Further evidence suggested that microglia-specific activation induced by SCFAs supplementation is associated with upregulation of the APOE-TREM2 signaling in the brain (COLOMBO et al., 2021; MOSSAD, ERNY, 2020). These data collectively suggest that the bacterial metabolic products are potentially related to microglial activation.

Metabolite-sensitive G protein-coupled receptors (GPCRs) rapidly recognize specific metabolites are the foundation of the mechanism of sensing endogenous metabolic intermediates. GPR41, GPR43, and GPR109a are three important GPCRs for SCFAs recognition (THORBURN et al., 2014). Our preliminary experiments observed GPR109a but not GPR41 and GPR43 at high expression levels in microglia. GPR109a is expressed mainly in white adipocytes, epithelial cells, and immune cells, including microglia, neutrophils, dendrites, and macrophages, but not in lymphocytes (OFFERMANN, SCHWANINGER, 2015). Recently, GPR109a, whose ligands include butyrate, ketone body β -hydroxybutyrate, nicotinic acid, and monomethyl fumarate, has been identified as a significant player in intestinal homeostasis regulation. It should be emphasized that the complete activation of GPR109a needs a high concentration of agonists. The ketone body β -hydroxybutyrate activates GPR109a with an EC_{50} of approximately 700 μ M, a concentration in the blood that reached only under fasting conditions and extended exercise. Under physiological conditions, GPR109a expressed by intestinal immune cells is most likely be activated where bacterial fermentation of dietary fiber provided high butyrate concentrations locally in the gut (OFFERMANN, 2017). It has been well-established that fasting and the ketogenic diet have anti-inflammatory effects such as suppressing microglia activation (KASHIWAYA et al., 2013). A study showed that GPR109a mRNA was expressed at low levels in unstimulated primary rat microglia and that its expression was correlated with the degree of microglial activation (FU et al., 2015).

GPR109a also has a high affinity for niacin with EC_{50} of $\sim 1 \mu\text{M}$ (TUNARU et al., 2003). It has been reported that niacin can directly act on GPR109a-expressing immune cells and increase the release of anti-inflammatory mediators in a GPR109a-dependent manner (BLAD et al., 2012). A prospective population-based study revealed an inverse association between niacin levels and the development of AD and cognitive decline, suggesting niacin deficiency enhances AD risk and age-related cognitive decline (MORRIS et al., 2004). In addition to niacin itself, its biologically active metabolites, nicotinamide adenine dinucleotide (NAD⁺), is also declined in the AD mice model (HOU et al., 2021; VAN DER VELPEN et al., 2021). Supplementation with NAD⁺ in APP/PS1 mice decreases neuroinflammation and reduces the activation of microglia and astrocytes (HOU et al., 2021).

4. AIM OF THIS WORK

In this study, we aimed to investigate the pathogenic role of GPR109a in APP-knock-in AD mice. Briefly, we answered the following three questions:

- (1) Does GPR109a knockout improve AD-associated pathologies in APP-knock-in mice?
- (2) Where is the GPR109a action site in AD mice? In the gut or on the endogenous microglia?
- (3) What are the potential mechanisms through which GPR109a modifies AD pathogenesis?

5. MATERIALS AND METHODS

5.1 Materials

5.1.1 Instruments

Instruments	Company
7500 Fast Real-Time PCR System	Applied Biosystems (Darmstadt, Germany)
Accu jet Pipettes Control	BrandTech Scientific (Essex, CT, USA)
Autoclave 3870 ELV	Systec (Wettenberg, Germany)
Autoclave V-150	Systec (Wettenberg, Germany)
Axiovert 25 inverted Microscope	Carl Zeiss Microscopy (Jena, Germany)
Axiovert 40 CFL Microscope	Carl Zeiss Microscopy (Jena, Germany)
Barnes Maze	Noldus Information Technology (Oberreifenberg, Germany)
Biofuge 13 Centrifuge	Heraeus (Hanau, Germany)
Biowizard KR-200 Bench	Kojair Tech Oy (Vilppula, Finland)
Coolbox KB 1001	Liebherr (Lindau, Germany)
Drying cabinet	Heraeus (Hanau, Germany)
Eclipse TS100 Invetiertes Microscop	Nikon Instruments (Melville, NY, USA)
Eclipse E600 Fluorescence Microscopy	Nikon Instruments (Melville, NY, USA)
FACSCanto II Flow Cytometer	BD Biosciences (Heidelberg, Germany)
Freezer Premium no frost	Liebherr (Lindau, Germany)
Freezer UF75-110 T	Colora (Frankfurt, Germany)
General Rotator STR4	Stuart Scientific (Staffordshire, UK)
HERAcell CO ₂ Incubators	Heraeus (Hanau, Germany)
HERAcell 150i CO ₂ Incubators	Thermo Scientific (Langenselbold, Germany)
HERAsafe HS 12 biological safety cabinet	Heraeus (Hanau, Germany)
Ice Machine	Eurfrigor Ice Makers Srl (Lainate, Italy)
Incubations hood TH-30	Edmund Bühler GmbH (Hechingen, Germany)
InoLab pH 720 pH-meter	WTW (Weilheim, Germany)
Jouan B4i Centrifuge	Thermo Scientific (Langenselbold, Germany)
Laboshaker	Gerhardt Analytical Systems (Königswinter, Germany)
Liquid Nitrogen Container	KGW-Isotherm (Karlsruhe, Germany)
Microwelle HF 26521	Siemens (München, Germany)
Mini-PROTEAN 3 Electrophoresis system	Bio-Rad Laboratories (München, Germany)
Mini Trans-Blot Cell	Bio-Rad Laboratories (München, Germany)
Multipette Plus	Eppendorf (Hamburg, Germany)
Nalgene Mr. Frosty Freezing Container	A. Hartenstein (Würzburg, Germany)
Nanodrop ND-1000 Spectrophotometer	PEQLAB Biotechnologie (Erlangen, Germany)
Optima Max Ultracentrifuge	Beckman Coulter (Krefeld, Germany)
Perfection V700 Photoscanner	Epson (Meerbusch, Germany)
Pipette PIPETMAN	Gilson (Middleton, WI, USA)
Pipette Single-Channel	Eppendorf (Hamburg, Germany)
Pipette Pipetus	Hirschmann (Eberstadt, Germany)

MATERIALS AND METHODS

PowerPac 200 Power Supply	Bio-Rad Laboratories (München, Germany)
Precision Balance scale 770	Kern & Sohn (Balingen, Germany)
Precision Balance scale CP 42023	Sartorius (Göttingen, Germany)
PS250 Power Supply	Hybaid (Heidelberg, Germany)
PTC 200 DNA Engine Thermal Cycler	MJ Research (St. Bruno, Canada)
PURELAB Ultra Water Purification system	Elga (Celle, Germany)
QuadroMACS™ Separator	Miltenyi Biotec (Bergisch Gladbach, Germany)
Refrigerated Laboratory Centrifuge	Eppendorf (Hamburg, Germany)
Refrigerator KG39VVI30	Siemens (München, Germany)
Refrigerator Premium	Liebherr (Lindau, Germany)
Refrigerator V.I.P. Series -86 °C Freezer	Sanyo (Wood Dale, IL, USA)
Rocky 3D	Labortechnik Frübel (Lindau, Germany)
Savant SpeedVac DNA 110	Thermo Scientific (Langenselbold, Germany)
Shakers SM-30	Edmund Bühler (Hechingen, Germany)
SmartSpec 3000 Spectralphotometer	Bio-Rad Laboratories (München, Germany)
Sunrise Microtiter plate reader	Tecan (Männedorf, Schweiz)
Tabletop Centrifuge 4K10	Sigma Laborzentrifugen (Osterode am Harz, Germany)
Tabletop Centrifuge 4K15C	Sigma Laborzentrifugen (Osterode am Harz, Germany)
Thermoblock TDB-120	BioSan (Riga, Latvia)
Thermomixer comfort	Eppendorf (Hamburg, Germany)
TLA-55 Rotor Package, Fixed Angle	Beckman Coulter (Krefeld, Germany)
Transsonic Ultrasonic Cleaning Units	Elma (Singen, Germany)
Ultrospec 3100 pro Spectralphotometer	Amersham Biosciences (München, Germany)
Vortex Genie 2	Scientific Industries (Bohemia, NY, USA)
Vortex Shaker REAX 2000	Heidolph (Schwabach, Germany)
Water bath	Köttermann (Hänigsen, Germany)
XCell SureLock Mini-Cell Electrophoreses system	Invitrogen (Darmstadt, Germany)

5.1.2 General experimental materials and consumables

Products	Company
Amersham Hyperfilm ECL	GE Healthcare (Buckinghamshire, UK)
Beackers	VWR (Darmstadt, Germany)
Biosphere Filter Tips (10 µl, 200 µl, 1000 µl)	Sarstedt (Nümbrecht, Germany)
Blotting Paper Grade GB003	Whatman (Dassel, Germany)
Cell Scrapers	TPP (Trasadingen, Schweiz)
Centrifugentubes (15 ml, 50 ml)	Sarstedt (Nümbrecht, Germany)
Combitips Plus (5 ml, 10 ml)	Eppendorf (Hamburg, Germany)
CryoPure tubes 1.8 ml	Sarstedt (Nümbrecht, Germany)
Cuvettes	Sarstedt (Nümbrecht, Germany)
Erlenmeyer Flasks	Schott (Mainz, Germany)
Falcon Multiwell Cell Culture Plates	BD Biosciences (Heidelberg, Germany)
Falcon Round bottom test tubes 5 ml	BD Biosciences (Heidelberg, Germany)
Filtropur Cell Strainer	Sarstedt (Nümbrecht, Germany)

MATERIALS AND METHODS

Filtropur Syringe Filter	Sarstedt (Nümbrecht, Germany)
Glass Bottles	Fisher Scientific (Schwerte, Germany)
Gloves, Latex	VWR (Darmstadt, Germany)
Gloves, Nitril	VWR (Darmstadt, Germany)
Hemocytometer	Brand (Wertheim, Germany)
LS Columns	Miltenyi Biotec (Bergisch Gladbach, Germany)
MicroAmp Optical 96-Well Reaction Plate	Applied Biosystems (Darmstadt, Germany)
MicroAmp Optical Adhesive Film	Applied Biosystems (Darmstadt, Germany)
Microlance™ needles	BD Biosciences (Heidelberg, Germany)
Microlon 600 96-Well Microplate	Greiner Bio-One (Frickenhausen, Germany)
Microscopic cover glasses 12x12 mm	R. Langenbrinck (Emmendingen, Germany)
Microtestplate 96-Well	Sarstedt (Nümbrecht, Germany)
Mini-PROTEAN 3 Short Plates	Bio-Rad Laboratories (München, Germany)
Mini-PROTEAN 3 Spacer Plates 1,5 mm	Bio-Rad Laboratories (München, Germany)
Mini-PROTEAN Comb (15 Wells, 1,5 mm)	Bio-Rad Laboratories (München, Germany)
Myelin Removal Beads II	Miltenyi Biotec (Bergisch Gladbach, Germany)
Nunc MaxiSorp 96-Well Plate, black	Thermo Scientific (Langenselbold, Germany)
Overhead Transparencies	R. Langenbrinck (Emmendingen, Germany)
Pasteur Pipettes	VWR (Darmstadt, Germany)
PCR Soft Tube 0.2 ml	Biozym Scientific (Oldendorf, Germany)
Pipette Tips (10 µl, 200 µl, 1000 µl)	Sarstedt (Nümbrecht, Germany)
Polyallomer Tube, 1.5 ml, Snap-On Cap	Beckman Coulter (Krefeld, Germany)
Precision Wipes Kimtech Science	Kimberly-Clark (Koblenz, Germany)
Pro-Gel 10-20% Tris-Tricin-Gel	Anamed Elektrophorese (Groß-Bieberau/Rodau, Germany)
Protran Nitrocellulose Transfermembranes	Whatman (Dassel, Germany)
PVDF Western Blotting Membranes	Roche (Mannheim, Germany)
Safe-Lock Tubes (0.5 ml, 1 ml, 2 ml)	Eppendorf (Hamburg, Germany)
Scalpel Blades	B. Braun (Melsungen, Germany)
Serological Pipettes (5 ml, 10 ml, 25 ml)	Sarstedt (Nümbrecht, Germany)
Slide Box	neoLab (Heidelberg, Germany)
Standing Cylinders	VWR (Darmstadt, Germany)
Syringes	B. Braun (Melsungen, Germany)
Tissue Culture Dish	Sarstedt (Nümbrecht, Germany)
Tissue Culture Flask	Sarstedt (Nümbrecht, Germany)
UV Quartz cuvette 10 mm	Hellma (Müllheim, Germany)

5.1.3 Chemicals, reagents, Kits, Antibodies

1. General chemicals and reagents

Chemicals and Reagents	Company
0.05% Trypsin/EDTA (1x)	Invitrogen (Darmstadt, Germany)

MATERIALS AND METHODS

(3-Aminopropyl) triethoxysilane	Sigma Aldrich (Taufkirchen, Germany)
β -Mercaptoethanol	Sigma Aldrich (Taufkirchen, Germany)
β -Secretase Substrate IV, Fluorogenic	Merck (Darmstadt, Germany)
γ -Secretase Substrate, Fluorogenic	Merck (Darmstadt, Germany)
Agarose	Biozym (Oldendorf, Germany)
Ammoniumpersulfat (APS)	Sigma Aldrich (Taufkirchen, Germany)
Antibiotic-Antimycotic 100x	Invitrogen (Darmstadt, Germany)
Bovine Serum Albumin (BSA)	Sigma Aldrich (Taufkirchen, Germany)
Borat	VWR (Darmstadt, Germany)
Bromphenol blue	Sigma Aldrich (Taufkirchen, Germany)
Casein	Fluka (Buchs, Switzerland)
Chloroform	Applichem (Darmstadt, Germany)
Citrate acid	Serva (Heidelberg, Germany)
Congo red	Sigma Aldrich (Taufkirchen, Germany)
Collagen Coating Solution	Sigma-Aldrich (Taufkirchen, Germany)
CX3CR1 antagonist 18a: AZD 8797	Axon Medchem BV (Groningen, Netherlands)
Cy3- labelled Streptavidin	Sigma-Aldrich (Taufkirchen, Germany)
Dimethylsulfoxid (DMSO)	Sigma Aldrich (Taufkirchen, Germany)
Diaminobenzidin-Hydrochlorid (DAB)	Sigma Aldrich (Taufkirchen, Germany)
DNA Ladder (100 bp, 1 kb)	New England Biolabs (Frankfurt am Main, Germany)
dNTP Mix	Roche (Mannheim, Germany)
Dithiothreitol (DTT)	Sigma Aldrich (Taufkirchen, Germany)
Digest-All 3 (Pepsin)	Thermo Fisher Scientific (Mannheim, Germany)
Dulbecco's Modified Eagle Medium (DMEM)	Invitrogen (Darmstadt, Germany)
Entellan®mounting media	VWR (Darmstadt, Germany)
Ethidiumbromid	Carl Roth (Karlsruhe, Germany)
Ethanol	Sigma Aldrich (Taufkirchen, Germany)
Ethylendiaminetetraacetat acid (EDTA)	Sigma Aldrich (Taufkirchen, Germany)
Ethylene glycol tetraacetic acid (EGTA)	Sigma Aldrich (Taufkirchen, Germany)
Fetal Bovine Serum (FBS)	Invitrogen (Darmstadt, Germany)
Glycine	Carl Roth (Karlsruhe, Germany)
Glycerol	Sigma Aldrich (Taufkirchen, Germany)
Guanidine Hydrochloride	Sigma Aldrich (Taufkirchen, Germany)
H ₂ O ₂	Otto Fishar (Saarbruecken, Germany)
H ₂ SO ₄	Fluka (Buchs, Switzerland)
HCl	Sigma Aldrich (Taufkirchen, Germany)
Ham's F-12 Medium	Invitrogen (Darmstadt, Germany)
Hank's Buffered Salt Solution (HBSS)	Sigma Aldrich (Taufkirchen, Germany)
Hexamer Random Primer	Invitrogen (Darmstadt, Germany)
HiLyte Fluor™ 488-conjugated A β 42	AnaSpec(Fremont, USA)
Isoflurane	Baxter (Unterschleißheim, Germany)

MATERIALS AND METHODS

Isopropanol	Carl Roth (Karlsruhe, Germany)
KHCO ₃	Merck (Darmstadt, Germany)
KCl	Merck (Darmstadt, Germany)
Lipopolysaccharide (LPS)	Axxora (Lörrach, Germany)
MgCl ₂	Fluka (Buchs, Switzerland)
MgSO ₄	Fluka (Buchs, Switzerland)
Methoxy-X04	Bio-Techne GmbH
Methanol	Sigma Aldrich (Taufkirchen, Germany)
MCC950	Sigma Aldrich (Taufkirchen, Germany)
Milk powder	Carl Roth (Karlsruhe, Germany)
NaCl	Merck (Darmstadt, Germany)
NaF	Merck (Darmstadt, Germany)
Na ₂ HPO ₄	Carl Roth (Karlsruhe, Germany)
NaH ₂ PO ₄ x H ₂ O	Merck (Darmstadt, Germany)
Na ₄ P ₂ O ₇	Sigma Aldrich (Taufkirchen, Germany)
Na ₃ VO ₄	Sigma Aldrich (Taufkirchen, Germany)
NH ₄ Cl	Sigma Aldrich (Taufkirchen, Germany)
Niacin	Sigma Aldrich (Taufkirchen, Germany)
Okadic acid	Sigma Aldrich (Taufkirchen, Germany)
Orange G	Merck (Darmstadt, Germany)
PageRuler Prestained Protein Ladder	Invitrogen (Darmstadt, Germany)
Paraformaldehyd (PFA)	Merck (Darmstadt, Germany)
Protease inhibitor Cocktail	Roche (Mannheim, Germany)
Penicillin-streptomycin	Sciencell Research Laboratories (Carlsbad, CA, USA)
Rotiphorese Gel 30	Carl Roth (Karlsruhe, Germany)
RPMI 1640	Invitrogen (Darmstadt, Germany)
Recombinant human IL-1 β	R&D Systems (Wiesbaden, Germany)
Sodium actate	Merck (Darmstadt, Germany)
Sodium dedecylsulfat (SDS)	Carl Roth (Karlsruhe, Germany)
Sucrose	VWR (Darmstadt, Germany)
Tetramethylethylendiamin (TEMED)	Serva (Heidelberg, Germany)
Tricine	Carl Roth (Karlsruhe, Germany)
Trizma®base	Sigma Aldrich (Taufkirchen, Germany)
Triton X-100	Sigma Aldrich (Taufkirchen, Germany)
TRizol	Sigma Aldrich (Taufkirchen, Germany)
Tween 20	Sigma Aldrich (Taufkirchen, Germany)
Western Lightning ECL Substrate	Perkin Elmer (Rodgau, Germany)
Xylene	Otto Fischar (Saarbrücken, Germany)
Xylene cyanol	Molekula (München, Germany)

2. Kits

MATERIALS AND METHODS

Products	Company
Bio-Rad Protein Assay	Bio-Rad Laboratories (München, Germany)
DyNAmo™ Flash probe qPCR Kit	Thermo Scientific (Bonn, Germany)
DyNAmo™ Flash SYBR Green qPCR Kit	Thermo Scientific (Bonn, Germany)
Human A β 40 ELISA Kit	Invitrogen (Darmstadt, Germany)
Human A β 42 ELISA Kit	Invitrogen (Darmstadt, Germany)
Mouse TNF-alpha DuoSet® ELISA	R&D Systems (Wiesbaden, Germany)
Mouse IL-10 DuoSet® ELISA	R&D Systems (Wiesbaden, Germany)
Mouse IL-1 β DuoSet® ELISA	R&D Systems (Wiesbaden, Germany)
MTT-based Cell Proliferation Kit I	Roche (Mannheim, Germany)
Neural Tissue Dissociation Kit (papain-based)	Miltenyi Biotec (B.V. & Co. KG, Bergisch Gladbach, Germany)
OptEIA™ TMB Substrate Reagent Set	BD Bioscience (Heidelberg, Germany)
RNeasy® Plus Mini Kit	Qiagen (Hilden, Germany)
RQ1 RNase-free DNase	Promega (Mannheim, Germany)
SuperScript® II Reverse Transcriptase	Invitrogen (Darmstadt, Germany)
VECTOR Blue Alkaline Phosphatase Substrate kit	Vector Laboratorie (Burlingame, USA)
VectaStain Elite ABC kit	Vector Laboratorie (Burlingame, USA)
VectaStain Elite ABC-AP kit	Vector Laboratorie (Burlingame, USA)

3. Oligonucleotides

Primers for the Real-Time-quantitative-PCR (SYBR® Green method)

Gene	Primer forward 5' - 3'	Primer reverse 5' - 3'
<i>mouse gpr41</i>	GTGACCATGGGGACAAGCTTC	CCCTGGCTGTAGGTTGCATT
<i>mouse gpr43</i>	CTGCCTGGGATCGTCTGTG	CATACCCTCGGCCTTCTGG
<i>mouse gpr81</i>	GGTGGCACGATGTCATGTT	GACCGAGCAGAACAAGATGATT
<i>mouse gpr109a</i>	TCCAAGTCTCAAAGGTGGT	TGTTTCTCTCCAGCACTGAGTT
<i>mouse gapdh</i>	ACAACCTTTGGCATTGTGGAA	GATGCACGGATGATGTTCTG
<i>mouse gata3</i>	CCTCTGGAGGAGGAACGCTAAT	GTTTCGGGTCTGGATGCCTTCT
<i>mouse t-bet</i>	CCACCTGTTGTGGTCCAAGTTC	CCACAAACATCCTGTAATGGCTTG

4. Antibody

Antibody	Company
<i>mouse monoclonal anti α-tubulin, clone: DM1A</i>	Abcam (Cambridge, UK)
<i>rabbit polyclonal anti β-actin, clone: 13E5</i>	Cell Signaling Technology (Europe)
<i>mouse monoclonal anti Amyloid β, clone: WO2</i>	Millipore (Schwalbach, Germany)
<i>mouse monoclonal anti Amyloid β, clone: 6F/3D</i>	Dako (Hamburg, Germany)
<i>rabbit monoclonal anti Amyloid β, clone: D12B2</i>	Cell Signaling Technology (Europe)
<i>rat monoclonal anti CD16/CD32, clone: 2.4G2</i>	BD Pharmingen (NJ, USA)
<i>Rat anti-mouse/human CD11b, clone: M1/70</i>	BioXCell (West Lebanon, NH)
<i>Dynabeads™ Mouse CD4 (L3T4)</i>	Invitrogen (Darmstadt, Germany)
<i>Dynabeads™ Sheep anti-Rat IgG</i>	Invitrogen (Darmstadt, Germany)

MATERIALS AND METHODS

<i>Alexa Fluor® 647 anti-mouse/human CD11b Antibody, clone: MI/70</i>	BioLegend (Germany)
<i>FITC anti-mouse/human CD11b Antibody, clone: MI/70</i>	BioLegend (Germany)
<i>Alexa Fluor® 488 anti-mouse CX3CR1 Antibody, clone: SA011F11</i>	BioLegend (Germany)
<i>Anti CD4 Monoclonal Antibody, PE-Cyanine5, eBioscience™, clone: RM4-5</i>	Invitrogen (Darmstadt, Germany)
<i>Anti TCR gamma/delta Monoclonal Antibody, APC, eBioscience™, clone: eBioGL3</i>	Invitrogen (Darmstadt, Germany)
<i>rabbit monoclonal anti PDGFRβ, clone: 28E1</i>	Cell Signaling Technology (Europe)
<i>rabbit monoclonal anti CD13/APN, clone: D6V1W</i>	Cell Signaling Technology (Europe)
<i>mouse monoclonal anti Iba1, clone:20A12.1</i>	Millipore (Schwalbach, Germany)
<i>rabbit polyclonal anti Iba1</i>	Wako (Neuss, Germany)
<i>rabbit polyclonal anti Munc18-1</i>	Cell Signaling (Cell Signaling Technology Europe)
<i>mouse monoclonal anti NeuN, clone: A60</i>	Millipore (Schwalbach, Germany)
<i>mouse monoclonal anti GFAP, clone:GA5</i>	Cell Signaling (Cell Signaling Technology Europe)
<i>mouse monoclonal anti PSD-95, clone, 6G6-1C9</i>	Abcam (Cambridge, UK)
<i>rabbit polyclonal anti RFP</i>	Rockland (Gilbertsville, USA)
<i>mouse monoclonal anti S100, clone:4C4.9</i>	Abcam (Cambridge, UK)
<i>rabbit monoclonal anti ABCB1, clone: E1Y7S</i>	Cell Signaling Technology (Europe)
<i>rabbit polyclonal anti LRP-1</i>	Cell Signaling Technology (Europe)
<i>rabbit monoclonal anti LRP-1, clone: EPR3724</i>	Abcam (Cambridge, UK)
<i>rabbit polyclonal anti amyloid Precursor Protein, C-Terminal</i>	Sigma Aldrich (A8717, Taufkirchen, Germany)
<i>rabbit monoclonal anti vinculin, clone: E1E9V</i>	Cell Signaling Technology (Europe)
<i>goat anti chicken Alexa 488 Conjugate</i>	Invitrogen (Darmstadt, Germany)
<i>goat anti rabbit Alexa 488 Conjugate</i>	Invitrogen (Darmstadt, Germany)
<i>goat anti rabbit cy3 Conjugate</i>	Cell Signaling Technology (Europe)
<i>goat anti mouse Alexa 546 Conjugate</i>	Invitrogen (Darmstadt, Germany)
<i>goat anti mouse Alexa 594 Conjugate</i>	Invitrogen (Darmstadt, Germany)
<i>goat anti rabbit biotin Conjugate</i>	Vector Laboratorie (Burlingame, USA)
<i>goat anti rat biotin Conjugate</i>	Vector Laboratorie (Burlingame, USA)
<i>goat anti mouse HRP Conjugate</i>	Dako (Hamburg, Germany)
<i>goat anti rabbit HRP Conjugate</i>	Promega (Mannheim, Germany)

5.1.4 Buffer

Recipe	Chemicals	Amount	Concentration
10x Citric buffer	Citric acid	2.014g	10mM
		Up to 1 Liter	
10x PBS	NaCl	400 g	1.37 M
	KCl	10 g	27 mM
	Na ₂ HPO ₄	71 g	100 mM
	NaH ₂ PO ₄ x H ₂ O	69 g	100 mM

MATERIALS AND METHODS

	dest. H ₂ O Adjust to pH 7.4	Up to 5 Liter	
10x TBS	Tris NaCl dest. H ₂ O Adjust to pH 7.4	302.5 g 425 g Up to 5 Liter	500 mM 1.45 M
5x DNA-Loading buffer	Bromphenol blue Xylene cyanol Orange G Sucrose 0.5 M EDTA [pH 8.0] dest. H ₂ O	1 mg 2 mg 2 mg 500 mg 2 µl Up to 1 ml	0.1% 0.2% 0.2% 50% 1 mM
5x TBE	Tris Borat 0.5 M EDTA [pH 8.0] dest. H ₂ O	270 g 137.5 g 100 ml Up to 5 Liter	446 mM 446 mM 10 mM
3x SDS-PAGE Loading buffer	1 M Tris/HCl [pH 6.8] 20% SDS Glycerol β-Mercaptoethanol 3% Bromphenol blue (w/v) dest. H ₂ O	187.5 µl 300 µl 300 µl 150 µl 10 µl Up to 1 ml	187.5 mM 6% 30% 15% 0.03%
10x SDS-Tris-Glycine Running buffer	Tris Glycine SDS dest. H ₂ O	151.5 g 720.5 g 50 g Up to 5 Liter	250 mM 1.92 M 1% (w/v)
10x SDS-Tris-Tricine running buffer	Tris Tricine SDS dest. H ₂ O	121 g 171 g 10 g Up to 1 Liter	1 M 1 M 1% (w/v)
10x Transfer buffer*	Tris Glycine dest. H ₂ O	30 g 138 g Up to 1 Liter	248 mM 1.84 M
* for use, mix 100 mL 10X Transfer buffer with 200 mL methanol and 700 mL dest. H ₂ O			
Western blot Blocking buffer	Nonfatty milk 1x PBS	5g Up to 50 ml	10%
DMEM media*	Dulbecco's Modified Eagle Medium (DMEM)(High Glucose) Fetal bovine serum Antibiotic-antimycotic(100x)	445 ml 50 ml 5 m	89% 10% 1%
* Fetal bovine serum should be inactivated in 56°C water bath for 30 min.			

MATERIALS AND METHODS

RPMI media*	RPMI 1640 Medium	445 ml	89%
	Fetal bovine serum	50 ml	10%
	Antibiotic-antimycotic(100x)	5 ml	1%
* Fetal bovine serum should be inactivated in 56°C water bath for 30 min.			
SDS-Cell lysis buffer	1 M Tris/HCl [pH 7.5]	2.5 ml	50 mM
	0.5 M EDTA [pH 8.0]	200 µl	2 mM
	0.5 M EGTA [pH 8.0]	200 µl	2 mM
	Protease inhibitor Cocktail	1 Tablet	1x
	20 µM Okadic acid	125 µl	50 mM
	0.25 M Na ₄ P ₂ O ₇	1 ml	5 mM
	1 M Na ₃ VO ₄	100 µl	100 µM
	1 M DTT	50 µl	1 mM
	1 M NaF	2.5 ml	50 mM
	20% SDS	5 ml	2%
	dest. H ₂ O	Up to 50 ml	

5.2 Mice

App^{NL-G-F/NL-G-F} knock-in mice (APP^{ki/ki}), provided by Prof. T. Saido from RIKEN Brain Science Institute, Japan, are used as AD mouse models for this project. *App*^{NL-G-F/NL-G-F} knock-in mice co-express the Swedish (KM670/671NL) and Beyreuther/Iberian (I716F) mutations (SAITO et al., 2014). *App*^{NL/NL} mice are inserted with only the Swedish mutation, which promotes β-cleavage of APP. *App*^{NL/NL} mice (APP^{wt}) were used as negative controls for APP^{ki/ki} mice because they generated equal amounts of APP and AICD, and the levels of CTF-β increased similarly between them in a gene dose-dependent manner. *App*^{NL-G-F/NL-G-F} knock-in mice develop Aβ deposition in the cortex within 2 months without overexpressing APP, and memory impairment by 6 months (SAITO et al., 2014). GPR109a-deficient (GPR109a^{-/-}) mice (TUNARU et al., 2003) provided by Prof. S. Offermanns, Max Planck Institute for Heart and Lung Research, Bad Nauheim. APP^{ki/ki} mice were mated with GPR109a^{-/-} mice to obtain homozygously (APP^{ki/ki}GPR109a^{-/-}) and heterogeneous (APP^{ki/ki}GPR109a^{+/-}) knockout of the GPR109a gene and wild-type (APP^{ki/ki}GPR109a^{+/+}) AD mice models for this study. *Gpr109a* expression reporter mice (GPR109a^{mRFP}) have been reported previously (HANSON et al., 2010), which overexpress red fluorescence protein (RFP) under the control of the *gpr109a* promoter. We crossbreed APP^{ki/ki} mice with GPR109a^{mRFP} to acquire a *Gpr109a* expression reporter AD mouse model, which we described as APP^{ki/ki}GPR109a^{mRFP} mice in this thesis.

GPR109a-deficient and wild-type AD mice with deficiency of IL-17a have been established in our laboratory through cross-breeding between APP^{ki/ki}GPR109a^{-/-} mice and IL-17a-Cre knock-in mice (The Jackson Laboratory, Stock No: 016879) (HIROTA et al., 2011). Knock-in expression of Cre abolishes the expression of endogenous IL-17a. APP^{ki/ki}IL-17a^{cre/cre}GPR109a^{-/-} and APP^{ki/ki}IL-17a^{cre/cre}GPR109a^{+/+} mice are used for experiments to examine whether deficiency of IL-17a eliminates the phenotypical difference between APP^{ki/ki}GPR109a^{-/-} and APP^{ki/ki}GPR109a^{+/+} mice. CX3CR1-CreERT2 mice, provided by Prof. Dr. Frank Kirchhoff and Dr. Wenhui Huang (Department of Physiology of Saarland University), were used to culture CX3CR1-deficient bone marrow-derived macrophages.

5.3 Methods

5.3.1 Y maze test

Y-Maze is an easy-to-use test used to assess the spatial learning and memory capabilities of mice based on their spontaneous exploration characteristics. Spontaneous alternation was used to measure spatial working memory, assessed by allowing mice to explore all three maze components without training and food restrictions. Rodents usually prefer to explore a new arm in a maze rather than return to previously visited areas, and the rodent's innate curiosity drives behavior. This behavior involves several brain regions, including the hippocampus, septum, basal forebrain, and prefrontal cortex.

The Y maze was experimented with using the published protocol (PRIEUR, JADAVJI, 2019; SAITO et al., 2014; WHYTE et al., 2018). All experiments were performed during the light phase (8:00-18:00), and we kept the start times of the experiments consistent. The Y-maze apparatus is made of gray, opaque plastic and consists of three identical components (3 cm (width), 30 cm (length), and 12 cm (height)) placed symmetrically (at 120° angle from each other) on a triangular central platform with equal sides (3 × 3 × 3 cm). After introducing the center platform, subjects are allowed free access to all three arms. When all four limbs are inside the arm, it is counted as a single entry. If the animal chooses a different component throughout multiple arm entries than that one it arrived in before, this choice is called an alteration. The access sequence is considered a valid response, while returning to the previous

arm is regarded as an error. We recorded total number of arm entries (T) and the number of valid triads (V), then calculate the percentage of alternations according to the formula: Alternations % = $V/(T-2) \times 100\%$.

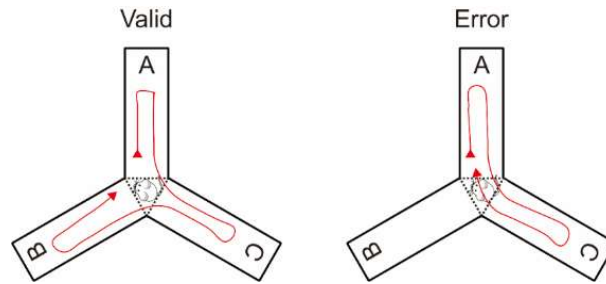


Fig. 5.3.1, Schematic diagram of Y maze test, showing examples of a valid (Left) and an error (Right) alternation in the Y-maze test.

5.3.2 Open field test

The open-field test (OFP) is used to analyze anxiety, exploratory behavior, and locomotion in mice. In our trials, the experimental installation consisted of a grey polyvinyl chloride (PVC) cube cage ($40 \times 40 \times 40$ cm) and a camera for monitoring movement in the center and peripheral areas of the test area. We define the central area as a 20×20 cm square in the middle of the box. The open field analysis is employed using published protocols (KRAEUTER et al., 2019). Each test mouse was allowed to explore the test area for 10 minutes. We analyzed the total distance moved, average velocity, frequency of entry into the central area, and time spent in the central area.

5.3.3 Tissue preparation

The animals were euthanized by inhaling isoflurane (Abbott, Wiesbaden, Germany). Whole blood was collected by intracardiac puncture and stored in EDTA-containing Eppendorf tubes. The mice were then perfused rapidly transcardially with ice-cold PBS, and the brains were removed and separated. The left side of the brain was fixed in 4% paraformaldehyde (PFA, Sigma) immediately for immunohistochemistry. A 0.5 mm thick piece of tissue was sagittally cut from the right hemisphere and placed in a tube containing 700 ul of Tizol (Life Technologies) for RNA isolation and extraction. The remainder of the right hemisphere was snap-frozen in liquid nitrogen for biochemical analysis (HAO et al., 2011; LIU et al., 2012).

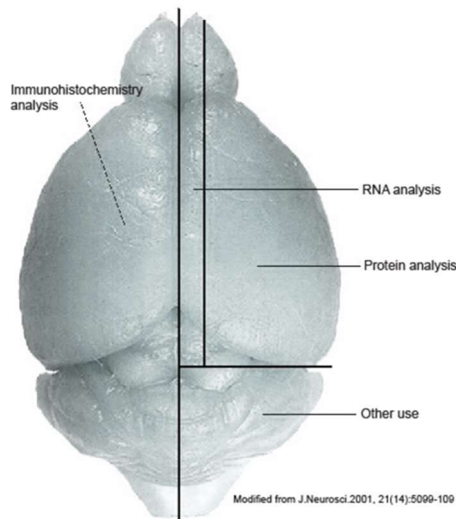


Fig. 5.3.3, Schematic diagram of the preparation of brain sample sections. The brain is divided into 4 parts. The left half of the brain was immediately fixed in 4% PFA and stored at 4°C for the immunohistochemical procedure. A 0.5 mm thick piece of brain tissue was sagittally cut from the right half of the brain and homogenized in Trizol for RNA isolation. The remainder of the right hemisphere was snap frozen in liquid nitrogen for biochemical analysis. The remaining portion was also frozen in liquid nitrogen.

5.3.4 Separation of cerebral vessels in mice

According to the published protocol, brain tissues were collected as described in section 3.3.3, dissection of the cortex and hippocampus of the remaining right hemisphere, and isolation of cerebral vessels (BOULAY et al., 2015; QUAN et al., 2021). Briefly, brain tissue was homogenized in Hanks Balanced Salt Solution (HBSS) containing HEPES and centrifuged at 4,400 g in HEPES-HBSS buffer supplemented with dextran from *Leuconostoc* spp. (molecular weight 70,000; Sigma-Aldrich Chemie GmbH) to remove the myelin. The vessel residue was suspended in HEPES-HBSS buffer supplemented with 1% bovine serum albumin (Sigma-Aldrich Chemie GmbH) and filtered through a 20 µm-mesh. Collect the vessel fragments from the filter membrane and store them at -80°C for biochemical analysis.

The steps are as follows:

- a) Solution preparation: B1, 5 ml of HEPES 1M in 500 ml of HBSS; B2, 0.9 g of Dextran 7000 in 5 ml of B1 (per hemisphere); B3, 5 g of BSA in 500 ml of B1.
- b) The brain tissue was collected as described above, and the right hemisphere tissue was placed in a 15 ml tube containing 3 ml of cold B1 solution.
- c) Manual mincing of brain tissue in B1 solution using ophthalmic shears, followed by obtaining small pieces of approximately 2 mm.

MATERIALS AND METHODS

- d) Homogenize brain tissue using an automatic Dounce homogenizer with 20 strokes at 400 rpm. Always keep the glass tube on ice. Ensure the upper half of the douncer is kept in solution when moving up and down to avoid the production of air bubbles. If more than one sample is prepared, wash the douncer with ionized water between each homogenization.
- e) Transfer the homogenate to a 15 ml polypropylene tube and centrifuge for 10 minutes at 4 °C at 2,000 g. A massive white interface (mainly myelin) will emerge on the top of the vessel pellet.
- f) Discard the supernatant. The whitish interface and the vessel pellet will remain contained. Add 5 mL of ice-cold B2 solution to each tube and aggressively shake it for 1 minute.
- g) Centrifugate again at 4,400 g for 15 minutes at 4°C. The myelin will now form a dense white layer on the surface of the supernatant.
- h) Hold the tube and slowly rotate it so that the supernatant passes along the tube wall, carefully separating the myelin layer from the tube wall. The supernatant is removed along with the myelin sheath. And the particles containing the vessel remain attached to the bottom of the tube.
- i) Blot the inside of the tube with absorbent paper wrapped around a 5 ml plastic pipette and remove any residual liquid, avoiding contact with the container particles. Place the tube upside down on the absorbent paper to drain the residual liquid.
- j) Suspend the pellet in 1 ml of ice-cold B3 solution by pipetting up and down with low-binding tips, keeping the tube on ice, then adding another 5 ml of B3 solution. Make sure that vessels are dispersed as much as possible and do not form aggregates.
- k) Assembling the filter set, then place a 20 µm-mesh filter on the filter set on the top of a beaker flask and equilibrate by applying 10 ml of ice-cold B3 solution.
- l) Prepare a beaker on ice with 30 ml of ice-cold B3 solution. Cover with parafilm to avoid air contamination.
- m) Rinse the membrane repeatedly with 40 ml ice-cold B3 solution in a beaker, and pour the beaker content in a 50 ml plastic tube and centrifuge at 2,000 g for 10 min at 4 °C.
- n) Add 1 ml of B3 solution to the tube to resuspend the precipitate, transfer to a 1.5 ml tube, centrifuge again at 2,000 g for 5 min at 4 °C.
- o) 50ul of RIPA solution was added to the vessel precipitates and treated with an Ultrasonic cracker for 1 minute. ABCB1, LRP1 and other protein levels were detected by quantitative Western blot.

5.3.5 Positive selection of CD11b⁺ cells in adult mouse brain

To determine the gene expression and cell surface antigen expression in microglia/brain macrophages, we carefully dissected the entire cerebrum from 9-month-old APP-transgenic mice with or without a deficiency of GPR109a and prepared a single-cell suspension. As described in previous study(XIE et al., 2013a), CD11b⁺ cells were selected with rat anti-mouse/human CD11b (BioXCell, clone: M1/70).

(1) Enzymatic Neural Tissue Dissociation: The enzymatic dissociation of brain tissue is beneficial in that cell suspension will contain less debris. Dissociated the right hemisphere into single-cell suspensions by enzymatic degradation of the extracellular matrix via the Neural Tissue Dissociation Kit (P) (Miltenyi Biotec):

- a) Reagent preparation: Prepare enzyme mix 1 (for digestion) and enzyme mix 2 (for dissolution of DNA) for one hemisphere (up to 400 mg tissue) according to the table below.

Enzyme mixture 1		Enzyme mixture 2	
Enzyme P: 50 μ l	Buffer X: 1900 μ l	Enzyme A: 10 μ l	Buffer Y: 20 μ l

- b) Prewarm the enzyme mixture 1 solution in a 37 °C water bath for 10 min before use.
- c) Remove the mouse brain. The weight of brain tissue was measured in 1 ml of cold HBSS to ensure that the weight did not exceed 400 mg per digestion.
- d) Remove the meninges, and mince the right hemisphere into small pieces on a petri dish to facilitate enzyme dissociation.
- e) Transfer brain tissues pieces to a 15 ml tube containing 1950 μ l preheated enzyme mixture 1, and incubated in a 37 °C water bath with continuous rotation for 10 min.
- f) Transfer 30 μ L of enzyme mixture 2 to a 15 ml tube. Gently invert the mixture and incubate sample again for 10 minutes at 37 °C with slow, continuous rotation.
- g) Place a 70 μ m strainer on a 50 mL tube to collect cell suspension and 10 mL of HBSS is applied to rinse the strainer.
- h) Centrifuge cell suspension at 700 \times g at 4 °C for 10 min and discard supernatant completely.
- i) Resuspend up to 10⁷ nucleated cells with per 1ml of buffer for further applications.

(2) Magnetic isolation of CD11b⁺ cells from brain cells suspension

- a) Blocking: preincubate cell suspension with Mouse BD Fc BlockTM purified anti-mouse CD16/32 mAb (clone: 2.4G2, BD) in 1 μ g/million cells at 4°C for 30 min to reduce Fc receptor-mediated binding by antibodies of CD11b, 10% FBS was added to prevent non-specific binding.

- b) Prepare rat anti-mouse/human CD11b (BioXCell, clone: M1/70) incubation buffer at a final dilution volume accommodating 1:50 to the preincubated cells. Mix well and incubate for 2 h at 4°C in the dark.
- c) Cells were washed 3 times with HBSS buffer and centrifuged at 4 °C, 700 × g for 10 min. Incubate cells in 300 µl DMEM solution containing 10% FBS, 20 µl of Dynabeads™ Sheep anti-Rat IgG antibody (Invitrogen) for at least 1 hour.
- d) Washing: wash cells with HBSS buffer three times again, place tube in the magnetic field of a suitable MACS separator 2 min, discard the untouched cell isolation (unlabelled cell fraction). Repeat the washing steps 3 times.
- e) Remove the tube from the MACS separator, and 700 µl lysis buffer was immediately added to CD11b+ cells for isolation of total RNA with the RNeasy Plus Mini Kit.

5.3.6 Isolation of T cells from mouse small intestinal lamina propria and Peyer's patches

The gut is the organ in our body that contains the largest number of immune cells, and the gut is essential for regulating adaptive and innate immune responses. We isolated T cells from small intestinal lamina propria and Peyer's patches using published protocols (BENAKIS et al., 2016).

(1) Preparation of solutions

- a) Extraction solution (per small intestine): 30 ml RPMI + 93 µl 5% (w/v) dithiothreitol (DTT) + 60 µl 0.5 M EDTA + 500 µl fetal bovine serum (FBS). Add the DTT immediately before use.
- b) Digestion solution (per small intestine): 25 ml RPMI + 12.5 mg Dispase + 37.5 mg collagenase II + 300 µl FBS. Add the Dispase and collagenase immediately before use.
- c) Prewarm solutions to 37 °C.

(2) Preparing a single cell suspension from the small intestinal lamina propria

- a) Mice were euthanized by inhalation of isoflurane followed by cervical dislocation.
- b) Exposed the abdominal cavity by an incision along the midline of the abdomen with scissors, separated the small intestine and stomach at the pyloric sphincter. Then the small intestine was gently removed in sequence and incised again at the ileo-cecum junction. Place the isolated small intestine in a 4 °C RPMI with 10% FBS.
- c) The small intestine was placed on a paper towel moistened with RPMI, and the fat was removed from the tissue with a blunt knife to remove residual fat.
- d) Gently flush the intestine with 15 - 20 ml of cold PBS using a syringe with an 18 g needle

MATERIALS AND METHODS

to remove the intestinal contents

- e) Peyer's patches were excised with scissors and collected in cold RPMI containing 5% fetal bovine serum. Peyer's patches are located on the antimesenteric side of the small intestine and appeared as multilobed white masses.
- f) Cut the small intestine into 6-8 cm pieces.
- g) Insert a curved forceps into the intestinal fragment, grasp the distal end of the tissue, and turn the tissue inside out.
- h) Tissue pieces are incubated in a 50 ml tube containing 30 ml of extraction medium, and stirred at 500 rpm for 15 minutes at 37 °C on a shaker.
- i) After incubation, the tissue pieces were collected with a steel strainer. Place the tissue on a dry paper towel and turn it over several times to facilitate removal of residual mucus.
- j) Tissue fragments were placed in 1.5 ml tubes containing 600 µl of digestion medium and chopped with scissors until the fragments no longer adhered to the scissors to facilitate digestion.
- k) The minced small intestine was transferred into a 50 ml tube containing 25 ml of digestion medium, stirred at 500 rpm for 30 minutes at 37 °C on a shaker.
- l) The digested tissues were filtered through a 100µm cell strainer into a 50 ml tube and the filter was rinsed with 20 ml of RPMI containing 10% FBS. The filtered solution was centrifuged at 700 g for 10 minutes at 4°C.
- m) The supernatant was removed and the pellet was resuspended in 1 ml of RPMI containing 10% FBS.
- n) Filter the suspended cells into a 50 ml tube with a 40 µm cell strainer. Rinse the filter with 20 ml of RPMI containing 10% FBS. Centrifuge filtered solution at 4 °C, 700 g for 10 min.
- o) The supernatant was carefully decanted and the pellet was resuspended in 1 ml of RPMI containing 2% FBS for later use.

(3) Preparation of a single cell suspension from Peyer's Patches

- a) transfer the Peyer's Patches collected in step (2e) to a 15 ml tube containing 2 ml of digestion medium and shake at 37 °C, 500 rpm for 10 min.
- b) The digested Peyer's Patches were then filtered into a 50 ml tube using a 40 µm cell filter, and the filter was rinsed with 10 ml of RPMI containing 10% FBS and centrifuged at 4°C for 10 min at 700 g.
- c) Remove supernatant and the pellet was resuspended in 1 ml of RPMI containing 2% FBS for later use.

After pelleting cells by centrifugation, 200 µl of blocking buffer containing 25 µg/ml rat

anti-mouse CD16/CD32 antibody (2.4G2, BD), 10% FBS was added to prevent non-specific binding. After 30 minutes of blocking at 4 °C, stained cells with 5 µg/ml PE-Cyanine 5-conjugated anti-Mo CD4 antibody (eBioscience™, clone: RM4-5) or APC- conjugated anti-Mo TCR gamma/delta Antibody (eBioscience™, clone: eBioGL3) for flow cytometric analysis by staining. Alternatively, cells were selected with Dynabeads™ Mouse CD4 (L3T4) antibody (Invitrogen) after blocking to separate CD4-positive cells. Lysis buffer was immediately added to the CD4-positive cells to isolate total RNA using RNeasy Plus Mini Kit (Qiagen GmbH).

5.3.7 Bone marrow-derived macrophages (BMDMs) culture and treatment

Bone marrow-derived macrophages were isolated from medullar cavities of femur and tibia of 8-week-old APP^{ki/ki}GPR109a^{-/-} and APP^{ki/ki}GPR109a^{+/+} littermate mice. Isolated and culture according to a published protocol (HAO et al., 2011).

(1) Isolation of bone marrow:

- a) Sacrifice the mice by cervical dislocation following the deep anesthesia with isoflurane.
- b) Remove both hind legs, strip tissue from femur and tibia, then keep the bones in ice-cold PBS.
- c) Cut the bones at both ends, using a 5 ml syringe containing 5 ml ice-cold PBS, wash the bone marrow into a small dish.

(2) Seeding the total bone marrow cells:

- a) Centrifuge the collected bone marrow at 4 °C, 1200 rpm for 8 min, then remove the supernatant.
- b) Resuspend the cell pellet in 5 ml lysing buffer (ACK Lysing Buffer, #A10492-01, Gibco). Leave for 5 min and add 5 ml PBS.
- c) Centrifuge again at 4 °C, 1200 rpm for 8 min, remove the supernatant and resuspend the cell pellet in 5 ml PBS.
- d) Centrifuge at 4 °C, 1200 rpm for 8 min to collect the cells, resuspend the pellet in 10 ml DMEM medium (10 % FBS and 1% Penicillin-Streptomycin in DMEM). Incubate at 37 °C for 24 hours.

(3) Re-seeding the macrophages:

- a) Collect the supernatant with all the swimming cells.
- b) Centrifuge at 4 °C, 1200 rpm for 8 min.
- c) Resuspend cell pellet with 10ml Culture medium (10 % L929 conditioned medium, 90 %

DMEM medium). Put them into a new culture dish, and incubate at 37 °C.

d) Change Culture every 3 to 4 days.

(4) Cell treatment

To investigate the effects of GPR109a in microglia, we administered LPS (Axxora) and niacin (Sigma Aldrich) to GPR109a wild-type and GPR109a deficiency BMDMs, respectively. Macrophages were treated with 0, 1, and 100 ng/ml of LPS and 0, 1, 10, and 100 µmol/l of niacin. After 12 hours of stimulation, the medium was collected for ELISA to detect inflammatory markers. Then macrophages were collected and labeled with Alexa Fluor® 488 Anti-Mouse CX3CR1 Antibody (BioLegend) and analyzed with a FACSCanto II flow cytometer (BD Biosciences).

5.3.8 Flow cytometric analysis of HiLyte Fluor™ 488-Aβ42 internalization in primary macrophages

The 42 amino acid form of human Aβ (Aβ42) was kindly provided by Dr. L. Fülöp (Albert Szent Gyorgyi Medical University, Szeged, Hungary). Oligomeric and fibrillar Aβ were prepared according to published protocols (LIU et al., 2014). Fluorescent Aβ was prepared by mixing HiLyte Fluor 488-labeled human Aβ42 (AnaSpec) and unlabeled Aβ at a ratio of 1:10.

To investigate the effect of GPR109a on internalized Aβ in macrophages, GPR109a-deficient and wild-type primary macrophages were cultured in 24-well plates (BD Biosciences) at a density of 3×10^5 cells/well and treated with 0.2 or 1.0 µM HiLyte Fluor 488-conjugated Aβ42. To investigate effects of niacin on Aβ internalization, GPR109a-deficient and wild-type primary macrophages were pretreated with 0, 1, 10, and 100 µmol/l niacin for 12 hours, followed by incubation with 1.0 µM fluorescent oligomeric Aβ42 aggregates for 6 h. Thereafter, macrophages were washed with a 1× solution of PBS and detached from the plate with trypsin-EDTA (Life Technologies). The mean fluorescence intensity (mFI) of internalized fluorophore-conjugated Aβ42 and the percentages of Aβ42 positive cells with intracellular proteins were immediately determined with a FACSCanto II flow cytometer (BD Biosciences).

5.3.9 Bio-Rad Protein Assay

The Bio-Rad Protein Assay is a simple colorimetric assay based on the Bradford dye-

binding method (BRADFORD, 1976). We use the Protein Assay Reagent (Bio-Rad) to measure total protein concentration by using standard procedures. The assay is used for samples with protein concentrations between 200 and 1,400 $\mu\text{g/ml}$ (20-140 μg in total). First, the protein concentration is estimated and diluted with dest.H₂O to bring the protein concentration within the measurement range. Briefly, in a high-concentration assay, loaded 20 μl sample or serially diluted standards were loaded on a 96-well format microplate, and then 200 μl 1 \times assay reagent was added to each well. Absorption at 595 nm was read with a Microplate reader, and protein concentration was determined according to a standard curve.

5.3.10 ELISA

TNF- α , IL-1 β , and IL-10 concentration in culture medium of primary BMDMs were determined by ELISA kits (all from R&D Systems). Procedure is as follows:

- (1) Dilute the capture antibody to working concentration in PBS without carrier protein. Coat ELISA microplate with 100 μl /well of diluted capture antibody. Seal the plate and incubate overnight at room temperature.
- (2) Aspirate each well and wash 3 times with > 400 μl /well of Wash Buffer. Soak in each wash step for approximately 1 minute to ensure washing effectiveness. Invert the plate and place it against the paper to remove any remaining Wash Buffer.
- (3) Block plates by adding 300 μl /well of Reagent Diluent (1% BSA in PBS, pH 7.2-7.4). Incubate at room temperature for a minimum of 1 h.
- (4) Repeat the aspiration/wash as in step (2).
- (5) Prepare samples and through serial dilution prepare the following standards as: 2000, 1000, 500, 250, 125, 62.5, 31.25, and 0 pg/ml Recombinant Mouse TNF- α or IL-10; and 1000, 500, 250, 125, 62.5, 31.25, 15.625, and 0 pg/ml Recombinant Mouse IL-1 β . Add 100 μl /well samples or standards. Cover with an adhesive strip and incubate for 2 hours at room temperature.
- (6) Repeat the aspiration/wash as in step (2).
- (7) Add 100 μl /well of the Detection antibody, diluted to working dilution by Reagent Diluent. Cover with a new adhesive strip and incubate for 2 hours at room temperature.
- (8) Repeat the aspiration/wash as in step (2).
- (9) Add 100 μl /well of the working dilution of Streptavidin-HRP. Seal the plate and incubate at room temperature for 30 minutes.
- (10) Repeat the aspiration/wash as in step (2).

- (11) Add 100 μ l/well Substrate Solution (R & D Systems, 1:1 mixture of color Reagent A and Reagent B). Incubate plate at room temperature for 20 minutes. Avoid placing the plate in direct light.
- (12) Add 50 μ l/well of Stop Solution. Gently tap the plate to ensure thorough mixing.
- (13) Determine the optical density of each well immediately, using a microplate reader set to 450 nm to get optical density (O.D.).

5.3.11 Extraction of A β from mouse brain into TBS-soluble, TBS-T-soluble, guanidine HCl-soluble fractions

The brain was homogenized as previously described (LIU et al., 2012). Following are the detailed steps:

(1) TBS-soluble fraction:

- a) Prepare 10 ml TBS extraction buffer: sterile 1x TBS + one tab of protease inhibitor cocktail.
- b) Weight frozen hemispheres quickly and keep the brain on ice until homogenization.
- c) Added four brain volumes (4 μ l/mg brain) ice-cold TBS extraction buffer to a 2ml Porter-Elvehjem (PE) homogenizer containing brain tissue on ice.
- d) Brain tissue were bounce-homogenized in the TBS-containing protease inhibitor cocktail and centrifuged at 16,000 g for 30 minutes at 4°C.
- e) Collected the supernatant as the TBS-soluble fraction and stored it at -80°C.

(2) TBS-T-soluble fraction:

- a) The pellets were re-suspended with 4 volumes (based on initial hemisphere weight) chilled TBS plus 1% Triton-X-100 (TBS-T).
- b) The remaining residue was lysed by sonication for 5 minutes in a 4°C ice bath.
- c) Centrifuged at 16,000 g for another 30 minutes at 4°C, then collected the supernatant and stored it as the TBS-T-soluble fraction at -80°C.

(3) Guanidine-soluble fraction:

- a) Dissolve guanidine hydrochloride in 50 mM Tris-solution to prepare a pH 8.0, 5 M guanidine hydrochloride buffer.
- b) The pellets were extracted using 4 volumes of ice-cold guanidine buffer for the third time.
- c) Vortex the tubes until the pellets move away from the bottom and disperse.
- d) Rotate overnight at 4°C to ensure thorough lysis.
- e) Centrifuged at 16,000 g for 30 minutes at 4°C. The supernatant was collected and stored at -80°C as the guanidine-soluble fraction.

- f) The protein concentration of all samples was measured using Bio-Rad Protein Assay (Bio-Rad Laboratories GmbH, Munich, Germany) and then normalized to the protein concentration of all samples for further analysis.

5.3.12 A β ELISA

A β 40 and A β 42 are quantified in three different fractions of brain homogenates by the Human A β 40 or A β 42 ELISA kit (Invitrogen). The assay identifies both natural and recombinant human A β . The procedure is as follows:

(1) Preparing solutions: Dissolve 2.31g Sodium Bicarbonate in 500mL deionized water and adjust the pH to 9.0 acquired an A β 40 standard reconstitution buffer (55 mM NaHCO₃ Buffer, pH 9.0). Dilute Wash Buffer Concentrate (25 \times) with deionized water to 1 \times Wash Buffer working solution.

(2) Dilute standards: reconstitute Human A β 40 and A β 42 Standard with standard reconstitution buffer (55 mM NaHCO₃ Buffer, pH 9.0) and deionized water, respectively. Then make serial dilutions of A β 40 standard as the follows: 500, 250, 125, 62.5, 31.25, 15.63, 7.81, and 0 pg/ml human A β 40; and A β 42 standard as the follows: 1000, 500, 250, 125, 62.5, 31.25, 15.63, and 0 pg/ml human A β 42. Mix thoroughly between steps.

(3) Samples preparation: Dilute the sample concentration to within the standard curve range using Standard Dilution Buffer. In our experiments, we dilute the TBS-soluble fraction 1:1, the TBST-soluble fraction 1:4, and the Guanidine-soluble fraction 1:100.

(4) Bind antigen and add detector:

a) Add 50 μ L of a serial Hu A β 40/A β 42 standard dilutions, controls, or samples to the plate wells and leave the wells empty for chromogenic blanks.

b) Add 50 μ L of Hu A β 40/A β 42 Detection Antibody solution into each well except the chromogen blanks.

c) Cover the plate with the plate cover and tap the side of the plate for mixing, then incubate at 4 $^{\circ}$ C with shaking overnight.

d) Thoroughly aspirate the solution and wash wells 4 times with 1 \times Wash Buffer.

(5) Add Anti-Rabbit IgG HRP solution:

a) Preparation of 1 \times Anti-Rabbit IgG HRP solution: For each 8-well strip used in the assay, aspirate 10 μ L of Anti-Rabbit IgG HRP solution (100 \times) and dispense the solution into a tube

containing 1 mL of HRP Diluent and mix thoroughly. Prepare the solution within 15 minutes of use.

- b) Add 100 μ l Anti-Rabbit IgG HRP into each well except the chromogen blanks.
- c) Cover the plate and tap the side of the plate to mix, then incubate at room temperature for 30 minutes.
- d) Thoroughly aspirate the solution and wash wells 4 times with 1 \times Wash Buffer.
- (6) Add 100 μ l of Stabilized Chromogen per well, and the substrate solution begins to turn blue. Incubate for 30 min at room temperature in the dark.
- (7) Add 100 μ l Stop Solution to each well. Tap the side of the plate to mix. The solution in the well changes from blue to yellow.
- (8) Read the plate with the absorbance at 450 nm. Read the plate within 2 hours after adding the Stop Solution.
- (9) Generate standard curves using curve-fitting software. Measure the concentration of the unknown sample and control by reading from the standard curve. Multiply the values obtained for the samples by the appropriate factor to correct for sample dilution.

5.3.13 Western blot analysis

Western blot is a scientific technique for qualitative or semiquantitative identification of specific protein molecules in a protein mixture by gel electrophoresis. The technique consists of three steps: separation of proteins from different samples, transfer to a solid support (e.g., PVDF membrane), and selective immunodetection of an immobilized antigen.

(1) Samples preparation

Frozen mouse brains were homogenized on ice in 5 \times radioimmunoprecipitation assay buffer (RIPA buffer; 50mM Tris [pH 8.0], 150mM NaCl, 0.1% SDS, 0.5% sodium oxy- cholate, 1% NP-40, and 5mM EDTA) supplemented with protease inhibitor cocktail (Sigma-Aldrich Chemie GmbH), and then centrifuged at 16,000 $\times g$ for 30 minutes at 4 $^{\circ}$ C to collect the supernatant containing the protein mixture. Isolated blood vessels were directly lysed in 2 \times sodium dodecyl sulfate-polyacrylamide gel electrophoresis (SDS-PAGE) sample loading buffer containing 4% SDS and ultrasonically lysed on ice for 1min before loading. Measure protein concentrations using the Bio-Rad protein assay, ensuring consistent concentrations

between samples and adding about 30 µg of total protein to each well. Samples were diluted at 1:2 in 3 × SDS-PAGE loading buffer and heated at 95°C for 5 minutes.

(2) Electrophoretic Separation of Proteins by SDS-PAGE

The SDS-PAGE is a technique for separating proteins based on the difference in their mobility in an applied electric field. The protein in the electric field moves or migrates at a rate determined by its charge/mass ratio. Protein samples treated with SDS show an equal amount per unit mass and migrate through the SDS gel only according to their molecular mass.

a) Gel preparation

The electrophoretic separation of proteins is most generally carried out in polyacrylamide gels. These gels are cast between two glass plates by polymerizing the acrylamide monomer solution into polyacrylamide chains and simultaneously cross-linking the chains into a semi-solid matrix. A completed gel consists of a lower separating gel and an upper stacking gel. By varying the concentrations of polyacrylamide and crosslinker, the pore size of the separating gel may be altered. We used 10% separating and 5% stacking gel. Proteins in brain homogenates were separated by 10-20% pre-casted Tris-Tricine gels (Anamed Elektrophorese GmbH, Groß-Bieberau/Rodau, Germany) to detect Aβ oligomers.

10% Separating gel (2 Gels)	Bisacrylamid	6.45 ml
	1M Tris-HCl (pH 8.8)	7.5 ml
	bidest. H ₂ O	4.95 ml
	20% SDS	97.5 µl
	10% APS	195 µl
	TEMED	24 µl
5% Stacking gel (2 Gels)	Bisacrylamid	840 µl
	1M Tris-HCl (pH 6.8)	1.88 ml
	bidest. H ₂ O	2.2 ml
	20% SDS	25 µl
	10% APS	50 µl
	TEMED	6 µl

APS: Ammonium persulfate, TEMED: N, N, N', N'-Tetramethyl ethylenediamine

b) Electrophoresis

The SDS-PAGE system used in this study is the Mini-PROTEAN^{®3} Cell electrophoresis system (Bio-Rad). The first step is to place the prepared gel into the electrophoresis apparatus, then pour the electrophoresis buffer into the electrophoresis apparatus, make sure the buffer completely

covers the gel and carefully remove the comb, and finally load the marker (5 μ l) or sample (20 μ l) into each well separately. Turn on the power for electrophoresis and run at 80V for 30 minutes, then switch to 120V until bromophenol blue flows from the bottom of the gel.

c) Electrotransfer

Electrotransfer is the most common method for transferring proteins from the gel, and we use wet electroblotting. The technique involves direct contact of the protein-containing polyacrylamide gel with a nitrocellulose membrane, polyvinylidene fluoride (PVDF) membrane, or other suitable protein-binding support. The gels are first equilibrated in transfer buffer, then the gel is cushioned by a pad and compacted together by a support grid in a "transfer sandwich" (filter paper-gel-membrane-filter paper). In our experiments, we use PVDF membranes (soaked in methanol for 1 minute before use) with 0.2 μ m or 0.4 μ m pore size depending on the size of the target protein. The sandwich is placed vertically in the transfer apparatus and ensures that the transfer chamber was filled with transfer buffer (pre-cooled at 4 °C) and completed the transfer at 250 mA for 90 to 120 min.

d) Blocking and immunoblotting

1. The membranes with immobilized proteins were blocked with 10% skimmed milk powder (w/v) in PBS for 1 hour at room temperature to seal the non-specific binding sites.
2. Then add primary antibody in 1% skimmed milk powder (w/v) and incubate overnight at 4°C on a shaker. Primary antibodies include: Munc18-1 protein mammalian homolog (Munc18-1), synaptosome-associated protein 25 (SNAP25), postsynaptic density protein 95 (PSD-95) (Catalog numbers: 13414, 3926 and 2507, respectively; Cell Signaling Technology) and mouse monoclonal synaptophysin antibody (clone SY38; Abcam), ABCB1, β -actin, and vinculin (clone: E1Y7S, 13E5 and E1E9V respectively; Cell Signaling Technology) and rabbit polyclonal antibodies against LRP1, and α -tubulin (Catalog numbers: 64099 and 2144, respectively; Cell Signaling Technology); anti-human A β mouse monoclonal antibody (clone W0-2; Merck Chemicals GmbH, Darmstadt, Germany).
3. The following day, the membrane was washed 3x10 min in TBS + 0.05% Tween 20 to remove the residual primary antibody.
4. Incubated the membrane with a secondary antibody diluted in PBS +1% skim milk powder (w/v) at room temperature for 2 hours.
5. Washing the membrane 3x10 min with TBS + 0.05% Tween 20 again.

- Using Western Lightning ECL substrate (PerkinElmer LAS GmbH, Rodgau, Germany) for developing. According to the instructions, substrate solutions A and B are mixed in a 1:1 ratio and cover the membrane uniformly. After 2 minutes, the substrate mixture is removed, and chemiluminescence is detected in a dark room using Amersham Hyperfilm ECL (GE Healthcare). Kodak GBX developer and fixer were used to make the signal visible.

Scan the western blot films with the Epson Perfection V700 Photo Scanner. Densitometric analyzes were performed with the image processing program Fiji (<https://imagej.net/software/fiji/>). The protein level was calculated for each sample as a ratio of target protein/ β -actin or α -tubulin or vinculin.

5.3.14 Methoxy-X04 staining for A β deposition

Methoxy-X04, a congo-red derivative, is a BBB permeable amyloid β fluorescent marker that selectively binds fibrillar β -sheet deposits with high affinity to detect plaque, tangles, and cerebrovascular amyloid in vivo. To quantify brain A β deposition, four paraffin brain sections from each mouse were selected with equal space and labelled with methoxy-X04 (Tocris Bioscience, Wiesbaden-Nordenstadt, Germany) after deparaffinization. The procedures are as follows:

- Preparing stock solutions for methoxy-X04: methoxy-X04 powder is dissolved in DMSO at a concentration of 10 mM and stored at -20 °C.
- Brain sections were deparaffinised sequentially in the solutions: 2 \times 5 min xylene, 2 \times 5 min 100% ethanol, 5 min 96% ethanol, 5 min 70% ethanol, and 5 min 50% ethanol.
- Rehydration of sections by rinsing in distilled water for 30 seconds, repeated 2-3 times.
- Antigen retrieval by cooking the sections in 1 x citrate buffer (10 mM, pH 6.0) for 1 hour in a steamer. Cool slowly to room temperature after cooking.
- Dilute the stock solution of methoxy-X04 1:1000 with a 1:1 mixture of DMSO and 0.9% NaCl solution.
- Brain sections incubated in methoxy-X04 working solution for 20 minutes.
- Wash 3 \times 10 min in PBST with gentle agitation.
- Mount with DAPI (1 μ l stock solution in 1ml Mowiol)-Mowiol.

The whole cortex and hippocampus were imaged and merged using MicroLucida (MBF Bioscience). Fluorescent-labelled areas were measured using the Fiji

(<https://imagej.net/software/fiji/>), and processing thresholds were fixed for all images. The percentage of A β coverage in the brain was calculated.

5.3.15 Immunofluorescent staining

Immunofluorescence (IF) is a required immunochemical method for detecting and localizing antigens in various types of tissue or cell preparations. An important basis for this technique is antigen binding to a specific antibody labelled with a fluorophore.

1. Frozen Section Preparation

- (1) 4% PFA-fixed left hemisphere (described as Section 5.3.3) was sequentially dehydrated in 10%, 20% and 30% sucrose (w/v) in PBS for 24h.
- (2) Dehydrated brain tissue is placed on a pre-labelled tissue base mold.
- (3) Cover the entire tissue block with Tissue-Tek® O.C.T.™ Compound (Sakura Finetek).
- (4) Base mould containing the embedded brain is placed in a beaker containing isopentane and then snap-frozen in liquid nitrogen. Store the frozen tissue block at -80°C until sectioning.
- (5) Transfer the frozen tissue blocks to cryotome cryostat (Leica CM3050 S, Leica Biosystems) 2-3 hours before slicing to equilibrate the temperature of the frozen tissue block with that of the cryotome.
- (6) Frozen tissue blocks are cut to 30 μ m sections using the cryotome. Tissue sections are placed on adhesive-coated, positively charged slides (Adhäsions-Objektträger SuperFrost® plus, R.Langensbrinck GmbH Labor-und Medizintechnik, Germany).
- (7) Dry the tissue sections overnight at room temperature.
- (8) Fix sections in -20°C acetone for 30 minutes. Sections can be stored in a sealed slide box at -80°C for later use.

2. Paraffin-Embedded Slide Deparaffinization and Rehydration

Paraffin-embedded brain tissue blocks were cut into 30 μ m sections and the slides were placed in an oven at 37°C overnight. The slides were deparaffinised sequentially in the solutions: 2 \times 5 min xylene, 2 \times 5 min 100% ethanol, 5 min 96% ethanol, 5 min 70% ethanol and 5 min 50% ethanol. Rehydration of sections by rinsing in distilled water for 30 seconds, repeated 2-3 times.

3. Antigen Retrieval

Cut the Paraffin-embedded brain tissue blocks into 30 μm sections, and the slides were placed in an oven at 37°C overnight. The slides were deparaffinised sequentially in the solutions: 2 \times 5 min xylene, 2 \times 5 min 100% ethanol, 5 min 96% ethanol, 5 min 70% ethanol, and 5 min 50% ethanol. Rehydration of sections by rinsing in distilled water for 30 seconds, repeated 2-3 times.

4. Immunostaining

- (1) Blocking: block slides with blocking buffer (0.2% Casein (w/v) + 0.1% Tween 20 + 0.1% Triton X-100 in PBS), RT, 1h.
- (2) Primary Antibody reaction: dilute the antibody with dilution buffer (0.02% casein (w/v) + 0.01% Tween 20 + 0.01% Triton X-100 in PBS solution). Rabbit polyclonal anti-Iba1 (Wako), mouse monoclonal anti-Iba1 (Millipore), rabbit polyclonal anti-RFP (Rockland), mouse monoclonal anti-human A β antibody (Dako), mouse monoclonal anti-NeuN (Millipore), mouse monoclonal anti-GFAP (Cell Signaling) dilute 1:500; the monoclonal rabbit anti-LRP1 (Abcam) and rabbit polyclonal anti-amyloid Precursor Protein (Sigma Aldrich) dilute 1:100. Incubate the primary antibody working solution at 4 °C overnight.
- (3) Rinse slides with PBST, 10 min \times 3 times.
- (4) Secondary Antibody reaction: with the 1:500 diluted goat anti-rabbit Alexa 488 Conjugate, or goat anti-mouse 546 Conjugate secondary antibodies in dilution buffer, RT, 2 hours.
- (5) Rinse slides with PBST, 10 min \times 3 times.
- (6) Coverslip slides with Mowiol with DAPI.
- (7) All images were acquired by Zeiss AxioImager.Z2 microscope (Carl Zeiss, Göttingen, Germany) equipped with a Stereo Investigator system (MicroBrightField, Williston, USA).

As we describe in previous studies (HAO et al., 2011; QUAN et al., 2021), the interaction between microglia and A β deposits and the morphology of microglia around A β or away from A β were investigated. Serial brain sections were stained with Iba-1 antibody (Wako Chemicals) and then co-staining with methoxy-X04 (Bio-Techne GmbH, Wiesbaden, Germany) and mouse monoclonal anti-human A β antibody (clone 6F/3D, Dako, Hamburg, Germany). Under Zeiss microscopy with 40 \times objective, A β deposits and surrounding microglia were imaged with Z-stack serial scanning from -10 to +10 μm . From each section, ≥ 10 randomly chosen areas were analyzed. The total number (> 200) of Iba-1-positive cells co-localizing with A β deposits were counted. Measure the area of A β by Fiji to adjust the microglial number around A β .

MATERIALS AND METHODS

Use the Stereological technique to count the number of microglia. Briefly, the entire hippocampus and cortex dorsal brain slices were systematically randomly sampled at 10-slice intervals for immunostaining first; then apply an Optical Fractionator as a stereological probe to quantify Iba-1-labelled cells with a 120×120×18 μm director and a 400×400 μm sampling grid. The coefficient of error (CE) calculated was less than 0.08. Tissue thickness was determined at each director location with a 0.1 m precision focus drive. Only Iba-1 positive cells with clear DAPI nuclei staining were counted in each direction. As described above, the microglia with dark blue nuclei were counted in the total hippocampus and cortex area in the randomly selected sections. Data were reported as the number of antibody-labeling cells divided by the total area (mm²) of interest. All immunohistochemical analyses were performed by an experimenter blinded to the genotype of mice.

We also co-stained LRP1 antibody (Abcam) with NeuN (Millipore) or GFAP (Cell signaling Technology) antibody to localize and quantify the expression of LRP1 in the brain. The average intensity of LRP1 fluorescence in neurons or astrocytes was also quantified using Fiji. Manually contour neurons and astrocytes based on NeuN or GFAP fluorescence signals, respectively. The mean fluorescence intensity in the LRP1 channel was measured; the selection was then moved to a nearby area without a significant LRP1 fluorescence signal, and the mean fluorescence intensity in the LRP1 channel was measured as the background; the normalized fluorescence intensity for each cell was calculated as the LRP1 fluorescence signal minus the background.

Axonal injury is a common feature of CNS injury. APP is a type I transmembrane protein with potential effects on neurodegeneration. Upregulation of APP is observed after brain insults and is considered a marker of CNS axonal injury. As described above, the brain sections were incubated overnight with rabbit antibody against amyloid Precursor Protein, C-Terminal (A8717, Sigma Aldrich). We assessed the intensity of APP around Aβ in APP^{ki/ki} mice with different expressions of GPR109a. Take the Aβ plaque as the center of the circle, draw concentric circles at a spacing of 5μm radius, and then calculate the fluorescence intensity of APP at different distances from Aβ.

To detect GPR109a-RFP positive cells in the brain of APP^{wt} and APP^{ki/ki} mice, we co-

stained rabbit polyclonal anti-RFP antibody with mouse monoclonal anti-Iba1 (Millipore), mouse monoclonal anti-NeuN (Millipore) and mouse monoclonal anti-GFAP (Cell Signaling), respectively. And co-stained with mouse monoclonal anti-human A β antibody (Dako) to explore the relationship between GPR109a-positive cells and A β plaques.

5.3.16 Analysis of microglial morphology

For the analysis of microglial morphology, published protocols and Fiji Image J were used (FERNANDEZ-ARJONA et al., 2017; YOUNG, MORRISON, 2018). PFA-fixed brain tissues were embedded in Tissue-Tek O.C.T. Compound (Sakura Finetek Europe B.V., AJ Alphen aan den Rijn, the Netherlands) as described in section 3.3.10. The brain was cut in 30- μ m sagittal sections. After fluorescent staining with Iba-1 antibody and methoxy-X04 (or A β antibody), a total of 10 A β plaques/mouse were randomly selected from the cortex dorsal to the hippocampus and imaged under 40 \times objective with Z-stack scanning with 1 μ m of interval. We defined plaque-associated regions as the area within a quadruple radius of the A β core plaque. Thus, microglia inside or outside the fourfold plaque radius were classified as plaque-associated or microglia away from the plaque, respectively. The serial images were Z-projected with maximal intensity, 8-bit grayscale transformed, Unsharp-Mask filter and despeckle-treated, and binarized to obtain a black and white image. For analysis, choose the cells with complete nuclei and branches without overlapping with neighboring cells. Eliminated the single-pixel background noise and filled the gaps along with processes under the view of the original image of the cell. The processed image was skeletonized and analyzed with the plugin Analyze Skeleton (2D/3D) (<http://imagej.net/AnalyzeSkeleton>) for the total number of primary branches, length of all branches, and the number of branch endpoints of each microglia. The whole analysis was done blinded to genotypes.

The Sholl analysis was performed using the Fiji plugin Simple Neurite Tracer (<https://imagej.net/plugins/snt/>) and published protocols (LONGAIR et al., 2011; TAVARES et al., 2017) by counting the number of microglial branches at a certain distance from the soma. Total 10 microglia from three APP^{ki/ki}GPR109a^{-/-} mice, 14 microglia from three APP^{ki/ki}GPR109a^{+/-}, and 14 microglia from three APP^{ki/ki}GPR109a^{+/+} littermates were analyzed.

Concentric circles (radius) were set with 10 μm of the interval from the soma to the longest branch.

5.3.17 Phagocytosis assays *in vivo*

Microglial phagocytosis plays an important role in A β clearance. We investigated microglia A β phagocytosis *in vivo* based on published flow cytometry-based methods (LAU et al., 2021). This method enables direct comparison of A β phagocytic capacity between different microglial subpopulations.

(1) *In vivo* labelling of amyloid plaques

Methoxy-X04 (MeX04) is an A β dye that can penetrate the blood-brain barrier. After MeX04 is intraperitoneally injected into mice, it enters the brain and binds to the surface of A β plaques. If microglia engulf amyloid plaques actively, MeX04 will be internalized along with A β . Following that, flow cytometry analysis allows the ability of microglia to phagocytose A β to be quantified.

- a) Prepare MeX04 stock solution (10 mg/ml) by dissolving in DMSO and storing in aliquots (200 μl) at -80 °C.

MeX04 working solution (1 ml, freshly prepared)		
Reagent	Final concentration	Volume (μl)
MeX04 stock (10 mg/ml)	2 mg/ml	200
DMSO	n/a	300
0.9 % saline, pH 12.0	n/a	500
Total	n/a	1000

- b) Intraperitoneal injection with MeX04: the working solution was heated in a 37°C water bath for 5 minutes. Weighted mice and injected intraperitoneally with MeX04 working solution at a dose of 10 mg/kg. Then mice were sacrificed 3 hours after injection, and brain tissue was collected.

(2) Brain dissociation and microglia staining

- a) Brain dissociation: described as section 5.3.3.
- b) Microglia staining: stain the microglia cell suspension (300 μl) with Alexa Fluor[®] 647 anti-mouse/human CD11b (M1/70) antibody (1:200) for 1 hour at 4 °C with rotation. In addition, prepare unstained controls using AD transgenic model mice and non-transgenic wild-type mice to serve as fluorescence-minus-one controls.

(3) Flow cytometry

- a) Turn on the flow cytometer (BD FACSCanto II) and start the machine with start-up procedure.
- b) Create the following diagram in the template:
 - i. Side-scatter (SSC) versus forward-scatter (FSC) are applied to identify cell populations.
 - ii. Pulse width trigger versus FSC (to identify singlets).
 - iii. PB660 versus FSC-A (to identify CD11b signal).
 - iv. PB450 versus PB660 (to identify MeX04 signal).
- c) A negative signal was set for MeX04 using a non-transgenic mouse brain sample and a negative signal for CD11b using an unstained control sample.
- d) Each sample was sequentially performed and MeX04 signals were recorded for 10,000 microglia using BD Trucount absolute counting tubes (BD Biosciences)
- e) Using FlowJo to analyze the data, the following information was obtained:
 - i. Proportion of MeX04 positive microglia = proportion of A β phagocytic microglia.
 - ii. Mean fluorescence intensity of MeX04 = A β phagocytic capacity.

5.3.18 Reverse transcription and quantitative PCR for analysis of gene transcripts

Real-time reverse transcription PCR (RT-PCR) is the most sensitive quantitative PCR method for detecting the amount of PCR template (e.g., DNA or cDNA) in a PCR reaction. There are two types of real-time PCR: intercalator-based and probe-based. Both approaches necessitate using a thermocycler with a sensitive camera that continuously monitors the fluorescence in each well of the 96-well plate during the PCR Reaction. The intercalator-based method (also known as the SYBR Green method) requires using a double-stranded DNA dye in the PCR reaction, which binds to the newly synthesized double-stranded DNA and emits fluorescence. Probe-based real-time PCR (also known as TaqMan PCR) requires a pair of PCR primers (as in conventional PCR), an additional fluorescent probe, a 20-26 nucleotide oligonucleotide with both a reporter fluorochrome and a quenching dye attached. The probes bound only the DNA sequences between two specific PCR primers. Only a particular PCR product may give a fluorescent signal in TaqMan PCR. Therefore, the TaqMan approach is more precise and reliable than the SYBR green method.

The 7500 Fast Real-Time PCR System (Life Technologies) was used to run real-time PCR using SYBR green (Roche Applied Science) or Taqman® probes (Life Technologies) in our

study. Gene transcripts were quantified with our established protocol (QUAN et al., 2021; XIE et al., 2013a).

1. Isolation of total RNA from brain tissue or selected cells

- (1) Sample preparation: 0.5-mm-thick tissue slices sagittally excised from the right hemisphere (see above in Tissue Preparation section 5.3.3) were homogenized in 1 mL of Trizol (Invitrogen).
- (2) Phase Separation: For complete dissociation of the nucleoprotein complex, the homogenized sample was first incubated for 5 minutes at room temperature. Add 0.2 ml of chloroform per ml of Trizol Reagent used. Cover the sample tightly, shake vigorously by hand for 15 sec, and then incubate at room temperature for 3 min. Centrifuge the resulting mixture at $12,000 \times g$ for 15 min at 4 °C. The sample mixture was separated into 3 phases: a lower red organic phase (containing protein), an interphase (containing DNA), and a colourless upper aqueous phase (containing RNA).
- (3) RNA precipitation: Transfer the colourless aqueous phase to a fresh tube and mix with 0.5 ml isopropyl alcohol per ml Trizol Reagent used in Sample Preparation section. Allow the mixture to stand for 10 min at room temperature and then centrifuge at $12,000 \times g$ for 10 min at 4 °C. The precipitated RNA is the gel-like pellet on the bottom side of the tube.
- (4) RNA wash: remove the supernatant and wash the RNA pellet by adding 1 ml 75% ethanol. Mix by vortexing and centrifuge at $7,500 \times g$ for 5 min at 4 °C. If the RNA pellets float, perform the wash in 75% ethanol at $12,000 \times g$ for 5 min at 4 °C.
- (5) Redissolve the RNA: Invert the tube, allow the RNA precipitate to briefly dry, and then dissolve it in an appropriate volume of RNase-free water. One sample of brain tissue is typically added to 100 μ l.

2. Isolation of total RNA from selected cell

Total RNA was extracted from selected CD11b-positive or CD4-positive cells using the RNeasy Plus Mini Kit (Qiagen) by the following steps:

- (1) Selected cells were lysed in 700 μ l Buffer RLT Plus and vortexed for 30 s.
- (2) Transfer the homogenized lysate to a gDNA Eliminator spin column placed in a 2 ml collection tube.
- (3) Centrifuge for 30 s at $8,000 \times g$. Discard the column, save the flow-through and add an equal volume (700 μ l) of 70% ethanol, mixing completely by pipetting.

MATERIALS AND METHODS

- (4) Transfer up to 700 μl of the sample, including any precipitate, to a RNeasy spin column placed in a 2 ml collection tube. Close the lid, and centrifuge for 30 s at $8,000 \times g$. Discard the flow-through.
- (5) Add 700 μl Buffer RPE to the RNeasy Mini spin column (in a 2 ml collection tube). Close the lid, and centrifuge for 30 s at $8,000 \times g$. Discard the flow-through.
- (6) Add 500 μl Buffer RW1 to the RNeasy Mini spin column. Close the lid, and centrifuge for 30 s at $8,000 \times g$. Discard the flow-through.
- (7) Add 500 μl Buffer RW1 to the RNeasy Mini spin column. Close the lid, and centrifuge for 2 min at $8,000 \times g$. Discard the flow-through. And then centrifuge at full speed for 1 min to further dry the membrane.
- (8) Place the RNeasy spin column in a new 1.5 ml collection tube. Add 30 μl RNase-free water directly to the spin column membrane. Close the lid, and centrifuge for 1 min at $8,000 \times g$ to elute the RNA.

3. Genomic DNA degradation prior to RT-PCR

To purify RNA samples of trace genomic DNA contamination, RQ1 (RNA Qualified) RNase-Free DNase (Promega), a DNase I that degrades double- and single-stranded DNA by endocytosis, was used. The reaction was set up as follows:

Components	Volume/10 μl reaction
RNA sample in water	8 μl
RQ1 RNase-Free DNase 10 \times Reaction buffer	1 μl
RQ1 RNase-Free DNase	1 U/ μg RNA
Nuclease-free water	To a final volume of 10 μl

Incubate at 37 $^{\circ}\text{C}$ for 30 min, and then the reaction is terminated by the addition of 1 μl of RQ1 DNase Stop solution. DNase is then inactivated by heating at 65 $^{\circ}\text{C}$ for 10 minutes.

4. First Strand cDNA Synthesis

First-strand cDNA was synthesized by priming total RNA with hexamer random primers (Invitrogen) and using Maxima Reverse Transcriptase (ThermoFisher Scientific), which is an enzyme with diminished RNase H activity with high thermal stability and enhanced processivity, thus providing robust performance in first-strand cDNA synthesis. Add reaction components into a sterile, nuclease-free tube on ice in the indicated order:

Components	Volume/20 μl reaction
Total RNA	3 μg
Rndom primer (250 ng/ μl)	1 μl
dNTP mix (10 mM each)	1 μl

MATERIALS AND METHODS

Nuclease-free water	To a final volume of 15 μ l
Mix gently, centrifuge briefly and incubate at 65°C for 5 min. Chill on ice for 2 min, briefly centrifuge again and place on ice. And then add:	
5 \times RT buffer	4 μ l
Maxima H Minus Reverse Transcriptase	1 μ l (200 U)
Mix gently and centrifuge briefly.	
Incubate for 10 min at 25 °C followed by 30 min 50°C.	
Terminate the reaction by heating at 85°C for 5 min.	
The cDNA can be ready for use.	

5. Real-time quantitative PCR

For quantification of *tnf- α* , *il-1 β* , *mrc1*, *chi3l3*, *inos*, *ccl2*, *il-10*, *il-4*, *il-17a*, *ifn γ* , *foxp3*, *trem2*, *apoe*, *CX3CR1*, *p2ry12*, *clec7a*, *lpl*, *tgfb*, *itgax*, *gapdh* transcription level, real-time quantitative PCR with the Taqman® gene expression assays were performed using the 7500 Fast real-time PCR system (Applied Biosystems) with a DyNAmo™Flash Probe qPCR kit (Roche Applied Science).

Reaction setup for Taqman probe:

Components	Volume	Concentration
2 \times DyNAmo™ Flash Probe Master Mix	10 μ l	1 \times
Primer Mix (10 μ M)	1 μ l	0.5 μ M
50 \times ROX reference dye	0.06 μ l	0.3 \times
cDNA	1 μ l	max. 150 ng
ddH2O	Up to 20 μ l	

Select FAM-labelled detectors and set up reaction system cycling to run:

step	purpose	temp	time	cycles
1	Initial denaturation	95 °C	10 min	1
2	Denaturation	95 °C	10 s	45
	Annealing + extension	60 °C	30 s	

By detecting the free FAM dye cleaved from the Taqman® probe, the amount of double-stranded PCR product generated in each cycle may be determined. The threshold cycle (Ct) value for each gene tested in the replicate PCR was normalized to the Ct value of the *gapdh* RNA control from the same cDNA preparations. The ratio of transcription of each gene was calculated as $2^{-\Delta Ct}$, where ΔCt is the difference Ct (*gapdh*) - Ct (test gene).

5.3.19 Statistical analysis

Data were presented as mean \pm SEM. For multiple comparisons, we used one-way or two-way ANOVA followed by Bonferroni, Tukey, or Dunnett T3 *post hoc* test (dependent on the

MATERIALS AND METHODS

result of Levene's test to determine the equality of variances). Two independent-samples Students *t*-test was used to compare means for two groups of cases. All statistical analyses were performed with GraphPad Prism 8 version 8.0.2. for Windows (GraphPad Software, San Diego, USA). Statistical significance was set at $p < 0.05$.

6. RESULTS

6.1 GPR109a specifically expresses in A β -associated microglia

We quantified the transcription of genes encoding *gpr41*, *gpr43*, *gpr109a*, and lactate receptor (*gpr81*) in microglia isolated from 9-month-old APP/PS1-transgenic (tg) and wild-type (wt) littermate mice. As shown in Fig. 6.1 A, only the *gpr109a* gene but not *gpr41*, *gpr43*, or *gpr81* gene is transcribed at a high level in microglia, and the transcription of *gpr109a* is up-regulated in APP-transgenic mice than wild-type controls (Fig. 6.1 A; t-test, $p < 0.05$). We then used the BAC-transgenic mouse line (*Gpr109a^{mRFP}*), in which the *Gpr109a* promoter controls the expression of monomeric red fluorescent protein (mRFP), to determine the expressions of GPR109a in various brain parenchymal cells. We observed that in APP^{wt}GPR109a^{mRFP} mice, mRFP is expressed only in Iba-1-positive cells but not in astrocytes and neurons (Fig. 6.1 B). And the mRFP-positive cells are recruited to A β plaques (Fig. 6.1 C).

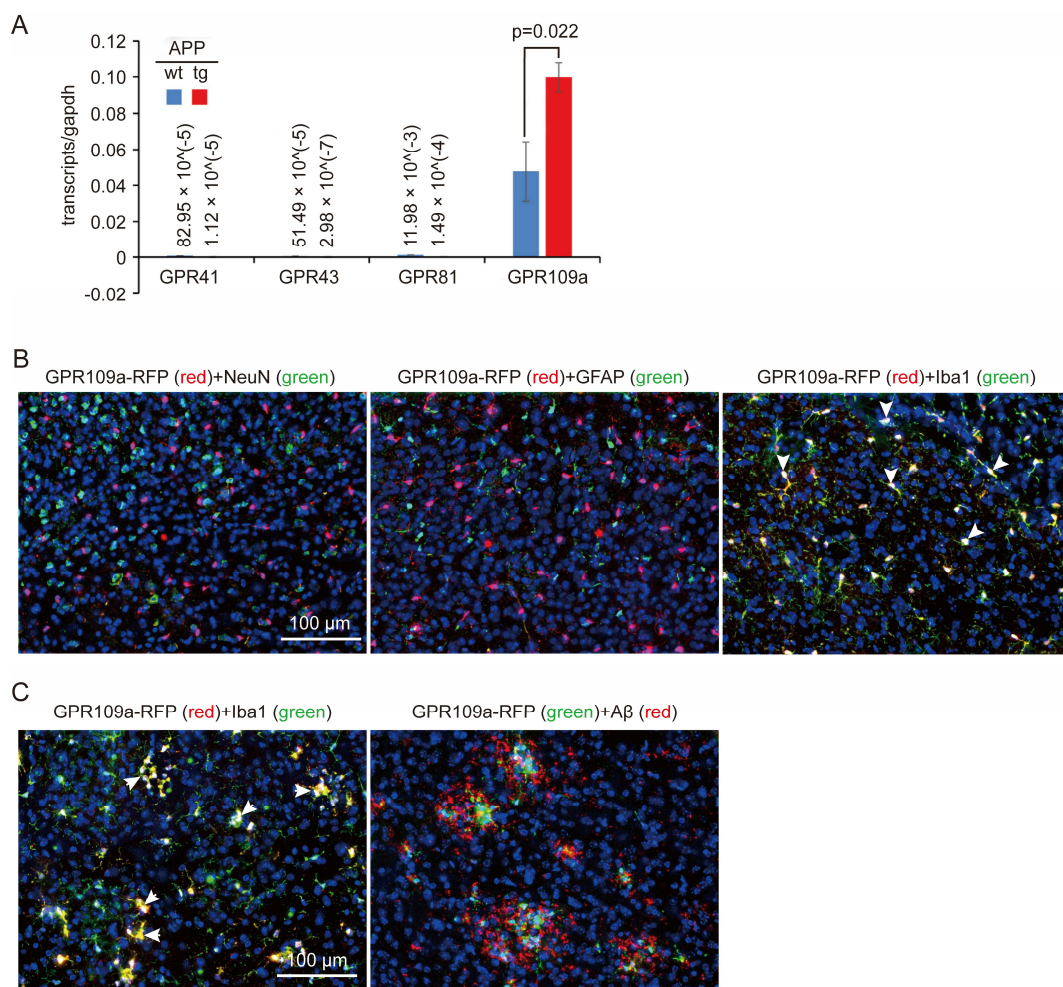


Fig. 6.1, GPR109a-positive microglia are recruited to A β deposits. Adult microglia, isolated from brains of 9-month-old APP/PS1 transgenic (tg) and wild-type (wt) littermate mice with magnetic beads-conjugated CD11b antibodies, were analysed for the transcription of *gpr41*, *gpr43*, *gpr109a* and *gpr81* genes with real-time PCR (A, t-test, $p < 0.05$; $n = 5$ per group). Brain sections from 3-month-old GPR109a-reporter mice were co-stained with fluorescence-labelled antibodies against RFP and NeuN, GFAP, and Iba1 (B). GPR109a-reporter mice were further mated with APP-knock-in AD mice. RFP co-staining with A β , we clearly observed that GPR109a-expressed cells are recruited specifically to A β deposits (C).

6.2 Deficiency of GPR109a ameliorates cognitive deficits in APP-knock-in mice

To investigate the effects of GPR109a on AD pathologies, we mated *App*^{NL-G-F/NL-G-F} mice (APP^{ki/ki}) with *Gpr109a* knockout mice (GPR109a^{-/-}) (TUNARU et al., 2003). Ten-month-old APP-knock-in littermate mice with different expressions of GPR109a were evaluated for cognitive function with the Y maze test (Fig. 6.2 A). Consistent with established research (SAITO et al., 2014), our experiments found that APP^{ki/ki} mice exhibit significantly impaired cognitive function with a reduced alternation in the Y maze test (Fig.6.2 B; one-way ANOVA, $p=0.006$). Interestingly, deficiency of GPR109a in APP^{ki/ki} mice increases the spontaneous alternation in a gene dose-dependent manner, which suggests that deficiency of GPR109a prevents the cognitive decline of AD mice (Fig.6.2 C; two-way ANOVA, $p=0.004$). Simultaneously, APP wild-type (*App*^{NL-F/NL-F}, APP^{wt}) littermate mice with different GPR109a expressions shown no significant differences in the alternation of the Y maze test (Fig.6.2 B; two-way ANOVA, $p>0.05$). The locomotion time has no difference between APP^{ki/ki}GPR109a^{-/-}, APP^{ki/ki}GPR109a^{+/-}, and APP^{ki/ki}GPR109a^{+/+} mice (Fig. 6.2 D; two-way ANOVA, $p>0.05$).

Open field test examines general locomotor activity, anxiety, and willingness to explore in animals (Fig. 6.2 E). In our experiments, deletion of GPR109a in either APP^{wt} or APP^{ki/ki} mice does not alter the frequency and duration in the central area of the open field test (Fig. 6.2F, G; two-way ANOVA, $p>0.05$). In conclusion, these behaviour test results suggest that GPR109a deficiency improves cognitive performances in APP^{ki/ki} mice but does not affect APP^{wt} mice. And knockout of GPR109a neither affect locomotion nor induce anxiety-like behaviour in APP^{ki/ki} mice.

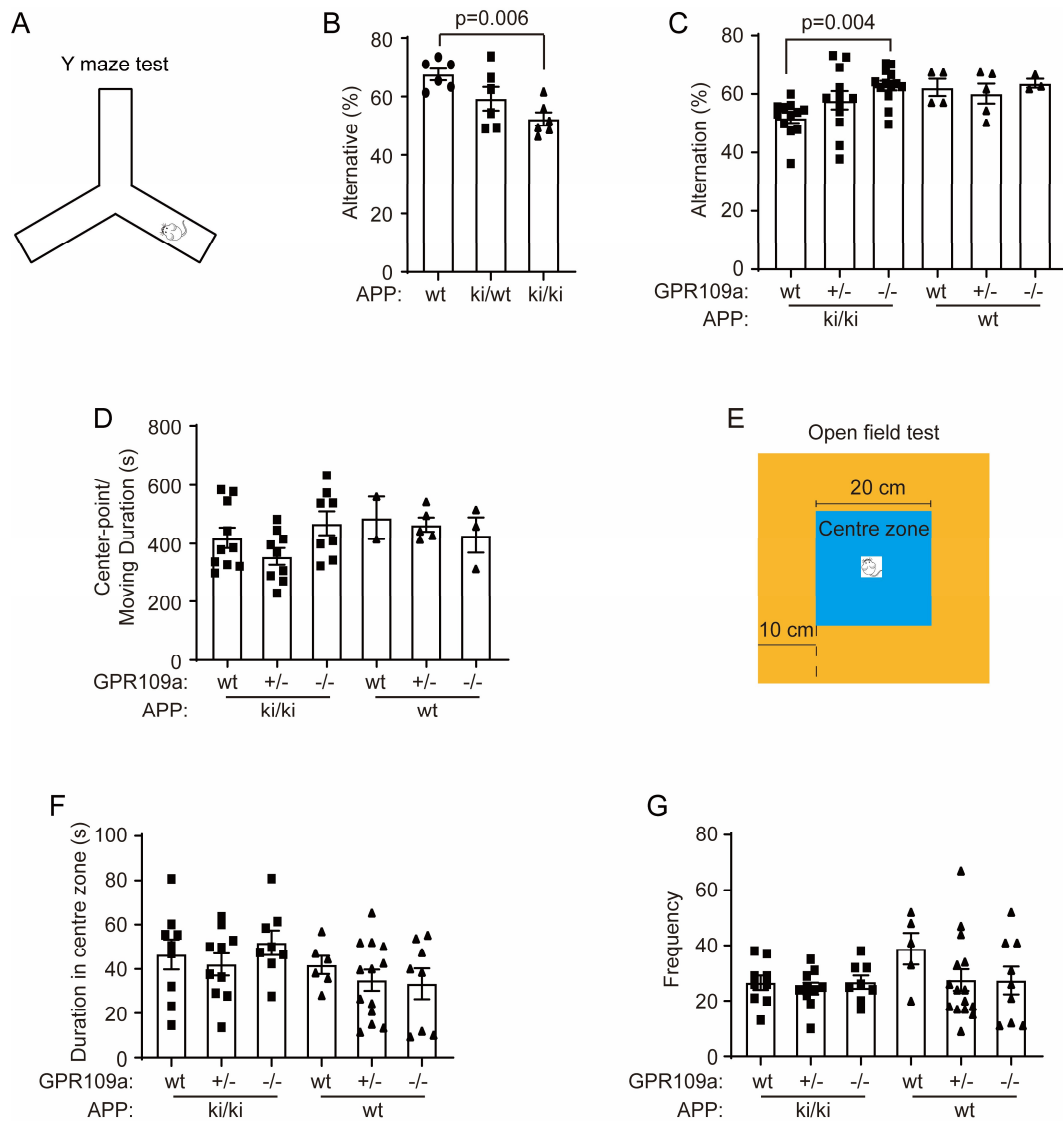


Fig. 6.2, Deficiency of GPR109a improves cognitive function of APP-KI AD mice. Ten-month-old APP-KI littermate mice with homozygous (-/-) and heterogeneous (+/-) knockout of GPR109a gene and wild-type (+/+) were analysed for cognitive function with Y maze (A). Significant reduction in the spontaneous alternation of APP^{ki/ki} mice in the Y-maze (B, one-way ANOVA followed by *Bonferroni post hoc test*, n = 6 per group). Deficiency of GPR109a has the potential to increase the alteration of AD mice in gene dose-dependent manner (C, two-way ANOVA followed by *Bonferroni post hoc test*, n ≥ 3 per group), but not affected movement (D, two-way ANOVA followed by *Bonferroni post hoc test*). Open field test (E). Deficiency of GRP109a does not change the duration in the centre zone, and frequency enters to centre zone in the open field test (F and G, one-way ANOVA followed by *Bonferroni post hoc test*, n ≥ 4 per group).

6.3 Deficiency of GPR109a reduces synaptic impairment of APP-knock-in AD mice

We measured the levels of synaptic-structure proteins Munc18-1, synaptophysin, SNAP25, and PSD-95 in the brain homogenates of 10-month-old APP wild-type and APP^{ki/ki} littermate

mice using Western blot analysis. As shown in Fig. 6.3.1 A-E, protein levels of Munc18-1 and PSD-95 in APP^{ki/ki} mice were significantly lower than those in APP^{wt} littermates (Fig. 6.3.1 B and C; one-way ANOVA, $p < 0.05$). Interestingly, deficiency of GPR109a reverses the loss of synaptic structural proteins induced by APP knock-in (Fig. 6.3.2 A-F; one-way ANOVA, $P < 0.05$). The amounts of Munc18-1, SNAP25, and PSD-95 proteins are significantly higher in brains from APP^{ki/ki}GPR109a^{-/-} mice than APP^{ki/ki}GPR109a^{+/-} and APP^{ki/ki}GPR109a^{+/+} control mice (Fig. 6.3.2 A-F; one-way ANOVA, $p < 0.05$). At the same time, there are no significant differences in the amount of SNAP25, Munc18-1, and PSD-95 between APP^{wt} GPR109a^{+/+} and APP^{wt}GPR109a^{-/-} (Fig. 6.3.2 G, H; one-way ANOVA, $p > 0.05$).

Besides the impairment of synaptic structural proteins, neuropathology is also associated with axonal dystrophy in the brain parenchyma, which can contribute to neuronal degeneration. Thus, we measured the volume of dystrophic neurites around individual amyloid plaques in brain sections from 10-month-old APP-knock-in mice with different expressions of GPR109a. Brain sections were co-stained with methoxy-X04 and an antibody against the C-terminal of APP, and the intensity of APP-positive signals were quantified at different distances from the plaque, with concentric circles for a 5 μm spacing. As shown in Fig. 6.3.2 I and J, abundant dystrophic neurites are accumulated around A β plaques in APP^{ki/ki} mice, while deletion of GPR109a reduces dystrophic neurites around A β plaques in a gene-dependent manner (Fig. 6.3.2 I and J; two-way ANOVA, $p < 0.05$).

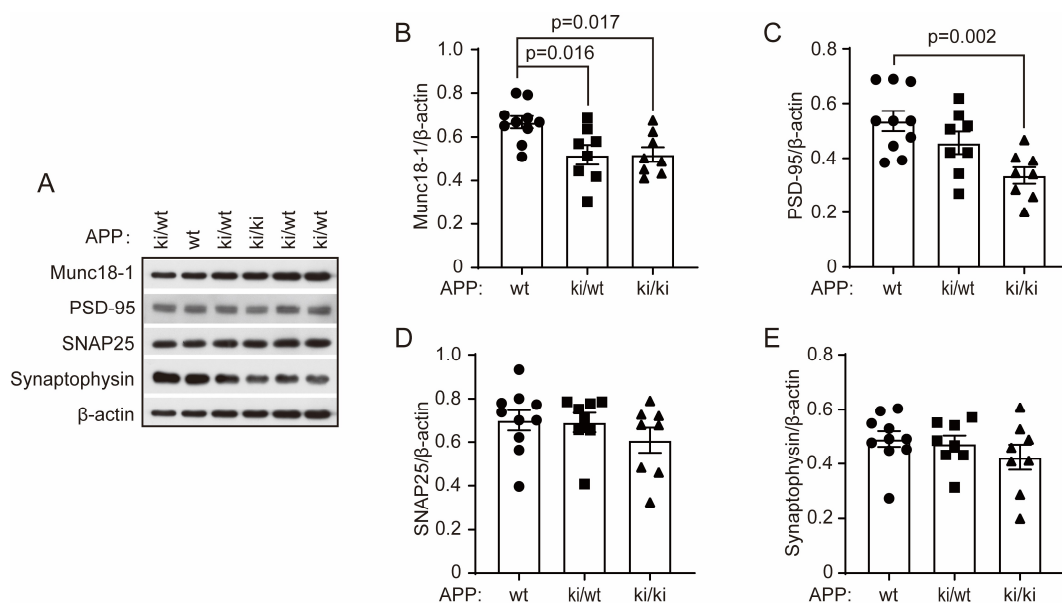


Fig. 6.3.1, Synaptic proteins decrease in APP-knock-in mice. Western blotting was used to detect the amounts of synaptic structure proteins in brain tissues from 10-month-old APP^{ki/ki}, APP^{ki/wt}, and APP^{wt} mice. Overexpression of APP significantly decreases Munc18-1 and PSD-95 amounts (A-C; one-way ANOVA followed by *Bonferroni post hoc test*, $p < 0.05$; $n \geq 8$ per group). However, the protein levels of SNAP25 and synaptophysin does not changed significantly (D and E; one-way ANOVA followed by *Bonferroni post hoc test*, $p > 0.05$; $n \geq 8$ per group).

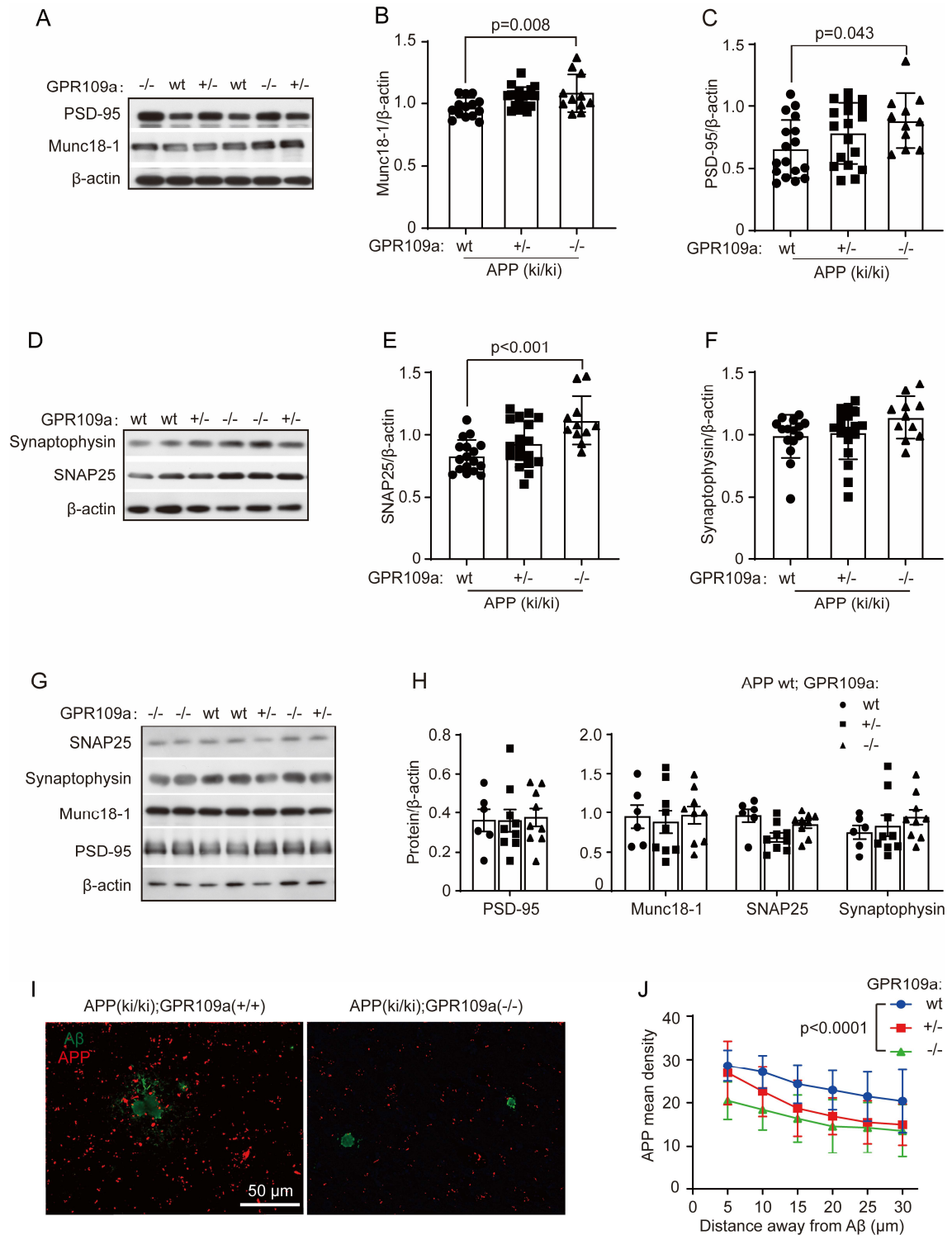


Fig. 6.3.2, Deletion of GPR109a reverses AD-associated loss of synaptic proteins and axonal dystrophy in APP^{ki/ki} mice. Western blotting was used to detect the amount of synaptic structure proteins, Munc18-1, SNAP25, synaptophysin, and PSD-95 in the 9-month-old APP^{ki/ki} and APP^{wt} mice (A-H). GPR109a deficiency are associated with higher levels of Munc18-1, PSD-95, and SNAP25 in the APP^{ki/ki} mice (A-F; one-way ANOVA followed by *Bonferroni post hoc test*; $n \geq 11$ per group), but not in the APP^{wt} mice (G and H, two-way ANOVA followed by *Bonferroni post hoc test*; $n \geq 6$ per group). GPR109a deficiency reduces plaque-associated axonal dystrophy (I and J). Visualization of amyloid-precursor-protein, C-Terminal-immunolabeled axonal dystrophy (red) around plaques in APP-KI mice brain (I). Quantification of dystrophy volume in APP^{ki/ki} mice with different *Gpr109a* genotypes (J; two-way ANOVA followed by *Bonferroni post hoc test*; $n \geq 3$ mice for each group, more than 8 plaques were analysed in each mouse).

6.4 Deficiency of GPR109a reduces A β load in the brain of APP-knock-in mice

Since A β accumulation is a key factor contributing to AD development, we further analysed whether GPR109a deficiency affect amyloid pathologies in the APP^{ki/ki} mice. We stained brain sections from 10-month-old APP^{ki/ki}GPR109a^{-/-}, APP^{ki/ki}GPR109a^{+/-}, and APP^{ki/ki}GPR109a^{+/+} littermate mice with methoxy-X04, which specifically recognizes the β -sheet secondary structure of A β . And quantitative results revealed that deficiency of GPR109a dramatically decreases the area of methoxy-X04 staining-positive A β plaques in both hippocampus and cortex of APP^{ki/ki} mice in a gene dose-dependent manner (Fig. 6.4.1 A, B; one-way ANOVA, $p > 0.05$). We then calibrated and quantified the volume of A β based on the volume of the assessed tissue using standard immunohistological and stereological Cavalieri methods. The immunoreactive A β volume in APP^{ki/ki}GPR109a^{-/-} mice are 2.7 ± 0.14 % positive in the cortex and 1.9 ± 0.78 % in the hippocampus respectively, which are significantly lower than that of APP^{ki/ki}GPR109a^{+/+} mice (3.3 ± 0.15 % in the cortex, $p < 0.0001$; 2.6 ± 0.86 % in the hippocampus; Fig. 6.4.1 C, D; one-way ANOVA, $p = 0.0014$).

We further measured the amount of differentially A β aggregates in brain homogenates by Western blotting with human A β -specific antibodies according to established biochemical methods (QUAN et al., 2021). Consistent with our histological results, we observed that all monomeric, dimeric, and trimeric A β are significantly decreased in APP^{ki/ki}GPR109a^{-/-} than in APP^{ki/ki}GPR109a^{+/-}, and APP^{ki/ki}GPR109a^{+/+} (Fig. 6.4.2 A-D; one-way ANOVA, $p < 0.05$). Protein levels of APP and its fragment C99, derived from cleavage of β -secretase, are not altered by deficiency of GPR109a (Fig. 6.4.2 E, F; one-way ANOVA, $p > 0.05$). Similarly, deletion of GPR109a markedly decrease the concentrations of A β 40 in TBS-soluble, and both

A β 40 and A β 42 in TBS plus 1% Triton X-100 (TBS-T)-soluble brain homogenates from APP^{ki/ki}GPR109a^{-/-} mice as compared to APP^{ki/ki}GPR109a^{+/+} mice (Fig. 6.4.3 A, D, E; one-way ANOVA, $p < 0.05$). However, neither A β 40 nor A β 42 are affected by GPR109a in Guanidine-hydrochloride-soluble brain homogenates enriched with high-molecular-weight aggregated A β (Fig. 6.4.3 G, H; one-way ANOVA, $p > 0.05$). Recently, several studies have demonstrated that the A β 42/40 ratio may more accurately reflect the changes in A β metabolism in AD pathogenesis than A β protein levels alone. According to our experiments, A β 42/40 ratio is decreased more than 2-fold in TBST soluble homogenate of APP^{ki/ki}GPR109a^{-/-} compared to APP^{ki/ki}GPR109a^{+/-}, and APP^{ki/ki}GPR109a^{+/+} mice (Fig. 6.4.3 E; one-way ANOVA, $p < 0.05$).

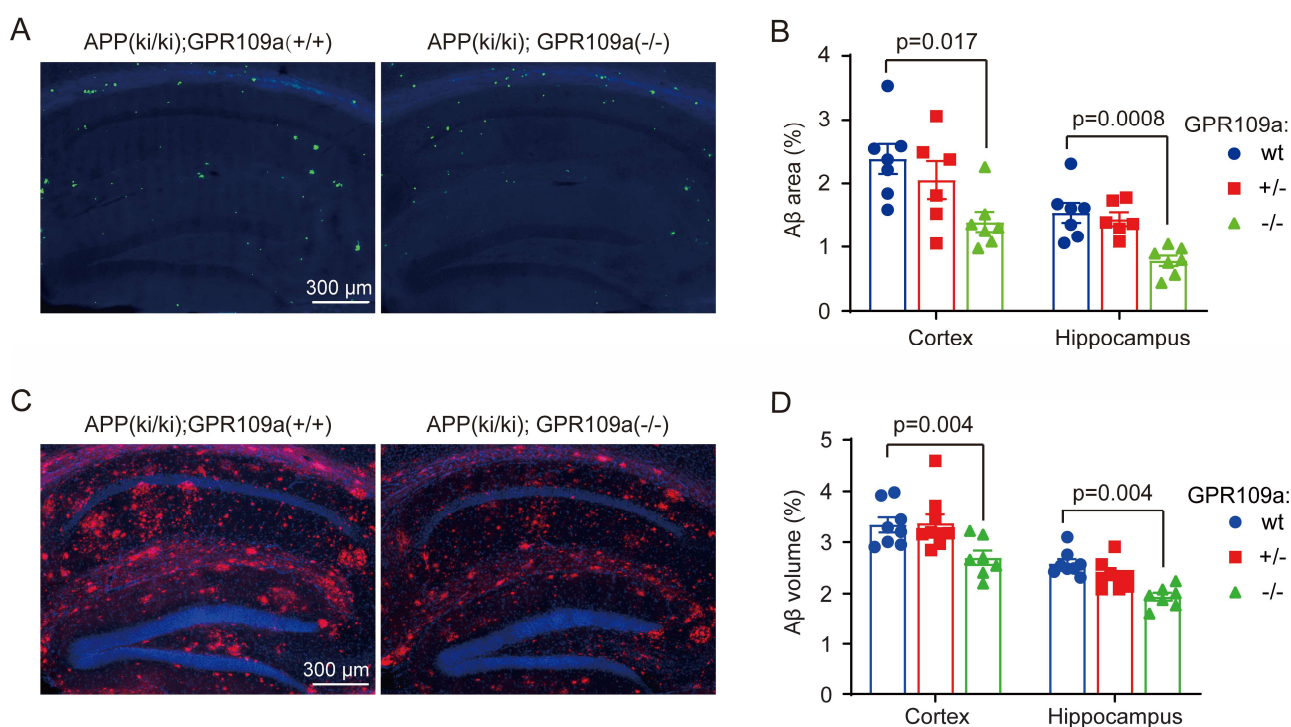


Fig. 6.4.1, Deficiency of GPR109a decreases A β load in APP^{ki/ki} mouse brain. Ten-month-old APP^{ki/ki} mice with different GPR109a expressions were stained cerebral A β with methoxy-X04 and A β antibody (clone D12B2, Cell Signaling Technology). Brain sections were first stained with methoxy-X04 and imaged with MicroLucida (A). The area of A β plaques were quantified and adjusted by the area of analysed brain tissues (B). Brain sections were further stained with human A β -specific antibody (C). The volume of immune reactive A β deposits in the hippocampus and cortex were estimated with the stereological Cavalieri method and adjusted by the volume of analysed tissues (D). Homozygous deletion of GPR109a significantly reduces the A β level both in the cortex and hippocampus (B and D, two-way ANOVA followed by *Bonferroni post hoc test*; $n \geq 7$ for each group).

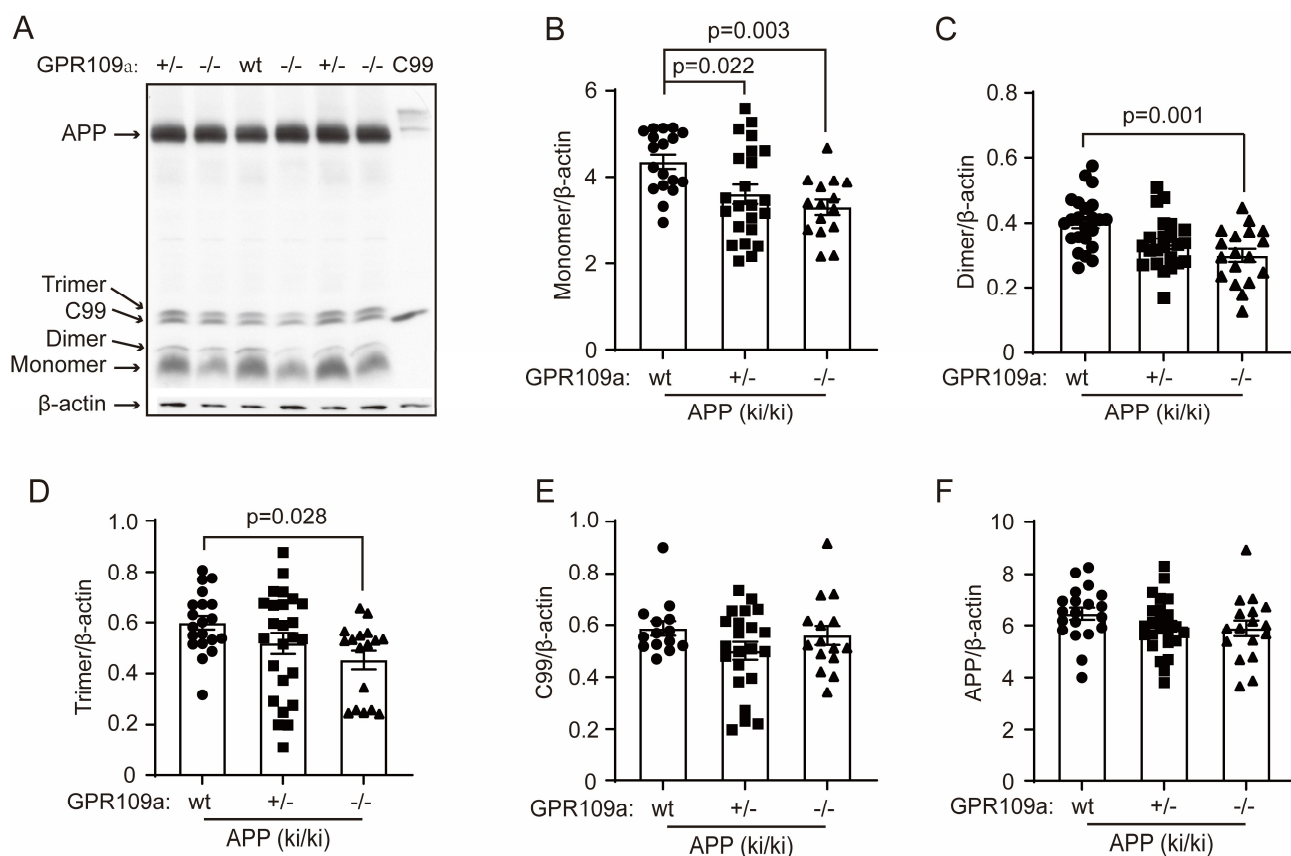


Fig. 6.4.2, Deficiency of GPR109a reduces A β monomers and oligomers in the brain of APP-knock-in mice. Brain lysate was prepared from 10-month-old APP^{ki/ki} littermate mice with homozygous (-/-), heterozygous (+/-) knockout of GPR109a gene and wild-type (+/+). Quantitative Western blot was used to detect monomer, dimer and trimer of A β , C99 and APP (A). Deficiency of GPR109a reduces monomeric (B), dimeric (C) and trimeric (D) A β , but not C99 (E) and APP (F) in the brain (One-way ANOVA followed by *Bonferroni post hoc test*, $n \geq 15$ per group). Cell lysate prepared from C99 fragment-overexpressing SH-SY5Y cells was used to identify the signal of C99 in Western blot.

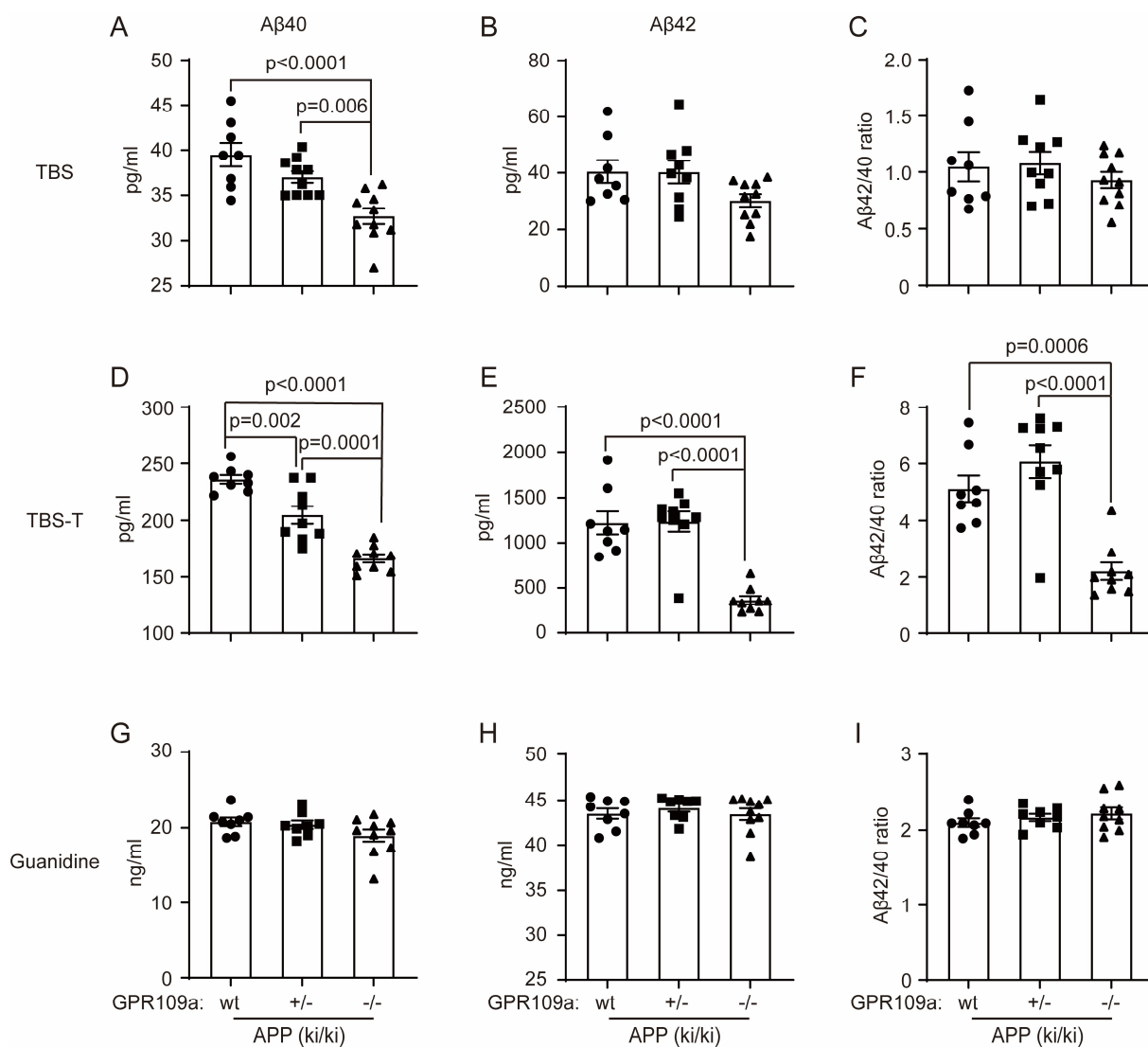


Fig. 6.4.3, Deficiency of GPR109a reduces Aβ42 and Aβ40 amounts in the brain of APP-knock-in mice. The concentration of Aβ40 and Aβ42 in the brain TBS, TBS-T, and Guanidine-soluble fractions were determined by Aβ40 and Aβ42 (Invitrogen) sandwich ELISA. Brain lysate was prepared from 10-month-old APP^{ki/ki} littermate mice with homozygous (-/-), heterozygous (+/-) knockout of GPR109a gene and wild-type (+/+). Brain TBS-soluble Aβ40 (A) decreases in GPR109a gene-dependent manner, whereas Aβ42 (B) and Aβ42/40 ratio (C) are unaffected by the expression of GPR09a. The concentration of Aβ40 (D), Aβ42 (E), and Aβ42/40 ratio in APP^{ki/ki}GPR109a^{-/-} mice brain TBS-T-soluble are significantly lower than APP^{ki/ki}GPR109a^{wt} mice. In the brain Guanidine-soluble, neither the amounts of Aβ40 (G) and Aβ42 (H) nor Aβ42/40 ratio is changed by the deletion of GPR109a (One-way ANOVA followed by *Bonferroni post hoc test*, n ≥ 8 per group).

6.5 Deficiency of GPR109a does not change neuroinflammatory activation in APP-knock-in mice

Microglia play two-edged sword in AD pathogenesis. On the one hand, microglial inflammatory activation exacerbates neurodegeneration (HENEKA et al., 2015) by releasing neurotoxic inflammatory mediators, such as TNF- α and IL-1 β ; on the other hand, they facilitate cerebral A β clearance through internalizing A β . We investigated the effects of GPR109a deficiency on neuroinflammation in APP^{ki/ki} mice by counting the microglial number and measuring inflammatory gene transcripts using our previously established method (QUAN et al., 2021). As shown in Fig. 6.5 A-B, the deficiency of GPR109a does not affect the number of Iba1 immunoreactive cells (representing microglia) either in the cortex or hippocampus.

We further measured transcripts of M1-inflammatory genes (*tnfa*, *il-1 β* , *inos*, and *ccl-2*) and M2-inflammatory genes (*il-10*, *chi3l3*, and *mrc1*) in the brains of 10-month-old APP^{ki/ki} littermate mice with different expressions of GPR109a gene and wild-type (+/+). In accordance with the immunohistochemical staining results, the transcription of inflammatory genes are not changed by GPR109a deficiency.

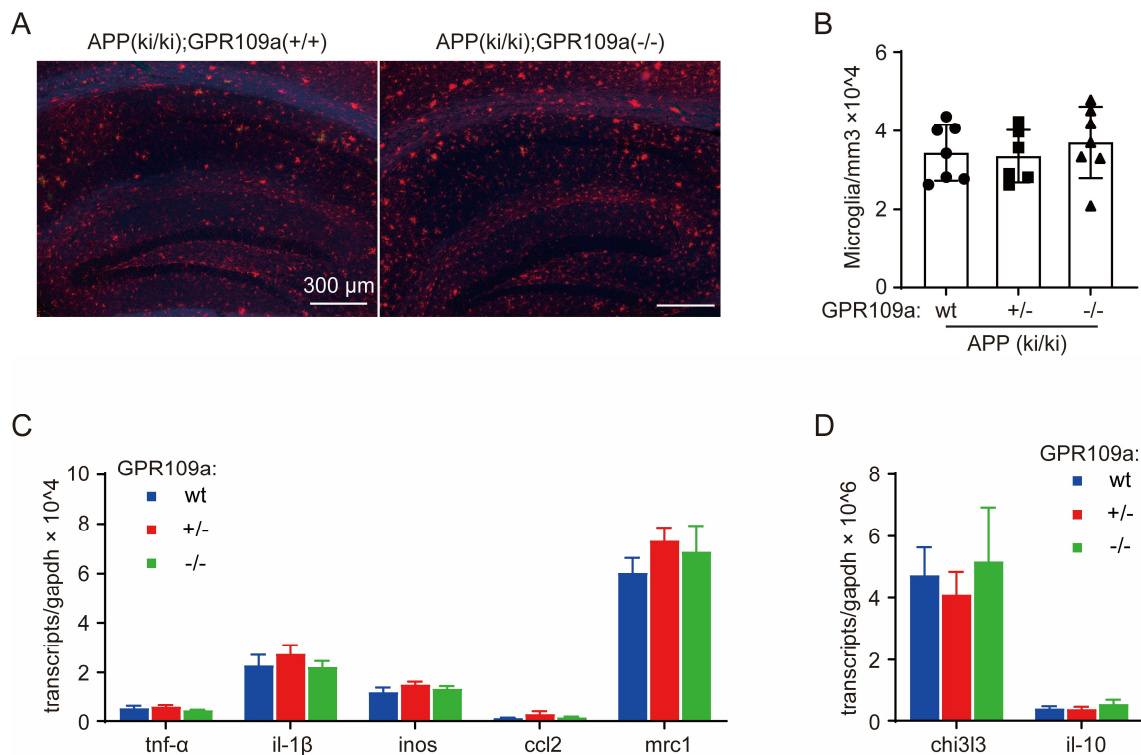


Fig. 6.5, Deficiency of GPR109a does not significantly change microglia-mediated inflammatory activation in APP-KI mouse brain. Ten-month-old APP-knock-in littermate mice with different expressions of GPR109a were used to assess inflammatory activation. Microglial cell numbers were estimated with a stereological method, Optical Fractionator, after immunohistochemical staining of Iba-1 (A and B; One-way ANOVA followed by *Bonferroni post hoc* test, $p > 0.05$; $n \geq 5$ per group). Inflammatory gene transcripts were measured by quantitative RT-PCR (C, D). The deficiency of GPR109a neither alter the number of Iba1-immunoreactive cells nor the transcription of inflammatory genes (One-way ANOVA followed by *Bonferroni post hoc* test, $p > 0.05$; $n \geq 7$ per group).

6.6 Deficiency of GPR109a regulates morphological changes of A β plaque-associated microglia in APP-knock-in mice

Microglial morphology is an important determinant of their activity, we investigated the morphological characteristics of plaque-associated microglia in the brain of 9-month-old APP-knock-in mice with different expressions of GPR109a. We evaluated the number of branches, endpoints, and length of branches of microglia. In GPR109a-deficient mice, plaque-associated microglia exhibited significantly more dendritic branches, as shown in Fig. 6.6 A-C, with a remarkable increase in both the number of branches and endpoints (Fig. 6.6 B and C; One-way ANOVA, $p < 0.05$). In addition, we also observed that GPR109a deficiency results in an obvious increase in the total length of dendritic branches of each microglia, but not in the average length of each branch (Fig. 6.6 D, E). We also analyzed microglia far from A β plaques (beyond the edge of 4-fold plaque radius); in contrast, there were no differences in the number of branches and endpoints or branch lengths in mice with different GPR109a expressions (data not shown).

Sholl analysis was further used to describe microglia branches. The Sholl intersection profile calculates the number of intersections of a hypothetical circle with a specific radius centred on the soma with the dendrites, which can digitize the complexity of the dendrites as one-dimensional data. As shown in Fig. 6.6 A, F, in APP^{ki/ki}GPR109a^{-/-} mice, there is a significant increase in the intersection frequency of concentric circles with microglia branches, especially at about 50 pixels from the soma. Collectively, our findings imply that microglia in APP^{ki/ki}GPR109a^{-/-} mice exhibit a ramified morphology with increased processes, the increase in total branch length is probably due to the increased number of branches.

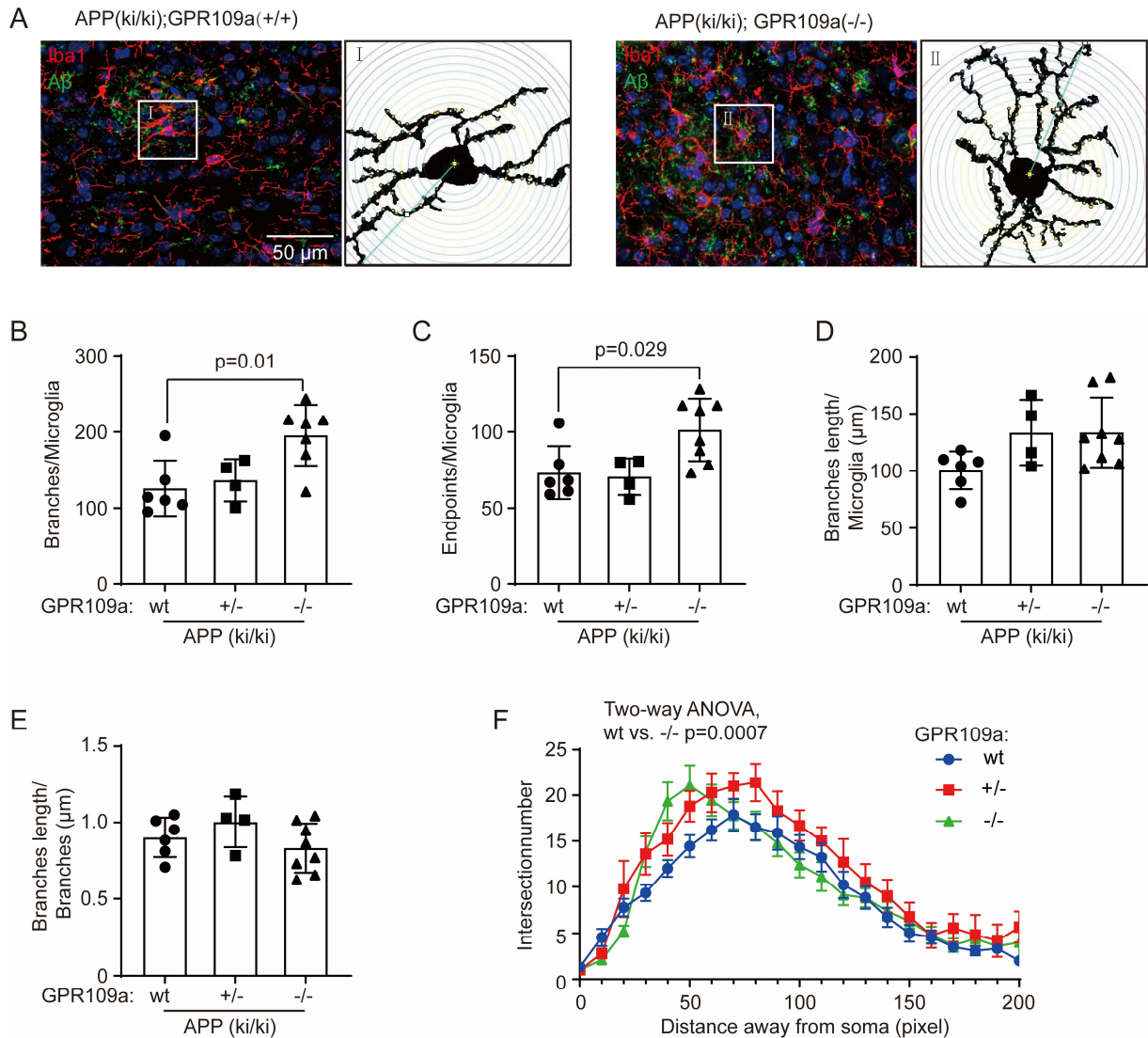


Fig. 6.6, Morphometric analysis of plaque-associated microglia. Brains from APP^{ki/ki}GPR109a^{-/-}, APP^{ki/ki}GPR109a^{+/-}, and APP^{ki/ki}GPR109a^{+/+} mice were fixed, sectioned, subjected to microscopy and analysis of microglia morphology contacted A β deposits. The brain sections were stained with antibodies against human A β (green) and Iba-1 (red) antibody. Maximum intensity projections of microscopy z-stack images illustrating representative microglia morphology in brain sections of 9-month-old GPR109a wild-type and GPR109a-deficient APP^{ki/ki} mice (A). Quantitative analysis of the number of microglia branches (B), endpoints (C), total branch length (D), and the average length of branches (E). GPR109a deficiency significantly increases the number of branches and endpoints of microglia (B and C, one-way ANOVA followed by *Bonferroni post hoc* test, $p < 0.05$; $n \geq 4$ per group). Sholl analysis of microglia was performed by placing concentric circles at 10 pixels intervals and centred on the soma (A). Quantification of the number of Sholl intersections along the microglia processes at all distances from soma revealed significant differences between the microglia from APP^{ki/ki}GPR109a^{-/-}, APP^{ki/ki}GPR109a^{+/-}, and APP^{ki/ki}GPR109a^{+/+} mice, especially in the circles ranging from 40 to 80 pixels (F, two-way ANOVA followed by *Bonferroni post hoc* test; 10 microglia from 3 GPR109a knockout mice, 14 microglia from 3 GPR109a heterogenous mice, and 14 microglia from 3 GPR109a wild-type mice were analysed; $p < 0.05$).

6.7 Deficiency of GPR109a shifts microglial activation to homeostatic profile

Recently, the disease-associated microglia (DAM or MGnD) phenotype has been defined. This signature is characterized by the repression of homeostatic genes and the induction of pro-inflammatory genes. We continued to detect transcripts of signature genes in selected CD11b⁺ microglia from GPR109a-deficient and wild-type APP-knock-in mice. We observed, in 9-month-old AD mice, that deletion of GPR109a: 1) significantly increases the transcription of *trem2* gene, which might promote microglia to respond to changes in the extracellular environment (Fig. 6.7 A; one-way ANOVA, $p < 0.05$); 2) significantly upregulates the transcription of *cx3cr1*, *p2ry12*, and *clec7a* genes (Fig. 6.7 C-E; one-way ANOVA, $p < 0.05$); and 3) does not change transcription of pro- nor anti-inflammatory genes, e.g. *tnf- α* , *il-1 β* , *ccl2*, *itgax* and *il-10* genes (Fig. 6.7 H - I; one-way ANOVA, $p > 0.05$). The upregulation of *cx3cr1*, *p2ry12* and *clec7a* genes is consistent with an increase in total process length in microglia from GPR109a-deficient mice.

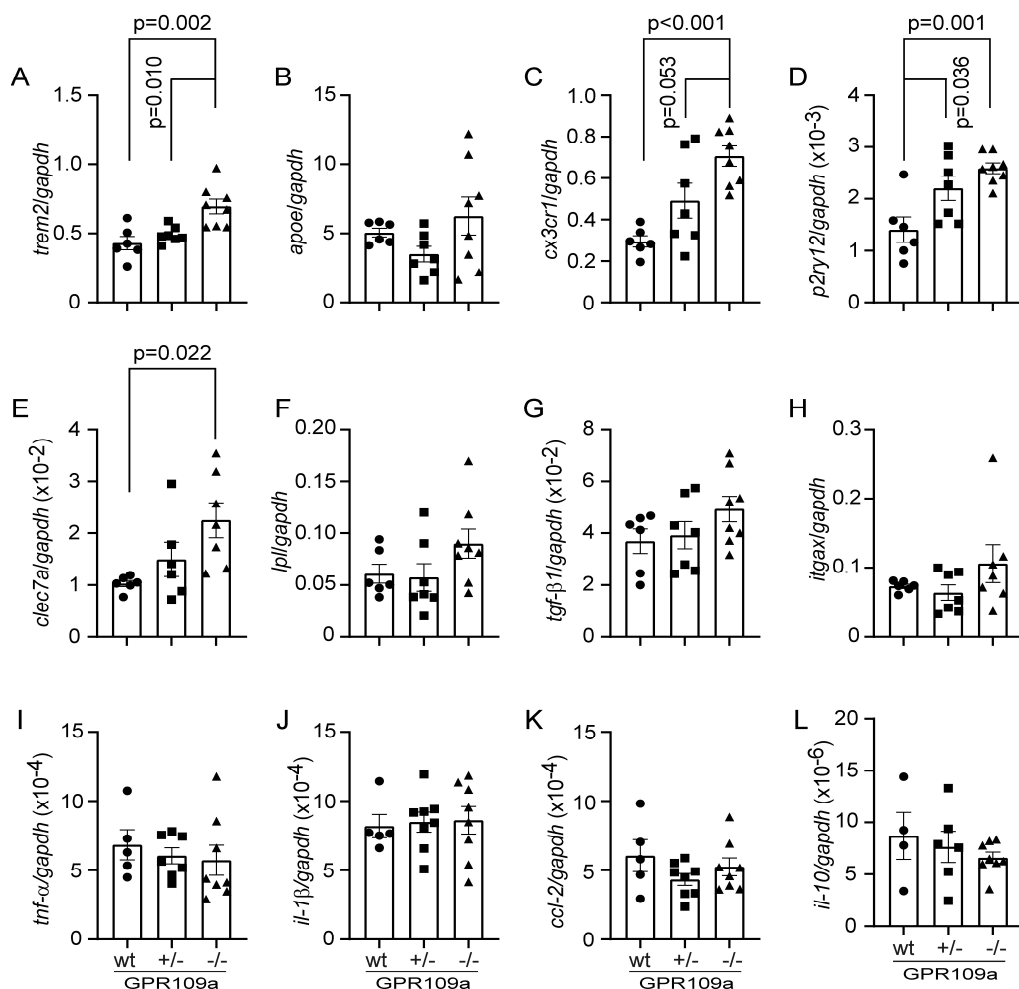


Fig. 6.7, Deletion of GPR109a shifts microglial activation to homeostatic profile in 9-month-old APP-knock-in mouse brain. Adult microglia were isolated with magnetic beads-conjugated CD11b antibodies from 9-month-old APP-knock-in mice with different expressions of GPR109a. The gene transcripts in microglia were detected with real-time PCR (one-way ANOVA followed by *Bonferroni post hoc* test; $n \geq 5$ per group).

6.8 Deficiency of GPR109a increases microglial recruitment around the plaques and promotes microglial A β phagocytosis

Microglial activation damages neurons by releasing neurotoxic substances and rescues neurons by cleaning A β in the brain. It has been reported that microglia clustering around A β deposits might form a physical barrier and compact A β into dense deposits, protecting against local neurite damage. Thus, we investigated the relationship between microglia and A β deposits by co-staining brain sections of 9-month-old APP^{ki/ki} mice with Iba-1-specific antibody and methoxy-X04. Immunofluorescent (IF) images revealed that abundant microglia are recruited around A β plaques in APP-knock-in mice (Fig. 6.8 A). Quantification of the microglia surrounding A β plaques revealed that there are considerably more microglia recruited around A β deposits in APP^{ki/ki}GPR109a^{-/-} mice ($2.34 \pm 0.1 \times 10^4$ cells/mm²) than in APP^{ki/ki}GPR109a^{+/-} ($1.79 \pm 0.06 \times 10^4$ cells/mm²) and APP^{ki/ki}GPR109a^{+/+} ($1.60 \pm 0.11 \times 10^4$ cells/mm²) mice (Fig. 6.8 B; one-way ANOVA, $p < 0.05$).

A β uptake by microglia is an important mechanism to remove A β in the AD brain. We used a flow cytometry-based approach to investigate whether the GPR109a deficiency facilitates microglial A β internalization in APP^{ki/ki} mice (LAU et al., 2021). Flow cytometry analysis showed that in 10-month-old APP^{ki/ki} mice without expression of GPR109a, 10.9 ± 0.89 % of microglia are methoxy-X04 positive, significantly higher than 7.9 ± 0.42 % in GPR109a wild-type mice, the proportion of methoxy-X04 positive microglia (representing A β phagocytic) is increased about 32.9 % (Fig. 6.8 C, D; t-test, $p < 0.05$). We further compared the A β fluorescent intensity within the Iba1 positive microglia in the brain of APP^{ki/ki}GPR109a^{-/-} mice with APP^{ki/ki}GPR109a^{+/+} mice. As shown in Fig. 6.8 E and F, A β intensity within microglia increases approximately 42.1% in GPR109a-deficient APP-knock-in mice. These results of co-immunostaining for A β and Iba1 confirmed the augmented uptake of A β by microglia in APP^{ki/ki}GPR109a^{-/-} mice. In conclusion, these findings implied that the deletion of GPR109a enhances microglia recruitment and phagocytosis in the region of plaques, boosting A β clearance in APP^{ki/ki} mice.

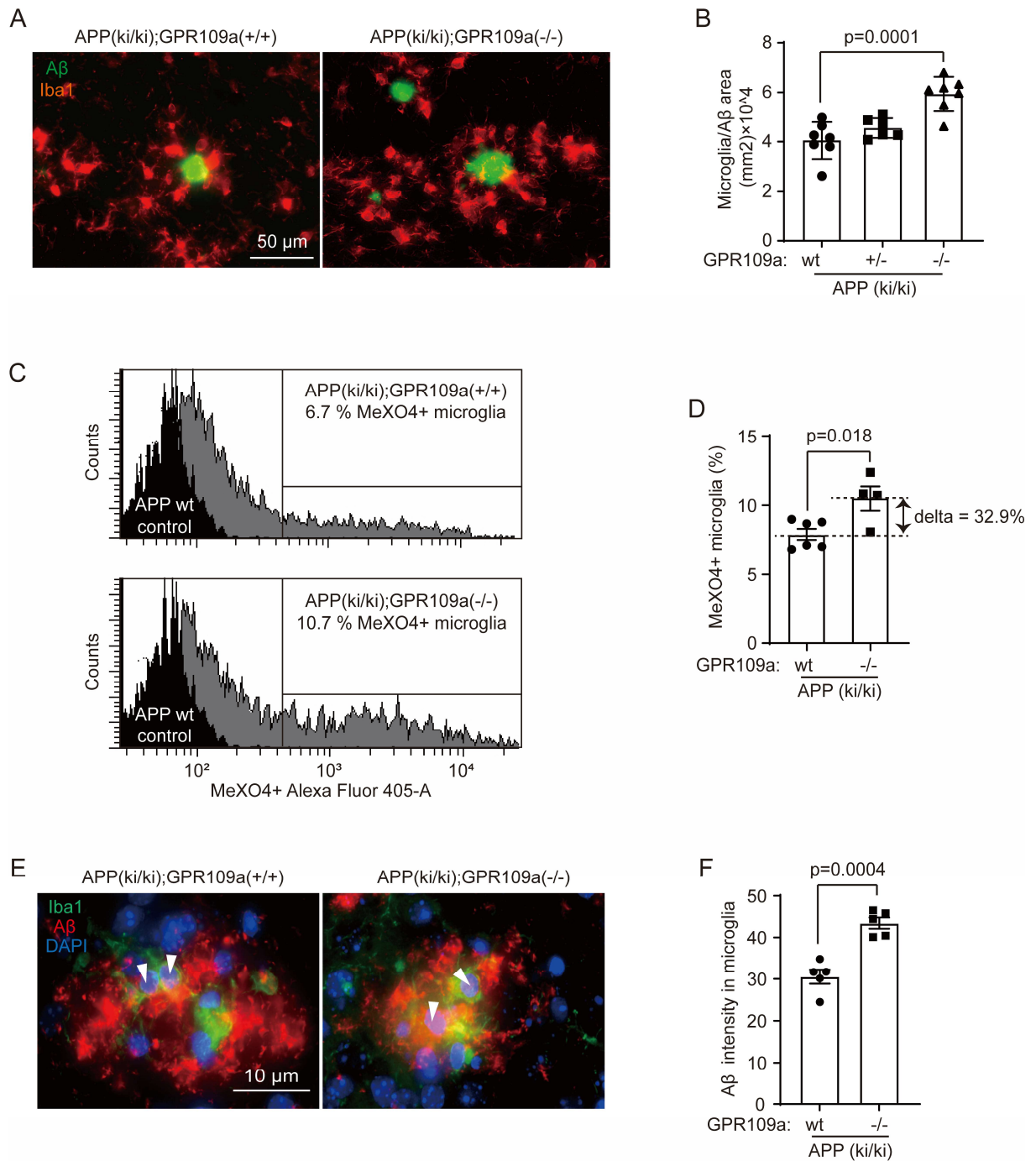


Fig. 6.8, GPR109a deficiency increases microglial recruitment around the plaques and promotes microglial amyloid- β phagocytosis. Microglia were labelled with Iba-1 antibody and co-stained with methoxy-X04 (A). Insufficiency of GPR109a significantly increases recruitment of microglia toward A β plaques (B; one-way ANOVA followed by *Bonferroni post hoc* test; $n \geq 6$ per group). Mice were injected intraperitoneally with methoxy-X04 to label cell populations that phagocytose A β . Brain tissues were collected 3 h after methoxy-X04 i.p., and stained with CD11b antibody, then flow cytometry analysis were used to identify CD11b⁺MeXO4⁺ cell populations. Histogram showing the methoxy-X04 signal intensity of A β phagocytic microglia (MeXO4⁺ microglia)

and non-A β phagocytic microglia (MeX04⁺ microglia) (C). The percentage of MeX04⁺ microglia from 6 APP^{ki/ki}GPR109a^{+/+} and 4 APP^{ki/ki}GPR109a^{-/-} mice brain shown the deficiency of GPR109a significantly increases the proportion of microglia that phagocytose A β (D; t-test; $n \geq 6$ per group). Representative immunofluorescence image of microglia phagocytosis A β in brain sections (E). The fluorescence intensity of A β in microglia are increased (F; t-test; $n = 5$ per group).

6.9 Deficiency of GPR109a enhances anti-inflammatory activation and A β phagocytosis in macrophages upon niacin treatment

We further investigated whether the differential responses and activities of microglia in GPR109a-deficient and wild-type APP^{ki/ki} mice are mediated by niacin, a high-affinity ligand of GPR109a. We cultured GPR109a-deficient and wild-type BMDMs and primed them with LPS or niacin from low to high concentrations for 12 hours. When exposed to low (1 mg/mL) or high (100 mg/mL) concentrations of LPS, GPR109a-deficient BMDMs secrete higher levels of TNF- α and IL-1 β but reduce IL-10 production compared to the GPR109a wild type (Fig. 6.9.1 A-C; one-way ANOVA, $p < 0.05$). Interestingly, in contrast to GPR109a-wildtype macrophages, GPR109a-deficient macrophages do not increase either TNF- α or IL-1 β secretion upon challenge with niacin (Fig. 6.9.1 A-B; one-way ANOVA, $p > 0.05$), but instead elevated the generation of IL-10 in a dose-dependent manner, which increased most pronounced at a niacin concentration of 10 μ M (Fig. 6.9.1 C; one-way ANOVA, $p < 0.05$). This finding indicates that the surrounding inflammatory milieu determines the inflammatory activity of GPR109a-deficient microglia during disease progression.

We observed a significant increase in *cx3cr1* gene transcription in microglia from APP^{ki/ki}GPR109a^{-/-} mice brain tissues, so we further evaluated whether niacin modulates the expression of CX3CR1 in macrophages. We detected the levels of CX3CR1 in BMDMs with or without GPR109a by flow cytometry. The expressions of CX3CR1 in GPR109a-deficient macrophages are significantly upregulated upon exposure to niacin, peaking at a concentration of 10 μ M (Fig. 6.9.1 E; two-way ANOVA, $p < 0.05$). Compared with GPR109a wild-type macrophages, the lack of GPR109a increases the expression of CX3CR1 in macrophages (Fig. 6.9.1 D and E; two-way ANOVA, $p < 0.05$). These results demonstrate that niacin facilitates the expression of CX3CR1 in GPR109a-deficient macrophages.

Many studies have shown that CX3CR1 is associated with microglial phagocytic activity (CASTRO-SANCHEZ et al., 2019; CHIDAMBARAM et al., 2020). In present study, we investigated whether the increases of CX3CR1 resulting from niacin stimulation are related to the phagocytosis. Firstly, we assessed the internalization of A β by GPR109a-deficient and GPR109a wild-type macrophages. As shown in Fig. 6.9.2 A-C, deletion of GPR109a dramatically promotes A β phagocytosis by macrophages upon exposure to niacin, with the increased proportion of A β -positive macrophages and A β fluorescence intensity (Fig. 6.9.2 A-C; two-way ANOVA, $p < 0.05$). Furthermore, we observed that GPR109a-deficient macrophages increase A β internalization most significantly at a concentration of 10 μ M niacin, indicating that niacin promotes the phagocytosis of A β in a concentration-dependent manner. Subsequently, we compared the A β phagocytic activity of CX3CR1-positive and -negative macrophages to investigate the relationship between CX3CR1 levels and A β phagocytosis. Flow cytometry results revealed that CX3CR1-positive macrophages have remarkably higher phagocytic activity for A β compared to that of CX3CR1-negative macrophages (Fig. 6.9.2 D and E; paired t-test, $p < 0.05$). In line with these findings, we used CX3CR1 knockout mice that had replaced CX3CR1 with a cDNA encoding enhanced green fluorescent protein (EGFP) (CX3CR1^{-/-} mice) further investigate the impacts of CX3CR1 in microglia phagocytosis. We observed that ablation of CX3CR1 significantly suppress the phagocytosis of A β by macrophages (Fig. 6.9.2 F; t-test, $p < 0.05$). We further incubated GPR109a-deficient and wildtype macrophages with 10 μ M AZD 8797, a selective and high-affinity inhibitor of CX3CR1 (RIDDERSTAD WOLLBERG et al., 2014), to validate the observation that increased CX3CR1 is associated with the microglial phagocytic activity. We observed that GPR109a deficiency did increase A β internalization in niacin-treatment macrophages. But concurrent treatment with AZD 8797, prevents niacin from promoting A β -phagocytosis by GPR109a-deficient macrophages (Fig. 6.9.2 G and H; t-test, $p < 0.05$). Our *in vitro* experiments demonstrate that deficiency of GPR109a enhances anti-inflammatory activation and A β phagocytosis in macrophages upon niacin treatment and is potentially mediated by CX3CR1.

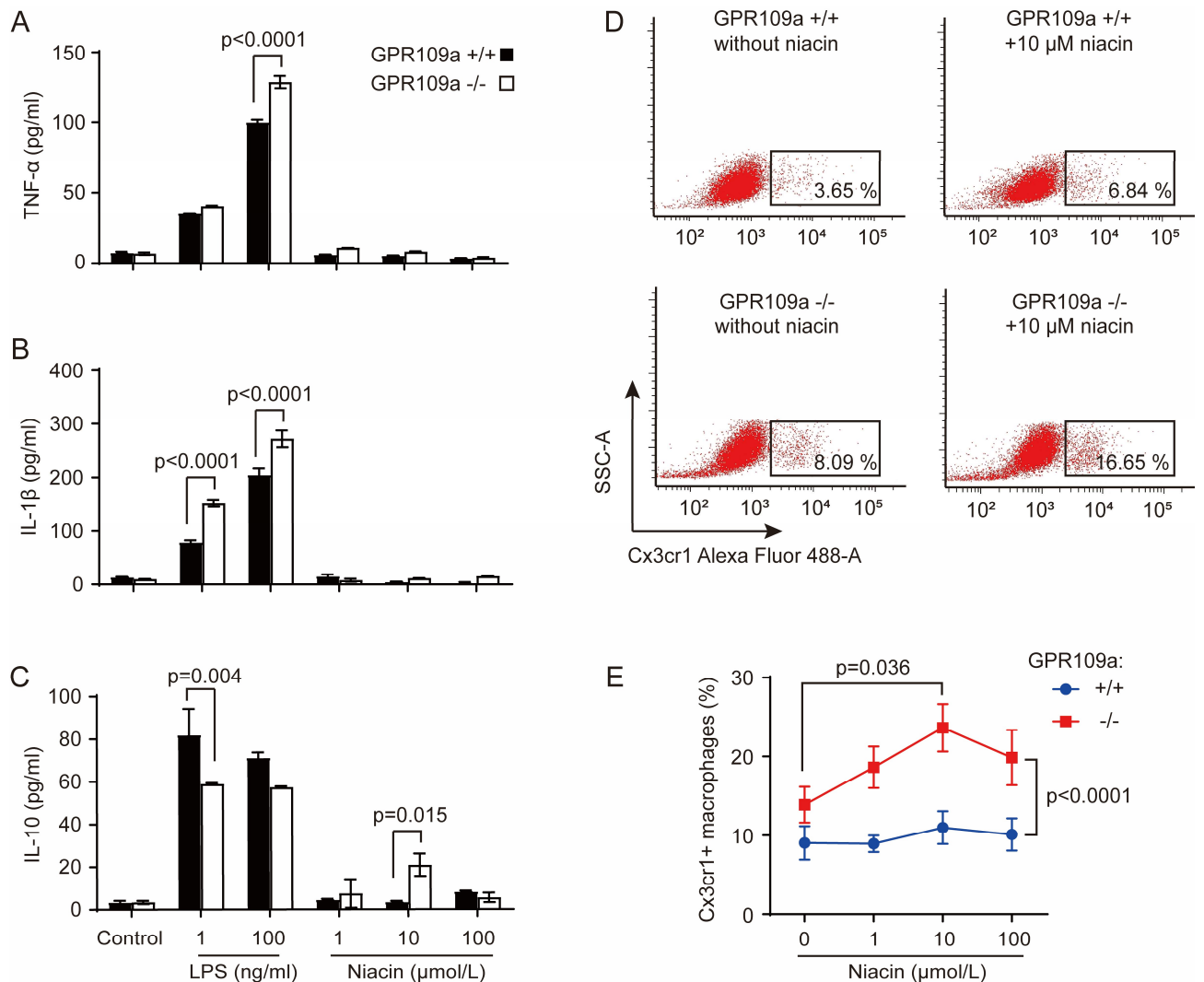


Fig. 6.9.1, Niacin inhibits inflammatory response and facilitates the expression of CX3CR1 in GPR109a-deficient macrophages. Bone marrow-derived macrophages in 48-well plate at a density of 2×10^5 cells per well were cultured from GPR109a-deficient (-/-) and wildtype (+/+) mice with our established protocol as describe in methods, and stimulated for 12 hours with LPS or niacin at different concentrations. Concentrations of TNF- α , IL-1 β , and IL-10 in the culture medium were measured with ELISA kits (R&D Systems) (A-C, t test, $n \geq 6$ per group). The protein levels of CX3CR1 were detected with flow cytometry after immunofluorescent staining of macrophages with Alexa Fluor[®] 488-labelled anti-mouse CX3CR1 Antibody (clone: SA011F11, BioLegend) (D). We counted the percentage of CX3CR1-positive macrophages in each group (E, two-way ANOVA followed by *Bonferroni post hoc* test, $n \geq 6$ per group).

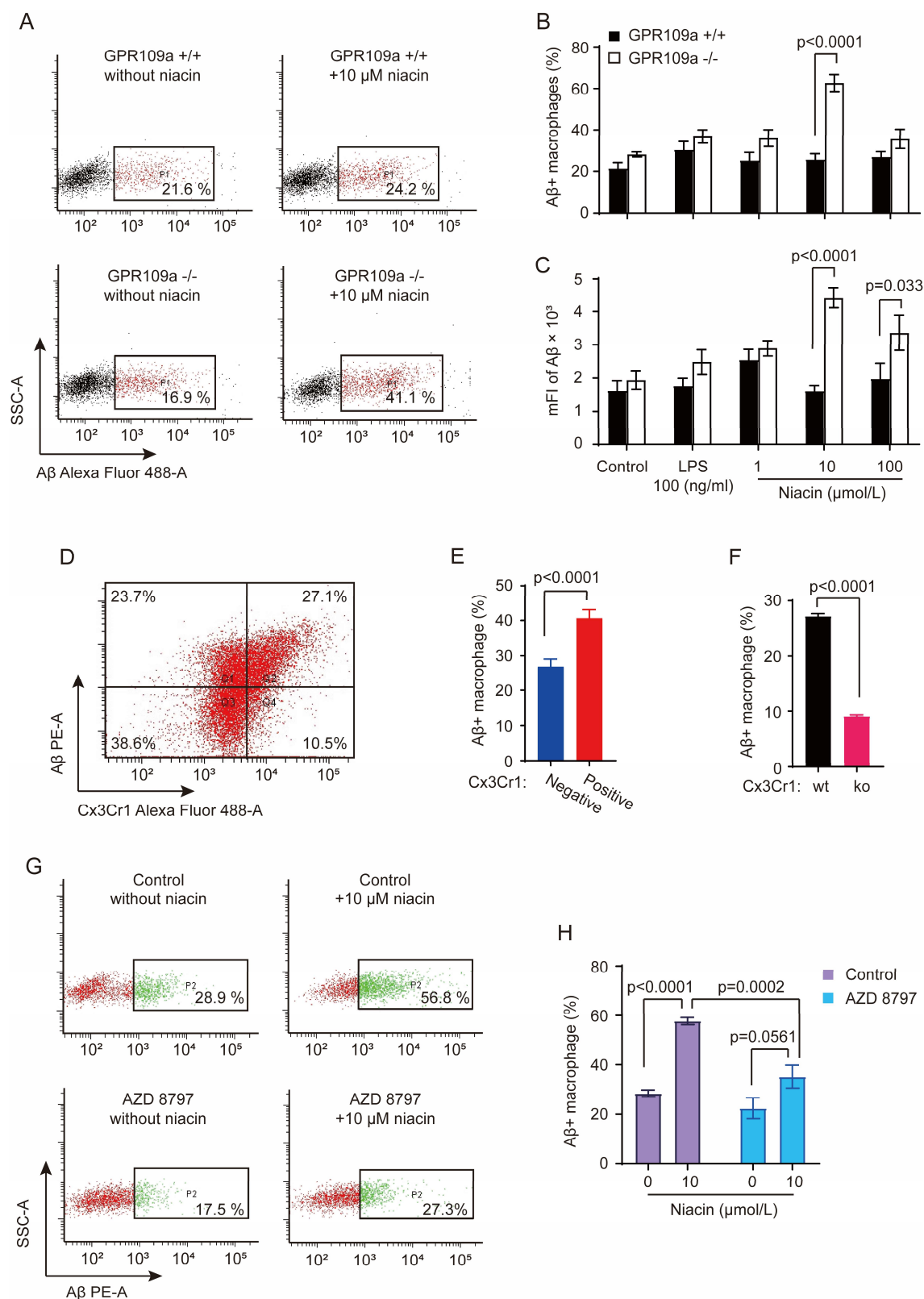


Fig. 6.9.2, Niacin promotes Aβ phagocytosis by GPR109a-deficient macrophages and is associated with CX3CR1. Fluorescent Aβ aggregates were prepared by mixing TAMRA-labelled human Aβ42 (Anaspec Inc.) and unlabelled Aβ42 (kindly provided by L. Fülöp, Albert Szent Gyorgyi Medical University, Szeged, Hungary) at a ratio of 1:10 and incubating 100 μM mixed peptides in phenol red-free Ham's F-12 for 24 hours. Thereafter,

macrophages were fed with 10 μ M TAMRA-conjugated oligomeric A β 42 and incubated for 6 hours at 37 °C. The internalization of A β was monitored by measuring the proportion of A β -positive macrophages and mean fluorescence intensity (mFI) with flow cytometry (A-C, t test, n \geq 6 per group). The proportion of A β -positive cells in CX3CR1-positive macrophages was counted and compared with that in CX3CR1-negative (D and E, t-test, n=8 per group, p < 0.05). CX3CR1-deficient macrophages phagocytose A β dramatically less efficiently than wildtype macrophages (F; t-test, n=6 per group, p < 0.05). Concurrent treatment with CX3CR1 inhibitor, AZD 8797, prevents niacin from promoting A β -phagocytosis by GPR109a-deficient macrophages (Fig. 6.9.2 G and H; t-test, n=8 per group, p < 0.05).

6.10 LRP1 upregulation in neurons and astrocytes from GPR109a-deficient APP^{ki/ki} mice

LRP1 and ABCB1 are thought to be involved in A β clearance and metabolism. We found that LRP1 protein levels are significantly lower in the brain of APP^{ki/ki} mice than APP^{wt} control mice (Fig. 6.10.1 A, B; one-way ANOVA, p < 0.05). Numerous studies have demonstrated that impairment of LRP1 in the brain leads to the accumulation of neurotoxic A β and drives AD pathology. To shed light on whether the deficiency of GPR109a affects the LRP1-mediated A β clearance, we compared the protein levels of LRP1 and ABCB1 in the brain from APP^{ki/ki} mice with different expressions of GPR109a. As shown in Fig. 6.10.1 D-F, the levels of LRP1 (Fig. 6.10.1 E; one-way ANOVA, p < 0.05), but not ABCB1 (Fig. 6.10.1 F; one-way ANOVA, p > 0.05), are increased significantly in a GPR109a gene-dose-dependent manner. Whereas in APP^{wt} control mice, deficiency of GPR109a neither alters the protein levels of LRP1 nor ABCB1 (Fig. 6.10.1 G-I; one-way ANOVA, p > 0.05). LRP1 has been shown to mediate A β removal from brain parenchyma to circulation via BBB transport. Therefore, we isolated micro-vessels from the brains of APP^{ki/ki} mice with different expressions of GPR109a. There are no differences in the expressions of either LRP1 or ABCB1 in microvascular tissues (Fig. 6.10.1 J-L; one-way ANOVA, p > 0.05). In conclusion, these Western blot results suggest that the deletion of GPR109a suppresses the reduction of LRP1 in AD mice brains, while that the increase in LRP1 does not appear to promote A β elimination via BBB.

LRP1 not only plays an important role in the systemic A β clearance via BBB. It is also essential for the endocytosis of A β , which is necessary for the cellular A β uptake and subsequent degradation. To further investigate the mechanism by which elevated LRP1 affects AD pathology, we compared the expression of LRP1 in brain parenchymal cells, such as neurons and astrocytes, of APP^{ki/ki}GPR109a^{-/-}, APP^{ki/ki}GPR109a^{+/-}, and APP^{ki/ki}GPR109a^{+/+}

mice brain. As shown in Fig. 6.10.2 A and B, compared with GPR109a wild-type mice, LRP1 fluorescence intensity is significantly upregulated in APP^{ki/ki}GPR109a^{-/-} mice neurons by 28.9% (Fig. 6.10.2 A, B; one-way ANOVA, $p < 0.05$). Similarly, the deficiency of GPR109a also increase the LRP1 protein level in astrocytes, although it is not as noticeable as the elevation in neurons (Fig. 6.10.2 C, D; one-way ANOVA, $p < 0.05$).

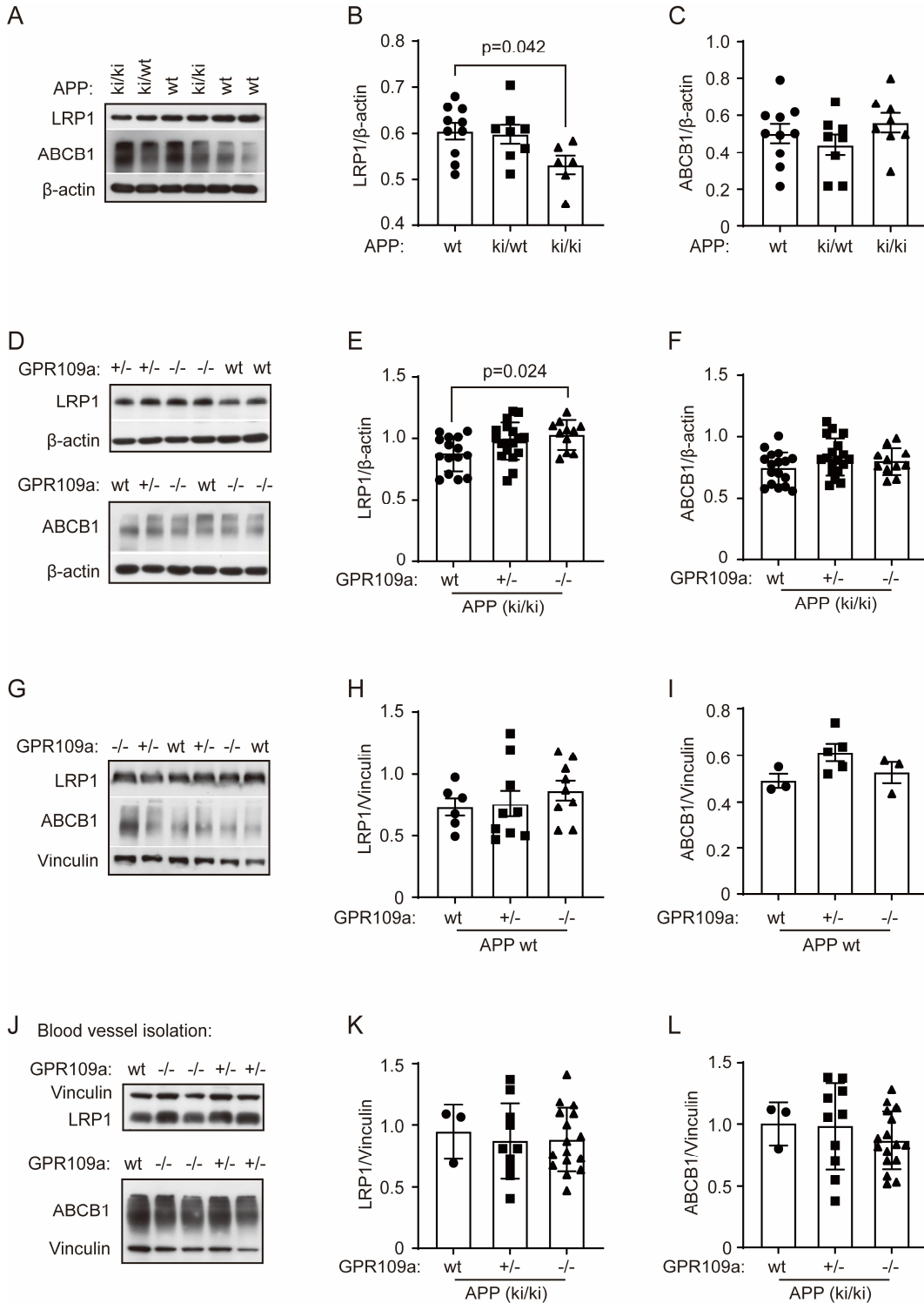


Fig. 6.10.1, Deficiency of GPR109a increases the expression of LRP1 in the APP^{ki/ki} mouse brain. Brain tissue and microvascular lysates from 9-month-old APP-knock-in littermate mice with homozygous (-/-) and heterogeneous (+/-) knockout of GPR109a gene and wild-type (+/+) were tested for Western blot to evaluate the expression of LRP1. The levels of LRP1 are decreased significantly in the brain lysates from APP^{ki/ki} than that in APP^{wt} mice, but ABCB1 is not affected by the expression of APP (A-C). Knockdown of GPR109a in APP^{ki/ki} mice reverses the reduction of LRP1 without effects on ABCB1 expression (D-F). And the expressions of LRP1 and ABCB1 in the brain of APP^{wt} mice are not regulated by GPR109a (G-I). Moreover, LRP1 and ABCB1 levels in the brain microvasculature of APP^{ki/ki} mice are not altered by GPR109a expression (G-I). (one-way ANOVA followed by *Bonferroni post hoc* test; $n \geq 5$ per group).

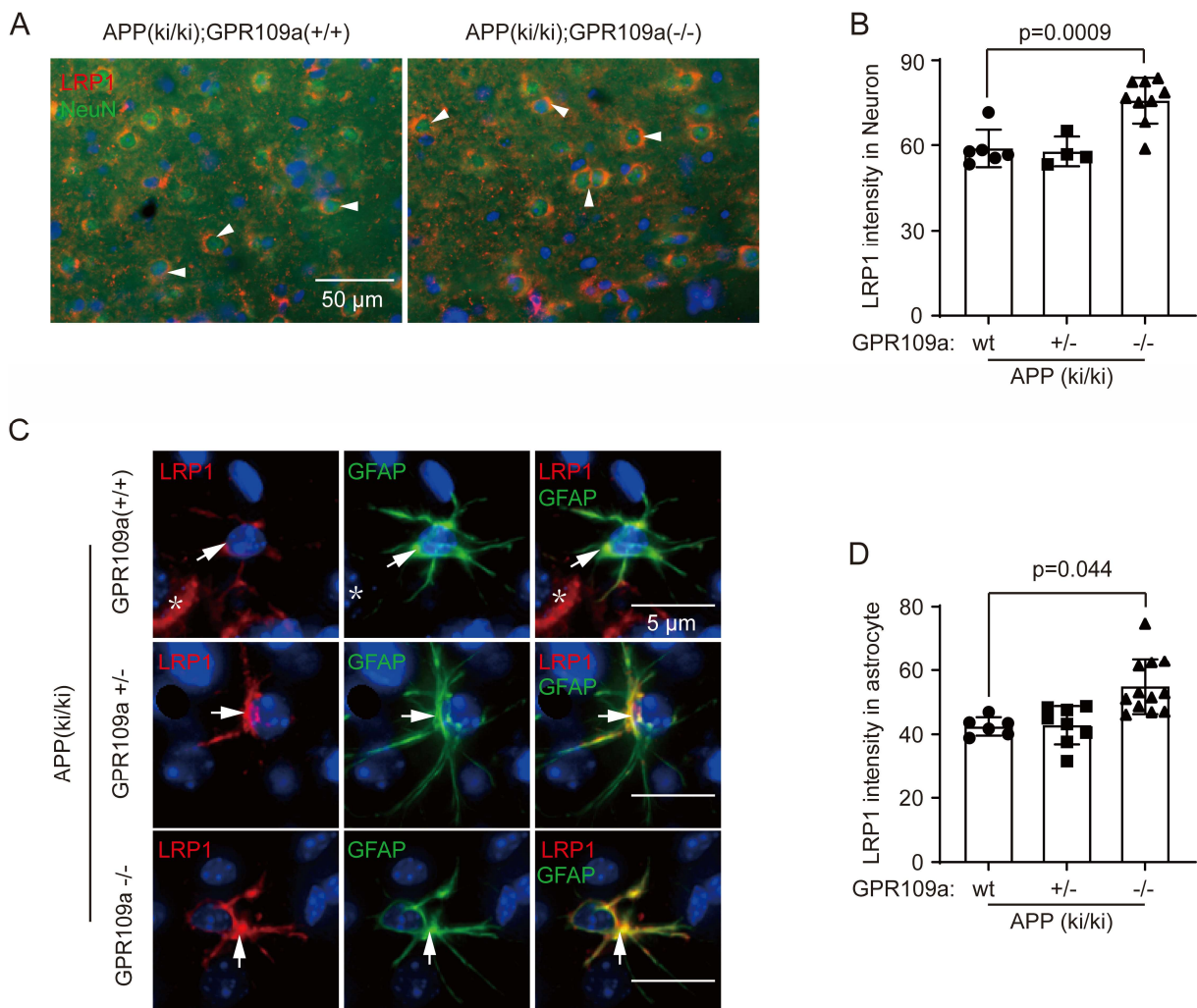


Fig. 6.10.2, Upregulation of LRP1 in neurons and astrocytes of GPR109a-deficient APP^{ki/ki} mice. Brain sections derived from 9-month-old APP^{ki/ki}GPR109a^{-/-} and APP^{ki/ki}GPR109a^{-/-} mice were stained for LRP1 (red) and marker protein of neurons NeuN (green) or astrocytes GFAP (green) (A, C). The quantification of the staining showed an elevation of LRP1 expression both in neurons (B) and astrocytes (D). (one-way ANOVA followed by *Bonferroni post hoc* test; $n \geq 6$ per group). White arrowheads represent LRP1 positive signal in neurons or astrocytes, asterisks represent LRP1 positive but GFAP negative.

6.11 Deficiency of GPR109a decreases IL-17a expression in intestinal CD4⁺ T lymphocytes of APP^{ki/ki} mice.

It is well documented that IL-17a-producing T cells are involved in the AD pathogenesis. We selected CD4⁺ spleen cells by magnetic beads-conjugated antibodies from 7-month-old APP^{ki/ki} and APP^{wt} littermate mice and observed that the transcriptions of both pro- and anti-inflammatory (*il-10*, *ifn-g*, *gata3*, *foxp3*, and *t-bet*) are significantly up-regulated in APP^{ki/ki} mice (Fig. 6.11.1 A; t-test, $p < 0.05$). The gene transcription of *il-17a* is also elevated, although no significant difference (Fig. 6.11.1 A; t-test, $p > 0.05$). Interestingly, among these genes, only transcription of the *il-17a* gene is significantly inhibited by the GPR109a deficiency in CD4⁺ positive splenocytes from APP^{ki/ki} mice (Fig. 6.11.1 B; t-test, $p < 0.05$), while transcriptions of other genes are unaffected (Fig. 6.11.1 B; t-test, $p > 0.05$).

We further selected CD4⁺ cells from the intestinal lamina propria and Peyer's patches of APP^{ki/ki} mice with different GPR109a expressions to evaluate whether the distribution of intestinal lymphocyte populations regulates by GPR109. We detected the transcription of lymphocyte marker genes by RT-PCR. GPR109a-deficient mice showed a dramatical reduction of *il-17a* gene transcription in CD4⁺ lymphocytes from lamina propria and Peyer's patches compared with aged-matched GPR109a-wild type mice (Fig. 6.11.2; A and E, one-way ANOVA, $p < 0.05$). This reduction is *gpr109a* gene dose-dependent. It suggests that GPR109a deficiency significantly reduce the generation of intestinal IL-17a⁺CD4⁺ lymphocytes (Th17). However, GPR109a elimination does not change the transcripts of marker genes for Th1 (*ifn- γ* and *t-bet*), Th2 (*il-4* and *gata3*), and Treg (*il-10* and *foxp3*) lymphocytes both in intestinal lamina propria (Fig. 6.11.2; B-D, one-way ANOVA, $p < 0.05$) and Peyer's patches (Fig. 6.11.2; F-G, one-way ANOVA, $p < 0.05$). Moreover, the cytometric analysis confirmed that the population of IL-17a⁺CD4⁺ lymphocytes in the intestinal lamina propria of APP^{ki/ki}GPR109a^{-/-} mice and APP^{ki/ki}GPR109a^{+/-} are lower than that in APP^{ki/ki}GPR109a^{+/+} mice (Fig. 6.11.3; A and B, one-way ANOVA, $p < 0.05$). In addition, we also found that deletion of GPR109a decreases the population of γ/δ ⁺ cells in the intestinal epithelium (Fig. 6.11.3; C and D, one-way ANOVA, $p < 0.05$), although we do not identify any IL-17a-expressing γ/δ T cells (γ/δ 17).

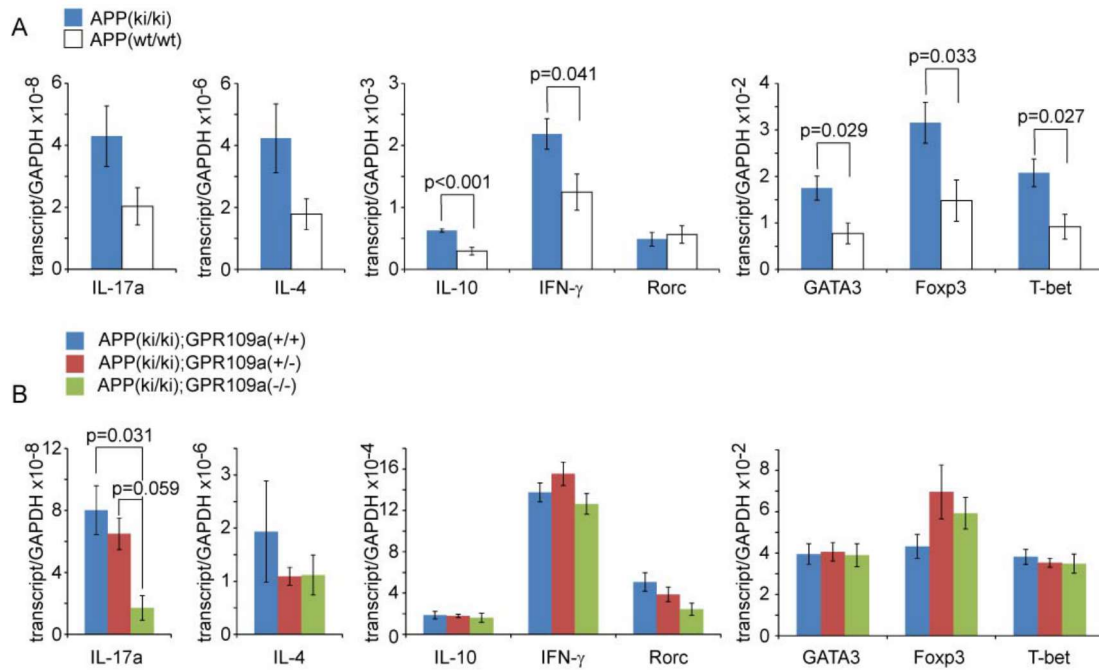


Fig. 6.11.1, Deficiency of GPR109a decreases genetic transcription of IL-17a in CD4-positive spleen cells. CD4-positive lymphocytes were selected with magnetic beads-conjugated antibodies from 7-month-old APP^{ki/ki} and APP^{wt} littermate mice (A; n = 6 and 4, respectively), from 7-month-old APP^{ki/ki} with different expression of GPR109a (B; n = 3, 6 and 4, respectively). Real-time PCR was used to quantify transcripts of marker genes for Th17 (*il-17a* and *rorc*), Th1 (*ifn-γ* and *t-bet*), Th2 (*il-4* and *gata3*) and Treg (*il-10* and *foxp3*) lymphocytes. T tests for A, and One-way ANOVA followed by *Bonferroni post hoc* test for B.

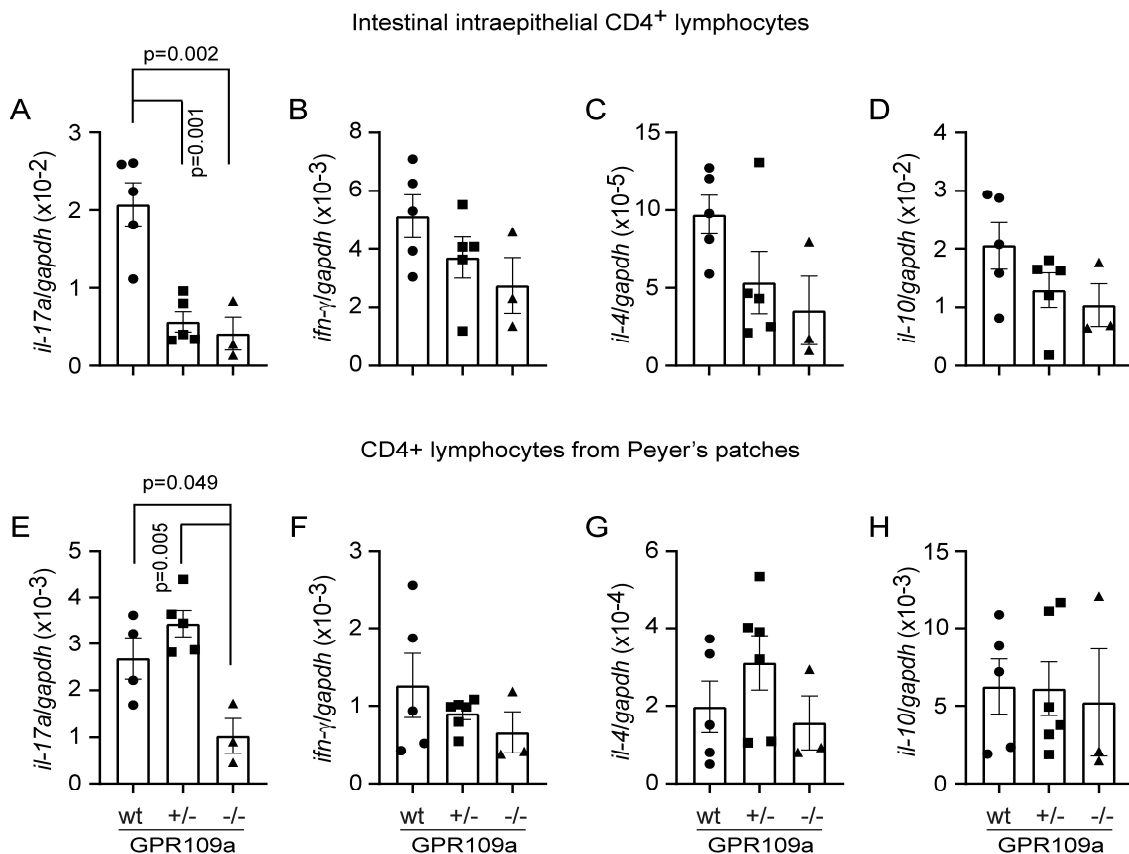


Fig. 6.11.2, Deficiency of GPR109a decreases *il-17a* gene transcription in CD4-positive lymphocytes in the gut. CD4-positive lymphocytes were selected with magnetic beads-conjugated antibodies from the epithelial layer and Peyer's patches of the gut of 9-month-old APP-knock-in mice with different expression of GPR109a. Real-time PCR was used to quantify transcripts of marker genes for Th17 (*il-17a*), Th1 (*ifn- γ*), Th2 (*il-4*) and Treg lymphocytes (*il-10*). (One-way ANOVA followed by *Bonferroni post-hoc* test. $n \geq 3$ per group).

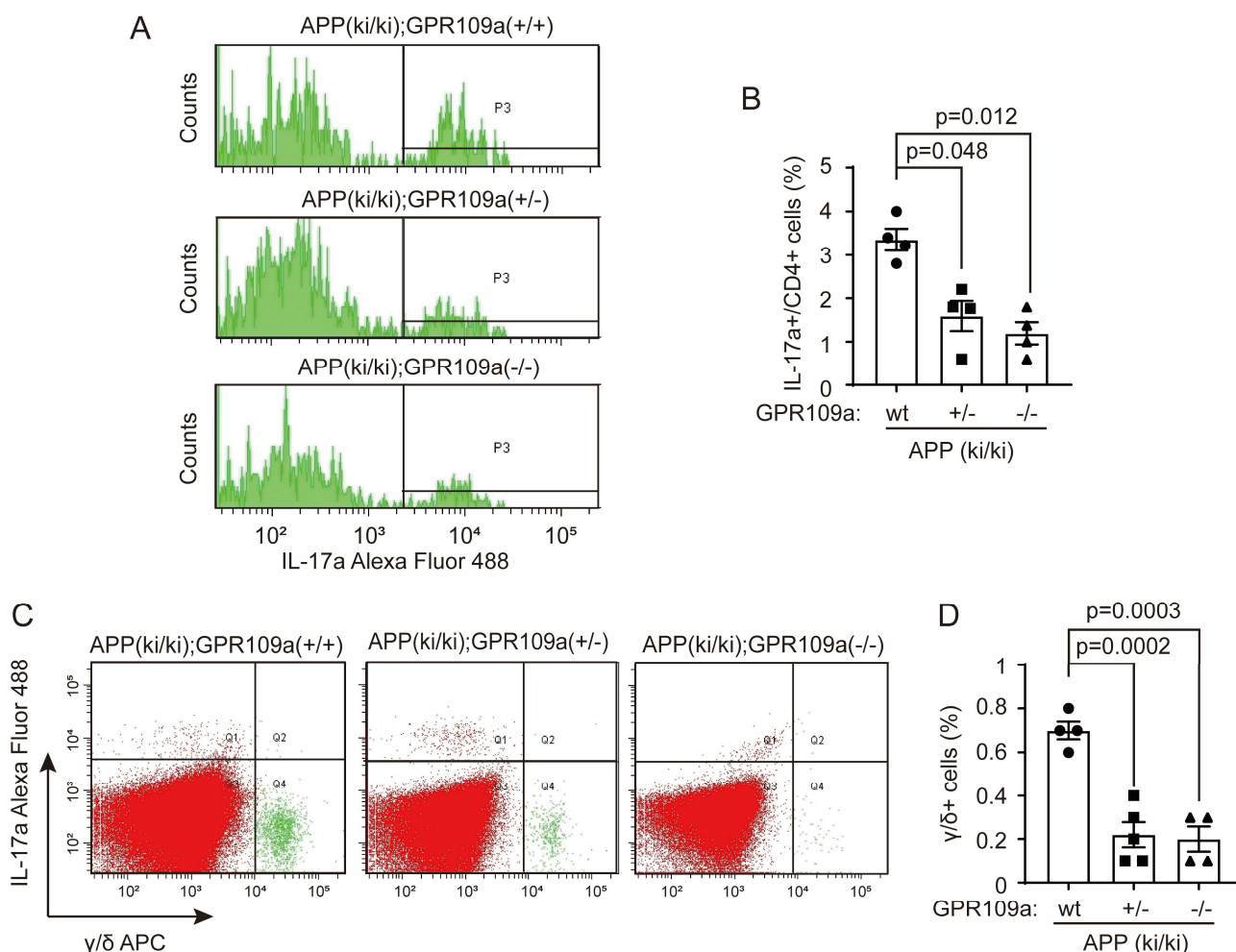


Fig. 6.11.3, Representative flow cytometry histograms of IL-17a fluorescence intensity from CD4+ lymphocytes in the intestinal epithelium (A). The percentage of IL-17a+ CD4+ lymphocytes is significantly lower in haploid and diploid insufficient GPR109a mice (B). Representative expression of IL-17a and marker of γ/δ cells in intestinal epithelium from 9-month-old APP-knock-in mice with different expression of GPR109a (C, D). In APP^{ki/ki}GPR109a^{+/-} and APP^{ki/ki}GPR109a^{-/-} mice, the frequency of γ/δ +IL-17a- cells (Q4) from the intestinal epithelium was significantly reduced (D). One-way ANOVA followed by *Bonferroni post hoc* test for B and D.

6.12 IL17a-expressing lymphocytes might be involved in the improvements of A β pathologies in GPR109a-deficient APP^{ki/ki} mice

To examine whether IL-17a-producing T lymphocytes mediate the effects of GPR109a

deficiency, we crossbred APP^{ki/ki}GPR109a^{-/-} mice with IL-17a knockout mice obtaining APP^{ki/ki}IL17a^{-/-}GPR109a^{+/+} (GPR109a wild-type with IL-17a knockout) and APP^{ki/ki}IL17a^{-/-}GPR109a^{-/-} (GPR109a-deficient with IL-17a knockout) mice. We performed a Y-maze test to analyse the cognitive function of APP^{ki/ki}IL17a^{-/-}GPR109a^{+/+} and APP^{ki/ki}IL17a^{-/-}GPR109a^{-/-} mice. In APP^{ki/ki}IL17a^{-/-} mice, GPR109a deletion does not ameliorate mice's alternation in the Y maze compared with GPR109a wild-type littermates (Fig. 6.12.1 A, t-test, $p > 0.05$). Moreover, we analysed the effects of IL-17a on A β load in the APP^{ki/ki}GPR109a^{-/-} mice. Quantitative Western blot results showed that the amount of A β monomer, dimer, and trimer in APP^{ki/ki}IL17a^{-/-}GPR109a^{-/-} mice have no differences between APP^{ki/ki}IL17a^{-/-}GPR109a^{+/+} littermates (Fig. 6.12.1 B and C, t-test, $p > 0.05$). We further stained brain sections from APP^{ki/ki}IL17a^{-/-}GPR109a^{+/+} and APP^{ki/ki}IL17a^{-/-}GPR109a^{-/-} mice with methoxy-X04 and A β antibody, the data revealed that homozygous knockout of *il-17a* gene eliminates the effects of GPR109a deficiency in reducing A β deposits in the brains of AD mice (Fig. 6.12.1 F-G, t-test, $p > 0.05$).

We observed that deficiency of GPR109a increases the expression of LRP1 in brain tissues (Fig. 6.10.1 A and B, one-way ANOVA, $p < 0.05$). However, the protein levels of LRP1 are not changed in APP^{ki/ki}IL17a^{-/-}GPR109a^{-/-} mice as compared with APP^{ki/ki}IL17a^{-/-}GPR109a^{+/+} mice (Fig. 6.12.2 A-C, t-test, $p > 0.05$), which indicated the knockout of the *il-17a* gene appeared to abolished the effects of GPR109a deficiency in LPR1 expression. Similarly, the significant elevation of A β -associated microglial recruitment in APP^{ki/ki}GPR109a^{-/-} mice is abolished by the homozygous knockout of IL-17a (Fig. 6.12.2 D and E, t-test, $p > 0.05$). Interestingly, IL-17a deficiency does not abrogate the alteration of microglia morphology by GPR109a, as shown in Fig. 6.12.2 F-K, with a significant increase in the branches and sholl analysis intersection number in APP^{ki/ki}IL17a^{-/-}GPR109a^{-/-} mice, consistent with that in APP^{ki/ki}GPR109a^{-/-} mice (Fig. 6.12.2 F-K, t-test, $p > 0.05$). In summary, IL-17a partially modulates the effects of GPR109a deficiency in AD mice.

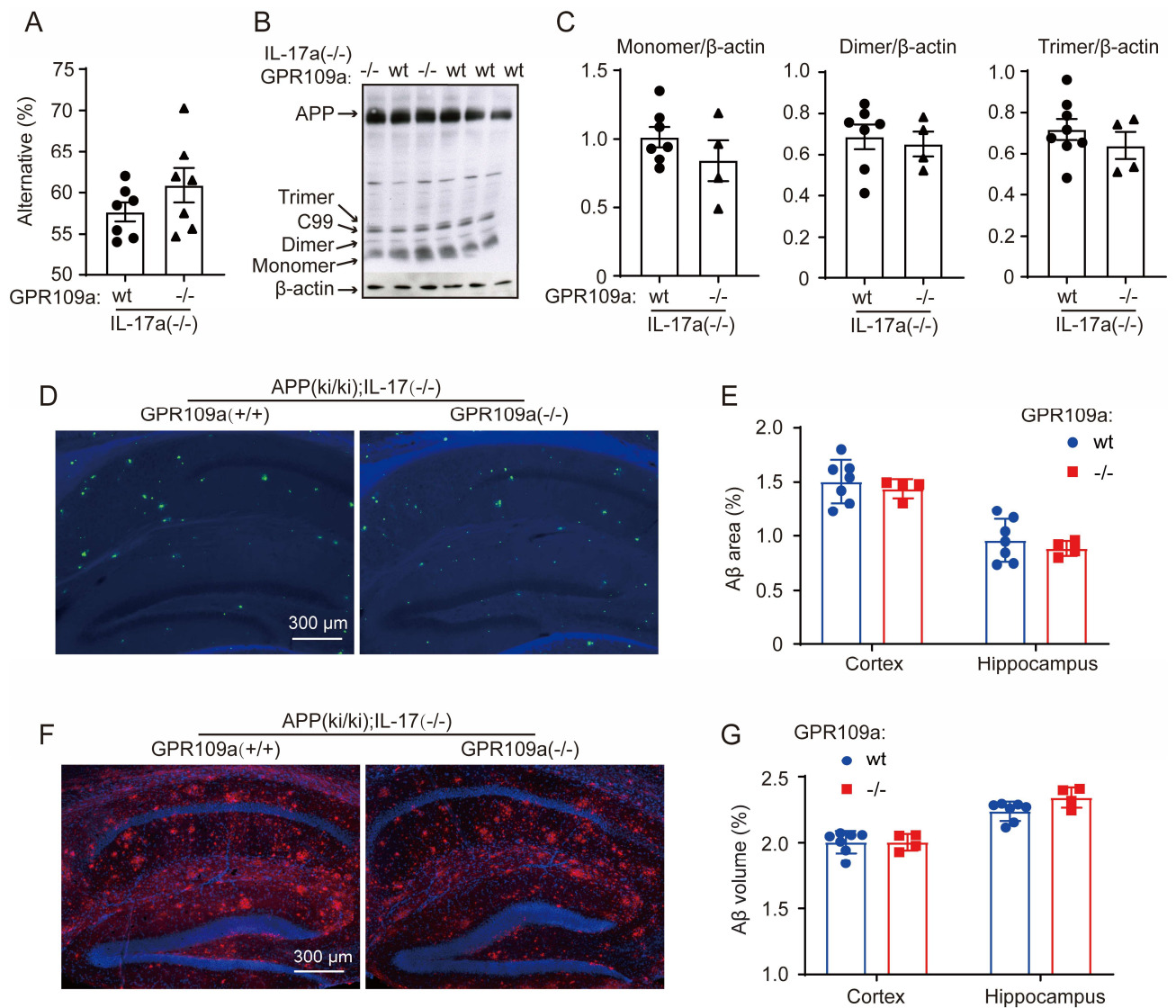


Fig. 6.12.1, Knockout of IL-17a eliminated the effects of GPR109a deficiency on the amyloid pathologies of in APP^{ki/ki} mice. APP^{ki/ki}GPR109a^{-/-} mice were cross-bred with IL-17a knockout (-/-) mice. 9-month-old APP^{ki/ki}IL17a^{-/-}GPR109a^{-/-} and APP^{ki/ki}IL17a^{-/-}GPR109a^{+/+} mice were used for the Y-maze test. When the *il-17a* gene was knocked out in APP^{ki/ki} mice, deficiency of GPR109a does not change the alteration in the Y maze (A, t-test, n = 7 per group, p ≥ 0.05). Moreover, the amounts of monomeric, dimeric, and trimeric Aβ in APP^{ki/ki}IL17a^{-/-}GPR109a^{-/-} mice have no difference compared with that in APP^{ki/ki}IL17a^{-/-}GPR109a^{+/+} mice (B and C, t-test, n ≥ 4 per group, p ≥ 0.05). Representative microscope images from brain sections staining with methoxy-X04 (D) or human Aβ-specific antibody (F). The area/volume of Aβ plaques in cortex and hippocampus are not changed by GPR109a deficiency when the *il-17a* gene was knocked out in APP^{ki/ki} mice (E and G, t-test, n ≥ 4 per group, p ≥ 0.05).

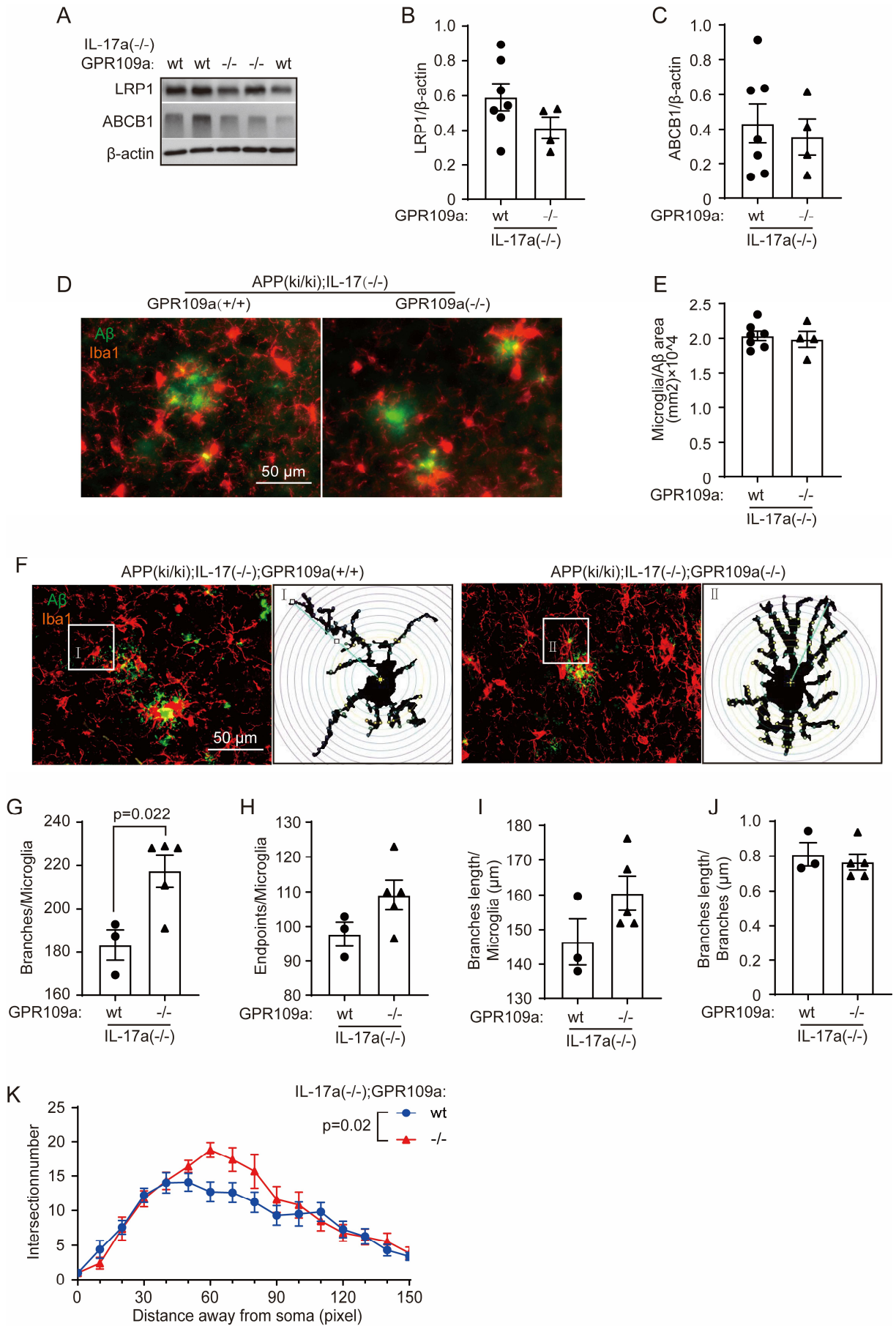


Fig. 6.12.2, IL-17a partially modulates the effects of GPR109a deficiency in AD mice. Deletion of GPR109a does not increase protein levels of LRP1 and ABCB1 in brain tissue of *il-17a* gene-deficient APP^{ki/ki} mice (A-C, t-test, $n \geq 4$ per group, $p \geq 0.05$). We have repeated the analysis of A β -associated microglia in 9-month-old APP-knock-in mice with (ko) and without (wt) GPR109a and with the homozygous knockout of IL-17a. IL-17a deficiency abolished the effect of GPR109a deficiency that promotes microglia to cluster around A β deposits (D and E, t-test, $n \geq 4$ per group, $p \geq 0.05$). Morphometric analysis of plaque-associated microglia was repeated in 9-month-old APP^{ki/ki}IL17a^{-/-}GPR109a^{-/-} and APP^{ki/ki}IL17a^{-/-}GPR109a^{+/+} mice's brain sections (F). In comparison with the aforementioned results, GPR109a deletion increases the microglial branches regardless of the presence or absence of the *il-17a* gene (G, t-test, $n \geq 3$ per group, $p \leq 0.05$). And the number of endpoints and branch lengths, although not yet significantly different, are on the rise (H and I, t-test, $n \geq 3$ per group, $p \geq 0.05$). And Sholl analysis revealed that the Sholl intersections along the microglial processes in APP^{ki/ki}IL17a^{-/-}GPR109a^{-/-} mice are increased obviously than that in APP^{ki/ki}IL17a^{-/-}GPR109a^{+/+} mice, especially in the circles ranging from 50 pixel to 80 pixel (K, two-way ANOVA followed by *Bonferroni post hoc test*; 10 microglia from 3 APP^{ki/ki}IL17a^{-/-}GPR109a^{-/-} mice, 10 microglia from 3 APP^{ki/ki}IL17a^{-/-}GPR109a^{+/+} mice were analyzed; $p < 0.05$).

7. DISCUSSION

7.1 Deficiency of GPR109a ameliorates Alzheimer's pathologies

Microglial activation has been extensively studied in the context of AD pathogenesis. It drives both inflammatory neurotoxicity, and A β clearance and neuronal survival. In this study, we observed that deficiency of GPR109a attenuates A β pathology and protects neurons in APP-knock-in AD mice. Specifically, knockout of *gpr109a* gene promotes microglial clustering around A β deposits and increases microglial internalization of A β in the brain of 9-month-old APP^{ki/ki} mice. GPR109a-deficient microglia display a homeostatic profile, with ramified morphology and an increase of *CX3CR1*, *trem2*, and *p2ry12* gene transcripts. GPR109a deficiency also enhances niacin treatment-induced anti-inflammatory activation (*e.g.*, secretion of IL-10) and A β phagocytosis, which is associated with an up-regulation of *CX3CR1* expression. Deficiency of GPR109a also increases LRP1 expression in neurons and astrocytes and facilitates LRP1-mediated A β clearance. Moreover, GPR109a deficiency reduces IL-17a-producing CD4-positive lymphocytes in the gut, which has the potential to regulate microglial activation and A β clearance in AD brain.

7.2 Deficiency of GPR109a modifies microglial activation and response in AD brain

Microglial pro- and anti-inflammatory activation are simultaneously increased in the brains of AD patients and animal models, which exert both deleterious and beneficial effects on AD (COLTON et al., 2006). Nowadays, the well-known M1 and M2 inflammatory profiles seem insufficient to characterize the microglial phenotypes. Next-generation sequencing methodologies, particularly single-cell and single-nucleus RNA sequencing, allow scientists to explore progressive changes in microglial gene transcription and epigenetic regulation in the AD brain at single-cell resolution (COLONNA, BRIOSCHI, 2020). Scientists have identified the phenotype of disease-associated microglia (DAM) in AD brain, which is characterized by a suppression of homeostatic genes (*e.g.*, *p2ry12*, *tmem119*, *tgfbr1*, *sall1*, *csflr*, and *CX3CR1*), and an induction of pro-inflammatory genes (including *il-1 β* , *ccl2*, *itgax*, and *csfl*), which might be shared by M1 profile. However, transcription of *apoe* and *trem2* genes is up-regulated in

DAM (KEREN-SHAUL et al., 2017), but down-regulated in M1 profile (KRASEMANN et al., 2017; LIU et al., 2020). It should also be pointed out that the characteristics of DAM in AD patients are not necessarily identical to those in AD mice. Homeostatic genes (*p2ry12*, *trem119*, and *CX3CR1*) down-regulated in microglia of AD mice were transcriptionally increased in AD patients (ZHOU et al., 2020). Similarly, protein C1QB and CD14, which are upregulated in microglia of AD patients, were not detected in AD animal models (LIU et al., 2005; MATHYS et al., 2019).

In our study, we observed that GPR109a deficiency significantly increases the transcription of *trem2*, *CX3CR1*, *p2ry12*, and *clec7a* genes in microglia of 9-month-old APP^{ki/ki} mice. But GPR109a deficiency not change pro- and anti-inflammatory genes in microglia, such as *tnf- α* , *il-1 β* , *ccl2*, and *il-10*. Deficiency of GPR109a appears to promote homeostatic transformation of microglial activation in AD mice, although the transcription of *trem2* gene is up-regulated.

TREM2 is the essential receptor for microglial sensing the environment. TREM2 enables microglia response in AD by maintaining microglial metabolic fitness; TREM2-deficient AD mice exhibit impaired cellular metabolism and increased microglia autophagy (ULLAND et al., 2017). TREM2-deficient microglia fail to recruit to A β plaques (ULLAND, COLONNA, 2018) and form a physical barrier around A β plaque to protect nearby neurons from A β toxicity (CONDELLO et al., 2015; ULLAND, COLONNA, 2018). It has been shown that microglia-covered plaques were compact and enriched in neurotoxic A β ₁₋₄₂ species, but non-microglia-covered plaques displayed a high degree of neuronal dystrophy (CONDELLO et al., 2015). Elevated microglial TREM2 expression reduces cerebral A β load, neuritic dystrophy, and cognitive deficits in 5xFAD transgenic mice, and enhances ramification and phagocytic capacity of plaque-associated microglia (LEE et al., 2018). However, the pathogenic role of TREM2 remains inclusive, since there were studies showing that TREM2 deficiency attenuates amyloid pathology in APPPS1-21 mice (JAY et al., 2015). Subsequent studies suggest that the consequences of TREM2 deficiency in AD are disease progression-dependent, with TREM2 deficiency improving amyloid pathology early but exacerbating it in the late disease stages (JAY et al., 2017).

In AD patients, the concentration of soluble TREM2 (sTREM2) in CSF fluctuates dramatically during the disease progresses, peaking in the early stages of the disease. In a 2-year prospective study of subjects from cognitively normal to symptomatic AD dementia, a higher level of sTREM2 in CSF at baseline is correlated with an increased A β accumulation in the brain in the follow-up examination (EWERS et al., 2020). However, in elderly subjects with decreased A β 42 and increased p-Tau in CSF, a higher level of sTREM2 CSF is associated with a slower decline of memory and cognition, and with a less conversion from cognitively normal to symptomatic stages or from MCI to AD dementia (EWERS et al., 2019).

The transcription of microglial homeostatic genes (*e.g.*, *p2ry12*, and *CX3CR1*) were reduced in *App^{NL-G-F/NL-G-F}* mice and associated with the degree of neuron loss (SOBUE et al., 2021). *P2ry12* regulates morphological changes and motility of microglia, with a lower expression level in aged microglia than in younger cells (BISHT et al., 2021). Its expression was reported to decrease or be absent in most microglia nearby A β deposits (JAIN et al., 2020; MILDNER et al., 2017). However, there is also a study showing that hyperactivated microglia, which interact with diffuse plaques, express abundant *P2ry12* (WALKER et al., 2020). Microglia in *P2ry12* knockout mice showed a diminished directional extension of branches toward lesion sites, suggesting that *P2ry12* is essential for microglial chemotaxis (HAYNES et al., 2006). *P2ry12*-mediated chemotaxis of microglia processes is needed for the rapid closure of the injured BBB (LOU et al., 2016). *P2ry12* contributes to, but is not necessary for, initial hyper-ramification of microglia (SIPE et al., 2016). It is, nevertheless, required for rapid morphological hyper-ramification involving the phagocytosis of synaptic components during development (SIPE et al., 2016).

CX3CR1 responds to the fractalkine ligand *CX3CL1* and drives the migration of microglia to their synaptic targets, where phagocytosis and synaptic refinement occur (PAOLICELLI et al., 2011). Under physiological conditions, mice lacking the *CX3CR1* exhibit impaired cognitive function and synaptic plasticity (ROGERS et al., 2011). Expression of *CX3CR1* decreases in AD brain, which promotes neuroinflammation, amyloid pathology and cytotoxicity (HEMONNOT et al., 2019; KEREN-SHAUL et al., 2017). (LIMATOLA, RANSOHOFF, 2014). *CX3CR1*-deficient microglia from young mice exhibit a premature

senescence transcriptomic signature with a down-regulated transcription of immune-related genes (GYONEVA et al., 2019). Late-onset AD patients with the *CX3CR1-V249I* mutation show more loss of neurons than AD patients without mutation in *CX3CR1* gene (LOPEZ-LOPEZ et al., 2018). It has been observed that tau and fractalkine competitively bind to CX3CR1, so that the down-regulation of fractalkine in AD brain promotes tau binding to CX3CR1 and its internalization by microglia (CHIDAMBARAM et al., 2020). The absence of CX3CR1 impairs microglial phagocytosis of tau (BOLOS et al., 2017). Deficiency of microglial CX3CR1 then accelerates tau spreading in the brain and exaggerates the impairment of memory in human tau-transgenic mice (MAPHIS et al., 2015). The effect of CX3CR1-deficient microglia on A β deposits is unclear. Some studies also indicated that CX3CR1 deficiency enhances A β phagocytosis by microglia and decreases cerebral A β load in various APP transgenic mice (HICKMAN et al., 2019; LEE et al., 2010; LIU et al., 2010). CX3CR1 deficiency even pushes microglial migration toward A β deposits (LIU et al., 2010).

Our experiments demonstrated that GPR109a deficiency enhances CX3CR1 expression induced by niacin treatment as compared with niacin-treated GPR109a wild-type cells. And CX3CR1 expression is correlated with phagocytosis of A β oligomers. Macrophages from CX3CR1^{-/-} mice showed substantially diminished phagocytosis of A β . Moreover, the concurrent treatment with CX3CR1 antagonist, AZD 8797, prevents niacin from promoting A β -phagocytosis by GPR109a-deficient macrophages. These results suggest that CX3CR1 is essential for microglial phagocytosis of A β and GPR109a deficiency enhances A β phagocytosis by up-regulating CX3CR1 expression. Our study is in line with a previous study that loss of CX3CR1 impairs the phagocytosis and migration of microglia (CASTRO-SANCHEZ et al., 2019).

7.3 Deficiency of GPR109a promotes construction of microglia physical barrier around A β deposits

It has been suggested that microglia cluster around A β deposits, form a physical barrier and condense A β into dense plaques, which protect local neurites from the damage by A β (CONDELLO et al., 2015; SPANGENBERG et al., 2019; WANG et al., 2016; YUAN et al.,

2016). In APP-transgenic mice, which express inducible diphtheria toxin (DT) receptor on microglia (CX3CR1-iDTR), induction of microglial deletion leads to an expansion of A β plaques and increases the impairment of neuronal dendrites crossing the plaques. Microglial deletion does not change the number of A β plaques. The repopulation of microglia after DT injection is able to discontinue the growth of A β plaques (ZHAO et al., 2017). We observed that GPR109a deficiency promotes microglia clustering around A β deposits in APP-knock-in mice. In parallel with the increased aggregation of microglia, synaptic structural proteins (e.g., PSD-95, SNAP25) are preserved and dystrophic neuritis are decreased around plaques in the brain of APP^{ki/ki}GPR109a^{-/-} mice.

The mechanism that drives microglia to migrate to A β deposits is unclear. We observed that GPR109a deficiency dramatically increases *trem2* gene transcription in microglia from APP-knock-in mice brain. Many studies have described that TREM2 mediates the relationship between microglial clustering and A β reduction in AD mice. TREM2 deficiency inhibits the recruitment of microglia to A β , demonstrating that it is a prerequisite for the formation of the neuroprotective microglia barrier (WANG et al., 2016). Further evidence supports this argument that administration of TREM2 agonist antibodies increases A β -associated microglia activation and proliferation, reducing A β pathology in an AD animal model (FASSLER et al., 2021; WANG et al., 2020).

7.4 Deficiency of GPR109a facilitates A β clearance in the brain

In our APP-knock-in mice, deficiency of GPR109a decreases cerebral A β deposits and soluble A β . It also dramatically decreases the ratio of A β 42/40. The ratio of A β 42/40 is a well-known biomarker for AD diagnosis. Elevated A β 42/A β 40 ratios positively correlate with the amyloid formation in sporadic AD (DOLEV et al., 2013). The increase of A β 42/40 ratio is linked to impairments of spontaneous synaptic activity, neuronal survival, and memory formation in AD animals (KUPERSTEIN et al., 2010). In a 3-D human neural cell culture models, A β 42/40 ratio rather than total A β levels (A β 40 or A β 42) determines A β aggregation (KWAK et al., 2020). The converging data suggests that A β accumulation is a crucial event in AD pathology, and progressive A β accumulation in the brain is thought to be the net

consequence of an imbalance between its production and clearance (HARDY, SELKOE, 2002; ZUROFF et al., 2017). Our data implicate that deficiency of GPR109a promotes microglia- and LRP1-mediated A β clearance in APP-knock-in mice.

7.4.1 Deficiency of GPR109a increases microglia-mediated A β clearance

Numerous studies have demonstrated microglia exert neuroprotective roles in early stages of AD by scavenging apoptotic cells and pathological protein aggregates (GALLOWAY et al., 2019; LEE, LANDRETH, 2010). The ability of microglia phagocytosing amyloid proteins decrease with aging. In the late stages of AD, repetitive pathogenic stimuli (*e.g.*, A β , tau) drive microglia reprogramming, resulting in a pro-inflammatory profile that reduces phagocytosis (BOCHE, GORDON, 2021; HENEKA et al., 2015; PERRY, HOLMES, 2014). Our study shows that deficiency of GPR109a promotes microglial phagocytosis of A β by around 32.9% in APP-knock-in mice as compared with GPR109a-wild-type control AD mice.

As a potential mechanism, we observed that GPR109a deficiency potentially increases niacin-induced anti-inflammatory activation (*e.g.*, secretion of IL-10) and A β phagocytosis. Niacin, a precursor for NAD⁺ and NADP⁺, is absorbed in the gut or transferred from tryptophan (GASPERI et al., 2019). Its concentration decreases in the brain of 3 \times Tg AD mice (VAN DER VELPEN et al., 2021). Niacin is a high-affinity GPR109a agonist (TUNARU et al., 2003). Our results obviously suggest that the immunomodulatory and anti-inflammatory effects of niacin are mediated by mechanisms other than GPR109a. An alternative receptor expressed by microglia might respond to niacin competitively with GPR109a (ROQUE et al., 2019). For example, G protein-coupled estrogen receptor (GPER, also known as GPR30), a seven-transmembrane GPCR, also acts as a niacin receptor with a lower affinity than GPR109a. It is widely expressed in various brain parenchymal cells in CNS. Studies have documented that GPER is involved in the anti-inflammatory effects of microglia (DU et al., 2018). One study reported that niacin binds to and activates GPER-mediated signaling in breast cancer cells and cancer-associated fibroblasts, preventing upregulation of ICAM-1 triggered by the pro-inflammatory cytokine TNF- α through GPER (SANTOLLA et al., 2014). Selective activation of GPER improves cognitive function in female 5XFAD AD mice (KUBOTA et al., 2016).

There is evidence showing that niacin insufficiency causes neurological symptoms, such as dementia and depression (GASPERI et al., 2019). A prospective study suggested that dietary niacin potentially prevents the cognitive decline related to AD and aging (MORRIS et al., 2004). Niacin treatment also increases hepatic X receptor expression, accelerating A β 42 clearance (FRICKER et al., 2018; VANMIERLO et al., 2011). Numerous studies in inflammatory and neurological diseases have shown that the anti-inflammatory properties of niacin and its neuroprotective effects are mediated by GPR109a (DIGBY et al., 2012; GIRI et al., 2019). For example, niacin reduces the secretion of pro-inflammatory mediators in LPS-activated human monocytes; knockdown of GPR109a abolishes this anti-inflammatory effect of niacin (DIGBY et al., 2012). And a most recent study on 5xFAD mouse model indicates that therapeutic doses of niacin induce a protective response of microglia to amyloid pathology mediated by GPR109a (MOUTINHO et al., 2022). However, it should be noted that in all previous therapeutic studies as well as in clinical practice, high doses (≥ 10 mM) of niacin was always used. In our cell culture experiments, we treated cells with niacin at 10 and 100 μ M that are closer to the physiological levels (SPECTOR, JOHANSON, 2007).

7.4.2 Deficiency of GPR109a elevates LRP1-mediated A β clearance

Transportation of A β from brain parenchyma to peripheral plasma might contribute 25% of total clearance of cerebral A β (ROBERTS et al., 2014). LRP1 and ABCB1 are two key transporters on blood-brain-barrier (BBB) responsible for A β efflux (KUHNKE et al., 2007; SHINOHARA et al., 2017). LRP1 expression in brain capillaries decreases with aging and the progression of AD (SHIBATA et al., 2000). Deletion or inhibition of endothelial LRP1 and ABCB1 resulted in A β accumulation in AD mouse brain (CIRRITO et al., 2005; STORCK et al., 2016). We observed that GPR109a deficiency increases the expression of LRP1 in the brain of APP-knock-in mice; however, our further experiments did not show an increase of LRP1 in cerebral capillaries of GPR109a-deficient mice, suggesting that GPR109a deficiency might promote LRP1-mediated A β clearance in the brain parenchyma.

LRP1 acts as an endocytic receptor for various ligands, including A β . It is also essential for A β removal by lysosomal degradation in the brain parenchymal cells. LRP1 is reduced in

the midfrontal cortex of AD patients compared with age-matched controls, and the amounts of LRP1 are strongly correlated with the age at the onset of AD (KANG et al., 2000). The protein level of PSD-95, indicating the preservation of synaptic connection, in postmortem tissues of AD patients is positively correlated with LRP1 (SHINOHARA et al., 2013). Conditional knockout of *lrp1* in forebrain neurons results in elevated A β and aggravated amyloid pathology in the brains of APP/PS1 mice, which appears to be caused by inhibition of LRP1-mediated neuronal A β uptake and degradation (KANEKIYO et al., 2013). Similarly, selective deletion of *lrp1* in astrocytes leads to reduced cellular A β uptake and degradation in astrocytes and downregulates the amounts of major extracellular A β degrading enzymes in the brain (e.g., MMP2, MMP9, and IDE) (LIU et al., 2017). Together, these lines of evidence suggest that restoring LRP1 expression and function in the brain may be an effective strategy to promote A β clearance and counteract amyloid pathology in AD. Although further experiments are needed to verify the concrete mechanisms of LRP1-mediated A β clearance in neurons and astrocytes in GPR109a-deficient APP-knock-in mice, our study has shed light on a possible pathway that deficiency of GPR109a facilitates A β clearance by brain cells besides microglia.

7.5 IL-17a-producing CD4-positive lymphocytes may regulate the pathogenic role of GPR109a in APP knock-in mice.

Peripheral circulating IL-17a-expressing lymphocytes might be a linker between gut bacteria and brain cells. It has been observed that deletion of gut bacteria reduces generation of IL-17a-expressing cells (BENAKIS et al., 2016; BERER, KRISHNAMOORTHY, 2012) and APP is expressed in myenteric neurons of the gut (SEMAR et al., 2013). We observed that deletion of GPR109a reduces the *il-17a* gene transcription in CD4-positive lymphocytes from lamina propria and splenocytes in APP knock-in mice. Elimination of GPR109a also reduces IL-17a-producing CD4-positive lymphocytes in the lamina propria, which reverses the increase in Th17 cells induced by APP knock-in. Moreover, in the context of IL-17a deficiency, the contribution of GPR109a deficiency in improving cognitive functions and amyloid pathologies in APP knock-in mice is eliminated. However, the morphological pattern of GPR109a-deficient microglia surrounding A β deposits is not changed by IL-17a-deficient in APP-knock-in mice.

Collectively, our data strongly suggests that IL-17a may at least partially mediate the pathogenic role of GPR109a in AD. Increased Th17 cells in the blood of AD patients have been documented (OBERSTEIN et al., 2018). IL-17a-expressing T lymphocytes accumulate in the meninges and brain of triple-transgenic AD mice (3×Tg-AD) (BRIGAS et al., 2021). In our future studies, it is worthwhile to reanalyze the pathogenic effects of GPR109a in AD mice based on IL-17a deficiency.

In summary, our study shows that deficiency of GPR109a modifies microglial activity, and increases A β clearance by microglia and possibly also by neurons and astrocytes, which subsequently attenuates amyloid pathology and protects neurons in AD mice. This study provides evidence for a potential GPR109a-independent pathway for the immunomodulatory and anti-inflammatory effects of niacin. Combining our current results with published studies, microglia "activation" is likely to involve dynamic responses to adaptive gene transcription and morphological changes. GPR109a deficiency might keep microglia in a neuroprotective homeostatic state rather than evolving into a late pro-inflammatory peak stage, but further studies are needed to verify this insight. These results contribute to a better understanding of underlying mechanisms that involve a potential therapeutic agent, niacin, for AD patients.

8. APPENDIX

Quan W, Luo Q^(Co-first author) et al., *Glia*, 2021Received: 23 February 2021 | Revised: 29 March 2021 | Accepted: 1 April 2021
DOI: 10.1002/glia.24007

WILEY

RESEARCH ARTICLE

Haploinsufficiency of microglial MyD88 ameliorates Alzheimer's pathology and vascular disorders in APP/PS1-transgenic mice

Wenqiang Quan^{1,2,3} | Qinghua Luo^{1,2} | Wenlin Hao^{1,2} | Inge Tomic^{1,2} |
Tomomi Furihata⁴ | Walter Schulz-Schäffer⁵ | Michael D. Menger⁶ |
Klaus Fassbender^{1,2} | Yang Liu^{1,2} ¹Department of Neurology, Saarland University, Homburg, Germany²German Institute for Dementia Prevention (DIDP), Saarland University, Homburg, Germany³Department of Clinical Laboratory, Tongji Hospital, Tongji University Medical School, Shanghai, China⁴Department of Clinical Pharmacy and Experimental Therapeutics, School of Pharmacy, Tokyo University of Pharmacy and Life Sciences, Hachioji, Tokyo, Japan⁵Department of Neuropathology, Saarland University, Homburg, Germany⁶Department of Experimental Surgery, Saarland University, Homburg, Germany**Correspondence**Yang Liu, Department of Neurology, Saarland University, Kirrberger Straße, Homburg 66421, Germany.
Email: a.liu@mx.uni-saarland.de**Funding information**

Bundesministerium für Bildung und Forschung, Grant/Award Number: 01ED1617B; Alzheimer Forschung Initiative, Grant/Award Number: #18009

Abstract

Growing evidence indicates that innate immune molecules regulate microglial activation in Alzheimer's disease (AD); however, their effects on amyloid pathology and neurodegeneration remain inconclusive. Here, we conditionally deleted one allele of *myd88* gene specifically in microglia in APP/PS1-transgenic mice by 6 months and analyzed AD-associated pathologies by 9 months. We observed that heterozygous deletion of *myd88* gene in microglia decreased cerebral amyloid β (A β) load and improved cognitive function of AD mice, which was correlated with reduced number of microglia in the brain and inhibited transcription of inflammatory genes, for example, *tnf- α* and *il-1 β* , in both brain tissues and individual microglia. To investigate mechanisms underlying the pathological improvement, we observed that haploinsufficiency of MyD88 increased microglial recruitment toward A β deposits, which might facilitate A β clearance. Microglia with haploinsufficient expression of MyD88 also increased vasculature in the brain of APP/PS1-transgenic mice, which was associated with up-regulated transcription of *osteopontin* and *insulin-like growth factor* genes in microglia. Moreover, MyD88-haploinsufficient microglia elevated protein levels of LRP1 in cerebral capillaries of APP/PS1-transgenic mice. Cell culture experiments further showed that treatments with interleukin-1 β decreased LRP1 expression in pericytes. In summary, haploinsufficiency of MyD88 in microglia at a late disease stage attenuates pro-inflammatory activation and amyloid pathology, prevents the impairment of microvasculature and perhaps also protects LRP1-mediated A β clearance in the brain of APP/PS1-transgenic mice, all of which improves neuronal function of AD mice.

KEYWORDS

Alzheimer's disease, LRP1, microglia, MyD88, vasculature

Wenqiang Quan and Qinghua Luo authors contributed equally to this study.

This is an open access article under the terms of the Creative Commons Attribution-NonCommercial License, which permits use, distribution and reproduction in any medium, provided the original work is properly cited and is not used for commercial purposes.

© 2021 The Authors. *GLIA* published by Wiley Periodicals LLC.

1 | INTRODUCTION

Alzheimer's disease (AD) is a progressive neurodegenerative disease pathologically characterized by extracellular amyloid β ($A\beta$) deposits, intracellular neurofibrillary tangles, and microglial activation (Heneka et al., 2015). Genome-wide association studies correlated microglial genes (i.e., *TREM2*, *APOE*, *CD33*, *ABCA7*, and *PLCG2*) with the occurrence of late-onset AD, which highlights an essential role of microglia in AD pathogenesis (Lewcock et al., 2020). In AD mouse models, which overexpress Alzheimer's amyloid precursor protein (APP) in neurons, microglia are activated and recruited to $A\beta$ deposits (Bolmont et al., 2008; Meyer-Luehmann et al., 2008), and are more closely correlated with the impairment of cognitive performance than $A\beta$ deposition (Focke et al., 2018). Elimination of microglia at a late disease stage with noticeable $A\beta$ already in the brain prevents the synaptic and neuronal loss in APP-transgenic mice (Spangenberg et al., 2016). However, activated microglia also exert a protective effect on neurons in AD mice by up-taking $A\beta$ peptides (Michaud et al., 2013) and promoting degradation of phosphorylated tau proteins in neurons (Qin et al., 2016).

Many studies through cross-breeding or bone marrow reconstruction have shown that the innate immune signaling regulates microglial activation in AD mice. Deficiency of CD14 (Reed-Geaghan, Reed, Cramer, & Landreth, 2010), Toll-like receptor (TLR) 2 (S. Liu et al., 2012), TLR4 (Song et al., 2011), myeloid differentiation factor 88 (MyD88) (Hao et al., 2011), interleukin receptor-associated kinase 4 (IRAK4) (Cameron et al., 2012), inhibitor of nuclear factor κ -B kinase subunit β (IKK β) (Y. Liu et al., 2014), or NLR family pyrin domain containing 3 (NLRP3) (Heneka et al., 2013) attenuates the degree of inflammation, shifts inflammatory activation from pro-inflammatory to anti-inflammatory profiles, or both in the brain of APP-transgenic mice. However, results on the effects of innate immunity on $A\beta$ pathology and neuronal degeneration in AD mice are often contradictory. For example, deletion of MyD88 or its downstream signaling molecule, IRAK4, and IKK β , or disruption of the interaction between TLR2 and MyD88, attenuates $A\beta$ pathology and neuronal death in APP-transgenic mice (Cameron et al., 2012; Hao et al., 2011; Lim et al., 2011; Y. Liu et al., 2014; Rangasamy et al., 2018), whereas, wild-type MyD88 was also reported to promote $A\beta$ clearance and protect neurons (Michaud, Richard, & Rivest, 2011, 2012). There was one study even showing that overall deletion of MyD88 in AD mice have no effects on neuroinflammation and $A\beta$ deposition (Weitz, Gate, Rezai-Zadeh, & Town, 2014). It is difficult to explain the apparently conflicting results delivered from different animal models and different experimental methods. However, in the investigation of MyD88 and AD, it should be noted that: (a) MyD88 functions not only in microglia, but also in other brain cells (e.g., neurons, astrocytes and endothelial cells; Gosselin & Rivest, 2008; Hung et al., 2018; Shen et al., 2016); and (b) overall deletion of MyD88 in AD mice alters development of the brain and is potentially fatal (Michaud et al., 2011; Schroeder et al., 2021). Thus, to clarify the pathogenic role of MyD88 in AD, MyD88 expression should be manipulated specifically in microglia or other brain cells within a designed time window in AD animals.

Growing evidence suggests that vascular disorders contribute to AD pathogenesis. AD patients often have vascular pathologies, which are from large artery atherosclerosis, cerebral amyloid angiopathy (CAA) to microvascular disease, and blood-brain-barrier (BBB) impairment (Cortes-Canteli & Iadecola, 2020). We observed a reduction of vasculature and blood flow in the hippocampus of APP- or tau-transgenic AD mice (Decker et al., 2018). Pericytes wrapping around endothelial cells are essential for the maintenance of normal structure and function of cerebral blood circulation, which include BBB homeostasis and angiogenesis (Sweeney, Ayyadurai, & Zlokovic, 2016). Pericytes are injured in AD at an early disease stage (Montagne et al., 2020; Nation et al., 2019). Deletion of pericytes increases permeability of BBB, decreases vasculature and blood flow, and exaggerates $A\beta$ accumulation in the brain of APP-transgenic mice (Montagne et al., 2018; Sagare et al., 2013). BBB is able to efficiently clean cerebral $A\beta$ by transporting $A\beta$ outside of brain (Roberts et al., 2014), which is at least partially mediated by low-density lipoprotein receptor-related protein 1 (LRP1) and ATP binding cassette subfamily B member 1 (ABCB1) (Kuhnke et al., 2007; Shinohara, Tachibana, Kanekiyo, & Bu, 2017). Interestingly, LRP1 also mediates $A\beta$ internalization by pericytes, thereby cleaning $A\beta$ locally at BBB (Ma et al., 2018). However, how microglia regulate microcirculation, pericyte function, and BBB-mediated $A\beta$ clearance in AD brain remains unclear.

In this study, we knocked out one allele of *myd88* gene specifically in microglia in APP/PS1-transgenic mice by 6 months and investigated amyloid pathology, neuroinflammation, and cerebral vasculature by 9 months. We observed that haploinsufficiency of MyD88 in microglia attenuated AD-associated pathologies and protected neurons.

2 | MATERIALS AND METHODS

2.1 | Animal models and Cross-breeding

APP/PS1-double transgenic mice over-expressing human mutated APP (KM670/671NL) and PS1 (L166P) under Thy-1 promoters (Radde et al., 2006) were kindly provided by M. Jucker, Hertie Institute for Clinical Brain Research, Tübingen, Germany; *myd88*-floxed mice (B6.129P2[SJL]-Myd88^{tm1Defr/J}; MyD88^{fl/fl}; Stock number: 008888; Hou, Reizis, & DeFranco, 2008) were imported from the Jackson Laboratory, Bar Harbor, ME; and Cx3Cr1-CreERT2 mice that express a fusion protein of Cre recombinase and an estrogen receptor ligand binding domain under the control of endogenous *cx3cr1* promoter/enhancer elements (Goldmann et al., 2013) were kindly provided by M. Prinz, University of Freiburg, Germany. APP/PS1-transgenic mice were cross-bred with MyD88^{fl/fl} and Cx3Cr1-Cre mice to obtain mice with the following genotypes: APP^{tg} or wtMyD88^{fl/wt}Cre^{+/-} and APP^{tg} or wtMyD88^{fl/wt}Cre^{-/-}. In order to minimize potential toxic effects of MyD88 deficiency on the physiological function, we used heterozygous *myd88*-floxed mice (MyD88^{fl/wt}) in the whole study. To induce the recombination of

myd88 gene, 6-month-old mice were injected (*i.p.*) with tamoxifen (Sigma-Aldrich Chemie GmbH, Munich, Germany; 100 mg/kg) in corn oil once a day over 5 days. The phenotype of APP/PS1-transgenic mice with or without haploinsufficient expression of MyD88 in microglia was compared between siblings. As a control experiment, APP/PS1-transgenic and Cx3Cr1-Cre mice were mated with *gpr43*-floxed mice (Tang et al., 2015) to obtain mice with APP^{tg}Gpr43^{fl/fl}Cre^{+/-} and APP^{tg}Gpr43^{fl/fl}Cre^{-/-} of genotypes. Control mice were treated completely the same as for MyD88-deficient mice. To identify cells, which express Gpr43, Gpr43-RFP reporter mice overexpressing monomeric red fluorescence protein (mRFP) under the control of *gpr43* promoter (Tang et al., 2015) were used. Both *gpr43*-floxed mice and Gpr43-RFP reporter mice were kindly provided by S. Offermanns, Max Planck Institute for Heart and Lung Research, Germany. All animal experiments were performed in accordance with relevant national rules and authorized by Landesamt für Verbraucherschutz, Saarland, Germany (permission numbers: 29/2016 and 14/2018).

2.2 | Morris water maze

The Morris water maze test, consisting of a 6-day training phase and a 1-day probe trial, was used to assess the cognitive function of APP/PS1-transgenic mice and their wild-type littermates, as previously described (Qin et al., 2016; Schnöder et al., 2020). During training phase, latency time, distance, and velocity were recorded with Ethovision video tracking equipment and software (Noldus Information Technology, Wageningen, the Netherlands). During the probe trial, the platform was removed and we measured the latency of first visit to the location of original platform, the frequency of crossing in that location, and the time spent in the platform area.

2.3 | Tissue collection and isolation of blood vessels

Animals were euthanized at 9 months of age by inhalation of isoflurane. Mice were then perfused with ice-cold PBS, and the brain was removed and divided. The left hemisphere was immediately fixed in 4% paraformaldehyde (Sigma-Aldrich Chemie GmbH) in PBS and embedded in paraffin for immunohistochemistry. For one part of mice, a 0.5- μ m-thick sagittal piece of tissue was cut from the right hemisphere. The cortex and hippocampus were carefully separated and homogenized in TRIzol (Thermo Fisher Scientific, Darmstadt, Germany) for RNA isolation. The remainder of the right hemisphere was snap-frozen in liquid nitrogen and stored at -80°C until biochemical analysis.

For the other part of mice, the cortex and hippocampus from right hemisphere were carefully dissected and brain vessel fragments were isolated according to the published protocol (Boulay, Saubamea, Declèves, & Cohen-Salmon, 2015). Briefly, brain tissues were homogenized in HEPES-contained Hanks' balanced salt solution (HBSS) and centrifuged at 4,400g in HEPES-HBSS buffer supplemented with

dextran from *Leuconostoc spp.* (molecular weight $\sim 70,000$; Sigma-Aldrich Chemie GmbH) to delete myelin. The vessel pellet was re-suspended in HEPES-HBSS buffer supplemented with 1% bovine serum albumin (Sigma-Aldrich Chemie GmbH) and filtered with 20 μ m-mesh. The blood vessel fragments were collected on the top of filter and stored at -80°C for biochemical analysis.

2.4 | Histological analysis

Serial 30- μ m-thick sagittal sections were cut from the paraffin-embedded hemisphere. For each animal, four sections with an interval of 10 layers between neighboring sections were examined. Human A β was stained with rabbit anti-human A β antibody (clone D12B2; Cell Signaling Technology Europe, Frankfurt am Main, Germany) and microglia labeled with rabbit anti-ionized calcium-binding adapter molecule (Iba)-1 antibody (Wako Chemicals, Neuss, Germany), and visualized with the VectaStain Elite ABC kit (Vector Laboratories, Burlingame, USA) or fluorescence-conjugated second antibodies. In the whole hippocampus, volumes of A β were estimated with the Cavalieri method, and Iba-1-positive cells were counted with Optical Fractionator as described previously (Y. Liu et al., 2014) on a Zeiss AxioImager.Z2 microscope (Carl Zeiss Microscopy GmbH, Göttingen, Germany) equipped with a Stereo Investigator system (MBF Bioscience, Williston, ND).

To evaluate the cerebral A β deposition, four serial brain sections from each animal were labeled with methoxy-XO4 (Tocris Bioscience, Wiesbaden-Nordenstadt, Germany) after deparaffinization. The whole cortex and hippocampus were imaged with MicroLucida (MBF Bioscience) and merged. Fluorescence-labeled areas were measured using the Image J software (<https://imagej.nih.gov/ij/>) with fixed thresholds for all compared animals. The percentage of A β coverage in the brain was calculated.

To detect the deposition of A β at blood vessels, brain sections were co-stained with human A β antibody (clone D12B2) and biotin-labeled *Griffonia simplicifolia* Lectin I isolectin B4 (Catalog number: B-1205; Vector Laboratories, Burlingame, CA), and Alexa488-conjugated anti-rabbit IgG and Cy3-conjugated streptavidin, respectively (Thermo Fisher Scientific). To identify Gpr43-expressing cells, brain sections from Gpr43-reporter mice were co-stained with rabbit anti-RFP antibody (Catalog number: 600-401-379; Rockland Immunochemicals, Limerick, PA) and mouse anti-Tmem119 antibody (clone: 195H4; Synaptic Systems GmbH, Göttingen, Germany), which were followed by incubation with Alexa488 or Cy3-conjugated second antibodies (Thermo Fisher Scientific).

The relationship between microglia and A β deposits was investigated as we did in a previous study (Hao et al., 2011). Serial brain sections were stained with Iba-1 antibody (Wako Chemicals) and Alexa546-conjugated anti-rabbit IgG (Thermo Fisher Scientific), and then co-stained with methoxy-XO4 (Bio-Techne GmbH). Under Zeiss microscopy with 40x objective, A β deposits were imaged with green fluorescence filter. Thereafter, Z-stack serial scanning from -10 to $+10$ μ m was performed under both green and orange fluorescence



filters. From each section, more than 10 randomly chosen areas were analyzed. The total number (>200) of Iba-1-positive cells co-localizing with A β deposits were counted. The area of A β was measured with Image J and used for the adjustment of microglial cell number.

To quantify vasculature in the brain, our established protocol was used (Decker et al., 2018; Quan et al., 2020). Four serial paraffin-embedded sections per mouse with 300 μ m of distance in between were deparaffinized, heated at 80°C in citrate buffer (10 mM, pH = 6) for 1 hr and digested with Digest-All 3 (Pepsin) (Thermo Fisher Scientific) for 20 min. Thereafter, brain sections were stained with rabbit anti-collagen IV polyclonal antibody (Catalog number: ab6586; Abcam, Cambridge, UK) and Alexa488-conjugated goat anti-rabbit IgG (Thermo Fisher Scientific). After being mounted, the whole hippocampus was imaged with MicroLucida (MBF Bioscience). The length, branching points, and density of collagen type IV staining-positive blood vessels were analyzed with a free software, AngioTool (<http://angiotool.nci.nih.gov>; Zudaire, Gambardella, Kurcz, & Vermeren, 2011). The mean diameter of blood vessels was calculated by dividing total area of blood vessels with the total length of vessels. The parameters of analysis for all compared samples were kept constant. The length and branching points were adjusted with brain area of interest.

2.5 | Western blot analysis

Frozen mouse brains were homogenized on ice in 5 \times radio-immunoprecipitation assay buffer (RIPA buffer; 50 mM Tris [pH 8.0], 150 mM NaCl, 0.1% SDS, 0.5% sodiumdeoxy-cholate, 1% NP-40, and 5 mM EDTA) supplemented with protease inhibitor cocktail (Sigma-Aldrich Chemie GmbH), followed by centrifugation at 16,000g for 30 min at 4°C to collect the supernatants. Isolated blood vessels were directly lysed in 2 \times SDS-PAGE sample loading buffer containing 4% SDS and sonicated before loading. The protein levels of synaptic proteins: Munc18-1 protein mammalian homolog (Munc18-1), synaptosome-associated protein 25 (SNAP-25), postsynaptic density protein 95 (PSD-95) and synaptophysin were detected with rabbit polyclonal antibodies (Catalog numbers: 13414, 3926, and 2507, respectively; Cell Signaling Technology) and mouse monoclonal antibody (clone SY38; Abcam). In the same sample, β -actin was detected as a loading control using rabbit monoclonal antibody (clone: 13E5; Cell Signaling Technology). For the detection of proteins in cerebral capillaries, rabbit monoclonal antibodies against platelet-derived growth factor receptor β (PDGFR β), CD13/APN, ABCB1, and vinculin (clone: 28E1, D6V1W, E1Y7S, and E1E9V respectively; Cell Signaling Technology) and rabbit polyclonal antibodies against LRP1 and α -tubulin (Catalog numbers: 64099 and 2144, respectively; Cell Signaling Technology), tight junction protein 1 (TJP1; Catalog numbers: NBP1-85047; Novus Biologicals, Wiesbaden-Nordenstadt, Germany), Claudin-5 (Thermo Fisher Scientific) and aquaporin 4 (AQP4; Proteintech Europe, Manchester, United Kingdom) were used. Western blots were visualized via the ECL method (PerkinElmer LAS GmbH, Rodgau, Germany). Densitometric analysis of bands was performed with the Image J software. For each sample, the protein level was calculated as a ratio of target protein/ β -actin, α -tubulin or vinculin.

For detection of A β oligomers, the proteins in the brain homogenate or in the isolated blood vessels were separated by 10–20% precasted Tris-Tricine gels (Anamed Elektrophorese GmbH, Groß-Bieberau/Rodau, Germany). For Western blot, anti-human A β mouse monoclonal antibody (clone W0-2; Merck Chemicals GmbH, Darmstadt, Germany), anti- β -actin, or anti- α -tubulin antibodies (Cell Signaling Technology) were used.

2.6 | β - and γ -secretase activity assays

Membrane components were purified from the brain homogenate of 9-month-old APP/PS1-transgenic mice with and without heterozygous deletion of *myd88* gene and β - and γ -secretase activity were measured by incubating the crude membrane fraction with secretase-specific FRET substrates according to our established methods (Hao et al., 2011; Xie et al., 2013).

2.7 | Positive selection of CD11b-positive microglia in the adult mouse brain

To determine the gene expression in microglia, CD11b-positive cells were isolated from the entire cerebrum of 9-month-old APP/PS1-transgenic mice with our established protocol (Y. Liu et al., 2014). A single-cell suspension was prepared with Neural Tissue Dissociation Kit (papain-based) (Miltenyi Biotec B.V. & Co. KG, Bergisch Gladbach, Germany) and selected with MicroBeads-conjugated CD11b antibody (Miltenyi Biotec). Lysis buffer was immediately added to CD11b-positive cells for isolation of total RNA with RNeasy Plus Mini Kit (Qiagen, Hilden, Germany).

2.8 | Quantitative PCR for analysis of gene transcripts

Total RNA was isolated from mouse brains or selected CD11b-positive cells and reverse-transcribed. Gene transcripts were quantified with our established protocol (Y. Liu et al., 2014) using Taqman gene expression assays of mouse *tumor necrosis factor (tnf- α)*, *interleukin-1 β (il-1 β)*, *inducible nitric oxide synthase (inos)*, *chemokine (C-C motif) ligand 2 (cd-2)*, *il-10*, *chitinase-like 3 (chi3l3)*, *mannose receptor C type 1 (mrc1)*, *insulin-like growth factor (igf)-1, triggering receptor expressed on myeloid cells 2 (trem2)*, *apoe*, *CX3C chemokine receptor 1 (cx3cr1)*, *purinergic receptor P2Y12 (p2ry12)*, *C-type lectin domain family 7 member A (clec7a)*, *lipoproteinlipase (lpl)*, *transforming growth factor β receptor 1 (tgfbr1)*, *integrin α X (itgax)*, *nephrilysin*, *insulin-degrading enzyme (ide)*, and *glyceraldehyde 3-phosphate dehydrogenase (gapdh)* (Thermo Fisher Scientific). The transcription of *osteopontin (opn)*, *vascular endothelial growth factor (vegf)*, and *peptidyl-prolyl cis-trans isomerase A (ppia)* genes in CD11b-positive cells was evaluated using the SYBR green binding technique with the following pairs of primers: *opn*, 5'-CAGCCATGAGTCAAGTCAGC-3' and 5'-TGTGGCTGTGAAACTTGTGG-3'; *vegf*, 5'-CCCTTCGTCTCTCTTACC-3' and

5'-AGGAAGGTAAGCCACTCAC-3'; and *ppia*, 5'-AGCATACAGGT CCTGGCATCTTGT-3' and 5'-CAAAGACCACATGCTTGCCATCCA-3'. The primer sequences for detecting the transcripts of various receptors of free fatty acids were listed in the legend of Figure S1.

2.9 | Pericyte culture and treatments

Human primary brain vascular pericytes (HBPC) were immortalized by infecting cells with tsSV40T lentiviral particles (Umehara et al., 2018). The selected immortalized HBPC clone 37 (hereafter referred to as HBPC/ci37) was used for our study. HBPC/ci37 cells were cultured at 33°C with 5% CO₂/95% air in pericyte medium (Catalog: # 1201; Sciencell Research Laboratories, Carlsbad, CA) containing 2% (v/v) fetal bovine serum, 1% (w/v) pericyte growth factors, and penicillin-streptomycin. Culture flasks and plates were treated with Collagen Coating Solution (Catalog: # 125-50; Sigma-Aldrich). HBPC/ci37 cells were used at 40–60 passages in this study.

To investigate the effects of inflammatory activation on expression of LRP1, PDGFR β , and CD13, pericytes were cultured in 12-well plate at 5.0×10^5 cells/well. Before experiments, the culture medium was replaced with serum-free pericyte medium and cells were cultured at 37°C for 3 days to facilitate the cell differentiation (Umehara et al., 2018). Thereafter, pericytes were treated with recombinant human IL-1 β (Catalog: # 201-LB; R&D Systems, Wiesbaden-Nordenstadt, Germany) at 0, 5, 10 and 50 ng/ml for 24 hr, or for 8 days with and without withdrawal of IL-1 β for the last 3 days. At the end of experiments, cultured cells were lysed in RIPA buffer supplemented with protease inhibitor cocktail. Protein levels of LRP1, PDGFR β , and CD13 were detected with quantitative Western blot as described in Section 2.5.

2.10 | Statistical analysis

Data were presented as mean \pm SEM. For multiple comparisons, we used one-way or two-way ANOVA followed by Bonferroni, Tukey, or Dunnett T3 post hoc test (dependent on the result of Levene's test to determine the equality of variances). Two independent-samples Students *t*-test was used to compare means for two groups of cases. All statistical analyses were performed with GraphPad Prism 8 version 8.0.2. for Windows (GraphPad Software, San Diego, CA). Statistical significance was set at $p < .05$.

3 | RESULTS

3.1 | Haploinsufficient expression of MyD88 in microglia protects neurons and improves cognitive function of APP/PS1-transgenic mice

To investigate effects of microglial MyD88 on AD pathogenesis, we mated APP/PS1-transgenic mice with MyD88^{fl/fl} mice and Cx3Cr1-CreERT2 mice. Littermate mice with APP^{tg}MyD88^{fl/wt}Cre^{+/-} and APP^{tg}MyD88^{fl/wt}Cre^{-/-}

of genotypes were injected with tamoxifen at 6 months of age. Tamoxifen-induced gene recombination should delete one allele of *myd88* gene in >93% microglia but not in other brain cells (Goldmann et al., 2013). Tamoxifen injection also knocks out loxP site-flanked *myd88* gene in peripheral Cx3Cr1-positive myeloid cells; however, normal MyD88-expressing myeloid cells produced from the bone marrow should replace these MyD88-deficient cells within 1 month (Goldmann et al., 2013). By detecting *myd88* gene transcripts in CD11b-positive brain cells from 9-month-old APP^{tg}MyD88^{fl/wt}Cre^{+/-} (MyD88^{het}) and APP^{tg}MyD88^{fl/wt}Cre^{-/-} (MyD88^{wt}) mice, we observed that the transcriptional level of *myd88* in microglia of MyD88^{het} mice was only 11.4% of that in MyD88^{wt} mice (*myd88/gapdh*: 0.178 \pm 0.054 [wt] and 0.020 \pm 0.004 [het]; *t* test, $p = .044$; $n = 3$ per group), which was in accordance with a previous observation that heterozygous knockout of *myd88* gene reduced *myd88* transcripts by 66% in the whole brain of APP-transgenic mice (Michaud et al., 2011). As a control, transcriptional levels of *myd88* (*myd88/gapdh*) in CD11b-positive blood cells were 0.100 \pm 0.023 and 0.123 \pm 0.025, in MyD88^{het} and MyD88^{wt} mice, respectively (*t* test, $p = .518$; $n = 4$ per group), which indicated that peripheral myeloid cells had been replenished by bone marrow-produced cells expressing MyD88 at a normal level.

We used the Morris water maze test to examine cognitive function of mice. During the acquisition phase, 9-month-old non-APP-transgenic (APP^{wt}) littermate mice with or without haploinsufficiency of microglial MyD88 (APP^{wt}MyD88^{fl/wt}Cre^{+/-} and APP^{wt}MyD88^{fl/wt}Cre^{-/-}) showed no significant differences in either swimming time or swimming distance before climbing onto the escape platform (Figure 1a,b; two-way ANOVA, $p > .05$). Compared to APP^{wt}MyD88^{fl/wt}Cre^{-/-} littermates, 9-month-old APP^{tg}MyD88^{fl/wt}Cre^{-/-} mice with normal MyD88 expression spent significantly more time (Figure 1a; two-way ANOVA, $p < .05$) and traveled longer distances (Figure 1b; two-way ANOVA, $p < .05$) to reach the escape platform. Interestingly, APP^{tg}MyD88^{fl/wt}Cre^{+/-} mice with the heterozygous deletion of microglial MyD88 performed significantly better than their APP^{tg}MyD88^{fl/wt}Cre^{-/-} littermates in searching and finding the platform after 3 days of training (Figure 1a,b; two-way ANOVA, $p < .05$). The swimming velocity did not differ between MyD88-deficient and wild-type APP-transgenic mice or for the same mice on different training dates (data not shown).

Twenty-four hours after the end of training phase, the escape platform was removed and a 5-min probe trial was conducted to test the memory of mice. Compared to APP^{wt}MyD88^{fl/wt}Cre^{-/-} littermates, APP^{tg}MyD88^{fl/wt}Cre^{-/-} mice crossed the region where the platform had been located with significantly less frequency, and remained for a significantly longer time in their first visit to the original platform region during the total 5-min probe trial (Figure 1c,d; one-way ANOVA followed by *post-hoc* test, $p < .05$). Interestingly, when compared to APP^{tg}MyD88^{fl/wt}Cre^{-/-} mice, APP^{tg}MyD88^{fl/wt}Cre^{+/-} mice were able to cross the region more frequently and reach the original platform region in less time (Figure 1c,d; one-way ANOVA followed by *post-hoc* test, $p < .05$). We observed differences in neither parameter analyzed in the probe trial between APP^{wt}MyD88^{fl/wt}Cre^{+/-} and APP^{wt}MyD88^{fl/wt}Cre^{-/-} littermate mice (Figure 1c,d; one-way ANOVA, $p > .05$).

In our previous study, we have observed that overexpression of APP/PS1 decreases protein levels of synaptic proteins

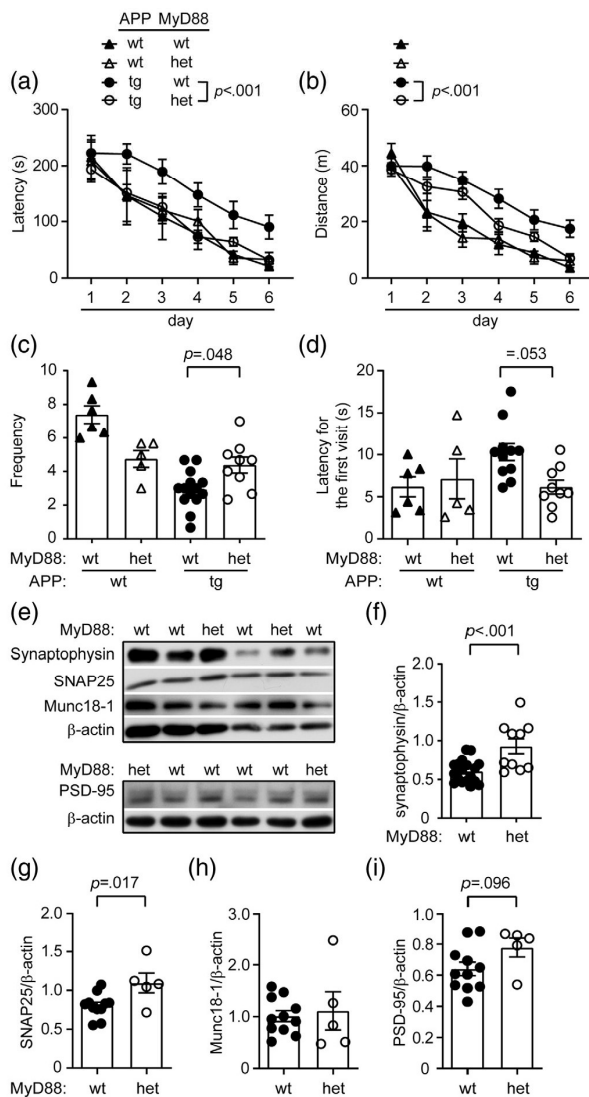


FIGURE 1 Haploinsufficiency of microglial MyD88 improves cognitive function and attenuates AD-associated loss of synaptic proteins in APP/PS1-transgenic mice. During the training phase of the water maze test, 9-month-old APP-transgenic mice (APPtg) spent more time and traveled longer distances to reach the escape platform than did their non-APP-transgenic littermates (APPwt). Compared to mice with normal expression of MyD88 (wt), heterozygous deletion of MyD88 in microglia (het) significantly reduced the traveling time and distance of APPtg mice but not of APPwt mice (a,b; two-way ANOVA followed by Bonferroni post hoc test; $n \geq 5$ per group). In the probe trial, APPtg mice crossed the region where the platform was previously located with significantly less frequency during the total 5-min experiment, and spent significantly longer time in the first visit to the platform region; heterozygous deletion of MyD88 in microglia recovered these APP expression-induced cognitive impairments (c,d; one-way ANOVA followed by Bonferroni post hoc test). Western blotting was used to detect the amount of synaptic structure proteins, Munc18-1, SNAP25, synaptophysin, and PSD-95 in the brain homogenate of 9-month-old APPtg mice (e–i). Haploinsufficiency of microglial MyD88 was associated with higher protein levels of synaptophysin and SNAP25 (t test; $n \geq 5$ per group)

(Schnöder et al., 2020). We further used Western blot analysis to quantify the levels of four synaptic structure proteins: Munc18-1, synaptophysin, SNAP-25, and PSD-95 in the brain homogenate of 9-month-old APP^{tg} littermate mice with different expression of MyD88. As shown in Figure 1e–g, protein levels of synaptophysin, and SNAP-25 in APP^{tg}MyD88^{fl/wt}Cre^{+/-} mice were significantly higher than levels of these proteins derived from APP^{tg}MyD88^{fl/wt}Cre^{-/-} littermate mice (t test, $p < .05$). Haploinsufficient expression of MyD88 in microglia tended to increase the protein level of PSD-95 in the brain as compared with MyD88-wildtype AD mice (Figure 1i; t test, $p = .096$).

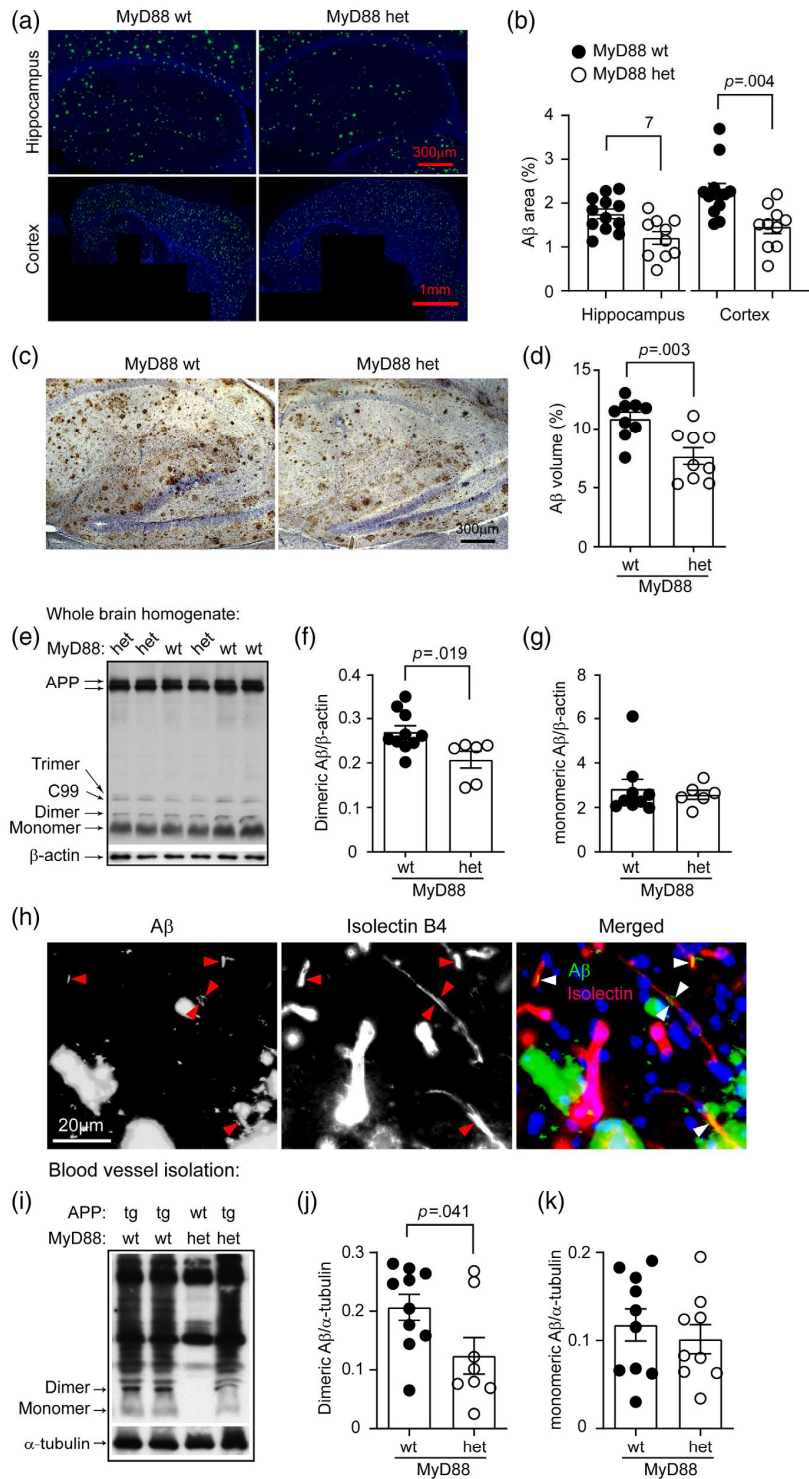
3.2 | Haploinsufficient expression of MyD88 in microglia reduces A β load in the brain parenchyma and blood vessels of APP/PS1-transgenic mice

After observing that heterozygous deletion of MyD88 in microglia attenuated cognitive deficits of APP^{tg} mice but not of APP^{wt} littermates, we analyzed the effects of microglial MyD88 on A β load in the APP^{tg} mice, as A β is the key molecule leading to neurodegeneration in AD (Mucke & Selkoe, 2012). We stained brain sections from APP^{tg}MyD88^{fl/wt}Cre^{+/-} and APP^{tg}MyD88^{fl/wt}Cre^{-/-} mice with methoxy-XO4, which specifically recognizes β -sheet secondary structure of A β . We observed that haploinsufficiency of microglial MyD88 significantly reduced the area of methoxy-XO4 staining-positive A β plaques in both hippocampus and cortex of APP/PS1-transgenic mice (Figure 2a,b; t test, $p < .05$). We then used standard immunohistological and stereological Cavalieri methods to evaluate A β volume, adjusted relative to the volume of analyzed tissues, in the hippocampus of 9-month-old APP^{tg}MyD88^{fl/wt}Cre^{+/-} and APP^{tg}MyD88^{fl/wt}Cre^{-/-} mice. The volume of $7.67\% \pm 0.71\%$ of APP^{tg}MyD88^{fl/wt}Cre^{+/-} mice was significantly lower than that of APP^{tg}MyD88^{fl/wt}Cre^{-/-} mice ($10.83\% \pm 0.56\%$; Figure 2c,d; t test, $p < .05$).

To measure the amount of oligomeric A β in brain tissues, quantitative Western blot was performed as we did in previous studies (Schnöder et al., 2016, 2020). We observed that the protein level of dimeric but not monomeric A β in 9-month-old APP^{tg}MyD88^{fl/wt}Cre^{+/-} mice was significantly lower than that in APP^{tg}MyD88^{fl/wt}Cre^{-/-} littermates (Figure 2e,f; t test, $p < .05$). Dimer has been considered as a toxic species of A β aggregates (Shankar et al., 2008).

A β is deposited not only in the brain parenchyma, but also at blood vessels (Stakos et al., 2020). Blood circulation contributes to A β clearance (Roberts et al., 2014). APP/PS1-transgenic mice used in our study were not a typical animal model for amyloid angiopathy; however, we observed an impairment of vasculature in their brain (Decker et al., 2018). Thus, we examined the potential localization of A β at blood vessels. We did observe that A β deposited in and around cerebral blood vessels of APP/PS1-transgenic mice (Figure 2h). To quantify the blood vessels-associated A β , we isolated capillaries from the brain homogenate and detected A β in the tissue lysate. Interestingly, the protein level of dimeric A β in APP^{tg}MyD88^{fl/wt}Cre^{+/-} mice was also significantly lower than that in APP^{tg}MyD88^{fl/wt}Cre^{-/-} littermate mice (Figure 2i,j; t test, $p < .05$). As a negative experimental control,

FIGURE 2 Haploinsufficiency of microglial MyD88 reduces cerebral A β load in APP/PS1-transgenic mice. Six-month-old APP^{tg}MyD88^{fl/wt}Cre^{+/-} (MyD88 het) and APP^{tg}MyD88^{fl/wt}Cre^{-/-} (MyD88 wt) were injected with tamoxifen and analyzed by 9 months of age for A β load in the brain. Brain sections were first stained with methoxy-XO4 and imaged with MicroLucida (a). The area of A β plaques were quantified and adjusted by the area of analyzed brain tissue (b). Brain sections were further stained with human A β -specific antibodies (c) and the volume of immune reactive A β deposits in hippocampus were estimated with stereological Cavalieri method and adjusted by the volume of analyzed tissues (d). Heterozygous deletion of microglial MyD88 significantly decreases A β deposits in the brain (b,d; *t* test; *n* \geq 9 per each group). The brains derived from 9-month-old microglial MyD88-het and wt APP-transgenic mice were also homogenized in RIPA buffer for Western blot analysis of soluble A β (monomeric and dimeric) (e). To demonstrate the relationship between blood vessels and A β , brain sections were co-stained A β antibodies and isolectin B4. Some A β deposits are located in and around the vessels (h; marked with arrow heads). Thereafter, micro blood vessels were isolated from 9-month-old MyD88-het and wt APP-transgenic mice and homogenized in RIPA buffer for Western blot analysis of monomeric and dimeric A β . Haploinsufficiency of MyD88 significantly reduces dimeric A β in the whole brain homogenate and isolated cerebral blood vessels of APP-transgenic mice (f,g,j,k; *t* test; *n* \geq 6 per each group) [Color figure can be viewed at wileyonlinelibrary.com]



oligomeric A β species could not be detected in capillaries isolated from non-APP transgenic mice (Figure 2i).

In APP^{tg}Myd88^{fl/wt}Cre^{+/-} mice, one allele of *cx3cr1* gene is replaced by the insertion of Cre-encoding sequence (Yona et al., 2013). To investigate the potential effects of heterozygous knockout of *cx3cr1* gene in

APP^{tg}Myd88^{fl/wt}Cre^{+/-} mice, we created APP/PS1-transgenic control mice with APP^{tg}Gpr43^{fl/fl}Cre^{+/-} and APP^{tg}Gpr43^{fl/fl}Cre^{-/-} of genotypes, in which *gpr43*, instead of *myd88* gene was loxP site-flanked. By detecting *gpr43* gene transcripts in CD11b-positive brain cells and staining RFP in the brain tissue of Gpr43-reporter mice, we observed that

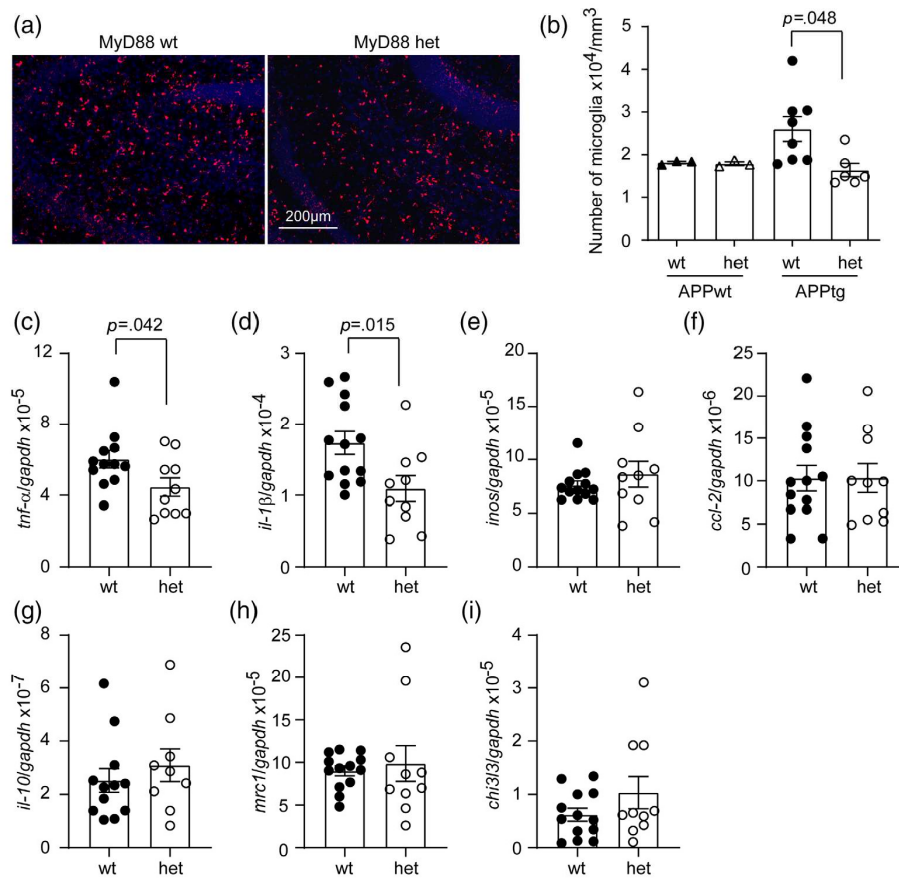


FIGURE 3 Haploinsufficiency of microglial MyD88 inhibits inflammatory activation in the brain of APP-transgenic mice. Six-month-old APP^{tg}MyD88^{fl/wt}Cre^{+/-} (MyD88 het) and APP^{tg}MyD88^{fl/wt}Cre^{-/-} (MyD88 wt) mice were injected with tamoxifen and analyzed at 9 months of age for neuroinflammation. Microglia were stained with fluorescence-conjugated Iba-1 antibodies (a) and counted with the stereological probe, Optical Fractionator. Haploinsufficiency of MyD88 reduced Iba-1-positive cells in 9-month-old APP-transgenic (APPtg) mice, but not in 9-month-old APP-wild-type (APPwt) mice (b); one-way ANOVA followed by Bonferroni post hoc test; $n \geq 6$ per group for APPtg mice and $n = 3$ per group for APPwt mice. The inflammatory activation in brain was further analyzed with real-time PCR to detect transcripts of both pro- and anti-inflammatory genes (c-i). Transcription of pro-inflammatory genes, *tnf- α* and *il-1 β* , was reduced by heterozygous deletion of MyD88 in 9-old APPtg mice (c and d; t test; $n \geq 9$ per group) [Color figure can be viewed at wileyonlinelibrary.com]

there was no expression (or expression at a very low level) of Gpr43 in microglia (see Figure S1a,b), which corroborated a previous observation (Emy et al., 2015). As Gpr43 was absent in microglia of both APP^{tg}Gpr43^{fl/fl}Cre^{+/-} and APP^{tg}Gpr43^{fl/fl}Cre^{-/-} mice, the phenotypical difference between these two groups of mice was caused by haploinsufficiency of Cx3Cr1. Surprisingly, with immunohistochemical methods, we did not detect changes of cerebral A β deposits in APP^{tg}Gpr43^{fl/fl}Cre^{+/-} mice compared with APP^{tg}Gpr43^{fl/fl}Cre^{-/-} littermate mice (see Figure S1c,d; t test, $p > .05$).

3.3 | Haploinsufficient expression of MyD88 in microglia inhibits pro-inflammatory activation in APP/PS1-transgenic mouse brain

Microglial inflammatory activation contributes to neuronal degeneration (Heneka et al., 2015). We observed that the number of Iba-1-

immunoreactive cells (representing microglia) in the hippocampus was significantly fewer in 9-month-old microglial MyD88-haploinsufficient APP/PS1-transgenic mice than in MyD88-wild-type APP/PS1-transgenic littermates (APP^{tg}MyD88^{fl/wt}Cre^{+/-} mice, $1.64 \pm 0.16 \times 10^4$ cells/mm³ vs. APP^{tg}MyD88^{fl/wt}Cre^{-/-} mice, $2.60 \pm 0.29 \times 10^4$ cells/mm³; t test, $p < .05$; Figure 3a,b). Haploinsufficiency of MyD88 in microglia did not change the number of Iba-1-positive cells in 9-month-old non-APP transgenic mice (Figure 3b; t test, $p > .05$).

We further measured transcripts of M1-inflammatory genes (*tnf- α* , *il-1 β* , *inos*, and *ccl-2*) and M2-inflammatory genes (*il-10*, *chi3l3*, and *mrc1*) in brains of 9-month-old APP^{tg}MyD88^{fl/wt}Cre^{+/-} and APP^{tg}MyD88^{fl/wt}Cre^{-/-} mice. As shown in Figure 3c,d, haploinsufficient expression of MyD88 in microglia significantly reduced cerebral *tnf- α* and *il-1 β* transcripts in APP-transgenic mice compared to MyD88-wildtype AD littermate mice (t test, $p < .05$). However, the transcription of other genes tested was not changed by MyD88 deficiency in microglia (Figure 3e-i).

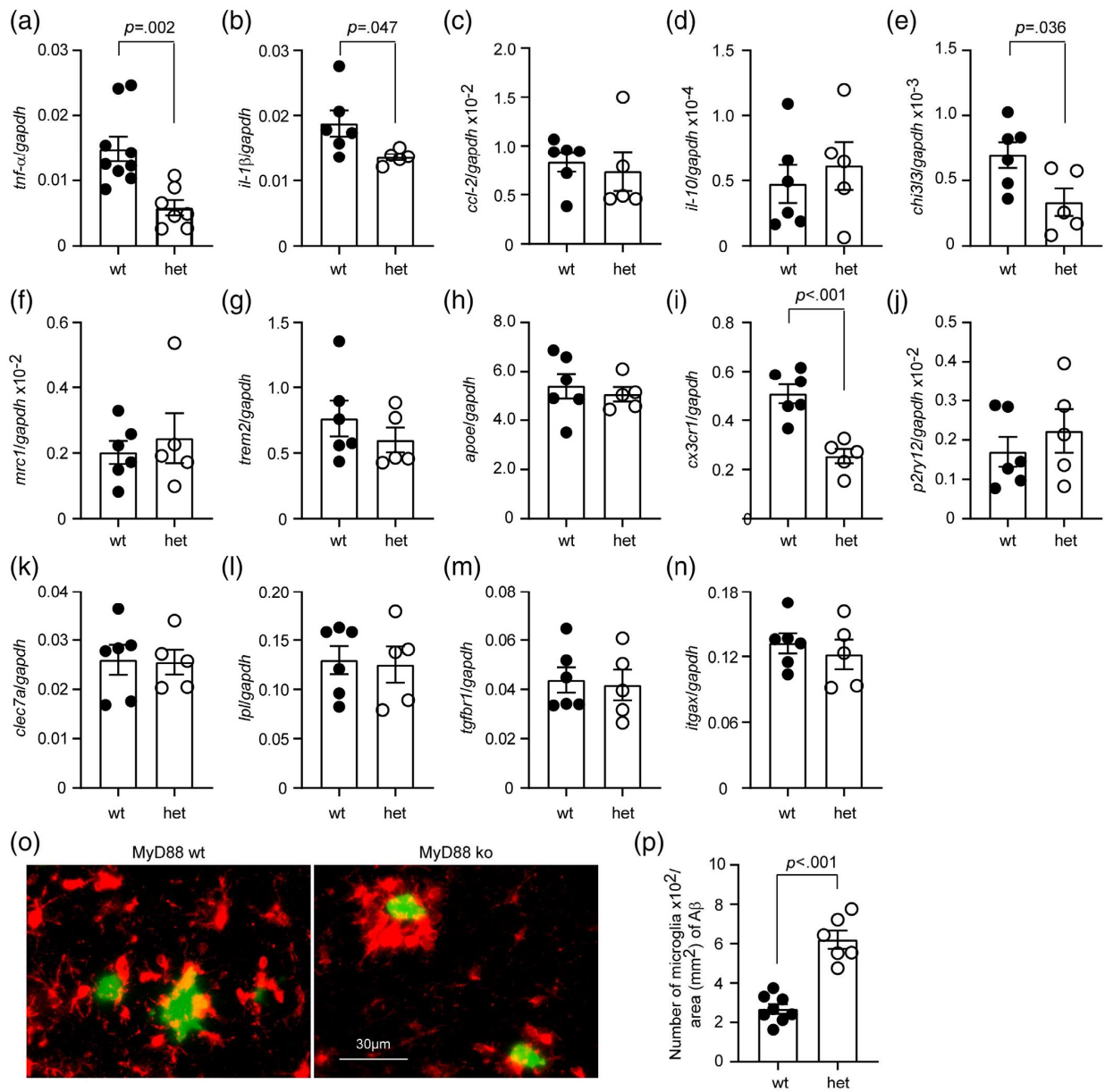


FIGURE 4 Haploinsufficiency of MyD88 inhibits pro-inflammatory activation in microglia and enhances microglial responses to A β deposits in the brain of APP-transgenic mice. Microglia were selected with magnetic beads-conjugated CD11b antibodies from 9-month-old tamoxifen-injected APP^{tg}MyD88^{fl/wt}Cre^{+/-} (MyD88 het) and APP^{tg}MyD88^{fl/wt}Cre^{-/-} (MyD88 wt) mice. Transcription of signature genes associated with neurodegenerative diseases were detected with real-time PCR. MyD88 deficiency significantly decreases transcripts of *tnf- α* , *il-1 β* , *chi3l3*, and *cx3cr1* genes (a,b,e,i; t test; $n \geq 5$ per group). *Iba-1* was also co-stained with methoxy-XO4, which recognizes aggregated A β (o). Haploinsufficiency of MyD88 significantly increases recruitment of microglia toward A β deposits (p ; t test; $n \geq 6$ per each group) [Color figure can be viewed at wileyonlinelibrary.com]

In additional experiments, we also detected transcripts of inflammatory genes (*tnf- α* , *il-1 β* , *ccl-2*, and *il-10*) in the brains of 9-month-old APP^{tg}Gpr43^{fl/fl}Cre^{+/-} and APP^{tg}Gpr43^{fl/fl}Cre^{-/-} mice, which were injected with tamoxifen by 6 months of age. As shown in Figure S1e-h, heterozygous deletion of *cx3cr1* gene did not change the inflammatory gene transcription in APP^{tg}Gpr43^{fl/fl}Cre^{+/-} mice as compared with Cx3Cr1-wild-type APP^{tg}Gpr43^{fl/fl}Cre^{-/-} mice (t test, $p > 0.05$).

3.4 | Haploinsufficient expression of MyD88 suppresses pro-inflammatory activation in microglia but enhances microglial responses to A β in APP/PS1-transgenic mice

Recently, disease-associated microglia (DAM) phenotype was defined after comparing microglial transcriptome between APP/PS1-transgenic

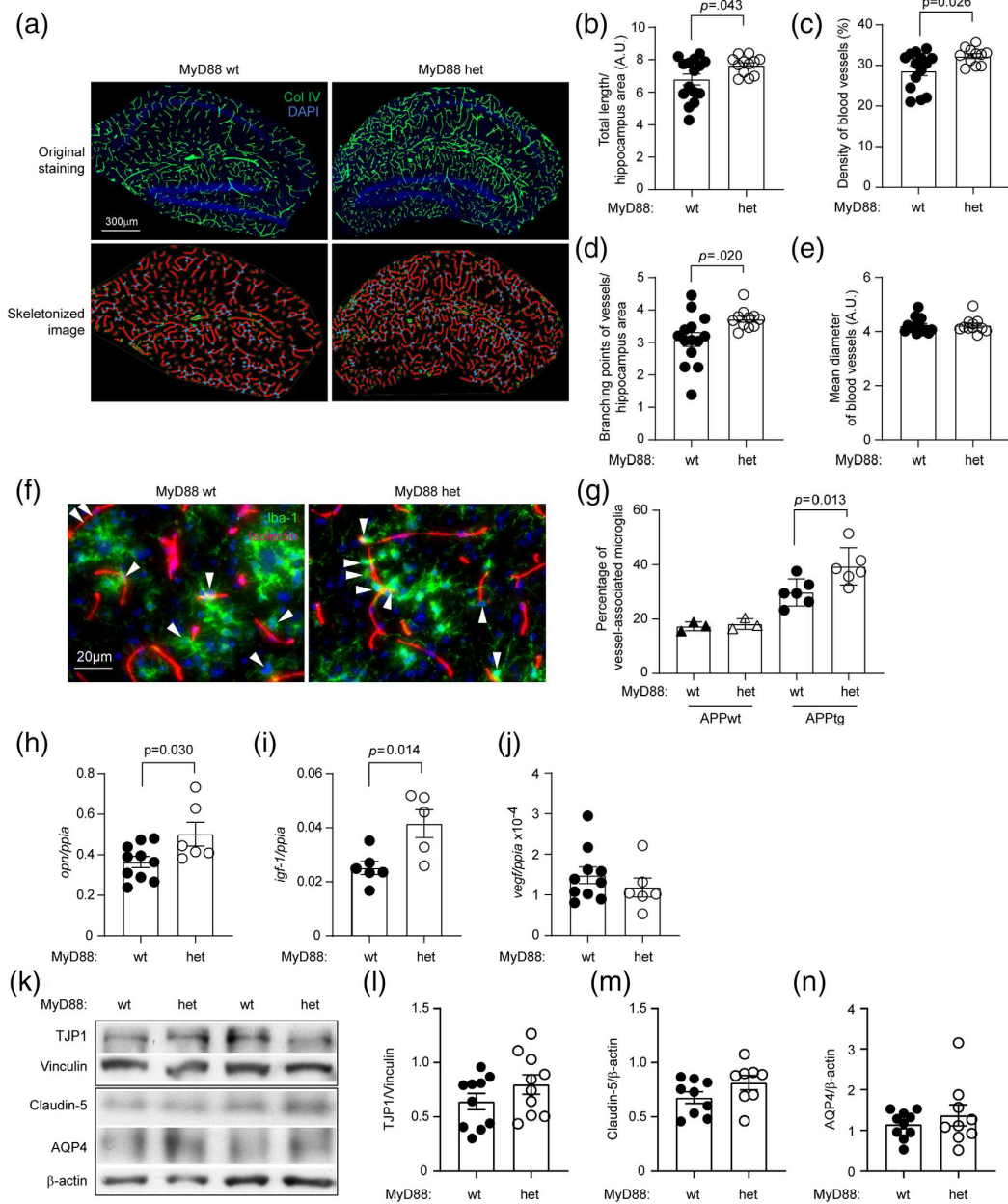


FIGURE 5 Haploinsufficiency of microglial MyD88 increases cerebral vasculature of APP/PS1-transgenic mice. The brains of 9-month-old tamoxifen-injected APP^{tg}MyD88^{fl/wt}Cre^{+/-} (MyD88 het) and APP^{tg}MyD88^{fl/wt}Cre^{-/-} (MyD88 wt) mice were stained for collagen type IV. The blood vessels in the hippocampus were thresholded and skeletonized. The skeleton representation of vasculature is shown in red and branching points of blood vessels are in blue (a). The total length, density and branching points of blood vessels were calculated and adjusted by area of analysis (b–d; *t* test, $n \geq 11$ per group). The mean diameter of blood vessels was calculated by dividing area of total blood vessels with total length of vessels (e). In order to analyze the relationship between vasculature and microglia, brain sections were co-stained with isolectin B4 (in red) and Iba-1 antibodies (in green) (f). Haploinsufficiency of MyD88 in microglia significantly increased the distribution of microglia around blood vessels (g; one-way ANOVA followed by Bonferroni post hoc test; $n = 6$ per group for APP-transgenic [tg] mice and $n = 3$ per group for APP-wildtype [wt] mice). Moreover, CD11b-positive brain cells were quantified for the transcription of pro-angiogenic genes. The transcription of *opn* and *igf-1* genes, but not of *vegfr* gene was significantly up-regulated by MyD88 deficiency (h, i; *t* test, $n \geq 5$ per group). In order to evaluate the integrity of BBB, isolated brain capillaries were detected for TJP1, Claudin-5, and AQP4 with quantitative Western blot (k). Haploinsufficiency of MyD88 in microglia did not significantly change the expression levels of all proteins tested (l–n; *t* test, $p > 0.05$, $n \geq 8$ per group) [Color figure can be viewed at wileyonlinelibrary.com]

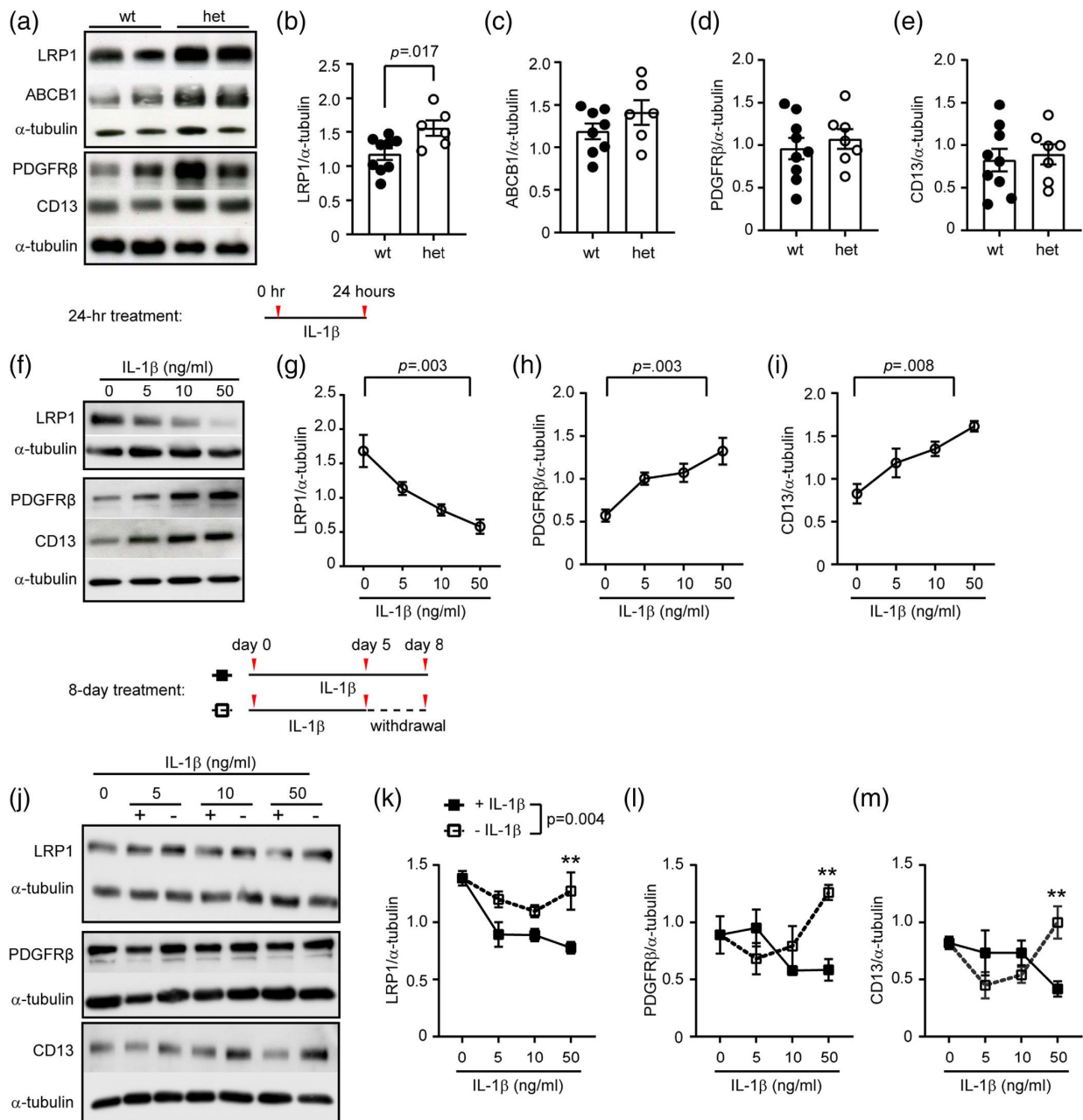


FIGURE 6 Haploinsufficiency of microglial MyD88 increases LRP1 in cerebral micro-vessels of APP/PS1-transgenic mice and IL-1 β treatment decreases LRP1 in cultured pericytes. Micro blood vessels were isolated from the brains of 9-month-old APP^{tg}/MyD88^{fl/wt}Cre^{+/-} (MyD88 het) and APP^{tg}/MyD88^{fl/wt}Cre^{-/-} (MyD88 wt) mice, which were injected with tamoxifen 3 months ago. Protein levels of LRP1, ABCB1, PDGFR β , and CD13 were determined with quantitative Western blot (a–e). Haploinsufficiency of MyD88 in microglia significantly elevates LRP1 protein level but not for other proteins tested, compared with MyD88-wildtype APP/PS1-transgenic mice (b; t test, $n \geq 6$ per group). Immortalized pericytes from human cerebral capillaries were cultured and treated with IL-1 β at various concentrations for 24 hr (f–i) or for 8 days with and without withdrawal of IL-1 β during the last 3 days (j–m). At the end of experiments, cell lysates were prepared from IL-1 β -treated pericytes and detected for LRP1, PDGFR β , and CD13 with quantitative Western blot. One-way ANOVA comparing levels of each tested protein at different concentrations of IL-1 β shows that: (1) IL-1 β treatments significantly decreases LRP1, but increases PDGFR β and CD13 in a concentration-dependent manner after a 24-hr treatment (g–i; p values are shown in the figure); (2) IL-1 β treatments significantly decreases LRP1 in a concentration-dependent manner after a 8-day treatment (k; $p < .001$); and (3) IL-1 β treatments does not significantly changes protein levels of PDGFR β and CD13 after a 8-day treatment (l,m). Two-way ANOVA comparing protein levels of LRP1, PDGFR β , or CD13 with and without withdrawal of IL-1 β in the last 3 days of experiments shows that withdraw of IL-1 β recovers expression of LRP1 (k; $p = .004$), but not for PDGFR β and CD13 (l,m). t test was used to analyze the difference of protein levels in cells treated with IL-1 β at 50 ng/ml shows that withdrawal of IL-1 β significantly recovers expression of LRP1, PDGFR β , and CD13 (k–m; $**$; $p < .01$). $n = 3$ or 4 per group [Color figure can be viewed at wileyonlinelibrary.com]

and wild-type mice. This signature is characterized by an induction of pro-inflammatory genes (including *il-1 β* , *cd2*, and *itgax*), and a suppression of homeostatic genes (e.g., *cx3cr1*, *p2ry12*, *tmem119*, *tgfbr1*, *sall1*, and *csf1r*). APOE and TREM2 are two signaling proteins essential for DAM development (Keren-Shaul et al., 2017; Krasemann et al., 2017). We quantified the transcription of several DAM signature genes to characterize the effects of MyD88 on microglial activation. We observed that haploinsufficiency of MyD88 significantly decreased transcripts of pro-inflammatory genes, *tnf- α* and *il-1 β* (Figure 4a,b; t test, $p < .05$), and also reduced the transcription of anti-inflammatory gene *chi3l3* (Figure 4e; t test, $p < .05$) and homeostatic gene *cx3cr1* (Figure 4i; t test, $p < .05$), as compared with MyD88-wildtype microglia.

In order to investigate the relationship between microglia and A β deposits, we co-stained brain sections of 9-month-old AD mice with Iba-1-specific antibodies and methoxy-XO4. There were significantly more microglia surrounding A β deposits in APP^{tg}Myd88^{fl/wt}Cre^{+/-} mice ($6.21 \pm 0.47 \times 10^2$ cells/mm²) than in APP^{tg}Myd88^{fl/wt}Cre^{-/-} mice ($2.68 \pm 0.24 \times 10^2$ cells/mm²; Figure 4o,p; t test, $p < .001$), which agrees with our previous observation in MyD88-deficient bone marrow chimeric APP-transgenic mice (Hao et al., 2011).

3.5 | Haploinsufficient expression of MyD88 in microglia increases cerebral vasculature in APP/PS1-transgenic mice

We observed that cerebral microvasculature is reduced in APP/PS1-transgenic mice (Decker et al., 2018). In this study, we asked whether haploinsufficiency of microglial MyD88 changed the vasculature in AD mouse brain. We stained brains of 9-month-old APP^{tg}Myd88^{fl/wt}Cre^{+/-} and APP^{tg}Myd88^{fl/wt}Cre^{-/-} mice with collagen type IV-specific antibodies, skeletonized and quantified the immunoreactive blood vessels (Figure 5a). As shown in Figure 5b–d, MyD88 deficiency in microglia significantly increased the total length, vessel density and branching points of micro blood vessels (t test, $p < .05$), but did not change the mean diameter of blood vessels (Figure 5e; t test, $p > .05$).

As resident microglia serve pro-angiogenic effects in the brain (Brandenburg et al., 2016; Jiang et al., 2020; Mastorakos et al., 2021), we co-stained Iba-1 and isolectin B4 on brain sections of 9-month-old APP^{tg}Myd88^{fl/wt}Cre^{+/-} and APP^{tg}Myd88^{fl/wt}Cre^{-/-} mice and counted microglia with and without contact with blood vessels in CA1 area of the hippocampus (Figure 5f). We observed that haploinsufficiency of MyD88 significantly increased the distribution of microglia to blood vessels (Figure 5g; one-way ANOVA followed by *post-hoc* test, $p < .05$). Furthermore, we quantified gene transcription of pro-angiogenic genes in CD11b-positive brain cells. As shown in Figure 5h–j, MyD88 deficiency significantly up-regulated the transcription of *opn* and *igf-1* genes (t test, $p < .05$).

To evaluate the integrity of BBB in AD mice, we quantified TJP1, Claudin-5 and AQP4 in blood vessels isolated from 9-month-old APP^{tg}Myd88^{fl/wt}Cre^{+/-} and APP^{tg}Myd88^{fl/wt}Cre^{-/-} mice. As shown in Figure 5k–n, haploinsufficiency of MyD88 in microglia did not significantly alter the protein levels of all proteins tested (t test, $p > .05$).

3.6 | Haploinsufficient expression of MyD88 in microglia increases LRP1 in cerebral capillaries of APP/PS1-transgenic mice

LRP1 mediates A β efflux and local clearance by pericytes at BBB (Ma et al., 2018; Shinohara et al., 2017). We isolated micro-vessels from brains of 9-month-old APP^{tg}Myd88^{fl/wt}Cre^{+/-} and APP^{tg}Myd88^{fl/wt}Cre^{-/-} mice and observed that haploinsufficiency of MyD88 in microglia significantly increased protein levels of LRP1, but not ABCB1 in APP/PS1-transgenic mice, as compared with MyD88-wildtype AD mice (Figure 6a–c; t test, $p < .05$). The protein levels of pericyte markers, PDGFR β , and CD13, were not changed by microglial deficiency of MyD88 (Figure 6d,e; t test, $p > .05$). In isolated blood vessels from non-APP-transgenic control mice (APP^{wt}Myd88^{fl/wt}Cre^{+/-} and APP^{wt}Myd88^{fl/wt}Cre^{-/-}), haploinsufficiency of MyD88 in microglia did not alter the protein levels of all molecules examined (data not shown).

To examine the effects of inflammatory activation on LRP1 expression, we treated cultured pericytes with recombinant IL-1 β either for 24 hr or for 8 days. As shown in Figure 6f,g,j,k, both short- and long-term treatments of IL-1 β significantly decreased the protein levels of LRP1 in a dose-dependent manner (one-way ANOVA, $p < .05$). In the 8-day treatment experiment, withdrawal of IL-1 β for the last 3 days restored expression of LRP1 in cultured pericytes (Figure 6j,k; two-way ANOVA, $p < .05$). The short-term treatment of IL-1 β markedly increased expression of PDGFR β and CD13, which corroborates our recent finding (Quan et al., 2020) (Figure 6f,h,i; one-way ANOVA, $p < .05$). The long-term treatment of IL-1 β only at a high concentration (e.g., 50 ng/ml) tended to decrease the expression of PDGFR β and CD13; however, it was not statistically significant (shown in Figure 6l,m with solid lines; one-way ANOVA, $p > .05$). The withdrawal of IL-1 β recovered the expression of PDGFR β and CD13 in cultured pericytes after treatment of IL-1 β at 50 ng/ml (Figure 6l,m; t test comparing cells with and without treatment of IL-1 β at 50 ng/ml, $p < .05$).

3.7 | Haploinsufficient expression of MyD88 in microglia decreases β - and γ -secretase activity but does not affect neprilysin and *ide* gene transcription in the brain of APP/PS1-transgenic mice

Cerebral A β level is determined by A β generation and clearance. We continued to ask whether MyD88-deficient microglia regulated A β production. Using our established protocols (Hao et al., 2011; Xie et al., 2013), we detected the activity of β - and γ -secretases in brains of 9-month-old APP^{tg}Myd88^{fl/wt}Cre^{+/-} and APP^{tg}Myd88^{fl/wt}Cre^{-/-} mice. Interestingly, the activity of both enzymes was significantly lower in the brain of APP^{tg}Myd88^{fl/wt}Cre^{+/-} mice than in MyD88-wildtype APP^{tg}Myd88^{fl/wt}Cre^{-/-} littermates (Figure 7a,b; two-way ANOVA, $p < .05$).

To further investigate the clearance of A β , we quantified gene transcripts of A β -degrading enzymes, neprilysin, and *ide* (Leissring et al., 2003). There were no changes in the transcription of neprilysin

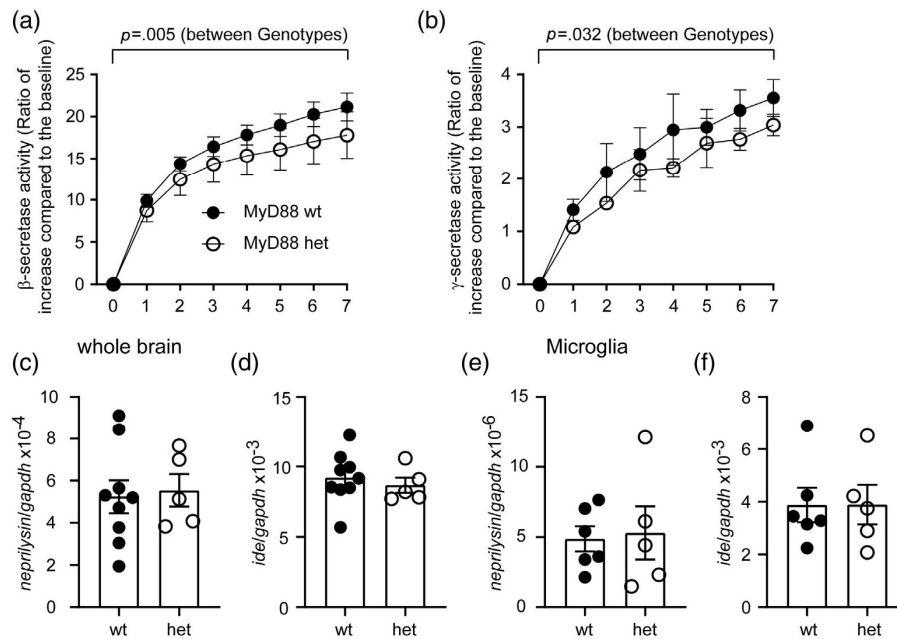


FIGURE 7 Haploinsufficiency of MyD88 in microglia decreases β - and γ -secretase activity, but does not affect the transcription of *neprilysin* and *ide* genes in the brain of APP/PS1-transgenic mice. The brains of 9-month-old tamoxifen-injected APP^{tg}MyD88^{fl/wt}Cre^{+/-} (MyD88 het) and APP^{tg}MyD88^{fl/wt}Cre^{-/-} (MyD88 wt) mice were used to prepare membrane components and RNA isolation. β - and γ -secretase activity was measured by incubating membrane components with fluorogenic β - and γ -secretase substrates, respectively (a,b, two-way ANOVA comparing MyD88 wt and het mice; $n = 4$ per group). The transcripts of *neprilysin* and *ide* genes in the brain tissue (c,e) and isolated microglia (d,f) were measured with real-time PCR, which showed that transcription of *neprilysin* and *ide* genes was not changed by the haploinsufficiency of MyD88 in microglia (t test; $n \geq 5$ per group)

and *ide* genes in both brain tissues and microglia from 9-month-old APP^{tg}MyD88^{fl/wt}Cre^{+/-} mice compared with APP^{tg}MyD88^{fl/wt}Cre^{-/-} mice (Figure 7c–f; t test, $p > .05$), suggesting that haploinsufficiency of MyD88 in microglia does not affect A β catabolism.

4 | DISCUSSION

Microglial activation has been extensively investigated in AD brain (Heneka et al., 2015), but microglial effects on A β pathology and neuronal degeneration remain inconclusive. In this study, we deleted one allele of *myd88* gene specifically in microglia in APP/PS1-transgenic mice by 6 months. Notably, by 9 months of age these animals showed attenuation both in the total number of microglia and in the transcription levels of pro-inflammatory genes (e.g., *tnf- α* and *il-1 β*) within the whole brain and individual microglia, correlating with decreased A β load and improved cognitive function. Interestingly, MyD88-haploinsufficient microglia might prevent APP/PS1 overexpression-induced changes of cerebral vasculature and LRP1 expression at BBB.

The regulating effects of innate immune signaling on the role of microglia in AD pathogenesis are highly heterogeneous. For example, TREM2 is essential for microglial response to A β in the brain (Ulland et al., 2017). One group reported that TREM2 deficiency in APP-

transgenic mice increases hippocampal A β burden and accelerates neuron loss (Y. Wang et al., 2015), while another group showed that TREM2 deletion reduces cerebral A β accumulation (Jay et al., 2015). Subsequent work suggested that TREM2 may have a protective effect at the early disease stage through phagocytic clearance of A β , but display a pathogenic effect at the later disease stage by triggering neurotoxic inflammatory responses (Jay et al., 2017; Parhizkar et al., 2019). In our studies, we reduced MyD88 expression in microglia or in bone marrow cells of APP-transgenic mice after noticeable A β had already developed in the brain, which decreases cerebral A β load and protects neurons (Hao et al., 2011). In the experiments by other groups, MyD88 expression was manipulated in APP-transgenic mice before the birth (by cross-breeding) or at 2 months of age (by bone marrow reconstruction) before A β deposits appeared in the brain. With such an experimental setting, MyD88-deficient microglia promote A β accumulation in the brain and accelerate spatial memory deficits (Michaud et al., 2011, 2012). Thus, the pathogenic role of innate immune molecules in microglia is shaped by the evolving cellular environment and should be analyzed dynamically during AD progression.

MyD88, as a common signaling adaptor for most TLRs and IL-1 receptor, plays an essential role in the innate immune response (O'Neill, Golenbock, & Bowie, 2013). It is not surprising that the heterozygous deletion of *myd88* gene inhibits the inflammatory activation of microglia in APP/PS1-transgenic mice. MyD88 deficiency

might reduce the generation of new microglia, as we previously observed that deletion of IKK β , a signaling molecule downstream to MyD88, decreases proliferating microglia in APP-transgenic mice (Y. Liu et al., 2014). It is unlikely that MyD88 deficiency induces microglial cell death in APP/PS1-transgenic mice, as blocking MyD88 signaling inhibits TLR4 activation-induced microglial apoptosis (Jung et al., 2005), while TLR4 is a receptor mediating microglial response to A β challenge (Walter et al., 2007). Interestingly, we observed that MyD88 deficiency promotes clustering of microglia around A β deposits as we observed in MyD88-deficient bone marrow chimeric AD mice (Hao et al., 2011). As deficiency of MyD88, IKK2, or TLR2 increases A β internalization by cultured microglia or macrophages (Hao et al., 2011; S. Liu et al., 2012; Y. Liu et al., 2014), the haploinsufficiency of MyD88 perhaps enhances microglial clearance of A β in AD brain. The relationship between microglial clustering and A β reduction in APP-transgenic mice has been described in many studies. For example, deficiency of TREM2 blocks microglial recruitment to A β , which is correlated with cerebral A β accumulation (Y. Wang et al., 2015). Administration of TREM2 agonist antibodies increases A β -associated microglia, which decreases A β in the brain (Fassler, Rappaport, Cuno, & George, 2021; Price et al., 2020; S. Wang et al., 2020). However, the molecular mechanisms, which mediate the migration of microglia toward A β and the following A β internalization, remain unclear.

The haploinsufficiency of MyD88 strongly decreases the transcription of *cx3cr1*, *chi3l3*, *tnf- α* , and *il-1 β* genes in microglia of our APP/PS1-transgenic mice. Cx3Cr1 expression is up-regulated in the brain of AD patients or animal models (Gonzalez-Prieto et al., 2021). Deficiency of Cx3Cr1 decreases cerebral A β in various APP-transgenic mice (Hickman, Allison, Coleman, Kingery-Gallagher, & El Khoury, 2019; Lee et al., 2010; Z. Liu, Condello, Schain, Harb, & Grutzendler, 2010). Homozygous knockout of *cx3cr1* gene was also observed to increase A β deposits-associated microglia and microglial phagocytosis of A β (Z. Liu et al., 2010). However, it should be noted that the reduction of *cx3cr1* transcription in our APP^{tg}Myd88^{fl/wt}Cre^{+/-} mice might be caused by the replacement of endogenous *cx3cr1* gene by Cre-encoding sequence (Yona et al., 2013). To address the question whether Cx3Cr1 haploinsufficiency in APP^{tg}Myd88^{fl/wt}Cre^{+/-} mice affects amyloidosis, we created APP^{tg}Gpr43^{fl/fl}Cre^{+/-} and APP^{tg}Gpr43^{fl/fl}Cre^{-/-} mice, in which *gpr43* instead of *myd88* gene was loxP site-flanked. As Gpr43 is not expressed in microglia in both APP^{tg}Gpr43^{fl/fl}Cre^{+/-} and APP^{tg}Gpr43^{fl/fl}Cre^{-/-} mice (Erny et al., 2015), any changes in APP^{tg}Gpr43^{fl/fl}Cre^{+/-} mice relative to APP^{tg}Gpr43^{fl/fl}Cre^{-/-} littermates should be due to the haploinsufficiency of Cx3Cr1. Our experiments revealed that the haploinsufficiency of Cx3Cr1 alters neither A β deposition nor transcription of inflammatory genes (e.g., *tnf- α* , *il-1 β* , *ccl-2*, and *il-10*) in the brain of our APP/PS1-transgenic mice. Thus, the pathological improvement in APP^{tg}Myd88^{fl/wt}Cre^{+/-} mice is a result from the haploinsufficiency of MyD88 instead of Cx3Cr1 deficiency in microglia.

Chi3l3 is a known marker for alternative activation of microglia and macrophages. Its transcription is also elevated in APP-transgenic mouse brain (Colton et al., 2006). However, the pathogenic function of microglial *Chi3l3* in AD mice is indeed unknown. Our serial studies

revealed that neuroinflammation and A β level are often simultaneously attenuated in the brain of APP-transgenic mice (Hao et al., 2011; S. Liu et al., 2012; Y. Liu et al., 2014). As pro-inflammatory activation inhibits phagocytosis of cultured microglia (Koenigsnecht-Talboo & Landreth, 2005), inhibition of proinflammatory activation in microglia might help A β clearance in AD brain. However, systemic injection of TLR4 or TLR9 agonist induces both pro- and anti-inflammatory activation and decreases A β in the brain of AD mice (Michaud et al., 2013; Scholtzova et al., 2014). Thus, how inflammatory activation regulates A β clearance in the brain is still an unanswered question.

There is growing evidence showing that microvascular circulation is damaged in AD brain; for example, capillary density and cerebral blood flow decrease, while BBB permeability increases (Watanabe et al., 2020). Our previous study showed that the blood flow goes down in correlation with a reduced vasculature in the hippocampus of APP-transgenic mice (Decker et al., 2018). A β -activated perivascular macrophages injure the neurovascular coupling through producing reactive oxygen species (Park et al., 2017). However, microglia were observed to serve pro-angiogenic effects in brains with glioma, ischemia, or direct vascular injury (Brandenburg et al., 2016; Jiang et al., 2020; Mastorakos et al., 2021). Transcription of *opn*, *vegf* and *igf1* genes in microglia is associated with angiogenesis (Jiang et al., 2020). Our study showed that haploinsufficiency of MyD88 in microglia increases cerebral vasculature, and distribution of microglia around blood vessels. MyD88 deficiency also up-regulates the transcription of *opn* and *igf-1* genes in microglia. As OPN enhances VEGF expression in endothelial cells (Dai et al., 2009) and IGF-1 drives the tissue repairment, including angiogenesis, in the brain (Vannella & Wynn, 2017), MyD88-haploinsufficient microglia might prevent vascular impairment in AD brain. However, a postmortem tissue study showed a higher density of capillaries in the brain of AD patients (Fernandez-Klett et al., 2020). Tg4510 tau-transgenic mice display increased capillaries, but with atypical and spiraling morphologies, and reduced luminal diameter of blood vessels (Bennett et al., 2018). Thus, more studies, especially functional analysis of the effects of microglia on the microvascular circulation in AD, are required.

BBB breakdown is an early biomarker of AD (Nation et al., 2019). APOE4 variant was recently linked to the loss of BBB integrity before the cognitive deficit (Montagne et al., 2020). The cerebrovascular leakage of ~100 nm nanoparticles was observed in APP-transgenic mice (Tanifum, Starosolski, Fowler, Jankowsky, & Annapragada, 2014). However, the effects of microglia on BBB integrity in AD brain remain unclear. In a mouse model of systemic lupus erythematosus, microglial activation around blood vessels protects BBB at the initial phase by expressing tight-junction protein Claudin-5, and impairs BBB by phagocytosing astrocytic end-feet after the inflammation is sustained (Haruwaka et al., 2019). In our study, we did not observe altered protein levels of TJP1, Claudin-5, and AQP-4 in microglial MyD88-haploinsufficient AD mice, although we were not able to exclude small damages in BBB integrity.

LRP1 contributes to A β clearance at BBB through mediating A β efflux and pericyte internalization of A β (Ma et al., 2018; Shinohara

et al., 2017). Deletion of LRP1 in endothelial cells accumulate A β in APP-transgenic mouse brain (Storck et al., 2016). LRP1 expression decreases in brain capillaries with aging and in AD (Shibata et al., 2000). Pro-inflammatory cytokines, such as IL-1 β , IL-6, and TNF- α , down-regulate LRP1 in cultured microvascular endothelial cells (Hsu, Rodriguez-Ortiz, Zumkehr, & Kitazawa, 2021). Our experiments showed that LRP1 expression is decreased by IL-1 β treatments in cultured pericytes. In APP/PS1-transgenic mice, MyD88-haploinsufficient microglia elevates LRP1 protein level in cerebral capillaries, which might be due to the inflammatory inhibition. It was supported by another observation that inflammatory activation in the brain by systemic administration of lipopolysaccharide decreases A β efflux at BBB (Erickson, Hansen, & Banks, 2012). PDGFR β and CD13 are two receptors on pericytes and essential for the survival and integration of pericytes in blood vessels (Lindahl, Johansson, Leveen, & Betsholtz, 1997; Rangel et al., 2007). The expression of PDGFR β and CD13 appeared to be resistant to inflammatory regulation, as haploinsufficiency of MyD88 did not change their protein levels in AD mice. Their expression in cultured pericytes was not altered, either, by IL-1 β at the concentrations sufficient for the down-regulation of LRP1 expression. There was a recent study showing that the density of pericytes is reserved during AD pathogenesis (Fernandez-Klett et al., 2020).

A β is produced after serial digestions of APP by β -(BACE1) and γ -secretases (Haass, Kaether, Thinakaran, & Sisodia, 2012). The expression of BACE1 in neurons is up-regulated by inflammatory activation (He et al., 2007; Sastre et al., 2006). Our studies showed that p38 α -MAPK deficiency promotes BACE1 degradation in neurons (Schnöder et al., 2016). Recently, inflammatory cytokines, such as interferon- γ and α , were shown to induce the expression of interferon-induced transmembrane protein 3 in neurons and astrocytes, which binds to γ -secretase and increases its activity (Hur et al., 2020). Thus, haploinsufficient expression of MyD88 in microglia in our APP/PS1-transgenic mice decreases neuroinflammation, and inhibits β - and γ -secretase activity in the brain, which might serve as another mechanism decreasing A β level in AD mice.

In summary, haploinsufficient expression of MyD88 in microglia at a late disease stage slows down the cognitive decline of APP/PS1-transgenic mice. MyD88 deficiency inhibits pro-inflammatory activation of microglia, but enhances microglial response to A β , which subsequently attenuates A β load in the brain. Haploinsufficiency of MyD88 might enhance pro-angiogenic effects of microglia, and prevent the loss of LRP1-mediated A β clearance at BBB in AD. However, the effects of microglia on the structure and function of micro-vessels in AD are far from being understood. To answer these questions will be a focus of our following studies.

ACKNOWLEDGMENTS

The authors thank Dr. M. Jucker (Hertie Institute for Clinical Brain Research, Tübingen) for providing APP/PS1-transgenic mice, Dr. M. Prinz (Department of Neuropathology, University of Freiburg, Freiburg) for Cx3Cr1-CreERT2 mice, and S. Offermanns (Max Planck Institute for Heart and Lung Research) for *gpr43*-floxed mice and *Gpr43*-RFP reporter mice. The authors appreciate Elisabeth Gluding

and Isabel Euler for their excellent technical assistance. This work was supported by "SNOWBALL," an EU Joint Programme for Neurodegenerative Disease (JPND; 01ED1617B; to Yang Liu and Klaus Fassbender); Alzheimer Forschung Initiative e.V. (#18009; to Yang Liu) and Medical Faculty of Universität des Saarlandes through HOMFOR2016 (to Yang Liu). Qinghua Luo holds a scholarship from China Scholarship Council (CSC; 201906820011). Open Access funding enabled and organized by Projekt DEAL.

CONFLICT OF INTEREST

The authors declare that they have no conflicts of interest with the contents of this article.

AUTHOR CONTRIBUTIONS

Yang Liu: conceptualized and designed the study, acquired funding, conducted experiments, acquired and analyzed data, and wrote the manuscript. **Wenqiang Quan, Qinghua Luo, Wenlin Hao, and Inge Tomic:** conducted experiments, acquired data, and analyzed data. **Tomomi Furihata:** provided pericyte cell line. **Walter Schulz-Schäffer:** provided technical support. **Michael D. Menger:** offered animal facility and supervised the study. **Klaus Fassbender:** acquired funding and supervised the study. All authors contributed to the article and approved the submitted version.

DATA AVAILABILITY STATEMENT

The data that support the findings of this study are available from the corresponding author upon reasonable request.

ORCID

Klaus Fassbender  <https://orcid.org/0000-0003-3596-868X>

Yang Liu  <https://orcid.org/0000-0002-7614-4233>

REFERENCES

- Bennett, R. E., Robbins, A. B., Hu, M., Cao, X., Betensky, R. A., Clark, T., ... Hyman, B. T. (2018). Tau induces blood vessel abnormalities and angiogenesis-related gene expression in P301L transgenic mice and human Alzheimer's disease. *Proceedings of the National Academy of Sciences of the United States of America*, 115(6), E1289–E1298. <https://doi.org/10.1073/pnas.1710329115>
- Bolmont, T., Haiss, F., Eicke, D., Radde, R., Mathis, C. A., Klunk, W. E., ... Calhoun, M. E. (2008). Dynamics of the microglial/amyloid interaction indicate a role in plaque maintenance. *The Journal of Neuroscience*, 28(16), 4283–4292. <https://doi.org/10.1523/JNEUROSCI.4814-07.2008>
- Boulay, A. C., Saubamea, B., Declèves, X., & Cohen-Salmon, M. (2015). Purification of mouse brain vessels. *Journal of Visualized Experiments*, 105, e53208. <https://doi.org/10.3791/53208>
- Brandenburg, S., Müller, A., Turkowski, K., Radev, Y. T., Rot, S., Schmidt, C., ... Vajkoczy, P. (2016). Resident microglia rather than peripheral macrophages promote vascularization in brain tumors and are source of alternative pro-angiogenic factors. *Acta Neuropathologica*, 131(3), 365–378. <https://doi.org/10.1007/s00401-015-1529-6>
- Cameron, B., Tse, W., Lamb, R., Li, X., Lamb, B. T., & Landreth, G. E. (2012). Loss of interleukin receptor-associated kinase 4 signaling suppresses amyloid pathology and alters microglial phenotype in a mouse model of Alzheimer's disease. *The Journal of Neuroscience*, 32(43), 15112–15123. <https://doi.org/10.1523/JNEUROSCI.1729-12.2012>

- Colton, C. A., Mott, R. T., Sharpe, H., Xu, Q., Van Nostrand, W. E., & Vittek, M. P. (2006). Expression profiles for macrophage alternative activation genes in AD and in mouse models of AD. *Journal of Neuroinflammation*, 3, 27. <https://doi.org/10.1186/1742-2094-3-27>
- Cortes-Cantelli, M., & Iadecola, C. (2020). Alzheimer's disease and vascular aging: JACC focus seminar. *Journal of the American College of Cardiology*, 75(8), 942–951. <https://doi.org/10.1016/j.jacc.2019.10.062>
- Dai, J., Peng, L., Fan, K., Wang, H., Wei, R., Ji, G., ... Guo, Y. (2009). Osteopontin induces angiogenesis through activation of PI3K/AKT and ERK1/2 in endothelial cells. *Oncogene*, 28(38), 3412–3422. <https://doi.org/10.1038/onc.2009.189>
- Decker, Y., Muller, A., Nemeth, E., Schulz-Schaeffer, W. J., Fatar, M., Menger, M. D., ... Fassbender, K. (2018). Analysis of the vasculature by immunohistochemistry in paraffin-embedded brains. *Brain Structure & Function*, 223(2), 1001–1015. <https://doi.org/10.1007/s00429-017-1595-8>
- Erickson, M. A., Hansen, K., & Banks, W. A. (2012). Inflammation-induced dysfunction of the low-density lipoprotein receptor-related protein-1 at the blood-brain barrier: Protection by the antioxidant N-acetylcysteine. *Brain, Behavior, and Immunity*, 26(7), 1085–1091. <https://doi.org/10.1016/j.bbi.2012.07.003>
- Emy, D., Hrabec de Angelis, A. L., Jaitin, D., Wieghofer, P., Staszewski, O., David, E., ... Prinz, M. (2015). Host microbiota constantly control maturation and function of microglia in the CNS. *Nature Neuroscience*, 18(7), 965–977. <https://doi.org/10.1038/nn.4030>
- Fassler, M., Rappaport, M. S., Cuno, C. B., & George, J. (2021). Engagement of TREM2 by a novel monoclonal antibody induces activation of microglia and improves cognitive function in Alzheimer's disease models. *Journal of Neuroinflammation*, 18(1), 19. <https://doi.org/10.1186/s12974-020-01980-5>
- Fernandez-Klett, F., Brandt, L., Fernandez-Zapata, C., Abuelnor, B., Middeldorp, J., Suijs, J. A., ... Priller, J. (2020). Denser brain capillary network with preserved pericytes in Alzheimer's disease. *Brain Pathology*, 30(6), 1071–1086. <https://doi.org/10.1111/bpa.12897>
- Focke, C., Blume, T., Zott, B., Shi, Y., Deussing, M., Peters, F., ... Brendel, M. (2018). Early and longitudinal microglial activation but not amyloid accumulation predict cognitive outcome in PS2APP mice. *Journal of Nuclear Medicine*, 60, 548–554. <https://doi.org/10.2967/jnumed.118.217703>
- Goldmann, T., Wieghofer, P., Muller, P. F., Wolf, Y., Varol, D., Yona, S., ... Prinz, M. (2013). A new type of microglia gene targeting shows TAK1 to be pivotal in CNS autoimmune inflammation. *Nature Neuroscience*, 16(11), 1618–1626. <https://doi.org/10.1038/nn.3531>
- Gonzalez-Prieto, M., Gutierrez, I. L., Garcia-Bueno, B., Caso, J. R., Leza, J. C., Ortega-Hernandez, A., ... Madrigal, J. L. M. (2021). Microglial CX3CR1 production increases in Alzheimer's disease and is regulated by noradrenaline. *Glia*, 69(1), 73–90. <https://doi.org/10.1002/glia.23885>
- Gosselin, D., & Rivest, S. (2008). MyD88 signaling in brain endothelial cells is essential for the neuronal activity and glucocorticoid release during systemic inflammation. *Molecular Psychiatry*, 13(5), 480–497. <https://doi.org/10.1038/sj.mp.4002122>
- Haass, C., Kaether, C., Thinakaran, G., & Sisodia, S. (2012). Trafficking and proteolytic processing of APP. *Cold Spring Harbor Perspectives in Medicine*, 2(5), a006270. <https://doi.org/10.1101/cshperspect.a006270>
- Hao, W., Liu, Y., Liu, S., Walter, S., Grimm, M. O., Kiliaan, A. J., ... Fassbender, K. (2011). Myeloid differentiation factor 88-deficient bone marrow cells improve Alzheimer's disease-related symptoms and pathology. *Brain*, 134(Pt 1), 278–292. <https://doi.org/10.1093/brain/awq325>
- Haruwaka, K., Ikegami, A., Tachibana, Y., Ohno, N., Konishi, H., Hashimoto, A., ... Wake, H. (2019). Dual microglia effects on blood brain barrier permeability induced by systemic inflammation. *Nature Communications*, 10(1), 5816. <https://doi.org/10.1038/s41467-019-13812-z>
- He, P., Zhong, Z., Lindholm, K., Berning, L., Lee, W., Lemere, C., ... Shen, Y. (2007). Deletion of tumor necrosis factor death receptor inhibits amyloid beta generation and prevents learning and memory deficits in Alzheimer's mice. *The Journal of Cell Biology*, 178(5), 829–841. <https://doi.org/10.1083/jcb.200705042>
- Heneka, M. T., Carson, M. J., El Khoury, J., Landreth, G. E., Brosseron, F., Feinstein, D. L., ... Kummer, M. P. (2015). Neuroinflammation in Alzheimer's disease. *Lancet Neurology*, 14(4), 388–405. [https://doi.org/10.1016/S1474-4422\(15\)70016-5](https://doi.org/10.1016/S1474-4422(15)70016-5)
- Heneka, M. T., Kummer, M. P., Stutz, A., Delekate, A., Schwartz, S., Vieira-Saecker, A., ... Golenbock, D. T. (2013). NLRP3 is activated in Alzheimer's disease and contributes to pathology in APP/PS1 mice. *Nature*, 493(7434), 674–678. <https://doi.org/10.1038/nature11729>
- Hickman, S. E., Allison, E. K., Coleman, U., Kingery-Gallagher, N. D., & El Khoury, J. (2019). Heterozygous CX3CR1 deficiency in microglia restores neuronal beta-amyloid clearance pathways and slows progression of Alzheimer's like-disease in PS1-APP mice. *Frontiers in Immunology*, 10, 2780. <https://doi.org/10.3389/fimmu.2019.02780>
- Hou, B., Reizis, B., & DeFranco, A. L. (2008). Toll-like receptors activate innate and adaptive immunity by using dendritic cell-intrinsic and -extrinsic mechanisms. *Immunity*, 29(2), 272–282. <https://doi.org/10.1016/j.immuni.2008.05.016>
- Hsu, H. W., Rodriguez-Ortiz, C. J., Zumkehr, J., & Kitazawa, M. (2021). Inflammatory cytokine IL-1beta downregulates endothelial LRP1 via MicroRNA-mediated gene silencing. *Neuroscience*, 453, 69–80. <https://doi.org/10.1016/j.neuroscience.2020.11.021>
- Hung, Y. F., Chen, C. Y., Shih, Y. C., Liu, H. Y., Huang, C. M., & Hsueh, Y. P. (2018). Endosomal TLR3, TLR7, and TLR8 control neuronal morphology through different transcriptional programs. *The Journal of Cell Biology*, 217(8), 2727–2742. <https://doi.org/10.1083/jcb.201712113>
- Hur, J. Y., Frost, G. R., Wu, X., Crump, C., Pan, S. J., Wong, E., ... Li, Y. M. (2020). The innate immunity protein IFITM3 modulates gamma-secretase in Alzheimer's disease. *Nature*, 586(7831), 735–740. <https://doi.org/10.1038/s41586-020-2681-2>
- Jay, T. R., Hirsch, A. M., Broihier, M. L., Miller, C. M., Neilson, L. E., Ransohoff, R. M., ... Landreth, G. E. (2017). Disease progression-dependent effects of TREM2 deficiency in a mouse model of Alzheimer's disease. *The Journal of Neuroscience*, 37(3), 637–647. <https://doi.org/10.1523/JNEUROSCI.2110-16.2016>
- Jay, T. R., Miller, C. M., Cheng, P. J., Graham, L. C., Bemiller, S., Broihier, M. L., ... Lamb, B. T. (2015). TREM2 deficiency eliminates TREM2+ inflammatory macrophages and ameliorates pathology in Alzheimer's disease mouse models. *The Journal of Experimental Medicine*, 212(3), 287–295. <https://doi.org/10.1084/jem.20142322>
- Jiang, L., Mu, H., Xu, F., Xie, D., Su, W., Xu, J., ... Hu, X. (2020). Transcriptomic and functional studies reveal underlined chemotactic and angiostimulatory properties of aged microglia during stroke recovery. *Journal of Cerebral Blood Flow & Metabolism*, 40(1 suppl), S81–S97. <https://doi.org/10.1177/0271678X20902542>
- Jung, D. Y., Lee, H., Jung, B. Y., Ock, J., Lee, M. S., Lee, W. H., & Suk, K. (2005). TLR4, but not TLR2, signals autoregulatory apoptosis of cultured microglia: A critical role of IFN-beta as a decision maker. *Journal of Immunology*, 174(10), 6467–6476. <https://doi.org/10.4049/jimmunol.174.10.6467>
- Keren-Shaul, H., Spinrad, A., Weiner, A., Matcovitch-Natan, O., Dvir-Szternfeld, R., Ulland, T. K., ... Amit, I. (2017). A unique microglia type associated with restricting development of Alzheimer's disease. *Cell*, 169(7), 1276–1290 e1217. <https://doi.org/10.1016/j.cell.2017.05.018>
- Koenigsknecht-Talbot, J., & Landreth, G. E. (2005). Microglial phagocytosis induced by fibrillar beta-amyloid and IgGs are differentially regulated by proinflammatory cytokines. *The Journal of Neuroscience*, 25(36), 8240–8249. <https://doi.org/10.1523/JNEUROSCI.1808-05.2005>
- Krasemann, S., Madore, C., Cialic, R., Baufeld, C., Calcagno, N., El Fatimy, R., ... Butovsky, O. (2017). The TREM2-APOE pathway drives

- the transcriptional phenotype of dysfunctional microglia in neurodegenerative diseases. *Immunity*, 47(3), 566–581 e569. <https://doi.org/10.1016/j.immuni.2017.08.008>
- Kuhnke, D., Jedlitschky, G., Grube, M., Krohn, M., Jucker, M., Mosyagin, I., ... Vogelgesang, S. (2007). MDR1-P-glycoprotein (ABCB1) mediates transport of Alzheimer's amyloid-beta peptides—Implications for the mechanisms of Abeta clearance at the blood-brain barrier. *Brain Pathology*, 17(4), 347–353. <https://doi.org/10.1111/j.1750-3639.2007.00075.x>
- Lee, S., Varvel, N. H., Konerth, M. E., Xu, G., Cardona, A. E., Ransohoff, R. M., & Lamb, B. T. (2010). CX3CR1 deficiency alters microglial activation and reduces beta-amyloid deposition in two Alzheimer's disease mouse models. *The American Journal of Pathology*, 177(5), 2549–2562. <https://doi.org/10.2353/ajpath.2010.100265>
- Leissring, M. A., Farris, W., Chang, A. Y., Walsh, D. M., Wu, X., Sun, X., ... Selkoe, D. J. (2003). Enhanced proteolysis of beta-amyloid in APP transgenic mice prevents plaque formation, secondary pathology, and premature death. *Neuron*, 40(6), 1087–1093. [https://doi.org/10.1016/s0896-6273\(03\)00787-6](https://doi.org/10.1016/s0896-6273(03)00787-6)
- Lewcock, J. W., Schlepckow, K., Di Paolo, G., Tahirovic, S., Monroe, K. M., & Haass, C. (2020). Emerging microglia biology defines novel therapeutic approaches for Alzheimer's disease. *Neuron*, 108, 801–821. <https://doi.org/10.1016/j.neuron.2020.09.029>
- Lim, J. E., Kou, J., Song, M., Pattanayak, A., Jin, J., Lalonde, R., & Fukuchi, K. (2011). MyD88 deficiency ameliorates beta-amyloidosis in an animal model of Alzheimer's disease. *The American Journal of Pathology*, 179(3), 1095–1103. <https://doi.org/10.1016/j.ajpath.2011.05.045>
- Lindahl, P., Johansson, B. R., Leveen, P., & Betsholtz, C. (1997). Pericyte loss and microaneurysm formation in PDGF-B-deficient mice. *Science*, 277(5323), 242–245. <https://doi.org/10.1126/science.277.5323.242>
- Liu, S., Liu, Y., Hao, W., Wolf, L., Kilian, A. J., Penke, B., ... Fassbender, K. (2012). TLR2 is a primary receptor for Alzheimer's amyloid beta peptide to trigger neuroinflammatory activation. *Journal of Immunology*, 188(3), 1098–1107. <https://doi.org/10.4049/jimmunol.1101121>
- Liu, Y., Liu, X., Hao, W., Decker, Y., Schomburg, R., Fulop, L., ... Fassbender, K. (2014). IKKbeta deficiency in myeloid cells ameliorates Alzheimer's disease-related symptoms and pathology. *The Journal of Neuroscience*, 34(39), 12982–12999. <https://doi.org/10.1523/JNEUROSCI.1348-14.2014>
- Liu, Z., Condello, C., Schain, A., Harb, R., & Grutzendler, J. (2010). CX3CR1 in microglia regulates brain amyloid deposition through selective protofibrillar amyloid-beta phagocytosis. *The Journal of Neuroscience*, 30(50), 17091–17101. <https://doi.org/10.1523/JNEUROSCI.4403-10.2010>
- Ma, Q., Zhao, Z., Sagare, A. P., Wu, Y., Wang, M., Owens, N. C., ... Zlokovic, B. V. (2018). Blood-brain barrier-associated pericytes internalize and clear aggregated amyloid-beta42 by LRP1-dependent apolipoprotein E isoform-specific mechanism. *Molecular Neurodegeneration*, 13(1), 57. <https://doi.org/10.1186/s13024-018-0286-0>
- Mastorakos, P., Mihelson, N., Luby, M., Burks, S. R., Johnson, K., Hsia, A. W., ... McGavern, D. B. (2021). Temporally distinct myeloid cell responses mediate damage and repair after cerebrovascular injury. *Nature Neuroscience*, 24(2), 245–258. <https://doi.org/10.1038/s41593-020-00773-6>
- Meyer-Luehmann, M., Sipres-Jones, T. L., Prada, C., Garcia-Alloza, M., de Calignon, A., Rozkaine, A., ... Hyman, B. T. (2008). Rapid appearance and local toxicity of amyloid-beta plaques in a mouse model of Alzheimer's disease. *Nature*, 451(7179), 720–724. <https://doi.org/10.1038/nature06616>
- Michaud, J. P., Halle, M., Lampron, A., Theriault, P., Prefontaine, P., Filali, M., ... Rivest, S. (2013). Toll-like receptor 4 stimulation with the detoxified ligand monophosphoryl lipid A improves Alzheimer's disease-related pathology. *Proceedings of the National Academy of Sciences of the United States of America*, 110(5), 1941–1946. <https://doi.org/10.1073/pnas.1215165110>
- Michaud, J. P., Richard, K. L., & Rivest, S. (2011). MyD88-adaptor protein acts as a preventive mechanism for memory deficits in a mouse model of Alzheimer's disease. *Molecular Neurodegeneration*, 6(1), 5. <https://doi.org/10.1186/1750-1326-6-5>
- Michaud, J. P., Richard, K. L., & Rivest, S. (2012). Hematopoietic MyD88-adaptor protein acts as a natural defense mechanism for cognitive deficits in Alzheimer's disease. *Stem Cell Reviews and Reports*, 8(3), 898–904. <https://doi.org/10.1007/s12015-012-9356-9>
- Montagne, A., Nation, D. A., Sagare, A. P., Barisano, G., Sweeney, M. D., Chakhoyan, A., ... Zlokovic, B. V. (2020). APOE4 leads to blood-brain barrier dysfunction predicting cognitive decline. *Nature*, 581(7806), 71–76. <https://doi.org/10.1038/s41586-020-2247-3>
- Montagne, A., Nikolakopoulou, A. M., Zhao, Z., Sagare, A. P., Si, G., Lazic, D., ... Zlokovic, B. V. (2018). Pericyte degeneration causes white matter dysfunction in the mouse central nervous system. *Nature Medicine*, 24(3), 326–337. <https://doi.org/10.1038/nm.4482>
- Mucke, L., & Selkoe, D. J. (2012). Neurotoxicity of amyloid beta-protein: Synaptic and network dysfunction. *Cold Spring Harbor Perspectives in Medicine*, 2(7), a006338. <https://doi.org/10.1101/cshperspect.a006338>
- Nation, D. A., Sweeney, M. D., Montagne, A., Sagare, A. P., D'Orazio, L. M., Pachicano, M., ... Zlokovic, B. V. (2019). Blood-brain barrier breakdown is an early biomarker of human cognitive dysfunction. *Nature Medicine*, 25(2), 270–276. <https://doi.org/10.1038/s41591-018-0297-y>
- O'Neill, L. A., Golenbock, D., & Bowie, A. G. (2013). The history of toll-like receptors—Redefining innate immunity. *Nature Reviews. Immunology*, 13(6), 453–460. <https://doi.org/10.1038/nri3446>
- Parhizkar, S., Arzberger, T., Brendel, M., Kleinberger, G., Deussing, M., Focke, C., ... Haass, C. (2019). Loss of TREM2 function increases amyloid seeding but reduces plaque-associated ApoE. *Nature Neuroscience*, 22, 191–204. <https://doi.org/10.1038/s41593-018-0296-9>
- Park, L., Uekawa, K., Garcia-Bonilla, L., Koizumi, K., Murphy, M., Pistik, R., ... Iadecola, C. (2017). Brain perivascular macrophages initiate the neurovascular dysfunction of Alzheimer Abeta peptides. *Circulation Research*, 121(3), 258–269. <https://doi.org/10.1161/CIRCRESAHA.117.311054>
- Price, B. R., Sudduth, T. L., Weekman, E. M., Johnson, S., Hawthorne, D., Woolums, A., & Wilcock, D. M. (2020). Therapeutic Trem2 activation ameliorates amyloid-beta deposition and improves cognition in the 5XFAD model of amyloid deposition. *Journal of Neuroinflammation*, 17(1), 238. <https://doi.org/10.1186/s12974-020-01915-0>
- Qin, Y., Liu, Y., Hao, W., Decker, Y., Tomić, I., Menger, M. D., ... Fassbender, K. (2016). Stimulation of TLR4 attenuates Alzheimer's disease-related symptoms and pathology in tau-transgenic mice. *Journal of Immunology*, 197(8), 3281–3292. <https://doi.org/10.4049/jimmunol.1600873>
- Quan, W., Luo, Q., Tang, Q., Furihata, T., Li, D., Fassbender, K., & Liu, Y. (2020). NLRP3 is involved in the maintenance of cerebral pericytes. *Frontiers in Cellular Neuroscience*, 14(276), 1–12. <https://doi.org/10.3389/fncel.2020.00276>
- Radde, R., Bolmont, T., Kaeser, S. A., Coomaraswamy, J., Lindau, D., Stoltze, L., ... Jucker, M. (2006). Abeta42-driven cerebral amyloidosis in transgenic mice reveals early and robust pathology. *EMBO Reports*, 7(9), 940–946. <https://doi.org/10.1038/sj.embor.7400784>
- Rangasamy, S. B., Jana, M., Roy, A., Corbett, G. T., Kundu, M., Chandra, S., ... Pahan, K. (2018). Selective disruption of TLR2-MyD88 interaction inhibits inflammation and attenuates Alzheimer's pathology. *The Journal of Clinical Investigation*, 128(10), 4297–4312. <https://doi.org/10.1172/JCI96209>
- Rangel, R., Sun, Y., Guzman-Rojas, L., Ozawa, M. G., Sun, J., Giordano, R. J., ... Pasqualini, R. (2007). Impaired angiogenesis in aminopeptidase N-null mice. *Proceedings of the National Academy of Sciences of the United States of America*, 104(11), 4588–4593. <https://doi.org/10.1073/pnas.0611653104>



- Reed-Geaghan, E. G., Reed, Q. W., Cramer, P. E., & Landreth, G. E. (2010). Deletion of CD14 attenuates Alzheimer's disease pathology by influencing the brain's inflammatory milieu. *The Journal of Neuroscience*, 30(46), 15369–15373. <https://doi.org/10.1523/JNEUROSCI.2637-10.2010>
- Roberts, K. F., Elbert, D. L., Kasten, T. P., Patterson, B. W., Sigurdson, W. C., Connors, R. E., ... Bateman, R. J. (2014). Amyloid-beta efflux from the central nervous system into the plasma. *Annals of Neurology*, 76(6), 837–844. <https://doi.org/10.1002/ana.24270>
- Sagare, A. P., Bell, R. D., Zhao, Z., Ma, Q., Winkler, E. A., Ramanathan, A., & Zlokovic, B. V. (2013). Pericyte loss influences Alzheimer-like neurodegeneration in mice. *Nature Communications*, 4, 2932. <https://doi.org/10.1038/ncomms3932>
- Sastre, M., Dewachter, L., Rossner, S., Bogdanovic, N., Rosen, E., Borghgraef, P., ... Heneka, M. T. (2006). Nonsteroidal anti-inflammatory drugs repress beta-secretase gene promoter activity by the activation of PPARgamma. *Proceedings of the National Academy of Sciences of the United States of America*, 103(2), 443–448. <https://doi.org/10.1073/pnas.0503839103>
- Schnöder, L., Gasparoni, G., Nordstrom, K., Schottek, A., Tomic, I., Christmann, A., ... Liu, Y. (2020). Neuronal deficiency of p38alpha-MAPK ameliorates symptoms and pathology of APP or tau-transgenic Alzheimer's mouse models. *The FASEB Journal*, 34, 9628–9649. <https://doi.org/10.1096/fj.201902731RR>
- Schnöder, L., Hao, W., Qin, Y., Liu, S., Tomic, I., Liu, X., ... Liu, Y. (2016). Deficiency of neuronal p38alpha MAPK attenuates amyloid pathology in Alzheimer disease mouse and cell models through facilitating lysosomal degradation of BACE1. *The Journal of Biological Chemistry*, 291(5), 2067–2079. <https://doi.org/10.1074/jbc.M115.695916>
- Scholtzova, H., Chianchiano, P., Pan, J., Sun, Y., Goñi, F., Mehta, P. D., & Wisniewski, T. (2014). Amyloid β and tau Alzheimer's disease related pathology is reduced by toll-like receptor 9 stimulation. *Acta Neuropathologica Communications*, 2(1), 101. <https://doi.org/10.1186/s40478-014-0101-2>
- Schroeder, P., Rivalan, M., Zaout, S., Kruger, C., Schuler, J., Long, M., ... Lehnardt, S. (2021). Abnormal brain structure and behavior in MyD88-deficient mice. *Brain, Behavior, and Immunity*, 91, 181–193. <https://doi.org/10.1016/j.bbi.2020.09.024>
- Shankar, G. M., Li, S., Mehta, T. H., Garcia-Munoz, A., Shepardson, N. E., Smith, I., ... Selkoe, D. J. (2008). Amyloid-beta protein dimers isolated directly from Alzheimer's brains impair synaptic plasticity and memory. *Nature Medicine*, 14(8), 837–842. <https://doi.org/10.1038/nm1782>
- Shen, Y., Qin, H., Chen, J., Mou, L., He, Y., Yan, Y., ... Zhou, Y. D. (2016). Postnatal activation of TLR4 in astrocytes promotes excitatory synaptogenesis in hippocampal neurons. *The Journal of Cell Biology*, 215(5), 719–734. <https://doi.org/10.1083/jcb.201605046>
- Shibata, M., Yamada, S., Kumar, S. R., Calero, M., Bading, J., Frangione, B., ... Zlokovic, B. V. (2000). Clearance of Alzheimer's amyloid-ss(1-40) peptide from brain by LDL receptor-related protein-1 at the blood-brain barrier. *The Journal of Clinical Investigation*, 106(12), 1489–1499. <https://doi.org/10.1172/JCI10498>
- Shinohara, M., Tachibana, M., Kanekiyo, T., & Bu, G. (2017). Role of LRP1 in the pathogenesis of Alzheimer's disease: Evidence from clinical and preclinical studies. *Journal of Lipid Research*, 58(7), 1267–1281. <https://doi.org/10.1194/jlr.R075796>
- Song, M., Jin, J., Lim, J. E., Kou, J., Pattanayak, A., Rehman, J. A., ... Fukuchi, K. (2011). TLR4 mutation reduces microglial activation, increases A β deposits and exacerbates cognitive deficits in a mouse model of Alzheimer's disease. *Journal of Neuroinflammation*, 8, 92. <https://doi.org/10.1186/1742-2094-8-92>
- Spangenberg, E. E., Lee, R. J., Najafi, A. R., Rice, R. A., Elmore, M. R., Blurton-Jones, M., ... Green, K. N. (2016). Eliminating microglia in Alzheimer's mice prevents neuronal loss without modulating amyloid-beta pathology. *Brain*, 139(Pt 4), 1265–1281. <https://doi.org/10.1093/brain/aww016>
- Stakos, D. A., Stamatelopoulos, K., Bampatsias, D., Sachse, M., Zormpas, E., Vlachogiannis, N. I., ... Stellos, K. (2020). The Alzheimer's disease amyloid-Beta hypothesis in cardiovascular aging and disease: JACC focus seminar. *Journal of the American College of Cardiology*, 75(8), 952–967. <https://doi.org/10.1016/j.jacc.2019.12.033>
- Storck, S. E., Meister, S., Nahrath, J., Meissner, J. N., Schubert, N., Di Spiezio, A., ... Pietrzik, C. U. (2016). Endothelial LRP1 transports amyloid-beta(1-42) across the blood-brain barrier. *The Journal of Clinical Investigation*, 126(1), 123–136. <https://doi.org/10.1172/JCI81108>
- Sweeney, M. D., Ayyadurai, S., & Zlokovic, B. V. (2016). Pericytes of the neurovascular unit: Key functions and signaling pathways. *Nature Neuroscience*, 19(6), 771–783. <https://doi.org/10.1038/nn.4288>
- Tang, C., Ahmed, K., Gille, A., Lu, S., Grone, H. J., Tunaru, S., & Offermanns, S. (2015). Loss of FFA2 and FFA3 increases insulin secretion and improves glucose tolerance in type 2 diabetes. *Nature Medicine*, 21(2), 173–177. <https://doi.org/10.1038/nm.3779>
- Tanifum, E. A., Starosolski, Z. A., Fowler, S. W., Jankowsky, J. L., & Annapragada, A. V. (2014). Cerebral vascular leak in a mouse model of amyloid neuropathology. *Journal of Cerebral Blood Flow and Metabolism*, 34(10), 1646–1654. <https://doi.org/10.1038/jcbfm.2014.125>
- Ulland, T. K., Song, W. M., Huang, S. C., Ulrich, J. D., Sergushichev, A., Beatty, W. L., ... Colonna, M. (2017). TREM2 maintains microglial metabolic fitness in Alzheimer's disease. *Cell*, 170(4), 649–663 e613. <https://doi.org/10.1016/j.cell.2017.07.023>
- Umehara, K., Sun, Y., Hiura, S., Hamada, K., Itoh, M., Kitamura, K., ... Furihata, T. (2018). A new conditionally immortalized human fetal brain pericyte cell line: Establishment and functional characterization as a promising tool for human brain pericyte studies. *Molecular Neurobiology*, 55(7), 5993–6006. <https://doi.org/10.1007/s12035-017-0815-9>
- Vannella, K. M., & Wynn, T. A. (2017). Mechanisms of organ injury and repair by macrophages. *Annual Review of Physiology*, 79, 593–617. <https://doi.org/10.1146/annurev-physiol-022516-034356>
- Walter, S., Letiembre, M., Liu, Y., Heine, H., Penke, B., Hao, W., ... Fassbender, K. (2007). Role of the toll-like receptor 4 in neuroinflammation in Alzheimer's disease. *Cellular Physiology and Biochemistry*, 20(6), 947–956. <https://doi.org/10.1159/000110455>
- Wang, S., Mustafa, M., Yuede, C. M., Salazar, S. V., Kong, P., Long, H., ... Colonna, M. (2020). Anti-human TREM2 induces microglia proliferation and reduces pathology in an Alzheimer's disease model. *The Journal of Experimental Medicine*, 217(9), e20200785. <https://doi.org/10.1084/jem.20200785>
- Wang, Y., Cella, M., Mallinson, K., Ulrich, J. D., Young, K. L., Robinette, M. L., ... Colonna, M. (2015). TREM2 lipid sensing sustains the microglial response in an Alzheimer's disease model. *Cell*, 160(6), 1061–1071. <https://doi.org/10.1016/j.cell.2015.01.049>
- Watanabe, C., Imaizumi, T., Kawai, H., Suda, K., Honma, Y., Ichihashi, M., ... Mizutani, K. I. (2020). Aging of the vascular system and neural diseases. *Frontiers in Aging Neuroscience*, 12, 557384. <https://doi.org/10.3389/fnagi.2020.557384>
- Weitz, T. M., Gate, D., Rezai-Zadeh, K., & Town, T. (2014). MyD88 is dispensable for cerebral amyloidosis and neuroinflammation in APP/PS1 transgenic mice. *The American Journal of Pathology*, 184(11), 2855–2861. <https://doi.org/10.1016/j.ajpath.2014.07.004>
- Xie, K., Liu, Y., Hao, W., Walter, S., Penke, B., Hartmann, T., ... Fassbender, K. (2013). Tenascin-C deficiency ameliorates Alzheimer's disease-related pathology in mice. *Neurobiology of Aging*, 34(10), 2389–2398. <https://doi.org/10.1016/j.neurobiolaging.2013.04.013>
- Yona, S., Kim, K. W., Wolf, Y., Mildner, A., Varol, D., Breker, M., ... Jung, S. (2013). Fate mapping reveals origins and dynamics of monocytes and tissue macrophages under homeostasis. *Immunity*, 38(1), 79–91. <https://doi.org/10.1016/j.immuni.2012.12.001>

Zudaire, E., Gambardella, L., Kurcz, C., & Vermeren, S. (2011). A computational tool for quantitative analysis of vascular networks. *PLoS One*, 6 (11), e27385. <https://doi.org/10.1371/journal.pone.0027385>

SUPPORTING INFORMATION

Additional supporting information may be found online in the Supporting Information section at the end of this article.

How to cite this article: Quan W, Luo Q, Hao W, et al. Haploinsufficiency of microglial MyD88 ameliorates Alzheimer's pathology and vascular disorders in APP/PS1-transgenic mice. *Glia*. 2021;1–19. <https://doi.org/10.1002/glia.24007>

9. REFERENCES

1. (2021) 2021 Alzheimer's disease facts and figures. *Alzheimers Dement* 17:327-406
2. Abdel-Haq R, Schlachetzki JCM, Glass CK, Mazmanian SK (2019) Microbiome-microglia connections via the gut-brain axis. *J Exp Med* 216:41-59
3. Albert MS, DeKosky ST, Dickson D, Dubois B, Feldman HH, Fox NC, Gamst A, Holtzman DM, Jagust WJ, Petersen RC, Snyder PJ, Carrillo MC, Thies B, Phelps CH (2011) The diagnosis of mild cognitive impairment due to Alzheimer's disease: recommendations from the National Institute on Aging-Alzheimer's Association workgroups on diagnostic guidelines for Alzheimer's disease. *Alzheimers Dement* 7:270-279
4. Asai H, Ikezu S, Tsunoda S, Medalla M, Luebke J, Haydar T, Wolozin B, Butovsky O, Kugler S, Ikezu T (2015) Depletion of microglia and inhibition of exosome synthesis halt tau propagation. *Nat Neurosci* 18:1584-1593
5. Aw E, Zhang Y, Carroll M (2020) Microglial responses to peripheral type 1 interferon. *J Neuroinflammation* 17:340
6. Benakis C, Brea D, Caballero S, Faraco G, Moore J, Murphy M, Sita G, Racchumi G, Ling L, Pamer EG, Iadecola C, Anrather J (2016) Commensal microbiota affects ischemic stroke outcome by regulating intestinal gammadelta T cells. *Nat Med* 22:516-523
7. Benveniste H, Liu X, Koundal S, Sanggaard S, Lee H, Wardlaw J (2019) The Glymphatic System and Waste Clearance with Brain Aging: A Review. *Gerontology* 65:106-119
8. Berer K, Krishnamoorthy G (2012) Commensal gut flora and brain autoimmunity: a love or hate affair? *Acta Neuropathol* 123:639-651
9. Bernaus A, Blanco S, Sevilla A (2020) Glia Crosstalk in Neuroinflammatory Diseases. *Front Cell Neurosci* 14:209
10. Bersch KL, DeMeester KE, Zagani R, Chen S, Wodzanowski KA, Liu S, Mashayekh S, Reinecker HC, Grimes CL (2021) Bacterial Peptidoglycan Fragments Differentially Regulate Innate Immune Signaling. *ACS Cent Sci* 7:688-696
11. Bisht K, Okojie KA, Sharma K, Lentferink DH, Sun YY, Chen HR, Uweru JO, Amancherla S, Calcuttawala Z, Campos-Salazar AB, Corliss B, Jabbour L, Benderoth J, Friestad B, Mills WA, 3rd, Isakson BE, Tremblay ME, Kuan CY, Eyo UB (2021) Capillary-associated microglia regulate vascular structure and function through PANX1-P2RY12 coupling in mice. *Nat Commun* 12:5289
12. Blacher E, Levy M, Tatirovsky E, Elinav E (2017) Microbiome-Modulated Metabolites at the Interface of Host Immunity. *J Immunol* 198:572-580
13. Blad CC, Tang C, Offermanns S (2012) G protein-coupled receptors for energy metabolites as new therapeutic targets. *Nat Rev Drug Discov* 11:603-619
14. Boche D, Gordon MN (2021) Diversity of transcriptomic microglial phenotypes in aging and Alzheimer's disease. *Alzheimers Dement*

REFERENCES

15. Boland B, Kumar A, Lee S, Platt FM, Wegiel J, Yu WH, Nixon RA (2008) Autophagy induction and autophagosome clearance in neurons: relationship to autophagic pathology in Alzheimer's disease. *J Neurosci* 28:6926-6937
16. Bolos M, Llorens-Martin M, Perea JR, Jurado-Arjona J, Rabano A, Hernandez F, Avila J (2017) Absence of CX3CR1 impairs the internalization of Tau by microglia. *Mol Neurodegener* 12:59
17. Boulay AC, Saubamea B, Decleves X, Cohen-Salmon M (2015) Purification of Mouse Brain Vessels. *J Vis Exp*:e53208
18. Bradford MM (1976) A rapid and sensitive method for the quantitation of microgram quantities of protein utilizing the principle of protein-dye binding. *Anal Biochem* 72:248-254
19. Brigas HC, Ribeiro M, Coelho JE, Gomes R, Gomez-Murcia V, Carvalho K, Faivre E, Costa-Pereira S, Darrigues J, de Almeida AA, Buee L, Dunot J, Marie H, Pousinha PA, Blum D, Silva-Santos B, Lopes LV, Ribot JC (2021) IL-17 triggers the onset of cognitive and synaptic deficits in early stages of Alzheimer's disease. *Cell Rep* 36:109574
20. Brionne TC, Tesseur I, Masliah E, Wyss-Coray T (2003) Loss of TGF-beta 1 leads to increased neuronal cell death and microgliosis in mouse brain. *Neuron* 40:1133-1145
21. Carabotti M, Scirocco A, Maselli MA, Severi C (2015) The gut-brain axis: interactions between enteric microbiota, central and enteric nervous systems. *Ann Gastroenterol* 28:203-209
22. Castro-Sanchez S, Garcia-Yague AJ, Kugler S, Lastres-Becker I (2019) CX3CR1-deficient microglia shows impaired signalling of the transcription factor NRF2: Implications in tauopathies. *Redox Biol* 22:101118
23. Cattaneo A, Cattane N, Galluzzi S, Provasi S, Lopizzo N, Festari C, Ferrari C, Guerra UP, Paghera B, Muscio C, Bianchetti A, Volta GD, Turla M, Cotelli MS, Gennuso M, Prella A, Zanetti O, Lussignoli G, Mirabile D, Bellandi D, Gentile S, Belotti G, Villani D, Harach T, Bolmont T, Padovani A, Boccardi M, Frisoni GB, Group I-F (2017) Association of brain amyloidosis with pro-inflammatory gut bacterial taxa and peripheral inflammation markers in cognitively impaired elderly. *Neurobiol Aging* 49:60-68
24. Chamera K, Trojan E, Szuster-Gluszczyk M, Basta-Kaim A (2020) The Potential Role of Dysfunctions in Neuron-Microglia Communication in the Pathogenesis of Brain Disorders. *Curr Neuropharmacol* 18:408-430
25. Chen GF, Xu TH, Yan Y, Zhou YR, Jiang Y, Melcher K, Xu HE (2017) Amyloid beta: structure, biology and structure-based therapeutic development. *Acta Pharmacol Sin* 38:1205-1235
26. Chidambaram H, Das R, Chinnathambi S (2020) Interaction of Tau with the chemokine receptor, CX3CR1 and its effect on microglial activation, migration and proliferation. *Cell Biosci* 10:109
27. Cirrito JR, Deane R, Fagan AM, Spinner ML, Parsadanian M, Finn MB, Jiang H, Prior JL, Sagare A, Bales KR, Paul SM, Zlokovic BV, Pivnicka-Worms D, Holtzman DM (2005) P-

- glycoprotein deficiency at the blood-brain barrier increases amyloid-beta deposition in an Alzheimer disease mouse model. *J Clin Invest* 115:3285-3290
28. Colombo AV, Sadler RK, Llovera G, Singh V, Roth S, Heindl S, Sebastian Monasor L, Verhoeven A, Peters F, Parhizkar S, Kamp F, Gomez de Aguero M, MacPherson AJ, Winkler E, Herms J, Benakis C, Dichgans M, Steiner H, Giera M, Haass C, Tahirovic S, Liesz A (2021) Microbiota-derived short chain fatty acids modulate microglia and promote Abeta plaque deposition. *Elife* 10
 29. Colonna M, Brioschi S (2020) Neuroinflammation and neurodegeneration in human brain at single-cell resolution. *Nat Rev Immunol* 20:81-82
 30. Colton CA, Mott RT, Sharpe H, Xu Q, Van Nostrand WE, Vitek MP (2006) Expression profiles for macrophage alternative activation genes in AD and in mouse models of AD. *J Neuroinflammation* 3:27
 31. Condello C, Yuan P, Schain A, Grutzendler J (2015) Microglia constitute a barrier that prevents neurotoxic protofibrillar Abeta42 hotspots around plaques. *Nat Commun* 6:6176
 32. Condello C, Yuan P, Grutzendler J (2018) Microglia-Mediated Neuroprotection, TREM2, and Alzheimer's Disease: Evidence From Optical Imaging. *Biol Psychiatry* 83:377-387
 33. Cryan JF, O'Riordan KJ, Sandhu K, Peterson V, Dinan TG (2020) The gut microbiome in neurological disorders. *Lancet Neurol* 19:179-194
 34. de Leon MJ, Li Y, Okamura N, Tsui WH, Saint-Louis LA, Glodzik L, Osorio RS, Fortea J, Butler T, Pirraglia E, Fossati S, Kim HJ, Carare RO, Nedergaard M, Benveniste H, Rusinek H (2017) Cerebrospinal Fluid Clearance in Alzheimer Disease Measured with Dynamic PET. *J Nucl Med* 58:1471-1476
 35. Deczkowska A, Keren-Shaul H, Weiner A, Colonna M, Schwartz M, Amit I (2018) Disease-Associated Microglia: A Universal Immune Sensor of Neurodegeneration. *Cell* 173:1073-1081
 36. Digby JE, Martinez F, Jefferson A, Ruparelina N, Chai J, Wamil M, Greaves DR, Choudhury RP (2012) Anti-Inflammatory Effects of Nicotinic Acid in Human Monocytes Are Mediated by GPR109A Dependent Mechanisms. *Arteriosclerosis Thrombosis and Vascular Biology* 32:669-U325
 37. Dolev I, Fogel H, Milshtein H, Berdichevsky Y, Lipstein N, Brose N, Gazit N, Slutsky I (2013) Spike bursts increase amyloid-beta 40/42 ratio by inducing a presenilin-1 conformational change. *Nat Neurosci* 16:587-595
 38. Du ZR, Feng XQ, Li N, Qu JX, Feng L, Chen L, Chen WF (2018) G protein-coupled estrogen receptor is involved in the anti-inflammatory effects of genistein in microglia. *Phytomedicine* 43:11-20
 39. Dubbelaar ML, Kracht L, Eggen BJJ, Boddeke E (2018) The Kaleidoscope of Microglial Phenotypes. *Front Immunol* 9:1753

REFERENCES

40. Erny D, Hrabce de Angelis AL, Jaitin D, Wieghofer P, Staszewski O, David E, Keren-Shaul H, Muhlrad T, Jakobshagen K, Buch T, Schwierzeck V, Utermohlen O, Chun E, Garrett WS, McCoy KD, Diefenbach A, Staeheli P, Stecher B, Amit I, Prinz M (2015) Host microbiota constantly control maturation and function of microglia in the CNS. *Nat Neurosci* 18:965-977
41. Esparza TJ, Zhao H, Cirrito JR, Cairns NJ, Bateman RJ, Holtzman DM, Brody DL (2013) Amyloid-beta oligomerization in Alzheimer dementia versus high-pathology controls. *Ann Neurol* 73:104-119
42. Ewers M, Franzmeier N, Suarez-Calvet M, Morenas-Rodriguez E, Caballero MAA, Kleinberger G, Piccio L, Cruchaga C, Deming Y, Dichgans M, Trojanowski JQ, Shaw LM, Weiner MW, Haass C, Alzheimer's Disease Neuroimaging I (2019) Increased soluble TREM2 in cerebrospinal fluid is associated with reduced cognitive and clinical decline in Alzheimer's disease. *Sci Transl Med* 11
43. Ewers M, Biechele G, Suarez-Calvet M, Sacher C, Blume T, Morenas-Rodriguez E, Deming Y, Piccio L, Cruchaga C, Kleinberger G, Shaw L, Trojanowski JQ, Herms J, Dichgans M, Alzheimer's Disease Neuroimaging I, Brendel M, Haass C, Franzmeier N (2020) Higher CSF sTREM2 and microglia activation are associated with slower rates of beta-amyloid accumulation. *EMBO Mol Med* 12:e12308
44. Farris W, Mansourian S, Leissring MA, Eckman EA, Bertram L, Eckman CB, Tanzi RE, Selkoe DJ (2004) Partial loss-of-function mutations in insulin-degrading enzyme that induce diabetes also impair degradation of amyloid beta-protein. *Am J Pathol* 164:1425-1434
45. Fassler M, Rappaport MS, Cuno CB, George J (2021) Engagement of TREM2 by a novel monoclonal antibody induces activation of microglia and improves cognitive function in Alzheimer's disease models. *J Neuroinflammation* 18:19
46. Fernandez-Arjona MDM, Grondona JM, Granados-Duran P, Fernandez-Llebrez P, Lopez-Avalos MD (2017) Microglia Morphological Categorization in a Rat Model of Neuroinflammation by Hierarchical Cluster and Principal Components Analysis. *Front Cell Neurosci* 11:235
47. Frenkel D, Wilkinson K, Zhao L, Hickman SE, Means TK, Puckett L, Farfara D, Kingery ND, Weiner HL, El Khoury J (2013) Scara1 deficiency impairs clearance of soluble amyloid-beta by mononuclear phagocytes and accelerates Alzheimer's-like disease progression. *Nat Commun* 4:2030
48. Fricker RA, Green EL, Jenkins SI, Griffin SM (2018) The Influence of Nicotinamide on Health and Disease in the Central Nervous System. *Int J Tryptophan Res* 11:1178646918776658
49. Friedman LG, Qureshi YH, Yu WH (2015) Promoting autophagic clearance: viable therapeutic targets in Alzheimer's disease. *Neurotherapeutics* 12:94-108
50. Fu SP, Wang JF, Xue WJ, Liu HM, Liu BR, Zeng YL, Li SN, Huang BX, Lv QK, Wang W, Liu JX (2015) Anti-inflammatory effects of BHBA in both in vivo and in vitro Parkinson's disease models are mediated by GPR109A-dependent mechanisms. *J Neuroinflammation* 12:9

REFERENCES

51. Galloway DA, Phillips AEM, Owen DRJ, Moore CS (2019) Phagocytosis in the Brain: Homeostasis and Disease. *Front Immunol* 10:790
52. Gasperi V, Sibilano M, Savini I, Catani MV (2019) Niacin in the Central Nervous System: An Update of Biological Aspects and Clinical Applications. *Int J Mol Sci* 20
53. Gatz M, Reynolds CA, Fratiglioni L, Johansson B, Mortimer JA, Berg S, Fiske A, Pedersen NL (2006) Role of genes and environments for explaining Alzheimer disease. *Arch Gen Psychiatry* 63:168-174
54. Gentier RJ, van Leeuwen FW (2015) Misframed ubiquitin and impaired protein quality control: an early event in Alzheimer's disease. *Front Mol Neurosci* 8:47
55. Giri B, Belanger K, Seamon M, Bradley E, Purohit S, Chong R, Morgan JC, Baban B, Wakade C (2019) Niacin Ameliorates Neuro-Inflammation in Parkinson's Disease via GPR109A. *Int J Mol Sci* 20
56. Gomez Perdiguero E, Klapproth K, Schulz C, Busch K, Azzoni E, Crozet L, Garner H, Trouillet C, de Bruijn MF, Geissmann F, Rodewald HR (2015) Tissue-resident macrophages originate from yolk-sac-derived erythro-myeloid progenitors. *Nature* 518:547-551
57. Guerreiro R, Wojtas A, Bras J, Carrasquillo M, Rogaeva E, Majounie E, Cruchaga C, Sassi C, Kauwe JS, Younkin S, Hazrati L, Collinge J, Pocock J, Lashley T, Williams J, Lambert JC, Amouyel P, Goate A, Rademakers R, Morgan K, Powell J, St George-Hyslop P, Singleton A, Hardy J, Alzheimer Genetic Analysis G (2013) TREM2 variants in Alzheimer's disease. *N Engl J Med* 368:117-127
58. Gyoneva S, Hosur R, Gosselin D, Zhang B, Ouyang Z, Cotleur AC, Peterson M, Allaire N, Challa R, Cullen P, Roberts C, Miao K, Reynolds TL, Glass CK, Burkly L, Ransohoff RM (2019) Cx3cr1-deficient microglia exhibit a premature aging transcriptome. *Life Sci Alliance* 2
59. Hanson J, Gille A, Zwykiel S, Lukasova M, Clausen BE, Ahmed K, Tunaru S, Wirth A, Offermanns S (2010) Nicotinic acid- and monomethyl fumarate-induced flushing involves GPR109A expressed by keratinocytes and COX-2-dependent prostanoid formation in mice. *J Clin Invest* 120:2910-2919
60. Hao W, Liu Y, Liu S, Walter S, Grimm MO, Kiliaan AJ, Penke B, Hartmann T, Rube CE, Menger MD, Fassbender K (2011) Myeloid differentiation factor 88-deficient bone marrow cells improve Alzheimer's disease-related symptoms and pathology. *Brain* 134:278-292
61. Harach T, Marungruang N, Duthilleul N, Cheatham V, Mc Coy KD, Frisoni G, Neher JJ, Fak F, Jucker M, Lasser T, Bolmont T (2017) Reduction of Abeta amyloid pathology in APPS1 transgenic mice in the absence of gut microbiota. *Sci Rep* 7:41802
62. Hardy J, Selkoe DJ (2002) The amyloid hypothesis of Alzheimer's disease: progress and problems on the road to therapeutics. *Science* 297:353-356
63. Haynes SE, Hollopeter G, Yang G, Kurpius D, Dailey ME, Gan WB, Julius D (2006) The P2Y12 receptor regulates microglial activation by extracellular nucleotides. *Nat Neurosci* 9:1512-1519

64. Hemonnot AL, Hua J, Ulmann L, Hirbec H (2019) Microglia in Alzheimer Disease: Well-Known Targets and New Opportunities. *Front Aging Neurosci* 11:233
65. Heneka MT, Carson MJ, El Khoury J, Landreth GE, Brosseron F, Feinstein DL, Jacobs AH, Wyss-Coray T, Vitorica J, Ransohoff RM, Herrup K, Frautschy SA, Finsen B, Brown GC, Verkhratsky A, Yamanaka K, Koistinaho J, Latz E, Halle A, Petzold GC, Town T, Morgan D, Shinohara ML, Perry VH, Holmes C, Bazan NG, Brooks DJ, Hunot S, Joseph B, Deigendesch N, Garaschuk O, Boddeke E, Dinarello CA, Breitner JC, Cole GM, Golenbock DT, Kummer MP (2015) Neuroinflammation in Alzheimer's disease. *Lancet Neurol* 14:388-405
66. Hickman S, Izzy S, Sen P, Morsett L, El Khoury J (2018) Microglia in neurodegeneration. *Nat Neurosci* 21:1359-1369
67. Hickman SE, Allison EK, El Khoury J (2008) Microglial dysfunction and defective beta-amyloid clearance pathways in aging Alzheimer's disease mice. *J Neurosci* 28:8354-8360
68. Hickman SE, Allison EK, Coleman U, Kingery-Gallagher ND, El Khoury J (2019) Heterozygous CX3CR1 Deficiency in Microglia Restores Neuronal beta-Amyloid Clearance Pathways and Slows Progression of Alzheimer's Like-Disease in PS1-APP Mice. *Front Immunol* 10:2780
69. Hirota K, Duarte JH, Veldhoen M, Hornsby E, Li Y, Cua DJ, Ahlfors H, Wilhelm C, Tolaini M, Menzel U, Garefalaki A, Potocnik AJ, Stockinger B (2011) Fate mapping of IL-17-producing T cells in inflammatory responses. *Nat Immunol* 12:255-263
70. Hou Y, Wei Y, Lautrup S, Yang B, Wang Y, Cordonnier S, Mattson MP, Croteau DL, Bohr VA (2021) NAD(+) supplementation reduces neuroinflammation and cell senescence in a transgenic mouse model of Alzheimer's disease via cGAS-STING. *Proc Natl Acad Sci U S A* 118
71. Huang Y, Happonen KE, Burrola PG, O'Connor C, Hah N, Huang L, Nimmerjahn A, Lemke G (2021) Microglia use TAM receptors to detect and engulf amyloid beta plaques. *Nat Immunol* 22:586-594
72. Iliff JJ, Wang M, Liao Y, Plogg BA, Peng W, Gundersen GA, Benveniste H, Vates GE, Deane R, Goldman SA, Nagelhus EA, Nedergaard M (2012) A paravascular pathway facilitates CSF flow through the brain parenchyma and the clearance of interstitial solutes, including amyloid beta. *Sci Transl Med* 4:147ra111
73. Iwata N, Tsubuki S, Takaki Y, Shirotani K, Lu B, Gerard NP, Gerard C, Hama E, Lee HJ, Saido TC (2001) Metabolic regulation of brain Abeta by neprilysin. *Science* 292:1550-1552
74. Jack CR, Jr., Bennett DA, Blennow K, Carrillo MC, Dunn B, Haeberlein SB, Holtzman DM, Jagust W, Jessen F, Karlawish J, Liu E, Molinuevo JL, Montine T, Phelps C, Rankin KP, Rowe CC, Scheltens P, Siemers E, Snyder HM, Sperling R, Contributors (2018) NIA-AA Research Framework: Toward a biological definition of Alzheimer's disease. *Alzheimers Dement* 14:535-562

REFERENCES

75. Jain P, Chaney AM, Carlson ML, Jackson IM, Rao A, James ML (2020) Neuroinflammation PET Imaging: Current Opinion and Future Directions. *J Nucl Med* 61:1107-1112
76. Jay TR, Miller CM, Cheng PJ, Graham LC, Bemiller S, Broihier ML, Xu G, Margevicius D, Karlo JC, Sousa GL, Cotleur AC, Butovsky O, Bekris L, Staugaitis SM, Leverenz JB, Pimplikar SW, Landreth GE, Howell GR, Ransohoff RM, Lamb BT (2015) TREM2 deficiency eliminates TREM2⁺ inflammatory macrophages and ameliorates pathology in Alzheimer's disease mouse models. *J Exp Med* 212:287-295
77. Jay TR, Hirsch AM, Broihier ML, Miller CM, Neilson LE, Ransohoff RM, Lamb BT, Landreth GE (2017) Disease Progression-Dependent Effects of TREM2 Deficiency in a Mouse Model of Alzheimer's Disease. *J Neurosci* 37:637-647
78. Jung CH, Ro SH, Cao J, Otto NM, Kim DH (2010) mTOR regulation of autophagy. *FEBS Lett* 584:1287-1295
79. Kanekiyo T, Cirrito JR, Liu CC, Shinohara M, Li J, Schuler DR, Shinohara M, Holtzman DM, Bu G (2013) Neuronal clearance of amyloid-beta by endocytic receptor LRP1. *J Neurosci* 33:19276-19283
80. Kanekiyo T, Bu G (2014) The low-density lipoprotein receptor-related protein 1 and amyloid-beta clearance in Alzheimer's disease. *Frontiers in Aging Neuroscience* 6
81. Kang DE, Pietrzik CU, Baum L, Chevallier N, Merriam DE, Kounnas MZ, Wagner SL, Troncoso JC, Kawas CH, Katzman R, Koo EH (2000) Modulation of amyloid beta-protein clearance and Alzheimer's disease susceptibility by the LDL receptor-related protein pathway. *J Clin Invest* 106:1159-1166
82. Karch CM, Goate AM (2015) Alzheimer's disease risk genes and mechanisms of disease pathogenesis. *Biol Psychiatry* 77:43-51
83. Karran E, Mercken M, De Strooper B (2011) The amyloid cascade hypothesis for Alzheimer's disease: an appraisal for the development of therapeutics. *Nat Rev Drug Discov* 10:698-712
84. Kashiwaya Y, Bergman C, Lee JH, Wan R, King MT, Mughal MR, Okun E, Clarke K, Mattson MP, Veech RL (2013) A ketone ester diet exhibits anxiolytic and cognition-sparing properties, and lessens amyloid and tau pathologies in a mouse model of Alzheimer's disease. *Neurobiol Aging* 34:1530-1539
85. Keren-Shaul H, Spinrad A, Weiner A, Matcovitch-Natan O, Dvir-Szternfeld R, Ulland TK, David E, Baruch K, Lara-Astaiso D, Toth B, Itzkovitz S, Colonna M, Schwartz M, Amit I (2017) A Unique Microglia Type Associated with Restricting Development of Alzheimer's Disease. *Cell* 169:1276-1290 e1217
86. Kierdorf K, Erny D, Goldmann T, Sander V, Schulz C, Perdiguero EG, Wieghofer P, Heinrich A, Riemke P, Holscher C, Muller DN, Luckow B, Brocker T, Debowski K, Fritz G, Opdenakker G, Diefenbach A, Biber K, Heikenwalder M, Geissmann F, Rosenbauer F, Prinz

- M (2013) Microglia emerge from erythromyeloid precursors via Pu.1- and Irf8-dependent pathways. *Nat Neurosci* 16:273-280
87. Kraeuter AK, Guest PC, Sarnyai Z (2019) The Open Field Test for Measuring Locomotor Activity and Anxiety-Like Behavior. *Methods Mol Biol* 1916:99-103
88. Krasemann S, Madore C, Cialic R, Baufeld C, Calcagno N, El Fatimy R, Beckers L, O'Loughlin E, Xu Y, Fanek Z, Greco DJ, Smith ST, Tweet G, Humulock Z, Zrzavy T, Conde-Sanroman P, Gacias M, Weng Z, Chen H, Tjon E, Mazaheri F, Hartmann K, Madi A, Ulrich JD, Glatzel M, Worthmann A, Heeren J, Budnik B, Lemere C, Ikezu T, Heppner FL, Litvak V, Holtzman DM, Lassmann H, Weiner HL, Ochando J, Haass C, Butovsky O (2017) The TREM2-APOE Pathway Drives the Transcriptional Phenotype of Dysfunctional Microglia in Neurodegenerative Diseases. *Immunity* 47:566-581 e569
89. Kubota T, Matsumoto H, Kirino Y (2016) Ameliorative effect of membrane-associated estrogen receptor G protein coupled receptor 30 activation on object recognition memory in mouse models of Alzheimer's disease. *J Pharmacol Sci* 131:219-222
90. Kuhnke D, Jedlitschky G, Grube M, Krohn M, Jucker M, Mosyagin I, Cascorbi I, Walker LC, Kroemer HK, Warzok RW, Vogelgesang S (2007) MDR1-P-Glycoprotein (ABCB1) Mediates Transport of Alzheimer's amyloid-beta peptides--implications for the mechanisms of Abeta clearance at the blood-brain barrier. *Brain Pathol* 17:347-353
91. Kuperstein I, Broersen K, Benilova I, Rozenski J, Jonckheere W, Debulpaep M, Vandersteen A, Segers-Nolten I, Van Der Werf K, Subramaniam V, Braeken D, Callewaert G, Bartic C, D'Hooge R, Martins IC, Rousseau F, Schymkowitz J, De Strooper B (2010) Neurotoxicity of Alzheimer's disease Abeta peptides is induced by small changes in the Abeta42 to Abeta40 ratio. *EMBO J* 29:3408-3420
92. Kurochkin IV, Guamera E, Berezovsky IN (2018) Insulin-Degrading Enzyme in the Fight against Alzheimer's Disease. *Trends Pharmacol Sci* 39:49-58
93. Kwak SS, Washicosky KJ, Brand E, von Maydell D, Aronson J, Kim S, Capen DE, Cetinbas M, Sadreyev R, Ning S, Bylykbashi E, Xia W, Wagner SL, Choi SH, Tanzi RE, Kim DY (2020) Amyloid-beta42/40 ratio drives tau pathology in 3D human neural cell culture models of Alzheimer's disease. *Nat Commun* 11:1377
94. Lau SF, Wu W, Seo H, Fu AKY, Ip NY (2021) Quantitative in vivo assessment of amyloid-beta phagocytic capacity in an Alzheimer's disease mouse model. *STAR Protoc* 2:100265
95. Lee CY, Landreth GE (2010) The role of microglia in amyloid clearance from the AD brain. *J Neural Transm (Vienna)* 117:949-960
96. Lee CYD, Daggett A, Gu X, Jiang LL, Langfelder P, Li X, Wang N, Zhao Y, Park CS, Cooper Y, Ferando I, Mody I, Coppola G, Xu H, Yang XW (2018) Elevated TREM2 Gene Dosage Reprograms Microglia Responsivity and Ameliorates Pathological Phenotypes in Alzheimer's Disease Models. *Neuron* 97:1032-1048 e1035

REFERENCES

97. Lee S, Varvel NH, Konerth ME, Xu G, Cardona AE, Ransohoff RM, Lamb BT (2010) CX3CR1 deficiency alters microglial activation and reduces beta-amyloid deposition in two Alzheimer's disease mouse models. *Am J Pathol* 177:2549-2562
98. Leissring MA, Farris W, Chang AY, Walsh DM, Wu X, Sun X, Frosch MP, Selkoe DJ (2003) Enhanced proteolysis of beta-amyloid in APP transgenic mice prevents plaque formation, secondary pathology, and premature death. *Neuron* 40:1087-1093
99. Leng F, Edison P (2021) Neuroinflammation and microglial activation in Alzheimer disease: where do we go from here? *Nat Rev Neurol* 17:157-172
100. Li X, Alafuzoff I, Soininen H, Winblad B, Pei JJ (2005) Levels of mTOR and its downstream targets 4E-BP1, eEF2, and eEF2 kinase in relationships with tau in Alzheimer's disease brain. *FEBS J* 272:4211-4220
101. Liddel SA, Guttenplan KA, Clarke LE, Bennett FC, Bohlen CJ, Schirmer L, Bennett ML, Munch AE, Chung WS, Peterson TC, Wilton DK, Frouin A, Napier BA, Panicker N, Kumar M, Buckwalter MS, Rowitch DH, Dawson VL, Dawson TM, Stevens B, Barres BA (2017) Neurotoxic reactive astrocytes are induced by activated microglia. *Nature* 541:481-487
102. Limatola C, Ransohoff RM (2014) Modulating neurotoxicity through CX3CL1/CX3CR1 signaling. *Front Cell Neurosci* 8:229
103. Liu CC, Hu J, Zhao N, Wang J, Wang N, Cirrito JR, Kanekiyo T, Holtzman DM, Bu G (2017) Astrocytic LRP1 Mediates Brain Abeta Clearance and Impacts Amyloid Deposition. *J Neurosci* 37:4023-4031
104. Liu S, Liu Y, Hao W, Wolf L, Kiliaan AJ, Penke B, Rube CE, Walter J, Heneka MT, Hartmann T, Menger MD, Fassbender K (2012) TLR2 is a primary receptor for Alzheimer's amyloid beta peptide to trigger neuroinflammatory activation. *J Immunol* 188:1098-1107
105. Liu W, Taso O, Wang R, Bayram S, Graham AC, Garcia-Reitboeck P, Mallach A, Andrews WD, Piers TM, Botia JA, Pocock JM, Cummings DM, Hardy J, Edwards FA, Salih DA (2020) Trem2 promotes anti-inflammatory responses in microglia and is suppressed under pro-inflammatory conditions. *Hum Mol Genet* 29:3224-3248
106. Liu Y, Walter S, Stagi M, Cherny D, Letiembre M, Schulz-Schaeffer W, Heine H, Penke B, Neumann H, Fassbender K (2005) LPS receptor (CD14): a receptor for phagocytosis of Alzheimer's amyloid peptide. *Brain* 128:1778-1789
107. Liu Y, Liu X, Hao WL, Decker Y, Schomburg R, Fulop L, Pasparakis M, Menger MD, Fassbender K (2014) IKK beta Deficiency in Myeloid Cells Ameliorates Alzheimer's Disease-Related Symptoms and Pathology. *Journal of Neuroscience* 34:12982-12999
108. Liu Z, Condello C, Schain A, Harb R, Grutzendler J (2010) CX3CR1 in microglia regulates brain amyloid deposition through selective protofibrillar amyloid-beta phagocytosis. *J Neurosci* 30:17091-17101
109. Livingston G, Huntley J, Sommerlad A, Ames D, Ballard C, Banerjee S, Brayne C, Burns A, Cohen-Mansfield J, Cooper C, Costafreda SG, Dias A, Fox N, Gitlin LN, Howard R, Kales HC, Kivimäki M, Larson EB, Ogunniyi A, Orgeta V, Ritchie K, Rockwood K, Sampson

- EL, Samus Q, Schneider LS, Selbæk G, Teri L, Mukadam N (2020) Dementia prevention, intervention, and care: 2020 report of the Lancet Commission. *The Lancet* 396:413-446
110. Longair MH, Baker DA, Armstrong JD (2011) Simple Neurite Tracer: open source software for reconstruction, visualization and analysis of neuronal processes. *Bioinformatics* 27:2453-2454
111. Lopez-Lopez A, Gelpi E, Lopategui DM, Vidal-Taboada JM (2018) Association of the CX3CR1-V249I Variant with Neurofibrillary Pathology Progression in Late-Onset Alzheimer's Disease. *Mol Neurobiol* 55:2340-2349
112. Lou N, Takano T, Pei Y, Xavier AL, Goldman SA, Nedergaard M (2016) Purinergic receptor P2RY12-dependent microglial closure of the injured blood-brain barrier. *Proc Natl Acad Sci U S A* 113:1074-1079
113. Louveau A, Smirnov I, Keyes TJ, Eccles JD, Rouhani SJ, Peske JD, Derecki NC, Castle D, Mandell JW, Lee KS, Harris TH, Kipnis J (2015) Structural and functional features of central nervous system lymphatic vessels. *Nature* 523:337-341
114. Lucin KM, O'Brien CE, Bieri G, Czirr E, Moshier KI, Abbey RJ, Mastroeni DF, Rogers J, Spencer B, Masliah E, Wyss-Coray T (2013) Microglial beclin 1 regulates retromer trafficking and phagocytosis and is impaired in Alzheimer's disease. *Neuron* 79:873-886
115. Malm TM, Jay TR, Landreth GE (2015) The evolving biology of microglia in Alzheimer's disease. *Neurotherapeutics* 12:81-93
116. Mandrekar S, Jiang Q, Lee CY, Koenigsknecht-Talboo J, Holtzman DM, Landreth GE (2009) Microglia mediate the clearance of soluble A β through fluid phase macropinocytosis. *J Neurosci* 29:4252-4262
117. Maphis N, Xu G, Kokiko-Cochran ON, Jiang S, Cardona A, Ransohoff RM, Lamb BT, Bhaskar K (2015) Reactive microglia drive tau pathology and contribute to the spreading of pathological tau in the brain. *Brain* 138:1738-1755
118. Martin Prince G-CA, Maëlenn Guerchet, Yu-Tzu Wu (2015) World Alzheimer's Report 2015, The Global Impact of Dementia An analysis of prevalence, incidence, cost and trends. Alzheimer's Disease International.
119. Mathys H, Davila-Velderrain J, Peng Z, Gao F, Mohammadi S, Young JZ, Menon M, He L, Abdurrob F, Jiang X, Martorell AJ, Ransohoff RM, Hafler BP, Bennett DA, Kellis M, Tsai LH (2019) Single-cell transcriptomic analysis of Alzheimer's disease. *Nature* 570:332-337
120. Mildner A, Huang H, Radke J, Stenzel W, Priller J (2017) P2Y12 receptor is expressed on human microglia under physiological conditions throughout development and is sensitive to neuroinflammatory diseases. *Glia* 65:375-387
121. Miners JS, Barua N, Kehoe PG, Gill S, Love S (2011) A β -degrading enzymes: potential for treatment of Alzheimer disease. *J Neuropathol Exp Neurol* 70:944-959

REFERENCES

122. Minter MR, Hinterleitner R, Meisel M, Zhang C, Leone V, Zhang X, Oyler-Castrillo P, Zhang X, Musch MW, Shen X, Jabri B, Chang EB, Tanzi RE, Sisodia SS (2017) Antibiotic-induced perturbations in microbial diversity during post-natal development alters amyloid pathology in an aged APPSWE/PS1DeltaE9 murine model of Alzheimer's disease. *Sci Rep* 7:10411
123. Morris MC, Evans DA, Bienias JL, Scherr PA, Tangney CC, Hebert LE, Bennett DA, Wilson RS, Aggarwal N (2004) Dietary niacin and the risk of incident Alzheimer's disease and of cognitive decline. *J Neurol Neurosurg Psychiatry* 75:1093-1099
124. Mossad O, Erny D (2020) The microbiota-microglia axis in central nervous system disorders. *Brain Pathol* 30:1159-1177
125. Moutinho M, Puntambekar SS, Tsai AP, Coronel I, Lin PB, Casali BT, Martinez P, Oblak AL, Lasagna-Reeves CA, Lamb BT, Landreth GE (2022) The niacin receptor HCAR2 modulates microglial response and limits disease progression in a mouse model of Alzheimer's disease. *Sci Transl Med* 14:eabl7634
126. Nakanishi A, Kaneko N, Takeda H, Sawasaki T, Morikawa S, Zhou W, Kurata M, Yamamoto T, Akbar SMF, Zako T, Masumoto J (2018) Amyloid beta directly interacts with NLRP3 to initiate inflammasome activation: identification of an intrinsic NLRP3 ligand in a cell-free system. *Inflamm Regen* 38:27
127. Nhan HS, Chiang K, Koo EH (2015) The multifaceted nature of amyloid precursor protein and its proteolytic fragments: friends and foes. *Acta Neuropathol* 129:1-19
128. Nixon RA (2007) Autophagy, amyloidogenesis and Alzheimer disease. *J Cell Sci* 120:4081-4091
129. Nixon RA (2017) Amyloid precursor protein and endosomal-lysosomal dysfunction in Alzheimer's disease: inseparable partners in a multifactorial disease. *FASEB J* 31:2729-2743
130. Oberstein TJ, Taha L, Spitzer P, Hellstern J, Herrmann M, Kornhuber J, Maler JM (2018) Imbalance of Circulating Th17 and Regulatory T Cells in Alzheimer's Disease: A Case Control Study. *Front Immunol* 9:1213
131. Offermanns S, Schwaninger M (2015) Nutritional or pharmacological activation of HCA(2) ameliorates neuroinflammation. *Trends Mol Med* 21:245-255
132. Offermanns S (2017) Hydroxy-Carboxylic Acid Receptor Actions in Metabolism. *Trends Endocrinol Metab* 28:227-236
133. Paolicelli RC, Bolasco G, Pagani F, Maggi L, Scianni M, Panzanelli P, Giustetto M, Ferreira TA, Guiducci E, Dumas L, Ragozzino D, Gross CT (2011) Synaptic pruning by microglia is necessary for normal brain development. *Science* 333:1456-1458
134. Peng W, Achariyar TM, Li B, Liao Y, Mestre H, Hitomi E, Regan S, Kasper T, Peng S, Ding F, Benveniste H, Nedergaard M, Deane R (2016) Suppression of glymphatic fluid transport in a mouse model of Alzheimer's disease. *Neurobiol Dis* 93:215-225

REFERENCES

135. Perry VH, Holmes C (2014) Microglial priming in neurodegenerative disease. *Nat Rev Neurol* 10:217-224
136. Prieur EAK, Jadavji NM (2019) Assessing Spatial Working Memory Using the Spontaneous Alternation Y-maze Test in Aged Male Mice. *Bio Protoc* 9:e3162
137. Prince M, Ali GC, Guerchet M, Prina AM, Albanese E, Wu YT (2016) Recent global trends in the prevalence and incidence of dementia, and survival with dementia. *Alzheimers Res Ther* 8:23
138. Prinz M, Priller J (2014) Microglia and brain macrophages in the molecular age: from origin to neuropsychiatric disease. *Nat Rev Neurosci* 15:300-312
139. Quan W, Luo Q, Hao W, Tomic I, Furihata T, Schulz-Schaffer W, Menger MD, Fassbender K, Liu Y (2021) Haploinsufficiency of microglial MyD88 ameliorates Alzheimer's pathology and vascular disorders in APP/PS1-transgenic mice. *Glia* 69:1987-2005
140. Rainey-Smith SR, Mazzucchelli GN, Villemagne VL, Brown BM, Porter T, Weinborn M, Bucks RS, Milicic L, Sohrabi HR, Taddei K, Ames D, Maruff P, Masters CL, Rowe CC, Salvado O, Martins RN, Laws SM, Group AR (2018) Genetic variation in Aquaporin-4 moderates the relationship between sleep and brain Abeta-amyloid burden. *Transl Psychiatry* 8:47
141. Rajan KB, Weuve J, Barnes LL, McAninch EA, Wilson RS, Evans DA (2021) Population estimate of people with clinical Alzheimer's disease and mild cognitive impairment in the United States (2020-2060). *Alzheimers Dement*
142. Rasmussen MK, Mestre H, Nedergaard M (2018) The glymphatic pathway in neurological disorders. *Lancet Neurol* 17:1016-1024
143. Reed-Geaghan EG, Savage JC, Hise AG, Landreth GE (2009) CD14 and toll-like receptors 2 and 4 are required for fibrillar A{beta}-stimulated microglial activation. *J Neurosci* 29:11982-11992
144. Reemst K, Noctor SC, Lucassen PJ, Hol EM (2016) The Indispensable Roles of Microglia and Astrocytes during Brain Development. *Front Hum Neurosci* 10:566
145. Ricciarelli R, D'Abramo C, Zingg JM, Giliberto L, Markesbery W, Azzi A, Marinari UM, Pronzato MA, Tabaton M (2004) CD36 overexpression in human brain correlates with beta-amyloid deposition but not with Alzheimer's disease. *Free Radic Biol Med* 36:1018-1024
146. Ridderstad Wollberg A, Ericsson-Dahlstrand A, Jureus A, Ekerot P, Simon S, Nilsson M, Wiklund SJ, Berg AL, Ferm M, Sunnemark D, Johansson R (2014) Pharmacological inhibition of the chemokine receptor CX3CR1 attenuates disease in a chronic-relapsing rat model for multiple sclerosis. *Proc Natl Acad Sci U S A* 111:5409-5414
147. Roberts KF, Elbert DL, Kasten TP, Patterson BW, Sigurdson WC, Connors RE, Ovod V, Munsell LY, Mawuenyega KG, Miller-Thomas MM, Moran CJ, Cross DT, 3rd, Derdeyn CP, Bateman RJ (2014) Amyloid-beta efflux from the central nervous system into the plasma. *Ann Neurol* 76:837-844

REFERENCES

148. Rogers JT, Morganti JM, Bachstetter AD, Hudson CE, Peters MM, Grimmig BA, Weeber EJ, Bickford PC, Gemma C (2011) CX3CR1 deficiency leads to impairment of hippocampal cognitive function and synaptic plasticity. *J Neurosci* 31:16241-16250
149. Roque C, Mendes-Oliveira J, Duarte-Chendo C, Baltazar G (2019) The role of G protein-coupled estrogen receptor 1 on neurological disorders. *Front Neuroendocrinol* 55:100786
150. Saido T, Leissring MA (2012) Proteolytic degradation of amyloid beta-protein. *Cold Spring Harb Perspect Med* 2:a006379
151. Saito T, Matsuba Y, Mihira N, Takano J, Nilsson P, Itohara S, Iwata N, Saido TC (2014) Single App knock-in mouse models of Alzheimer's disease. *Nat Neurosci* 17:661-663
152. Santolla MF, De Francesco EM, Lappano R, Rosano C, Abonante S, Maggiolini M (2014) Niacin activates the G protein estrogen receptor (GPER)-mediated signalling. *Cell Signal* 26:1466-1475
153. Scheltens P, De Strooper B, Kivipelto M, Holstege H, Chetelat G, Teunissen CE, Cummings J, van der Flier WM (2021) Alzheimer's disease. *Lancet* 397:1577-1590
154. Semar S, Klotz M, Letiembre M, Van Ginneken C, Braun A, Jost V, Bischof M, Lammers WJ, Liu Y, Fassbender K, Wyss-Coray T, Kirchhoff F, Schafer KH (2013) Changes of the enteric nervous system in amyloid-beta protein precursor transgenic mice correlate with disease progression. *J Alzheimers Dis* 36:7-20
155. Shibata M, Yamada S, Kumar SR, Calero M, Bading J, Frangione B, Holtzman DM, Miller CA, Strickland DK, Ghiso J, Zlokovic BV (2000) Clearance of Alzheimer's amyloid-ss(1-40) peptide from brain by LDL receptor-related protein-1 at the blood-brain barrier. *J Clin Invest* 106:1489-1499
156. Shinohara M, Petersen RC, Dickson DW, Bu G (2013) Brain regional correlation of amyloid-beta with synapses and apolipoprotein E in non-demented individuals: potential mechanisms underlying regional vulnerability to amyloid-beta accumulation. *Acta Neuropathol* 125:535-547
157. Shinohara M, Tachibana M, Kanekiyo T, Bu G (2017) Role of LRP1 in the pathogenesis of Alzheimer's disease: evidence from clinical and preclinical studies. *J Lipid Res* 58:1267-1281
158. Shirotani K, Tsubuki S, Iwata N, Takaki Y, Harigaya W, Maruyama K, Kiryu-Seo S, Kiyama H, Iwata H, Tomita T, Iwatsubo T, Saido TC (2001) Neprilysin degrades both amyloid beta peptides 1-40 and 1-42 most rapidly and efficiently among thiorphan- and phosphoramidon-sensitive endopeptidases. *J Biol Chem* 276:21895-21901
159. Sipe GO, Lowery RL, Tremblay ME, Kelly EA, Lamantia CE, Majewska AK (2016) Microglial P2Y12 is necessary for synaptic plasticity in mouse visual cortex. *Nat Commun* 7:10905
160. Sobue A, Komine O, Hara Y, Endo F, Mizoguchi H, Watanabe S, Murayama S, Saito T, Saido TC, Sahara N, Higuchi M, Ogi T, Yamanaka K (2021) Microglial gene signature

reveals loss of homeostatic microglia associated with neurodegeneration of Alzheimer's disease. *Acta Neuropathol Commun* 9:1

161. Spangenberg E, Severson PL, Hohsfield LA, Crapser J, Zhang J, Burton EA, Zhang Y, Spevak W, Lin J, Phan NY, Habets G, Rymar A, Tsang G, Walters J, Nespi M, Singh P, Broome S, Ibrahim P, Zhang C, Bollag G, West BL, Green KN (2019) Sustained microglial depletion with CSF1R inhibitor impairs parenchymal plaque development in an Alzheimer's disease model. *Nat Commun* 10:3758

162. Spector R, Johanson CE (2007) Vitamin transport and homeostasis in mammalian brain: focus on Vitamins B and E. *J Neurochem* 103:425-438

163. Sperling RA, Aisen PS, Beckett LA, Bennett DA, Craft S, Fagan AM, Iwatsubo T, Jack CR, Jr., Kaye J, Montine TJ, Park DC, Reiman EM, Rowe CC, Siemers E, Stern Y, Yaffe K, Carrillo MC, Thies B, Morrison-Bogorad M, Wagster MV, Phelps CH (2011) Toward defining the preclinical stages of Alzheimer's disease: recommendations from the National Institute on Aging-Alzheimer's Association workgroups on diagnostic guidelines for Alzheimer's disease. *Alzheimers Dement* 7:280-292

164. Storck SE, Meister S, Nahrath J, Meissner JN, Schubert N, Di Spiezio A, Baches S, Vandenbroucke RE, Bouter Y, Prikulis I, Korth C, Weggen S, Heimann A, Schwaninger M, Bayer TA, Pietrzik CU (2016) Endothelial LRP1 transports amyloid-beta(1-42) across the blood-brain barrier. *J Clin Invest* 126:123-136

165. Takahashi RH, Milner TA, Li F, Nam EE, Edgar MA, Yamaguchi H, Beal MF, Xu H, Greengard P, Gouras GK (2002) Intraneuronal Alzheimer abeta42 accumulates in multivesicular bodies and is associated with synaptic pathology. *Am J Pathol* 161:1869-1879

166. Tavares G, Martins M, Correia JS, Sardinha VM, Guerra-Gomes S, das Neves SP, Marques F, Sousa N, Oliveira JF (2017) Employing an open-source tool to assess astrocyte tridimensional structure. *Brain Struct Funct* 222:1989-1999

167. Tay TL, Savage JC, Hui CW, Bisht K, Tremblay ME (2017) Microglia across the lifespan: from origin to function in brain development, plasticity and cognition. *J Physiol* 595:1929-1945

168. Teeling JL, Cunningham C, Newman TA, Perry VH (2010) The effect of non-steroidal anti-inflammatory agents on behavioural changes and cytokine production following systemic inflammation: Implications for a role of COX-1. *Brain Behav Immun* 24:409-419

169. Thorburn AN, Macia L, Mackay CR (2014) Diet, metabolites, and "western-lifestyle" inflammatory diseases. *Immunity* 40:833-842

170. Tolar M, Abushakra S, Sabbagh M (2020) The path forward in Alzheimer's disease therapeutics: Reevaluating the amyloid cascade hypothesis. *Alzheimers Dement* 16:1553-1560

171. Tse JKY (2017) Gut Microbiota, Nitric Oxide, and Microglia as Prerequisites for Neurodegenerative Disorders. *ACS Chem Neurosci* 8:1438-1447

172. Tseng BP, Green KN, Chan JL, Blurton-Jones M, LaFerla FM (2008) Abeta inhibits the proteasome and enhances amyloid and tau accumulation. *Neurobiol Aging* 29:1607-1618

REFERENCES

173. Tunaru S, Kero J, Schaub A, Wufka C, Blaukat A, Pfeffer K, Offermanns S (2003) PUMA-G and HM74 are receptors for nicotinic acid and mediate its anti-lipolytic effect. *Nat Med* 9:352-355
174. Ulland TK, Song WM, Huang SC, Ulrich JD, Sergushichev A, Beatty WL, Loboda AA, Zhou Y, Cairns NJ, Kambal A, Loginicheva E, Gilfillan S, Cella M, Virgin HW, Unanue ER, Wang Y, Artyomov MN, Holtzman DM, Colonna M (2017) TREM2 Maintains Microglial Metabolic Fitness in Alzheimer's Disease. *Cell* 170:649-663 e613
175. Ulland TK, Colonna M (2018) TREM2 - a key player in microglial biology and Alzheimer disease. *Nat Rev Neurol* 14:667-675
176. van Assema DM, Lubberink M, Bauer M, van der Flier WM, Schuit RC, Windhorst AD, Comans EF, Hoetjes NJ, Tolboom N, Langer O, Muller M, Scheltens P, Lammertsma AA, van Berckel BN (2012) Blood-brain barrier P-glycoprotein function in Alzheimer's disease. *Brain* 135:181-189
177. van der Velpen V, Rosenberg N, Maillard V, Teav T, Chatton JY, Gallart-Ayala H, Ivanisevic J (2021) Sex-specific alterations in NAD⁺ metabolism in 3xTg Alzheimer's disease mouse brain assessed by quantitative targeted LC-MS. *J Neurochem* 159:378-388
178. Van Gool B, Storck SE, Reekmans SM, Lechat B, Gordts P, Pradier L, Pietrzik CU, Roebroek AJM (2019) LRP1 Has a Predominant Role in Production over Clearance of Aβeta in a Mouse Model of Alzheimer's Disease. *Mol Neurobiol* 56:7234-7245
179. Vanmierlo T, Rutten K, Dederen J, Bloks VW, van Vark-van der Zee LC, Kuipers F, Kiliaan A, Blokland A, Sijbrands EJ, Steinbusch H, Prickaerts J, Lutjohann D, Mulder M (2011) Liver X receptor activation restores memory in aged AD mice without reducing amyloid. *Neurobiol Aging* 32:1262-1272
180. Versele R, Corsi M, Fuso A, Sevin E, Businaro R, Gosselet F, Fenart L, Candela P (2020) Ketone Bodies Promote Amyloid-beta1-40 Clearance in a Human in Vitro Blood-Brain Barrier Model. *Int J Mol Sci* 21
181. Vogt NM, Kerby RL, Dill-McFarland KA, Harding SJ, Merluzzi AP, Johnson SC, Carlsson CM, Asthana S, Zetterberg H, Blennow K, Bendlin BB, Rey FE (2017) Gut microbiome alterations in Alzheimer's disease. *Sci Rep* 7:13537
182. Walker DG, Tang TM, Mendsaikhan A, Tooyama I, Serrano GE, Sue LI, Beach TG, Lue LF (2020) Patterns of Expression of Purinergic Receptor P2RY12, a Putative Marker for Non-Activated Microglia, in Aged and Alzheimer's Disease Brains. *Int J Mol Sci* 21
183. Wang D, Chen F, Han Z, Yin Z, Ge X, Lei P (2021) Relationship Between Amyloid-beta Deposition and Blood-Brain Barrier Dysfunction in Alzheimer's Disease. *Front Cell Neurosci* 15:695479
184. Wang S, Mustafa M, Yuede CM, Salazar SV, Kong P, Long H, Ward M, Siddiqui O, Paul R, Gilfillan S, Ibrahim A, Rhinn H, Tassi I, Rosenthal A, Schwabe T, Colonna M (2020) Anti-human TREM2 induces microglia proliferation and reduces pathology in an Alzheimer's disease model. *J Exp Med* 217

REFERENCES

185. Wang Y, Szretter KJ, Vermi W, Gilfillan S, Rossini C, Cella M, Barrow AD, Diamond MS, Colonna M (2012) IL-34 is a tissue-restricted ligand of CSF1R required for the development of Langerhans cells and microglia. *Nat Immunol* 13:753-760
186. Wang Y, Ulland TK, Ulrich JD, Song W, Tzaferis JA, Hole JT, Yuan P, Mahan TE, Shi Y, Gilfillan S, Cella M, Grutzendler J, DeMattos RB, Cirrito JR, Holtzman DM, Colonna M (2016) TREM2-mediated early microglial response limits diffusion and toxicity of amyloid plaques. *J Exp Med* 213:667-675
187. Wang Y, Wang Z, Wang Y, Li F, Jia J, Song X, Qin S, Wang R, Jin F, Kitazato K, Wang Y (2018) The Gut-Microglia Connection: Implications for Central Nervous System Diseases. *Front Immunol* 9:2325
188. Wesen E, Jeffries GDM, Matson Dzebo M, Esbjorner EK (2017) Endocytic uptake of monomeric amyloid-beta peptides is clathrin- and dynamin-independent and results in selective accumulation of Aβ(1-42) compared to Aβ(1-40). *Sci Rep* 7:2021
189. Whyte LS, Hemsley KM, Lau AA, Hassiotis S, Saito T, Saido TC, Hopwood JJ, Sargeant TJ (2018) Reduction in open field activity in the absence of memory deficits in the App(NL-G-F) knock-in mouse model of Alzheimer's disease. *Behav Brain Res* 336:177-181
190. Wolf AJ, Underhill DM (2018) Peptidoglycan recognition by the innate immune system. *Nat Rev Immunol* 18:243-254
191. Wong CO (2020) Endosomal-Lysosomal Processing of Neurodegeneration-Associated Proteins in Astrocytes. *Int J Mol Sci* 21
192. Wymore Brand M, Wannemuehler MJ, Phillips GJ, Proctor A, Overstreet AM, Jergens AE, Orcutt RP, Fox JG (2015) The Altered Schaedler Flora: Continued Applications of a Defined Murine Microbial Community. *ILAR J* 56:169-178
193. Xia M, Yang L, Sun G, Qi S, Li B (2017) Mechanism of depression as a risk factor in the development of Alzheimer's disease: the function of AQP4 and the glymphatic system. *Psychopharmacology (Berl)* 234:365-379
194. Xie K, Liu Y, Hao W, Walter S, Penke B, Hartmann T, Schachner M, Fassbender K (2013a) Tenascin-C deficiency ameliorates Alzheimer's disease-related pathology in mice. *Neurobiol Aging* 34:2389-2398
195. Xie L, Kang H, Xu Q, Chen MJ, Liao Y, Thiyagarajan M, O'Donnell J, Christensen DJ, Nicholson C, Iliff JJ, Takano T, Deane R, Nedergaard M (2013b) Sleep drives metabolite clearance from the adult brain. *Science* 342:373-377
196. Xu Z, Xiao N, Chen Y, Huang H, Marshall C, Gao J, Cai Z, Wu T, Hu G, Xiao M (2015) Deletion of aquaporin-4 in APP/PS1 mice exacerbates brain Aβ accumulation and memory deficits. *Mol Neurodegener* 10:58
197. Yasojima K, McGeer EG, McGeer PL (2001) Relationship between beta amyloid peptide generating molecules and neprilysin in Alzheimer disease and normal brain. *Brain Res* 919:115-121

REFERENCES

198. Yeh FL, Wang Y, Tom I, Gonzalez LC, Sheng M (2016) TREM2 Binds to Apolipoproteins, Including APOE and CLU/APOJ, and Thereby Facilitates Uptake of Amyloid-Beta by Microglia. *Neuron* 91:328-340
199. Young K, Morrison H (2018) Quantifying Microglia Morphology from Photomicrographs of Immunohistochemistry Prepared Tissue Using ImageJ. *J Vis Exp*
200. Yuan P, Condello C, Keene CD, Wang Y, Bird TD, Paul SM, Luo W, Colonna M, Baddeley D, Grutzendler J (2016) TREM2 Haplodeficiency in Mice and Humans Impairs the Microglia Barrier Function Leading to Decreased Amyloid Compaction and Severe Axonal Dystrophy. *Neuron* 90:724-739
201. Zeppenfeld DM, Simon M, Haswell JD, D'Abreo D, Murchison C, Quinn JF, Grafe MR, Woltjer RL, Kaye J, Iliff JJ (2017) Association of Perivascular Localization of Aquaporin-4 With Cognition and Alzheimer Disease in Aging Brains. *JAMA Neurol* 74:91-99
202. Zhang Y, Chen X, Zhao Y, Ponnusamy M, Liu Y (2017) The role of ubiquitin proteasomal system and autophagy-lysosome pathway in Alzheimer's disease. *Rev Neurosci* 28:861-868
203. Zhao R, Hu W, Tsai J, Li W, Gan WB (2017) Microglia limit the expansion of beta-amyloid plaques in a mouse model of Alzheimer's disease. *Mol Neurodegener* 12:47
204. Zhou Y, Song WM, Andhey PS, Swain A, Levy T, Miller KR, Poliani PL, Cominelli M, Grover S, Gilfillan S, Cella M, Ulland TK, Zaitsev K, Miyashita A, Ikeuchi T, Sainouchi M, Kakita A, Bennett DA, Schneider JA, Nichols MR, Beausoleil SA, Ulrich JD, Holtzman DM, Artyomov MN, Colonna M (2020) Human and mouse single-nucleus transcriptomics reveal TREM2-dependent and TREM2-independent cellular responses in Alzheimer's disease. *Nat Med* 26:131-142
205. Zhuang ZQ, Shen LL, Li WW, Fu X, Zeng F, Gui L, Lu Y, Cai M, Zhu C, Tan YL, Zheng P, Li HY, Zhu J, Zhou HD, Bu XL, Wang YJ (2018) Gut Microbiota is Altered in Patients with Alzheimer's Disease. *J Alzheimers Dis* 63:1337-1346
206. Zuroff L, Daley D, Black KL, Koronyo-Hamaoui M (2017) Clearance of cerebral Abeta in Alzheimer's disease: reassessing the role of microglia and monocytes. *Cell Mol Life Sci* 74:2167-2201

10. LIST OF FIGURES AND COOPERATIONS

Fig. 3.3	Alzheimer's disease (AD) continuum lasts 15-25 years. Picture from: 2021 Alzheimer's disease facts and figures
Fig. 3.3.2	Microglia response to amyloid-β. Picture from: Fangda Leng and Paul Ed ison
Fig. 5.3.1	Schematic diagram of Y maze test. Picture from: Qinghua Luo
Fig. 5.3.3	Schematic diagram of the preparation of brain sample sections. Picture from: Shirong Liu
Figure 6.1	GPR109a-positive microglia are recruited to Aβ deposits. Real time PCR: Alex Liu; Immunohistochemistry: Qinghua Luo
Figure 6.2	Deficiency of GPR109a tends to improve cognitive function of APP-knock-in AD mice. Behaviour test and data analysis: Qinghua Luo
Figure 6.3.1	Synaptic proteins decrease in APP-KI mice. Western blot and data analysis: Qinghua Luo
Figure 6.3.2	Deletion of GPR109a attenuates AD-associated loss of synaptic proteins and axonal dystrophy in APP^{ki/ki} mice. Western blot, immunohistochemistry and data analysis: Qinghua Luo
Figure 6.4.1	Deficiency of GPR109a decreases Aβ load in APP^{ki/ki} mouse brain Immunohistochemistry and data analysis: Qinghua Luo
Figure 6.4.2	Deficiency of GPR109a reduces Aβ monomers and oligomers in the brain of APP-knock-in mice. Western blot: Inge Tomic; Data analysis: Qinghua Luo
Figure 6.4.3	Deficiency of GPR109a reduces Aβ42 and Aβ40 amounts in the brain of APP-knock-in mice. ELISA and data analysis: Qinghua Luo
Figure 6.5	Deficiency of GPR109a does not significantly change microglia-mediated inflammatory activation in APP-KI mouse brain. Real time PCR: Alex Liu; Immunohistochemistry: Qinghua Luo
Figure 6.6	Morphometric analysis of plaque-associated microglia. Immunohistochemistry and microglial morphology analysis: Qinghua Luo
Figure 6.7	Deletion of GPR109a shifts microglial activation to homeostatic profile in 9-month-old APP-knock-in mouse brain. Real time PCR: Qinghua Luo; Data analysis: Alex Liu
Figure 6.8	GPR109a deficiency increases microglial recruitment around the plaques and promotes microglial amyloid-β phagocytosis. Immunohistochemistry, flow cytometry and data analysis: Qinghua Luo
Figure 6.9.1	Niacin inhibits inflammatory response and facilitates the expression of CX3CR1 in GPR109a-deficient macrophages. ELISA, flow cytometry and data analysis: Qinghua Luo
Figure 6.9.2	Niacin promotes Aβ phagocytosis by GPR109a-deficient macrophages and is associated with CX3CR1. Flow cytometry and data analysis: Qinghua Luo
Figure 6.10.1	Deficiency of GPR109a increases the expression of LPR1 in the APP^{ki/ki} mouse brain. Western blot and data analysis: Qinghua Luo
Figure 6.10.2	Upregulation of LRP1 in neurons and astrocytes of GPR109a-deficient APP^{ki/ki} mice.

LIST OF FIGURES AND COOPERATIONS

	Immunohistochemistry and data analysis: Qinghua Luo
Figure 6.11.1	Deficiency of GPR109a decreases genetic transcription of IL-17a in CD4-positive spleen cells. Real time PCR and data analysis: Alex Liu
Figure 6.11.2	Deficiency of GPR109a decreases il-17a gene transcription in CD4-positive lymphocytes in the gut. Real time PCR: Qinghua Luo; Data analysis: Alex Liu
Figure 6.11.3	Representative flow cytometry histograms of IL-17a fluorescence intensity from CD4⁺ lymphocytes in the intestinal epithelium. Flow cytometry and data analysis: Qinghua Luo
Figure 6.12.1	Knockout of IL-17a eliminated the beneficial effects of GPR109a deficiency in APP^{ki/ki} mice. Western blot: Inge Tomic; Immunohistochemistry and data analysis: Qinghua Luo
Figure 6.12.2	Deletion of GPR109a does not increase protein levels of LRP1 and ABCB1 in brain tissue of <i>il-17a</i> gene-deficient APP^{ki/ki} mice; IL-17a deficiency abolished the effect of GPR109a deficiency that promotes microglia to cluster around Aβ deposits. Western blot, immunohistochemistry and microglial morphology analysis: Qinghua Luo

11. PUBLICATIONS AND PRESENTATIONS

11.1 Publications

1. Quan W, **Luo Q** (Co-first authorship), Hao W, Tomic I, Furihata T, Schulz-Schaffer W, Menger MD, Fassbender K, Liu Y (2021) Haploinsufficiency of microglial MyD88 ameliorates Alzheimer's pathology and vascular disorders in APP/PS1-transgenic mice. *Glia* 69:1987-2005.
2. **Luo Q**, Li D, Bao B, Wan X, Pan B, Tu J, Wang H, Ouyang Y, Chen Z, Yin X (2019) NEMO-binding domain peptides alleviate perihematomal inflammation injury after experimental intracerebral hemorrhage. *Neuroscience* 409:43-57.
3. Hao W, **Luo Q**, Menger MD, Fassbender K, Liu Y (2021) Treatment With CD52 Antibody Protects Neurons in Experimental Autoimmune Encephalomyelitis Mice During the Recovering Phase. *Front Immunol* 12:792465.
4. Quan W, **Luo Q**, Tang Q, Furihata T, Li D, Fassbender K, Liu Y (2020) NLRP3 Is Involved in the Maintenance of Cerebral Pericytes. *Frontiers in Cellular Neuroscience* 14.
5. Ouyang Y, Li D, Wang H, Wan Z, **Luo Q**, Zhong Y, Yin M, Qing Z, Li Z, Bao B, Chen Z, Yin X, Zhu LQ (2019) MiR-21-5p/dual-specificity phosphatase 8 signaling mediates the anti-inflammatory effect of haem oxygenase-1 in aged intracerebral haemorrhage rats. *Aging Cell* 18:e13022.
6. Zhao J, Zhang G, Li M, **Luo Q**, Leng Y, Liu X (2018) Neuro-protective effects of aloperine in an Alzheimer's disease cellular model. *Biomed Pharmacother* 108:137-143.

11.2 Poster presentations

1. **Luo QH**, Quan WQ, Hao WL, Fassbender K and Liu Y. Haploinsufficiency of microglial MyD88 ameliorates Alzheimer's pathology and vascular disorders in APP/PS1-transgenic mice. XV European Meeting on Glial Cells in Health and Disease. 2021, 09.
2. **Luo QH**, Fassbender K and Liu Y. The pathologic role of GPR109a in Alzheimer's disease. AD/PDTM 2022. Barcelona, Spain, 2022, 03.

12. ACKNOWLEDGEMENTS

First and foremost, I would like to express my deepest gratitude to my thesis supervisor Dr. Yang Liu, Prof. Dr. Klaus Fassbender, and Prof. Dr. Frank Kirchhoff. They continuously headed this project with their enthusiasm and wealth of knowledge and always steered me in the right direction whenever I needed them. I sincerely thank Dr. Yang Liu, whose office door is always open to me whenever I come into a snag or have questions about my research or writing even my life. Also, I am heartily grateful to Prof. Dr. Klaus Fassbender and Prof. Dr. Frank Kirchhoff, who always tried their utmost to help me, thanks to their patience with me and sacrificed their time to support me. Once again, I want to convey my gratitude to all of my advisors. Without their help and enthusiastic guidance, this dissertation would not have been conducted successfully.

I would like to thank my friendly and upbeat colleagues at AG Fassbender, Dr. Wenlin Hao, Dr. Wenqiang Quan, Dr. Laura Schnöder, Tomic Inge, Andrea Schottek, and Dr. Yann Decker, for making the last three years so enjoyable. I am incredibly grateful to Dr. Wenlin Hao, both a teacher and a friend. She is always willing to assist me in my thesis and guide me through the experimental procedures. Thanks to Dr. Wenqiang Quan for his patient explanation and guidance on various techniques. Dr. Laura Schnöder was always enthusiastic to help me when I needed it and introduced me to some German traditions. Ms. Tomic Inge and Ms. Andrea Schottek provided expert technical support to advance my thesis. Anytime I reach out to them, they are pleased to assist me, whether for academic or personal reasons. It has definitely been a fantastic experience in this lab. Especially, thanks to Dr. Xu Liu for introducing me to AG Fassbender and his heart-warming instructions and advice. I'd also like to express my gratitude to Dr. Yang Liu, without his assistance and wise advice this research would not have been possible! My sincere thanks to all the members of the AG Fassbender research team for their energy, understanding and help throughout the project.

I appreciated Prof. T. Saïdo (RIKEN Brain Science Institute, Japan) provided *App^{NL-G-F/NL-G-F}* knock-in mice; Prof. S. Offermanns (Max Planck Institute for Heart and Lung Research, Bad Nauheim) provided GPR109a-deficient mice; and Prof. Dr. Frank Kirchhoff, Dr. Wenhui

ACKNOWLEDGEMENTS

Huang (Department of Physiology of Saarland University) provided CX3CR1-CreERT2 mice.

I would like to acknowledge Alzheimer Forschung Initiative e.V. (#18009; to Yang Liu) for providing sufficient financial assistance for my thesis study. I gratefully thank the China Scholarship Council for providing scholarships (CSC: 201906820011) to guarantee my study and life.

Furthermore, I cannot forget my friends, who have always been there for me through thick and thin, cheering me on and celebrating each accomplishment. I would like to express my gratitude to Wenqiang Quan, Yiwen Yao, Qing Liu, Anqi Sheng, Wenyong Xian, Lipao Fang, Qilin Guo, Xiaoyu Cai, Weikun Meng, ect.

Finally, I deeply thank my most loving parents, Liyong Luo and Chengmei Tang, for their unconditional trust, timely encouragement, and endless patience. Without their wholehearted backing and encouragement, I believe I would not have had the fortitude to complete my Ph.D., and their love gave me the greatest motivation to get back on my feet. I appreciate my sister, Xiaoyan Luo, for her generous love and encouragement. Also, I offer my regards to my aunts, Manlin Luo and Xiaolin Luo, for their exceptionally help and affection during my Ph.D.. To all my loving family, I dedicate this dissertation.

The curriculum vitae was removed from the electronic version of the doctoral thesis for reasons of data protection.

